THE MID-ORDOVICIAN OOLITIC IRONSTONES OF NORTH WALES

by

Robert John Baxter Trythall, M.A. (Oxon.), F.G.S.,

Faculty of Applied Sciences,
Luton College of Higher Education,
Park Square,
Luton,
Beds.
LU1 3JU

Collaborating Institute: Camborne School of Mines

Thesis submitted in partial fulfillment of the degree of Doctor of Philosophy of the Council for National Academic Awards (CNAA).

October 1988

Gold is for the mistress,
silver for the maid,
copper for the craftsman,
cunning at his trade.

'Good!' said the Baron,
sitting in his hall,
'But Iron - Cold Iron
is master of them all.'

Cold Iron - Rudyard Kipling
(Rewards and Fairies 1910)

CONTENTS

LIST OF FIGURES

LIST OF TABLES

ACKNOWLEDGEMENTS

The author would like to acknowledge the receipt of a Beds. County Council LEA research studentship grant, whilst at Luton College. The receipt of monies from Luton College for field work and equipment expenses are gratefully acknowledged. I would like to thank my Director of Studies, Dr. Gordon Taylor, my Supervisor, Dr. Charles Eccles, and my external supervisor, Dr. Alan Bromley (Camborne School of Mines), for all the help they have put into this project. The support offered especially by other members of the Geology staff, by staff at Luton College, and by the Dean of Faculty, Dr. Mike Daniel , is acknowledged. The services of the geology technical staff, Mike Ashton, Maz Iqbal, Andy Willits, Jenny Matthews and Phil Rumford, are gratefully acknowledged, for thin sections, general technical support and games of cricket. The support of other technical, library and secretarial staff is also gratefully acknowledged.

The following institutions have offered the use of analytical and other facilities for this project, and this is gratefully acknowledged. These are as follows: The Open University (rock crushing facilities); Nottingham University, Drs. Peter Harvey and Brian Atkin (XRF analyses); Cambridge University, Dr. Andy Buckley (EPMA); Oxford University, Professor Vincent and Colin Fagg (XRD); Oxford Polytechnic, Anton Kearsley and Dr. Bill Perkins (ICP and SEM). Camborne School of Mines, Tony Ball, Steve and Lil (XRD, rock crushing facilities, mineral separation, microscope facilities, preparation of sections). The British Geological Survey have offered much support during this project, and is gratefully acknowledged. I would like to thank Dr. Stuart Molyneux (Keyworth) for his collaboration, and joint publication, on the ironstones. I would like to thank the staff at Abersytwyth for their help for use of facilities. I would like to thank Dr. Baruch Spiro (Grays Inn Road) for Isotope analyses.

I would like to thank a number of people who have provided useful discussions on ironstones and North Wales geology; especially Dr. Tony Reedman and Martin Smith (BGS Aberystwyth), Anton Kearsley (Oxford Polytechnic) and Tim Young (Sheffield University). Thanks also go to the delegates of the Phanerozoic Ironstones Symposium, Sheffield April 1987, who attended the North Wales Ironstones field trip, for their discussions in the field. Geologists from Aberystwyth University, Br. Bill Fitches and Warren Pratt, are thanked for their help.

Finally a number of people have made my stay at Luton infinitely more enjoyable than I thought possible. Firstly, much love and thanks go to my parents for their moral support throught this time, and to my father for the English lessons. Secondly, various staff, students, secretaries, technicians and old friends who have helped to pass the time during my institutionalisation at Luton, and without whose help all this would probably finished much sooner, but with much less fun. There are too many names to say thank you to, but they know who they are!

DECLARATION

The material of this thesis is based on the authors previously unpublished independant research. Material used from other sources is acknowledged within the text where applicable.

PERMISSION TO COPY

ABSTRACT

The Mid-Ordovician Oolitic Ironstones of North Wales - Robert Trythall

Oolitic ironstones occur within the Lower Palaeozoic Welsh Basin as isolated deposits found over a wide geographical area. There are two phases of ironstone deposition, a minor Upper Arenig phase and a Mid-Ordovician (Upper Llanvirn to basal Caradoc) phase. Both correlate with eustatic falls of sea level which exposed the Irish Sea Landmass lying immediately to the northwest. This exposure resulted in deep chemical weathering and generation of lateritic soils. Erosion of this material formed the source for the oolitic ironstones in the Welsh Basin.

The ironstones formed above stratigraphic hiatuses on sediment starved shallow water shoals, formed by synsedimentary faulting. These shoals were the favourable sites for the formation of berthierine peloids, which formed the nuclei for ooids. Additionally, they were also the site for the accumulation of berthierine mud, which was closely linked with the development of ferruginous algal mats. Bacterial reduction of organic material associated with ironstones, supplied the necessary reducing conditions for the formation and preservation of berthierine from a kaolinite/iron oxide precursor. Ooids formed by rolling over the muddy surface and mechanically accreting berthierine.

Subsequent tidal current reworking of this sediment resulted in the formation of the characteristic lithological features of the ironstones, representing a shallowing-up sequence. Progressive current winnowing led to the formation of a sequence with an upward increasing ooid content and decreasing mud content. The upper facies of the ironstones is an ooid bar deposit worked by tidal currents. Cessation of current reworking allowed faunal colonisation of the bar with significant bioturbation of the sediment, destroying primary sedimentary structures. The presence of some grain-ironstones indicate the original sedimentary state of the upper facies. Tectonic instability during deposition, by synsedimentary faulting, resulted in the formation of disturbed ironstones, and debris flows within the ironstone sequences.

Many features of the ironstones are diagenetic in origin, especially the formation of phosphate nodules within the ironstone sequence. These formed just below the sediment/sea water interface, and some nodules were reworked into overlying beds. The source was phosphorus released from adsorption on clays and iron oxides, and also released from organic material. Later siderite development in the ironstones is indicated by the presence of primary cements in grain-ironstones and secondary alterations in pack-ironstones. The generation of diagenetic siderite was dependant upon the amount of organic material within the ironstones, bacterial reduction of which resulted in the formation of bicarbonate and ferrous ions.

Some ironstones were subsequently altered during the Caradoc phase of volcanic activity. The formation of magnetite and stilpnomelane within the ironstones were caused by metasomatic activity associated with dolerite sills and microgranite intrusions. Siderite alteration and base metal sulphides resulted from late stage hydrothermal activity by some microgranites. Contact metamorphism by granophyric intrusions led to the extensive replacement of the ironstones by pyrite. Regional metamorphism resulted in the progressive change of berthierine to chamosite and increased lattice ordering of chamosite.

1 INTRODUCTION

1.1 INTRODUCTION

The volcanic history of the Welsh Basin, and by implication its tectonic setting, has been the main focus of research on Welsh geology. By contrast little attention has been paid to the oolitic ironstones. These occur throughout North Wales, in the mountainous areas of Snowdonia and Cadair Idris, but can also be found in the low-lying areas of Anglesey and the Llŷn Peninsula. The exposures of these ironstones are predominantly within abandoned mines and adits. These ironstones, mainly exploited from Victorian times up to the end of the First World War, are the only example in Britain of an oolitic ironstone that has undergone metamorphism (Hallimond in Pulfrey 1933a).

1.1.1 Distribution of North Wales Ironstones

Oolitic ironstones are distributed sporadically in the Ordovician North Wales Basin. They can be found in the Anglesey, Llŷn Peninsula, Snowdonia and Cadair Idris regions (Figure 1.1). On the basis of their age the ironstones can be divided into two distinct phases of development, an uppermost Arenig/basal Llanvirn phase, and a Mid-Ordovician phase (Figure 1.1).

The first phase consists of poorly developed ironstone horizons which occur at the top of the Arenig or the base of the Llanvirn (Beckley 1987). This interval has been noted as favourable for the formation of ironstones (Young 1989b). These ironstones occur in the Bangor district (Greenly 1944; Howells *et al.* 1985), the Llŷn Peninsula (Nicholas 1915; Crimes 1970; Cattermole & Romano 1981), the Arenig area (Beckley 1986), near Dolgellau (Cox & Wells 1927; Kokelaar 1979) and in the Arans (Dunkley 1978). The majority of these deposits are dated by graptolite faunas which place them in the *hirundo* Biozone. Those ironstones not dated by graptolites are placed at the top of the Arenig on the basis of local lithostratigraphic correlations (Beckley 1986,1987).

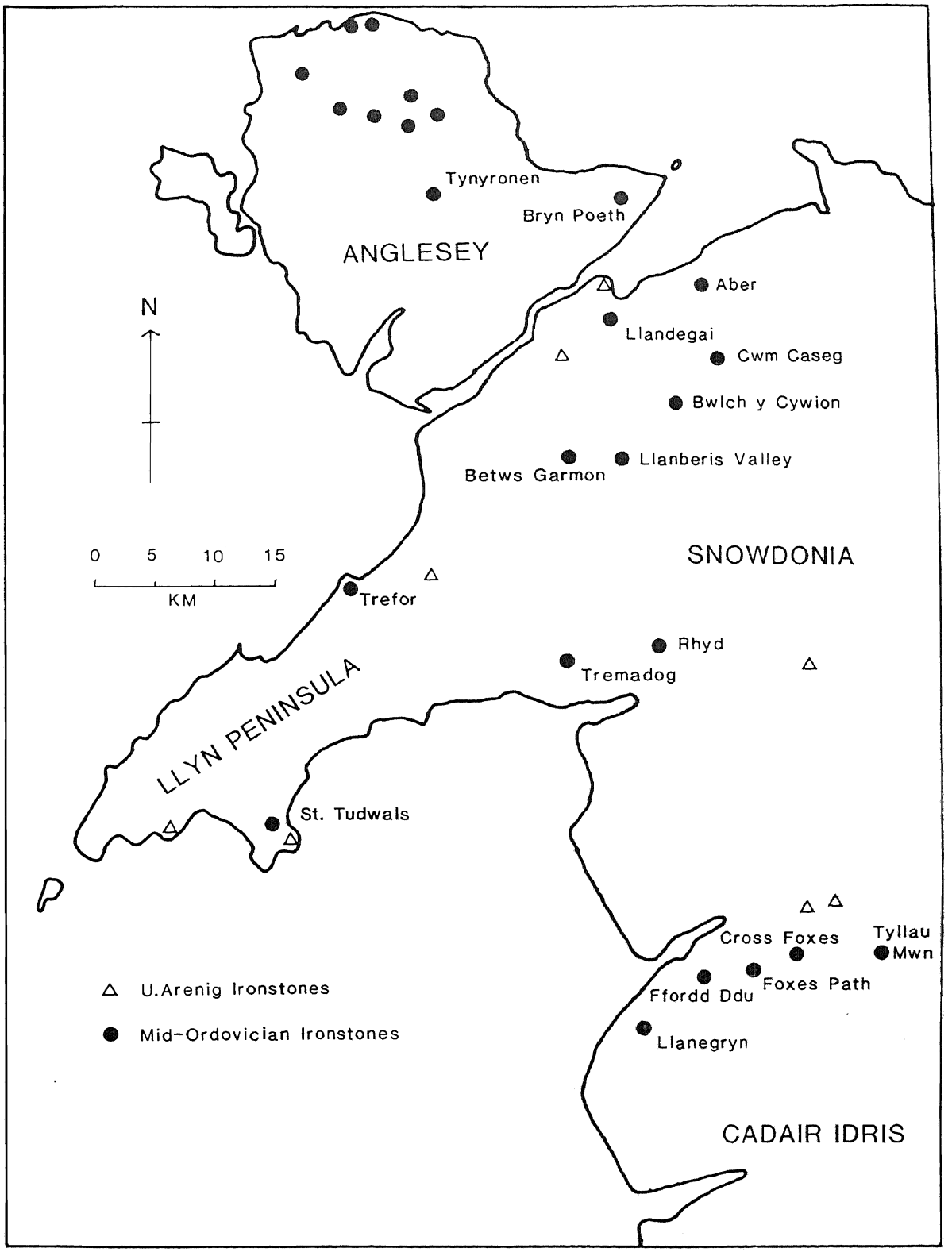

Figure 1.1 Location of the North Wales Ironstones. A distinction is made between Upper Arenig and Mid-Ordovician oolitic ironstones. The main Mid-Ordovician localities have been named.

The Mid-Ordovician Ironstones form the second phase (Trythall et al. 1987; Trythall 1989). These ironstones, which are the subject of this investigation, are found in Anglesey (Greenly 1919; Bates 1972), the Llŷn Peninsula (Nicholas 1915; Crimes 1969; Tremlett 1962), Snowdonia (Greenly 1944; Reedman et al. 1983; Smith 1987; Bromley 1963) and Cadair Idris (Cox 1925; Jones 1933; Dunkley 1978).

1.1.2 History of Research on the North Wales Ironstones

Little attention has been paid to the North Wales Ironstones since Pulfrey (1933a) first described their petrology. Strahan et al. (1920) reviewed the occurrence and field relationships of the ironstones, and Pulfrey's (1933a) research relied heavily on the descriptions of Strahan et al. (1920). There were, however, other research workers who mentioned the occurrence of ironstones in their mapping area (Fearnsides 1910; Nicholas 1915; Greenly 1919; Cox 1925). Fearnsides (1910) suggested that the Tremadog ironstone was a metasomatic deposit formed by the intrusion of a dolerite sill along a thrust plane, with metasomatic fluids flowing along other thrust planes. Subsequent researchers proposed that the North Wales Ironstones were sedimentary in nature (Nicholas 1915; Strahan et al. 1920; Cox 1925). This suggestion was accepted when Pulfrey (1933a) presented his paper. Cox (1925) suggested that the thick sequence of spilitic lavas beneath the Cadair Idris ironstone could be the source of iron. Pulfrey's (1933a) proposition was the formation and deposition of ooids within a ferruginous gel to form the ironstones.

Weinberg (1973) concluded that the ironstones all occurred in the gracilis Biozone at the base of the Caradoc. Material from lateritic weathering of the Lake District Borrowdale Volcanics was eroded during the gracilis transgression and formed the source of material for the ironstones. The ooids were formed as mud-balls during the rapid erosion of deposited argillaceous sediment. When the current waned the ooids were deposited in poorly-sorted, graded bedded sediments. Mineralogical differences within ooid laminae were subsequently formed beneath the sediment/sea water interface. More recent research, in which the ironstones are referred to, has attempted to place the ironstones within a regional stratigraphy, with little or no explanation of their mode of origin (Tremlett 1962; Evans 1968; Crimes 1969; Davies 1969; Cattermole & Jones 1970; Bates 1972; Ridgway 1976; Dunkley 1978; Roberts 1979; Reedman et al. 1983; Howells et al. 1985).

1.1.3 Mining History

The North Wales Lower Palaeozoic rocks contain a varied collection of mineral deposits. The main period of mining was in the 19th Century. The principle metals extracted were gold, copper, zinc, lead, barium, manganese and iron (Foster-Smith 1977 a&b). Of these only gold has been exploited over the last ten years, mainly recovered from quartz veins in carbonaceous shales to the north of Dolgellau (Bottrell *et al.* 1988). Copper, lead and zinc were mined throughout North Wales (Archer 1959). These deposits are all hydrothermal in origin, either volcanogenic (Reedman *et al.* 1985), magmatic (Rice & Sharp 1976; Allen *et al.* 1976) or orogenic (Dunham *et al.* 1978). By comparison, the iron and manganese deposits in North Wales are thought to be wholly of sedimentary origin. Manganese occurs in the Cambrian in the Harlech Dome, and in the Cambrian and Ordovician in the Llŷn Peninsula (Bennett 1987).

The peak of mining of the North Wales Ironstones, outlined by Strahan *et al.* (1920), was in the 19th Century; some were mined up to the end of the First World War. Ironstone workings were known to have existed at Betws Garmon and Tyllau Mwn as early as 1°38. But the majority of mines were opened during the 1850's. The Tremadoc ironstone was discovered when digging in search of coal in black shales associated with the ironstone. Most of the mining ceased during the 1870's, although the Aber and Gorddinog mines were discovered and exploited 1915-1916, and the Betws Garmon and Llandegai ironstones were mined up to the end of the First World War. Most of the ironstone mines were worked at a shallow depth as open pits, but a few were mined underground (Betws Garmon and Cross Foxes). The main economic viability of these ores was handicapped by their phosphorus and sulphur contents, which was reduced by weathering. This explains why most ironstones were only exploited in shallow pits. In the case of those ironstones mined underground, the hardness of the ore obtained was detrimental to its market value. Approximately 300,000 tonnes of iron ore were removed from North Wales (Strahan *et al.* 1920), of which one third came from Betws Garmon. The ore from the ironstones was shipped to the steel works of South Wales.

1.2 GEOLOGICAL EVOLUTION OF THE NORTH WALES BASIN

The North Wales region is composed mostly of Lower Palaeozoic sediments and volcanics, with minor exposures of Precambrian, Devonian and Carboniferous rocks. During the Lower Palaeozoic the Welsh Basin was bound to the northwest by the Irish Sea Landmass, which separated it from the Lake District-Leinster Basin further to the northwest. Further northwest again lay the closing Iapetus Ocean, while to the southeast lay the Midland Platform. Gibbons & Gayer (1985) and Hutton (1987) have interpreted the Caledonides as a series of discreet terranes (Figure 1.2). They interpret the juxtaposition of the Irish Sea Landmass (Mona terrane) as a suspect terrane which docked against the Welsh Basin at the start of the Cambrian.

The Welsh Basin was founded on immature continental crust of Precambrian age, younger than 900 Ma (Kokelaar et al. 1984), which crop out on Anglesey and the Llŷn Peninsula (Figure 1.3). The northwest and southeast margins of the Welsh Basin were defined by reactivated northeast to southwest basement faults which, with north to south trending faults (Figure 1.3), controlled the topology, sedimentation and volcanism throughout the Lower Palaeozoic (Kokelaar et al. 1984). The tensional Welsh Basin was continuously active throughout its Lower Palaeozoic history, with no quiescent periods (Fitches & Woodcock 1987).

1.2.1 Lower Palaeozoic History

An outline of the geology of North Wales is given in Figure 1.3. This also shows the distribution of the major faults which were active during the Lower Palaeozoic. The earliest record of volcanic activity in North Wales is represented by the early Cambrian Arfon Group (Reedman et al. 1984). Large thicknesses of acid volcanic rocks accumulated in major fault controlled grabens which were subsequently infilled by marine sediments during the Cambrian. Uplift and erosion at the end of the Tremadoc, associated with island arc type volcanism (Bevins et al. 1984), was followed by a renewed transgression in the early Arenig (Beckley 1987), where sediments onlapped onto progressively older rocks to the northwest. Sedimentation, dominated by fine-grained shelf siliciclastics, continued up to the Caradoc, which was marked by the onset of major volcanism in North Wales (Kokelaar et al. 1984; Howells et al. 1985). The volcanism,

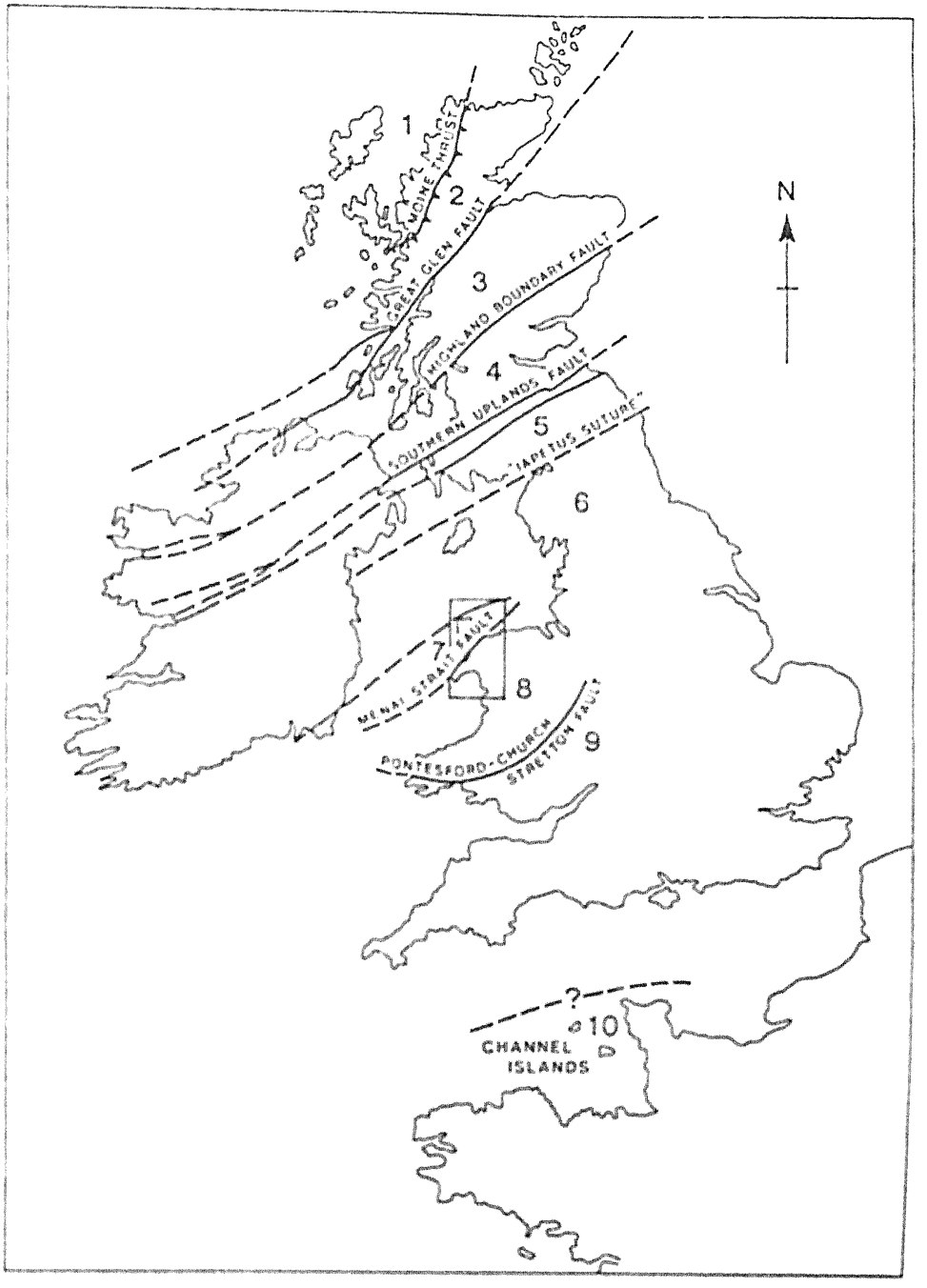

Figure 1.2 British Caledonian Terranes (after Gibbons 1987). 1) Northwest Foreland; 2) Northern Highland (Moine); 3) Grampian (Dalradian); 4) Midland Valley; 5) Southern Uplands; 6) Lakesman; 7) Monian; 8) Welsh Basin; 9) Midland Platform; 10) North Armorican. Except for the Moine Thrust, terrane boundaries are either dominantly steep fault systems (Great Glen, Highland Boundary, Southern Uplands, Menai Strait, Pontesford-Church Stretton) or are unexposed. The study area for the ironstones is outlined.

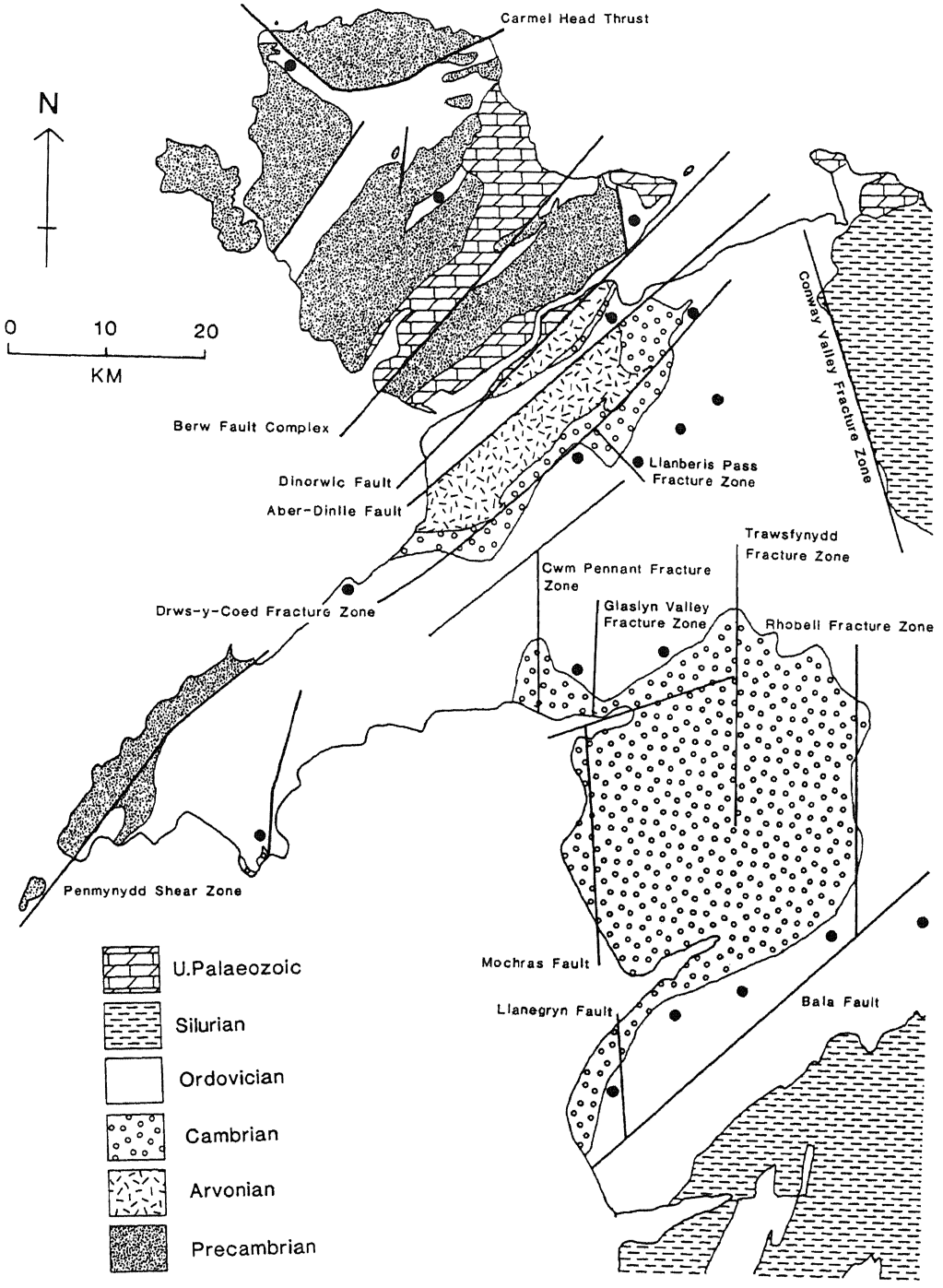

Figure 1.3 Outline of the Geology of North Wales, showing the distribution of major faults or fracture zones active during the Lower Palaeozoic. Location of the main ironstones are shown as dots, names after Figure 1.1.

sedimentation and tectonic activity in the Welsh Basin have been placed within a general model of Ordovician plate tectonics (Campbell et al. 1988; Kokelaar et al. 1984). It is proposed that the Welsh Basin was transitional from a volcanic arc to a marginal basin in a back arc setting (Bevins et al. 1984), underlain by immature continental basement undergoing extension (although no oceanic crust was formed).

1.2.2 Deformation and Metamorphism

During the Caledonian Orogeny (end Silurian to early Devonian) the previously tensional regime for the Welsh Basin became a compressional one, which inverted the basin with a component of renewed reactivation along the basement faults (Fitches & Woodcock 1987). The deformation in North Wales is characterised by northeast to southwest trending upright folding, with an arcuate pattern and a penetrative axial planar cleavage (Coward & Siddans 1979; Campbell et al. 1985; Smith 1987; Wilkinson 1987; Wilkinson & Smith 1988). Discrete zones contrast markedly with this regional pattern and have been interpreted as deformation above basement faults or fractures (Wilkinson & Smith 1988 and Figure 1.3).

Recent publications on metamorphism in North Wales (Roberts 1981; Bevins & Rowbotham 1983; Merriman & Roberts 1985; Roberts & Merriman 1985; Robinson & Bevins 1986) have used metabasite assemblages and illite crystallinity of metapelites to determine metamorphic grade, showing that the highest grades are low-grade greenschist facies (epizone) in Central Snowdonia and the Harlech Dome, with grades decreasing away from this area (Figure 1.4). The metamorphic grades reflect burial metamorphism, at a P/T gradient of 25^{o}C/km (Robinson & Bevins 1986). The highest grades reflect the area of thickest accumulation of sediment, although it may also have been affected by the intrusion of a number of plutons. However, it has been proposed that metamorphism was pre-deformation due to a high heat flux because of crustal thinning due to extension (Bevins & Robinson 1988).

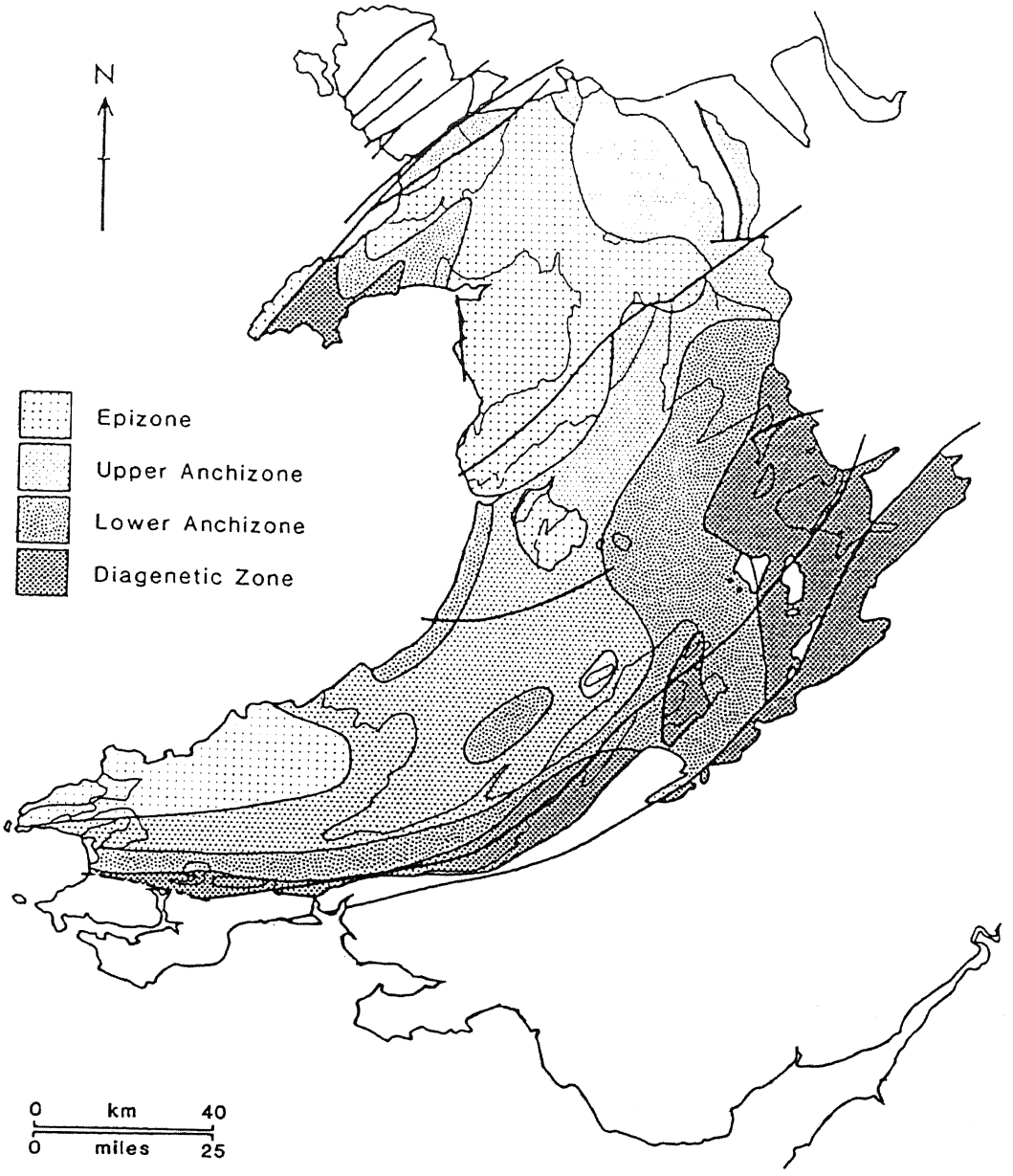

Figure 1.4 Metamorphic map of the Lower Palaeozoic rocks of Wales and the Welsh Borderlands, based on illite crystallinity studies (after Robinson & Bevins 1986). Major faults are thick and geological boundaries thin black lines (after Robinson & Bevins 1986, Figure 1).

1.3 AIMS OF THE INVESTIGATION

The sedimentary sequences in which the ironstones are contained are fine-grained siliciclastic sediments. Stratigraphic and sedimentological research of these sequences in the past has been hampered by poor biostratigraphy and low-grade metamorphic overprinting of the diagnostic sedimentary structures, textures and mineralogy. In turn this has hampered any research into the ironstones, which occur as discrete bodies within the fine argillites. Despite this deformation and metamorphism, sufficient sedimentary textures are preserved for a sedimentological study of the North Wales Ironstones.

1.3.1 Objectives of the Investigation

The aim of this work is to study the sedimentation, diagenesis and subsequent alteration of the North Wales Ironstones, and then to place the ironstones within the context of current knowledge of the Welsh Basin and Phanerozoic ironstones. The specific objectives are:

1) To establish the distribution of the ironstones and detail their field relationships.

2) To determine the ages of the ironstones and place them within a regional stratigraphy.

3) To determine the environments of deposition of the ironstones.

4) To document the diagenetic history of the ironstones.

5) To document further alterations of the ironstones.

6) To compare and contrast the history of the ironstones obtained to current knowledge of the Welsh Basin (Fitches & Woodcock 1987; Kokelaar et al. 1984) and to other oolitic ironstones (Young & Taylor 1989).

1.3.2 Outline of the Thesis

The thesis is presented through a geological history of the development of the ironstones, from the origins and sedimentation, through the diagenesis to metasomatic and hydrothermal alterations. The distribution and stratigraphy of the ironstones (Chapter 2) are followed by the sedimentation of the ironstones (Chapter 3), including a description of their geochemistry. Diagenesis of the ironstones

(Chapter 4) is mainly a petrological study supplemented by X-ray diffraction (XRD), electron probe micro-analysis (EPMA) and X-ray fluorecence (XRF) analysis. The same techniques are also used to determine the metasomatic and hydrothermal alterations of the ironstones (Chapter 5). This work is concluded (Chapter 6) by a comparison of the North Wales Ironstones to the more problematic areas of Phanerozoic Ironstone formation and Welsh Basin history.

1.3.3 Methodology

A number of analytical techniques have been used to supplement the field and petrographic descriptions of the ironstones. Samples collected in the field for further study (XRD, EPMA, XRF and inductively coupled plasma emission spectroscopy (ICP)) are detailed in Appendix 1, which gives sample numbers, their location and analytical techniques used.

A total of 32 samples was analysed by XRD at Oxford University to identify and study the structure of the iron-bearing sheet silicate in the ironstones. Bulk rock XRD was used to identify the mineralogy of the ironstones studied in thin section. The analytical conditions and results are given in appendix 3. Electron probe micro-analysis was undertaken at Cambridge University on 16 polished thin sections to study chamosite, apatite, siderite and stilpnomelane compositions (Appendix 4). From the EPMA spot size only siderite, stilpnomelane and large chamosite crystals could be analysed with confidence. Therefore, Appendix 4 gives analytical conditions, methodology for ensuring pure analyses and EPMA results.

A total of 37 samples were analysed by XRF at Nottingham University for the major and 18 trace elements. These samples consisted of 4 grain-ironstones, 25 pack-ironstones, 6 wacke-ironstones, 1 chamositic mud-ironstone and 1 feebly oolitic sideritic ironstone. The XRF data presents the major elements as weight percent oxides, and the trace elements as parts per million (ppm) element. Total iron, $Fe_2O_3(T)$, was calculated as Fe_2O_3. The Fe^{II}/Fe^{III} ratio was subsequently determined by wet chemical methods (Appendix 5). The results of the XRF data are given in Appendix 5. The XRF data was studied using a multivariate statistical analysis package (Heley 1980) and a MINITAB data handling package on a VAX mainframe computer. Multivariate statistical analysis of the data showed up the natural groupings and associations of the data set. These groupings were then studied using MINITAB, which can

plot any element against another, calculate the Pearson Correlation Coefficient (r) and the equation for the regression line. ICP analysis for the rare earth elements (REE) was also undertaken on 18 of the XRF samples, the results of which are given in Appendix 5. The samples were analysed by ICP at Oxford Polytechnic, the method of preparation after Jarvis & Jarvis (1986).

1.4 CLASSIFICATION OF IRONSTONES AND NOMENCLATURE

Until recently there was confusion over the definition of ironstones, over the distinction of oolitic ironstones from Banded Iron Formations (BIF), and over the nomenclature used in describing ironstones. For example, there is confusion in the use of such terms as 'Clinton type ironstones' and 'Minette type ironstones', and in the use of the terms chamosite and chamositic. These uncertainties have been largely resolved by a workshop during the 'Phanerozoic Ironstones' Symposium (Sheffield University, April 1987). The recommendations, which are adopted in this thesis, will be published elsewhere (Young 1989a).

1.4.1 Definition of an Ironstone

An ironstone is defined as a ferruginous sedimentary rock of any age containing 15% or more Fe of primary origin (depositional or diagenetic) (James 1966, Kimberley 1978, Van Houten & Bhattacharrya 1982). Oolitic ironstones are distinguished from 'Banded Iron Formations' in that they are dominantly Phanerozoic, predominantly contain coated grains, are commonly aluminous, contain no chert, and are not banded. The dominant iron-minerals are berthieroid, goethite, siderite and haematite (Maynard 1983, James 1966).

Phanerozoic Ironstones (SCOS-IF, sandy, clayey and oolitic, shallow inland-sea iron formation - Kimberley 1978) have previously been referred to as 'Minette' and 'Clinton' type ironstones (Gross 1970). These terms are not used as they are not adequate as standard facies types to be used as a reference type. While a facies term to distinguish different Phanerozoic Ironstone types is needed, more work is required before such a scheme can be suggested (Young 1989a). The term 'ironstone formation' (Van Houten & Bhattacharrya 1982, Howard 1985) refers to a mappable rock unit composed mostly of ironstone (*sensu stricto*). It should not be confused with the Precambrian 'Banded Iron Formations'.

1.4.2 Nomenclature of ironstones

In describing the North Wales Ironstones, Weinberg (1973) used the classification scheme of Taylor (1949). A similar scheme was used earlier by Pulfrey (1933a). Taylor's (1949) scheme proposed that the

primary classification of the rock (either ironstone, sandstone or mudstone) should be determined by the nature of the matrix, with secondary subdivisions based on the nature of the ooids. Adjectival prefixes are used for the minerals of the groundmass and substantive prefixes for for those of the ooids. Therefore a rock with limonite ooids in a siderite matrix is a sideritic limonite oolite (Taylor 1949). The main disadvantage of this scheme are that it includes no textural information. The mineralogy of ironstones is diagenetically very variable, hence the lack of consistency in adopting a purely mineralogical description (Dimroth 1975). It is probably more useful in ironstones to stress the textural information in the nomenclature, leaving the user to add as much or as little mineralogical information as the context requires.

The nomenclature proposed for Phanerozoic Ironstones (Young 1989a), is an adaptation of the limestone classification scheme of Dunham (1962). One suggested qualification is the use of '..stone' in the Dunham scheme should be replaced by '..-ironstone' (eg mud-ironstone, pack-ironstone). This is because of the occurrence of both ironstones and limestones in a single sedimentary sequence. The nomenclature for the allochems within the ironstones follows those of limestones, with an '..idal' termination of allochem names (eg ooidal grain-ironstone, oncoidal wacke-ironstone). To include mineralogy, it should be given as a noun for the allochem and as an adjective (if the adjectival form is available) for the groundmass. Thus a matrix-supported ironstone with 15% goethite ooids in a chamosite-rich matrix would be termed a goethite ooidal chamositic wacke-ironstone.

This classification is suitable for the majority of oolitic ironstones, but it would not give a complete textural description of the North Wales Ironstones for two reasons. The North Wales Ironstones contain ferruginous oncoids and stromatolites, and also reworked sedimentary clasts. These two aspects are not covered unless the modifications to the Dunham scheme by Embry & Klovan (1971) are included in the ironstone classification scheme. Therefore the terms float-ironstone, rud-ironstone and bind-ironstone should be incorporated. Secondary subdivisions of the matrix follow the Dunham scheme. Therefore an ooidal pack-ironstone containing cobble-sized phosphatic clasts which do not support each other, would be a phosphatic float-ironstone in an ooidal pack-ironstone.

This nomenclature to describe the North Wales Ironstones replaces the one previously used by Trythall et al. (1987). Table 1.1 equates

the nomenclature used here with that of Trythall et al. (1987).

Trythall et al. (1987)	This Work
chamositic mudstone	chamositic mud-ironstone
oolitic pisolitic mudstone	ooidal wacke-ironstone
massive oolitic ironstone	ooidal pack-ironstone
massive oolitic ironstone with a sparry cement	ooidal sideritic grain-ironstone

Table 1.1 Nomenclature of the North Wales Ironstone facies: a comparison of this work with Trythall et al. (1987).

Throughout this work, the chlorite terminology is after AIPEA (1980). Therefore chamosite is a 2:1 iron-rich trioctahedral 1.4nm chlorite with Fe^{II} as the dominant divalent octahedral cation, while berthierine is an Fe-rich 1:1 layer silicate of the serpentine group (0.7nm repeat) having appreciable tetrahedral aluminium. However, a field and petrographic term for an iron-rich clay is needed (previously 'chamositic') and it is recommended that the term berthieroid should be used (Young 1989a).

1.4.3 Terminology of the coated grains

The North Wales Ironstones have previously been described as oolitic and pisolitic (Pulfrey 1933a, Weinberg 1973), although neither author recognised the relative abundance of oncoids within the ironstones. The nomenclature of allochems follows the recommendations of Young (1989a) although with some minor differences, detailed below. These are due to the peculiarities of the North Wales Ironstones. As ferruginous ooids are morphologically similar to recent calcareous ooids (Kimberley 1983), the nomenclature for ferruginous allochems follows that of calcareous allochems. Richter (1983a) in describing coated grains uses the descriptive terms ooids and oncoids, which are

adopted here. Richter (1983b) describes ooids as:

1) formed by a cortex and nucleus variable in composition and size,
2) as having a smoothly laminated cortex,
3) increasing in sphericity with growth,
4) lacking constructive biogenic structures.

Oncoids are distinct from ooids in that their laminae are irregular (often wavy) and usually discontinuous. However the term oncoid also has a genetic implication of an algal/organic origin (Dahanayake 1977). The terms pisoid (an ooid larger than 2mm - Richter 1983b; Young 1989a) or the term microoncoid (an oncoid less than 2mm in size - Young 1989a; Dahanayake & Krumbein 1986) are not used in this work. This is because ooids and oncoids have a continuum in size and therefore it would be misleading to place an artificial size barrier on allochem classification. However, the size of allochems (and clasts and nodules) is important in classifying the texture of the ironstones.

2 DISTRIBUTION AND STRATIGRAPHY OF THE IRONSTONES

2.1 INTRODUCTION

The North Wales Ironstones may be grouped into four geographical areas: Anglesey, Llŷn, Snowdonia and Cadair Idris (including the Arans). In this chapter the occurrence of ironstones within each area is described. Although the ironstones are distributed over a wide geographical area, their occurrence is sporadic being separated by large areas of non-occurrence. A field guide to the main ironstone localities is to be published elsewhere (Trythall 1989). It is the intention of this chapter to document all Mid-Ordovician ironstone localities and describe the features exposed.

2.1.1 General Characteristics

Throughout North Wales, the ironstones can easily be distinguished from the adjacent fine-grained clastic sediments by their poorly cleaved or uncleaved nature and by their darker colour, which weathers to a strong orange/brown colour. The typical sequence is of basal chamositic mud-ironstones interbedded with mudstones, siltstones and shales. This is followed upwards by a transitional facies (ooidal wacke-ironstones, or alternating lenses of pack-ironstone, wacke-ironstone or float-ironstone in mud-ironstone) with an upward increasing ooid and oncoid content and decreasing mud content. The top of the ironstone is marked by an ooidal pack-ironstone, ooidal wacke-ironstone with pack-ironstone patches or float-ironstone (more rarely an ooidal grain-ironstone), which reverts abruptly to overlying clastic mudstones.

Within the ironstone sequence early diagenetic phosphate nodules, up to 10cm in length, are a conspicuous feature. Nodules do not occur in the ooidal grain-ironstones. In the ooidal pack-ironstones they are amoeboid in shape with diffuse margins (Figure 2.1.a). In the underlying muddier facies they are rounded, with sharp, well defined, margins; some localities show a pronounced bedding alignment. When fresh, the nodules are dark grey and show little of the internal

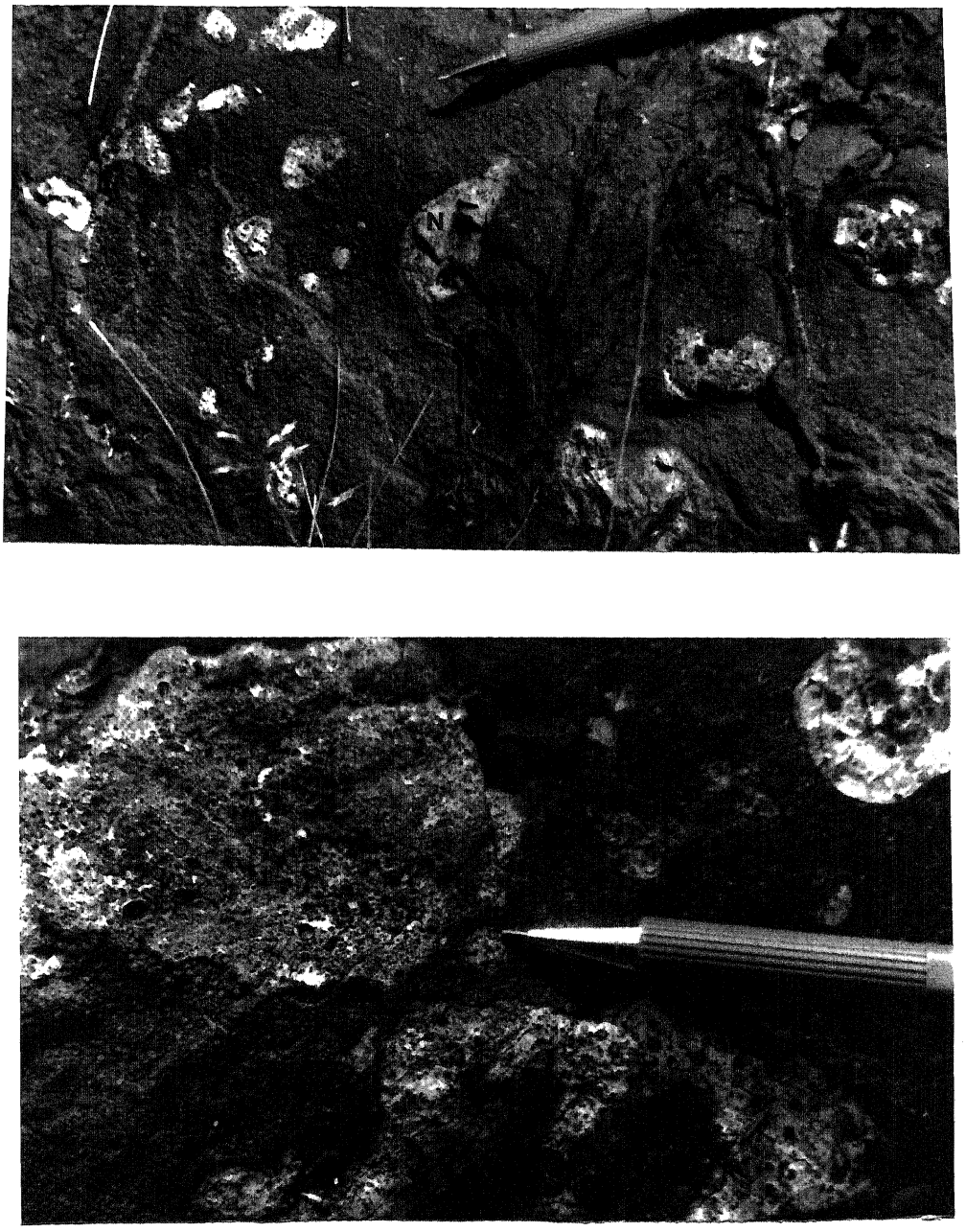

Figure 2.1 Phosphate nodules within ooidal pack-ironstones (Pen y Gaer SH 2992 2821). a) Nodules (N) are distinctive by their white colour when weathered. b) A loose packing of ooids can be seen within the nodules.

texture, but on weathered surfaces they are white, displaying randomly scattered ooids and oncoids (Figure 2.1.b), brachiopod fragments and sponge spicules (Pulfrey 1933b).

2.1.2 Biostratigraphy

The North Wales ironstones do not commonly contain stratigraphically useful fossils. In the past various ironstones have been assigned to different stratigraphic levels in the Ordovician (and Cambrian), although some ironstones have already been reliably dated as they contain good graptolite faunas. To clarify the stratigraphic position of all the North Wales Ironstones, selected ironstone samples, or mudstones immediately adjacent to ironstones, were collected for age determination using acritarchs, in collaboration with Dr. Stuart Molyneux (BGS Keyworth). This lead to the publication of new ages for the ironstones (Trythall et al. 1987). Work on Ordovician acritarch dating in Britain is still at a preliminary stage, but it is now possible to assign ages to most of the ironstones, based on the known ranges of acritarchs in Britain, their occurrence elsewhere, and the composition of the associated published graptolite faunas (Figure A).

Trythall et al. (1987) found three differing acritarch assemblages for the North Wales Ironstones. The first is an U.Llanvirn assemblage (Bryn Poeth), the next is a Lower or Middle Llandeilo assemblage (St. Tudwals, Betws Garmon, Llandegai, Trefor) and the third is a basal Caradoc assemblage (Tremadog). The stratigraphic age of each ironstone locality will be included with the description of its lithology.

2.2 ANGLESEY

The ironstones on Anglesey have previously been described by Greenly (1919), Strahan et al. (1920) and Bates (1972). Since these works were published, most of the smaller localities are no longer, and so they have been located from Greenly's original field slips (at the British Geological Survey, Aberystwyth). Their description is taken from the above three authors. Greenly (1919) described three types of ironstone on Anglesey, feebly oolitic grey siderite rocks, feebly oolitic ferrified grits and oolitic ironstones. The distribution of the localities and the different ironstone types are shown in Figure 2.2. In only four pits are ironstones now exposed: Porth Padrig, Fferam Uchaf, Tynyronen and Bryn Poeth.

2.2.1 Porth Padrig [SH 3756 9434]

This ironstone, plus the Penterfyn [SH 382 946] and Porth Pridd [SH 407 945] ironstones, occur in Caradoc outliers on the Gwna Melange (Bates 1972). These ironstones are dated, by graptolite faunas recovered from shales adjacent to the ironstone, as occurring in the gracilis Biozone (Greenly 1919). These ironstones are the feebly oolitic siderite ironstones of Greenly (1919). At Porth Padrig the ironstone is exposed in the cliff (Figure 2.3) as a pale brown, strongly weathered, featureless ironstone. However on the foreshore are exposures of fresh grey and feebly oolitic ironstone.

2.2.2 Fferam Uchaf [SH 3626 8675]

All the ironstones in this central zone (Figure 2.2), apart from Mynydd y Garn (an oolitic ironstone), are feebly oolitic ferruginous grits occurring within the basal beds of the gracilis transgression across central Anglesey (Bates 1972). This ironstone is dated by shales of the gracilis Biozone exposed in Fferam Uchaf Farm (Bates 1972). The Fferam Uchaf ironstone outcrops in a small pit just to the northwest of Fferam Uchaf Farm (Bates & Davies 1981), which exposes 1.5m of dark flaggy chamositic mud-ironstones with thin interbedded grits and conglomerates with sparse ooids. The ironstone rests on murchisoni Biozone shales exposed to the south of the farm (Bates & Davies 1981).

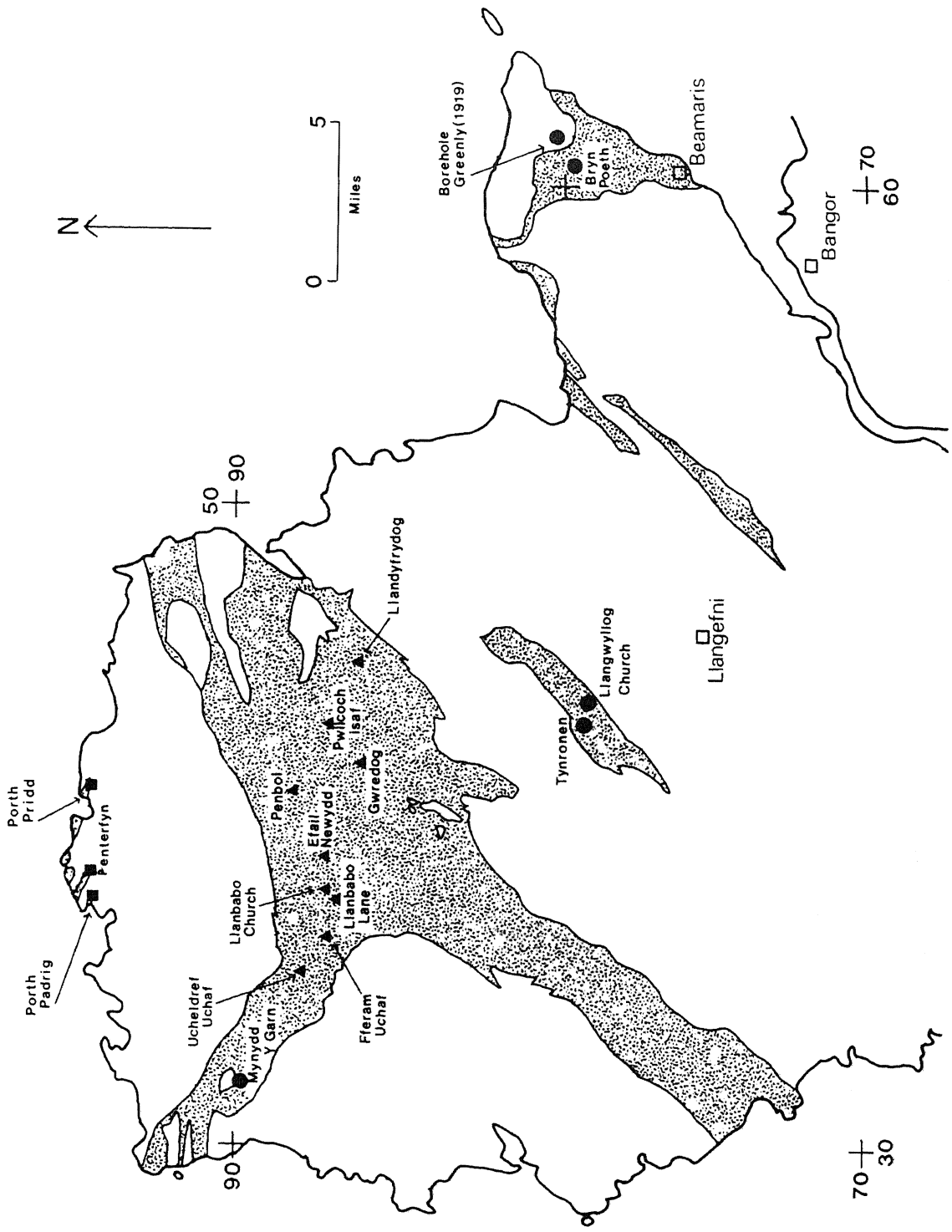

Figure 2.2 Location of the ironstones on Anglesey, showing the distribution of the three different ironstone types, squares - feebly oolitic sideritic ironstones, triangles - feebly oolitic ferrified grits, circles - oolitic ironstones. Shaded area is the Ordovician outcrop.

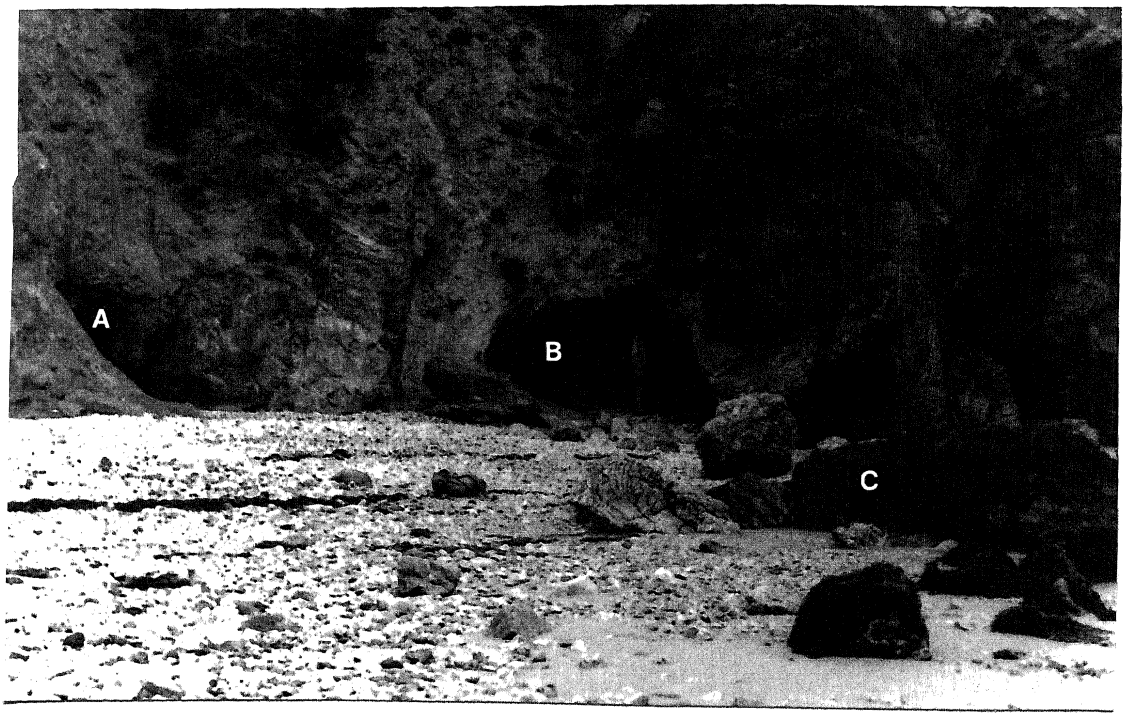

Figure 2.3 The Porth Padrig ironstone [SH 3756 9434]. The adit on the left (A) is into gracilis Biozone shales. Intensively weathered ironstone is exposed in the main adit to the right (B) while fresh ironstone is exposed on the foreshore (C).

2.2.3 Tynyronen [SH 4327 7932]

This ironstone is also of gracilis Biozone age (Greenly 1919) and is a small exposure 300m to the northeast of Tynyronen Farm. Most of the pit is of cleaved chamositic mud-ironstone with abundant phosphate nodules. In the southwest corner of the pit is a small exposure of strongly weathered oolitic ironstone. Near Llangwyllog church [SH 439789], 800m to the southeast of Tynyronen Farm, Bates (1972) described a small quarry with nodular oolitic ironstone, now no longer exposed.

2.2.4 Bryn Poeth [SH 6016 7958]

The Ordovician sequence exposed in southeast Anglesey, described by Greenly (1919) and Bates (1972), consists of Arenig grits resting unconformably on Precambrian schists, succeeded by U.Arenig shales (Beckley 1987). Greenly (1919) noted the absence of the bifidus Biozone in this area, as the next exposure in the stratigraphic sequence is the Bryn Poeth ironstone with an U.Llanvirn graptolite fauna (Greenly 1919, p432).

The Bryn Poeth ironstone is uncleaved and undeformed and therefore preserves the best sedimentary structures of all the ironstone localities in North Wales. The vertical sequence exposed is shown in Figure 2.4. Bedding at this locality strikes 200° and dips 16°W. In the lower part of the unit (Figure 2.4; section B) the base of the unit consists of clastic shales and feldspathic sandstones, with thin beds of chamositic mud-ironstone, all with sparse ooids. This grades up into a unit with laminated silty chamositic mud-ironstone at the base into lenses of ooidal pack-ironstone or oncoidal float-ironstone in chamositic mud-ironstone. Cutting into this is a small channel infilled with a fining-up sequence (Figure 2.5). This is followed by two units, each approximately 0.5m thick, of basal laminated muddy siltstone to chamositic mud-ironstone, which grades up into ooidal pack-ironstone by increasing the thickness and frequency of the ooidal pack-ironstone lenses and decreasing the chamosite mud content. Each cycle is capped by a thin ooidal grain-ironstone, now strongly weathered, which has a number of erosional surfaces within it.

The lenses of pack-ironstone in mud-ironstone plus the beds of pack-ironstone also contain detrital quartz and feldspar grains, not seen in the mud-ironstone. Graptolites and inarticulate brachiopods

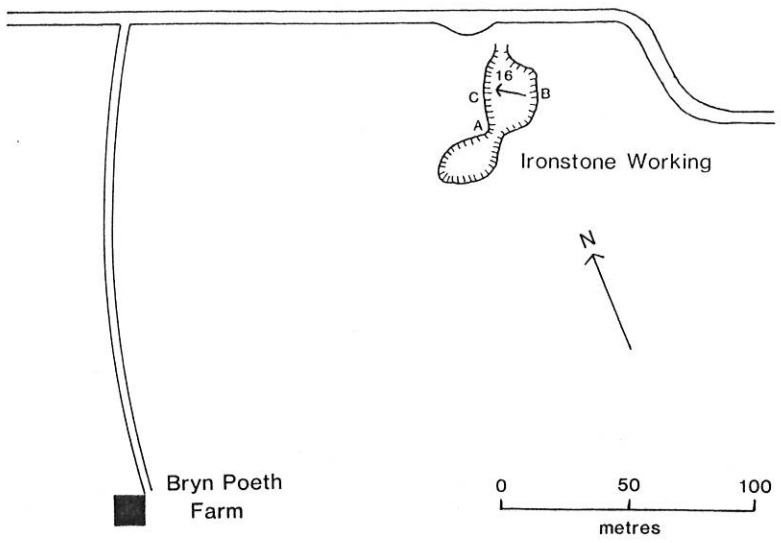

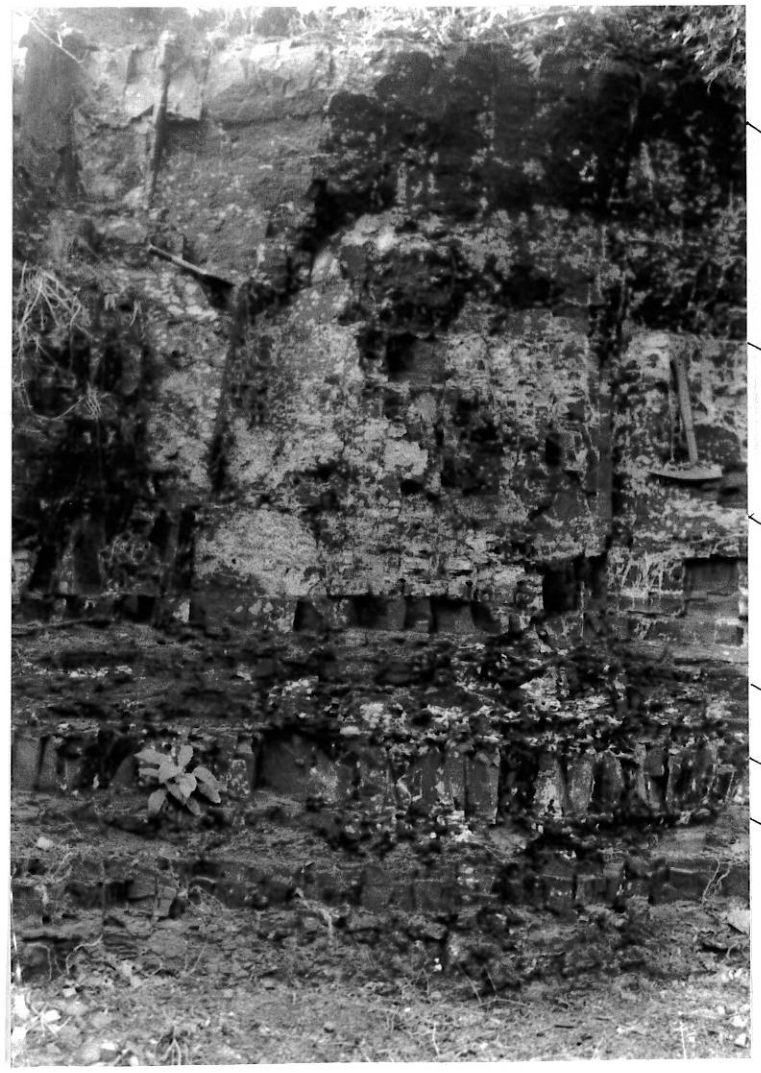

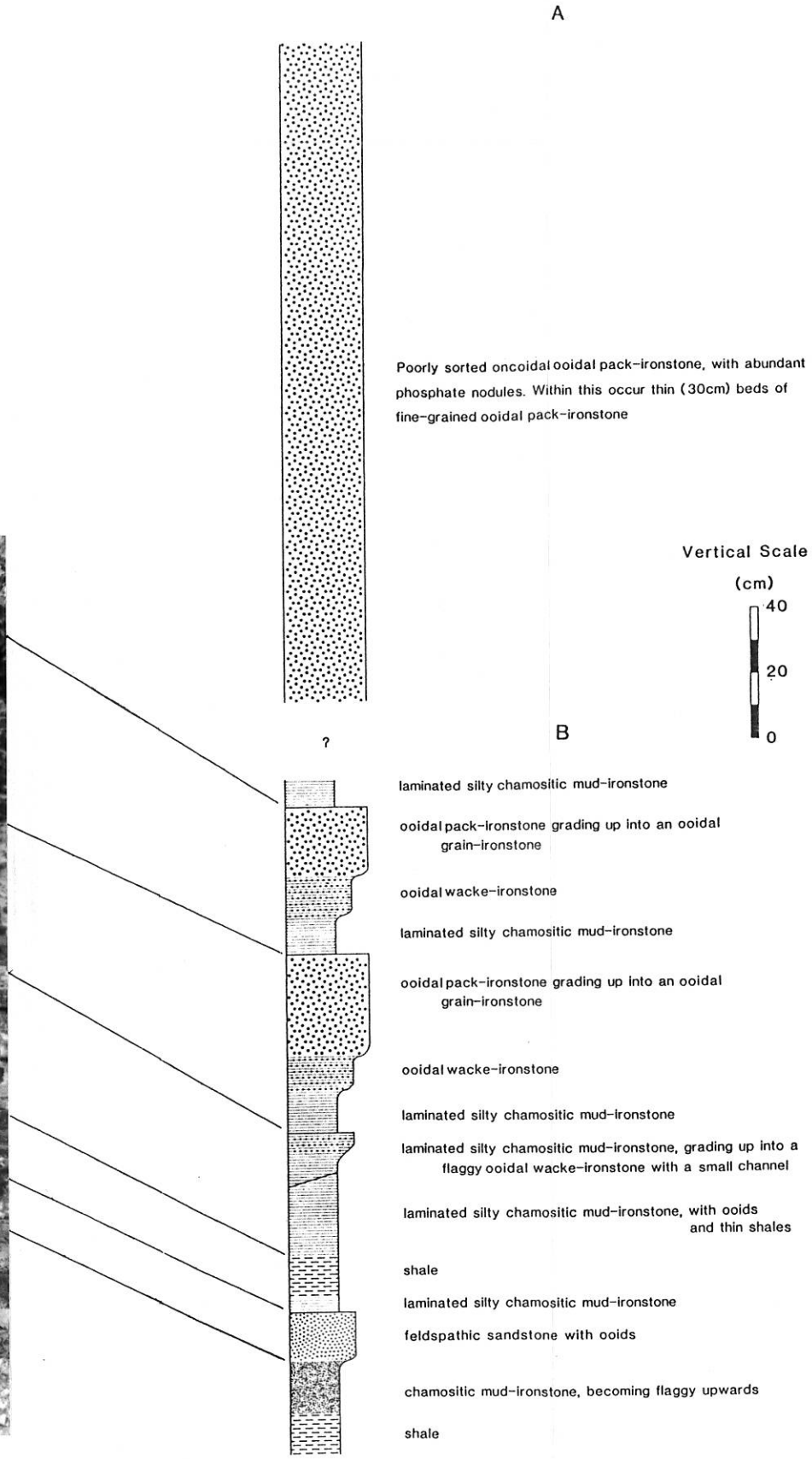

Figure 2.4 Lithological log of the Bryn Poeth ironstone [SH 6016 7958]. A the exposure of the upper part of the sequence on the southwest side of the pit, and B is the exposure of the lower part of the ironstone sequence on the east side of the pit. C is exposures of nodular shales immediately above the ironstone.

Figure 2.5 Scour and fill structure in the top of a lense of pack-ironstone in chamositic mud-ironstone (Figure 2.4), Bryn Poeth [SH 6016 7958]. The base of the scour is marked by reworked phosphate nodules and oncoids, with mud and ooids infilling the remainder of the scour.

are found in this sequence and burrow mottling indicates some bioturbation of these sediments, although it is not sufficient to disturb the laminated sediments or the lenses of ooidal pack-ironstone.

The top oncoidal float-ironstone in ooidal pack-ironstone (Figure 2.4; section A) is lithologically heterogenous, poorly sorted and contains early diagenetic siderite. Within it are thin (30cm) beds of fine-grained ooidal pack-ironstone, with a high detrital quartz and feldspar content. This ironstone sequence is succeeded by shales with diagenetic phosphate nodules (Figure 2.4;C).

2.3 LLYN

Two ironstones are exposed in the Llŷn Peninsula, at Trefor (Tremlett 1962) and in the St. Tudwals (Crimes 1969; Nicholas 1915).

2.3.1 Trefor [SH 3715 4747 to SH 3677 4739]

Little is published on the geology of the Trefor region, apart from studies by Tremlett (1962) and Roberts (1979). The ironstone is exposed on the Trwn y Tâl Peninsula. The sediments adjacent to the ironstones on the peninsula are fine-grained laminated sandstones, siltstones and silty mudstones of possible Arenig age (Roberts 1979), although Trythall *et al.* (1987) assign a Llandeilo age to the ironstone based on acritarchs collected from mudstones and siltstones immediately adjacent to the ironstone.

The eastern ironstone locality consists of two pits (Figure 2.6.a), but only the upper pit exposes ironstone (Figure 2.6.b). Bedding is near vertical striking ESE to WNW, and the beds young to the north. The southern wall of the pit is made up of cleaved chamositic mud-ironstone with abundant phosphate nodules. Slickenside planes and chloritic pressure solution seams cut through the mud-ironstone, and the phosphate nodules are broken up by quartz veins and by chloritic pressure solution seams. The back (west) wall of the pit exposes ooidal wacke-ironstone interbedded with laminated siltstones. The North Wall is composed of oncoidal float-ironstone in ooidal pack-ironstone, and is cut up by numerous (now weathered) pyrite veins. Just above the north wall pale laminated muddy sandstones showing small-scale cross bedding are exposed.

In the central part of the Trwn y Tâl peninsula at the edge of the cliff [SH 3687 4741] is another ironstone working. This exposure consists of fault bounded blocks of oncoidal float-ironstone in ooidal pack-ironstone, where the faults are now filled with pyrite, with pyrite also disseminated within the ironstone. Numerous slickenside planes and boudinaged quartz veins can be seen.

The most westerly exposure of the ironstone [SH 3675 4739] consists of three parallel trenches, where the bedding strikes 234° with vertical dip. The northernmost trench (the main exposure), where bedding youngs to the south, exposes 2m of oncoidal float-ironstone in ooidal pack-ironstone, with cleaved pale grey mudstones above the ironstone exposed along the south wall (Figure 2.7). The

a)

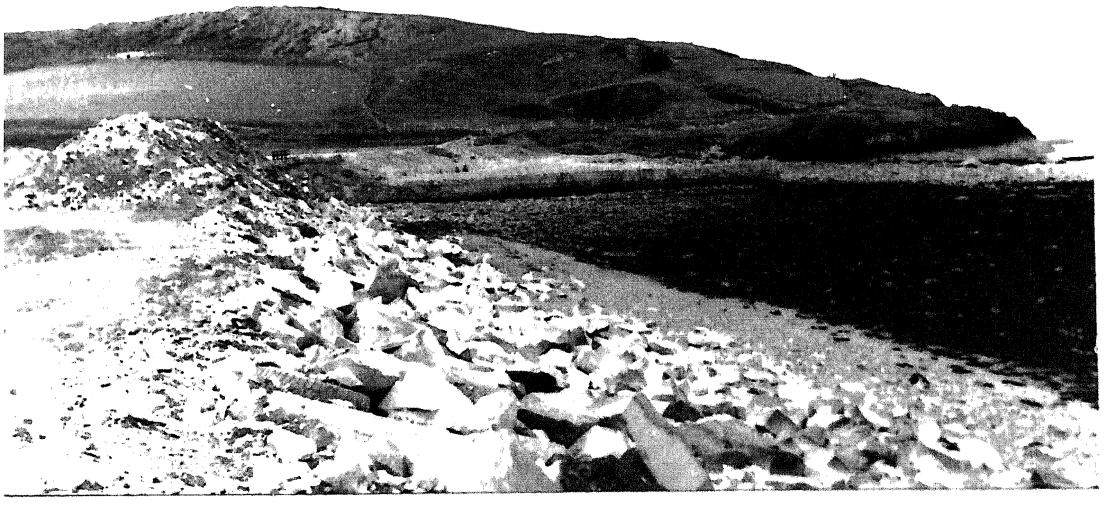

b)

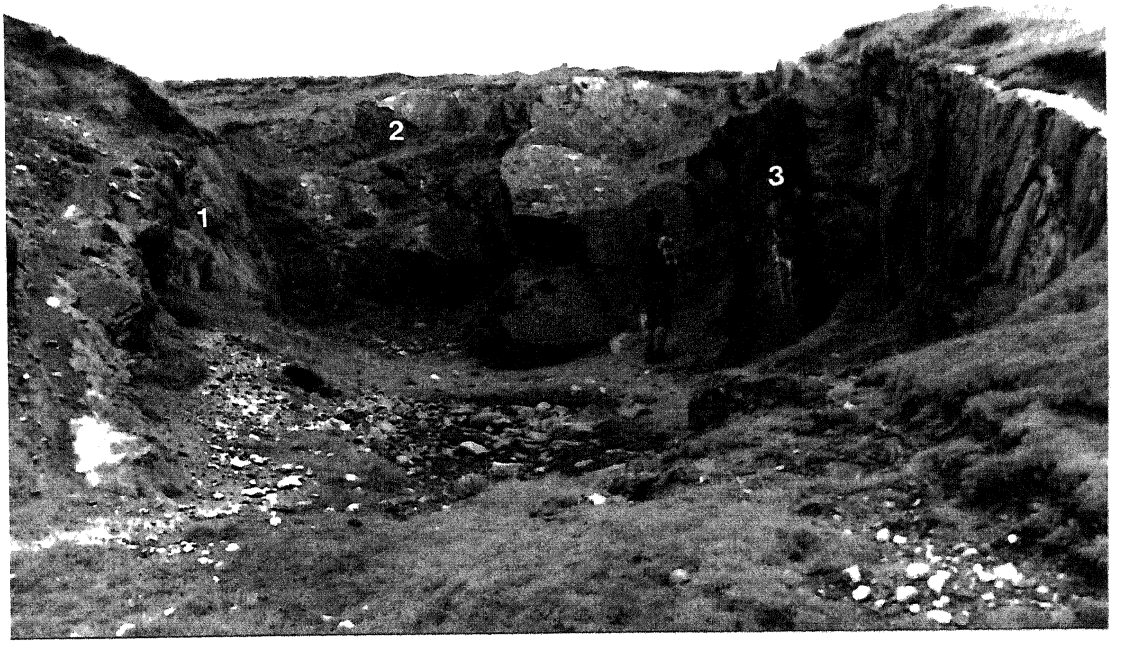

Figure 2.6 The Trefor ironstone. a) The easterly ironstone exposure on the Trwn y Tâl peninsula looking westward. Only the upper of the two pits [SH 3715 4747] exposes the ironstone. The westerly exposure of ironstone is on the left side of the photograph just over the rise of the hill. b) Details of the easterly exposure looking west, the younging sequence to the right (north), 1 nodular chamositic mud-ironstone, 2 ooidal wacke-ironstone interbedded with siltstone, 3 ooidal pack-ironstone strongly pyrite rich.

Figure 2.7 Trefor west pit [SH 3675 4739], facing westwards. Younging direction is to the left (south). 1 cleaved pale grey mudstones, 2 oncoidal ooidal pack-ironstone. The right wall also exposes a thin oncolite bed (Figure 2.8) which is only intermittently exposed because of offset by faults.

float-ironstone is poorly sorted, containing stromatolite crusts and abundant variously shaped oncoids (Figure 2.8.a), which are composed of chamosite and phosphate lamellae around a chamositic core, and are up to 4cm in size. A thin (10cm) oncolite bed is exposed at this locality (Figure 2.8.b), with some oncoids showing partial replacement of the chamosite by haematite.

2.3.2 St. Tudwals [SH2984 2829 to SH3002 2714]

In the St. Tudwals peninsula, Cambrian sediments are unconformably overlain by the Tudwals Sandstones, succeeded by the Llanengan Mudstones (Figure 2.9 and Nicholas 1915), both of hirundo Biozone age (Beckley 1987). These are unconformably overlain in turn, although with little apparent discontinuity, by the Hen dy Capel Ironstone and Pen y Gaer Mudstones (Crimes 1969). Originally this unconformity was interpreted as a thrust (Nicholas 1915), similar to that found at Tremadog (Fearnsides 1910). Similar tectonic disruption can be seen within the ironstones in both areas. Trythall et al. (1987) assigned an age to this ironstone of early Middle Llandeilo at the base of the gracilis Biozone. The St. Tudwals region is bounded just to the north by a thrust zone (Crimes 1969; Roberts & Merriman 1985), where Tremadoc and Arenig sediments of different character to those found in the St. Tudwals region occur to the north of this thrust.

The Pen y Gaer ironstone has been used as the key section for this area as it shows the least effects of tectonic disturbance. The ironstone sequence is exposed in two pits. A minimum thickness of 16m is estimated for this ironstone. The lower sequence is exposed on the side of the hill [SH 2984 2829]; the upper sequence of the ironstone is seen on the top of Pen y Gaer [SH 2992 2821] (Figure 2.9). Bedding in the lower sequence dips 40° to the northwest, although in an adjacent ironstone pit also exposing the lower part of the ironstone sequence the bedding is vertical and youngs toward the southeast. However by studying way-up structures, the ironstone sequence can be demonstrated to be overturned. The cleavage is steeper than bedding (Figure 2.9) dipping to the southeast, which is axial planar associated with the NNE to SSW open folding in the area (Crimes 1969). Therefore there must have been a phase of folding without cleavage first, either slump folding or other deformation, possibly related to thrusting to the north of St. Tudwals. This was then followed by Caledonian open folding with an axial planar cleavage.

a)

b)

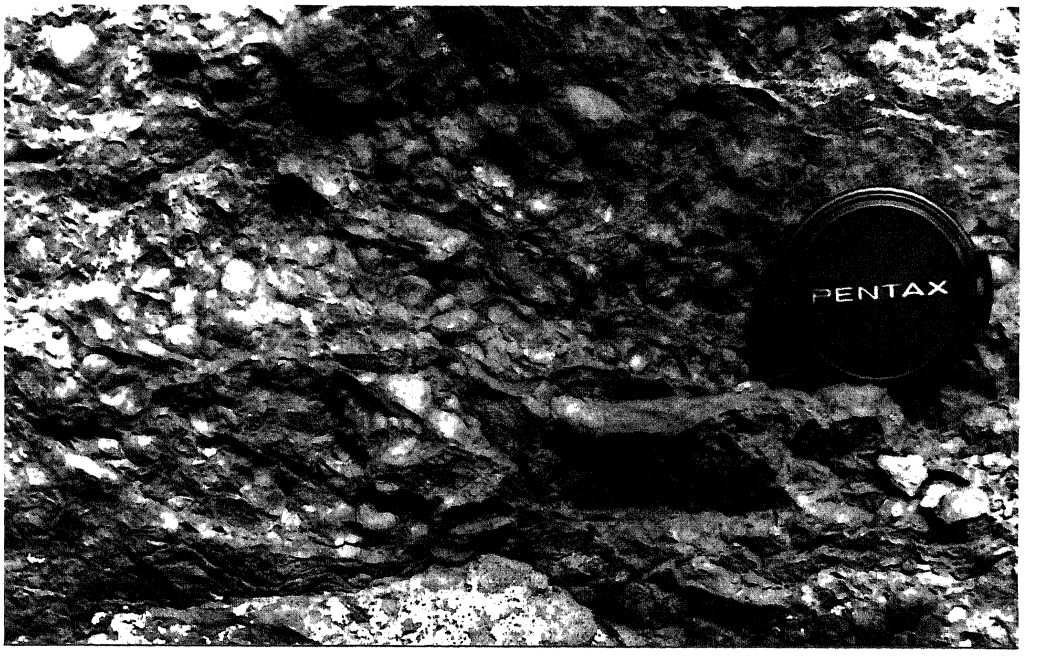

Figure 2.8 Trefor west pit. a) oncoidal ooidal pack-ironstone showing, top centre, a large phosphate nodule (white) with loosely packed ooids, and also oncoids with interlaminated chamosite (dark) and phosphate (white). b) oncolite bed composed of partially haematised chamosite oncoids.

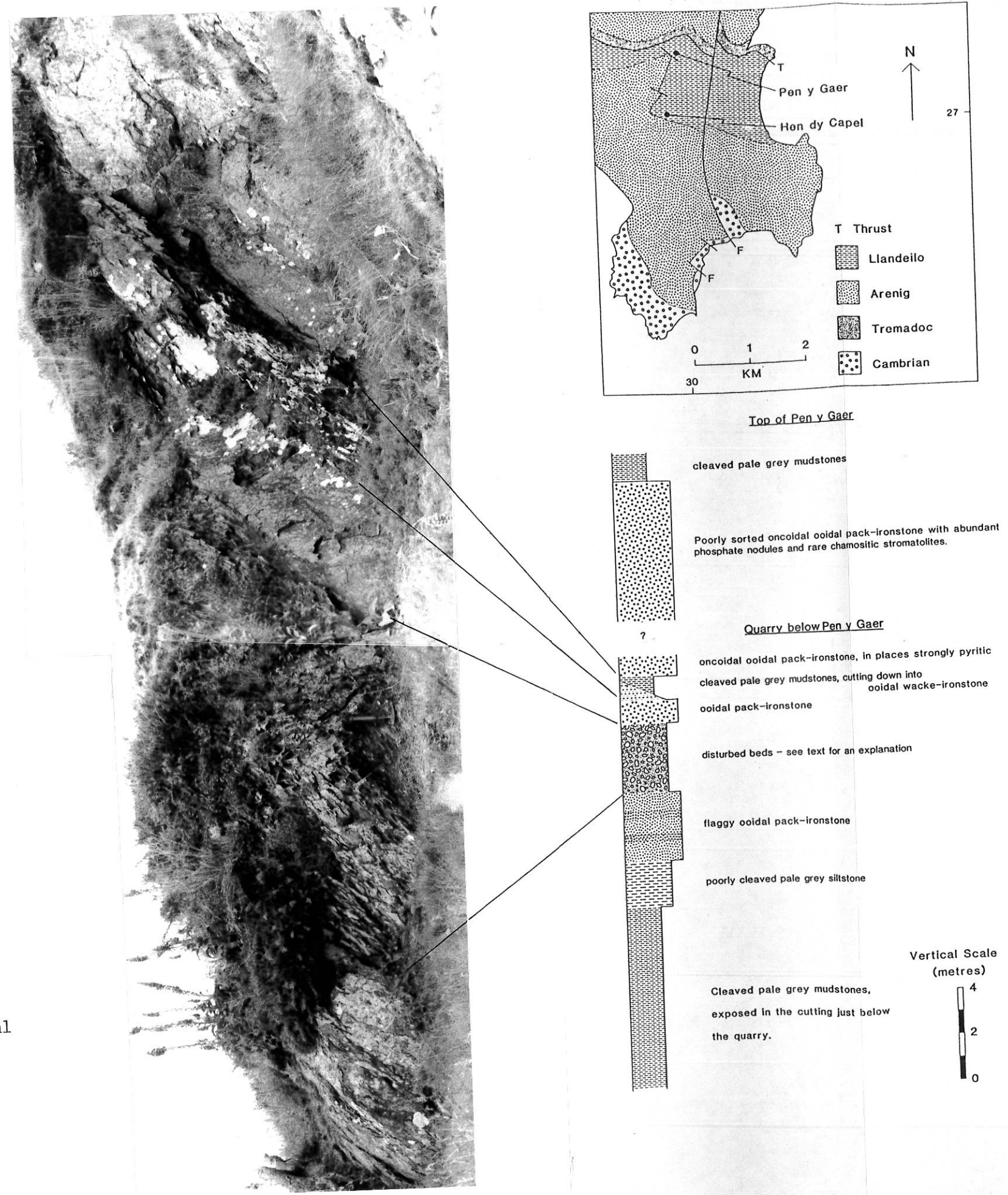

Figure 2.9 Lithological log of Pen y Gaer and Geology of the St. Tudwals region (after Crimes 1969).

In the lower sequence, the disturbed beds (Figure 2.9) are of particular interest. They consist of a variety of rock types, including ooidal wacke-ironstones, cleaved pale grey mudstones, lenses of oncoidal pack-ironstones and silty mudstones. The latter contain reworked and broken ooids and phosphate nodules, ripped-up rafts of chamosite mud, ripped up and deformed laminated silty mudstones and volcanic clasts, all suggesting a debris flow deposit. Ironstone containing volcanic clasts in a debris flow is also exposed 600m to the south next to Craigfryn Farm [SH 2971 2766]. Throughout this lower sequence the ooids and phosphate nodules in the ironstones show strong evidence of having been reworked and broken, and some of the pack-ironstones take on a flaggy nature. The upper part of the ironstone sequence, exposed on the top of Pen y Gaer, is a thick, massive and poorly sorted ooidal oncoidal pack-ironstone containing abundant phosphate nodules. The ironstone is brown on exposed surfaces, due to weathering of siderite within the ironstones.

Half way between the Pen y Gaer and Hen dy Capel ironstone exposures lies the Llanengan quarry [SH 2947 2731]. Exposed on the western side of the quarry is bedded ooidal pack-ironstone, with the bedding dipping towards the east. On the eastern side is massive ooidal pack-ironstone.

A marked facies change is apparent between the Pen y Gaer and Hen dy Capel exposures. At Hen dy Capel [SH 3002 2714] the ironstone consists of metre thick lenses of reworked or slumped ironstone, containing chamositic stromatolite crusts and abundant oncoids, within slumped and deformed mudstones containing ripped up sedimentary clasts (the 'crushed shales' of Nicholas 1915). These changes occur along strike toward a major north-south trending fault (Figure 2.9). The ironstone does not occur on the other side of this fault.

2.4 SNOWDONIA

A number of ironstones of differing ages are exposed in Snowdonia, although there is still uncertainty as to the ages of the Aber and Rhyd ironstones. Of these ironstones, only Llandegai is no longer exposed.

2.4.1 Llandegai [SH 5984 7004]

The Llandegai ironstone lies low in the Nant Ffrancon Formation (Howells *et al.* 1985), which has the Arenig Graianog Sandstone at its base. However, acritarch ages, combined with published graptolite faunas (Greenly 1944), for this ironstone place it in the Llandeilo (Trythall *et al.* 1987). Greenly (1944) reported that *murchisoni* biozone graptolites were missing from this region, implying a stratigraphic hiatus beneath the ironstone.

The Llandegai ironstone is no longer exposed, as the pit was filled in during the construction of the A55 Bangor Bypass. Logs of this section are given by Strahan *et al.* (1920) and the British Geological Survey (BGS) on 1:10,000 field slips. The log below is taken from BGS field slips:

Oolitic ironstone, dark grey, coarsely pisolitic at base	3.90m
Oolitic ironstone, dark grey and red, thinly bedded	0.23m
Oolitic ironstone, dark grey, fine grained	0.53m
Mudstone, pyritiferous, pyrite nodules	0.28m
Siltstone, with thin oolitic ironstone bands	3.00m

2.4.2 Aber [SH 6689 7243 to SH 6789 7294]

Little is known of the geology of the Aber region. The most recent work was by Davies (1969), who described the ironstone as occurring at the base of the *gracilis* Biozone at the base of the Caradoc, although no fauna have been found in this region. Recent work by the BGS (Reedman *et al.* 1983) describe the ironstone as occurring low in the Nant Ffrancon Formation above the Arenig Graianog Sandstone. Acritarchs collected from this ironstone proved to be inconclusive in determining its age (Trythall *et al.* 1987). The Aber ironstone has been deformed and has undergone hydrothermal alteration. Strahan *et al.* (1920) attributed the intermittent exposure of the ironstone to strike faults. Subsequent mineralisation has been concentrated along

these fault planes and this relationship is best shown in the western pit at Aber (Figure 2.11).

The ironstone in the Aber region is intermittently exposed for 1km (Figure 2.10). Three pits are exposed along strike at Aber and one pit at Gorddinog. The general sequence of the ironstone is difficult to determine as the contact between different rock units are tectonic not sedimentary. However, all three exposures at Aber show the same general sequence. To the south of each pit, but exposed within the western pit [SH 6689 7243], are cleaved pale grey mudstones that strike 042^{o} and dip 84^{o}S. In the western pit these cleaved mudstones have quartz injected along the cleavage planes.

Ooidal wacke-ironstones are exposed on the southern edge of each pit. In the western pit the contact between this and the cleaved nmudstones, and this and the ooidal grain-ironstone, can be demonstrated as faulted and mineralised (Figure 2.11). The majority of the exposure in each pit is of the upper facies of the ironstone, which is generally a pale grey colour with a thin dark brown weathering rim around fresh samples. This are predominantly ooidal grain-ironstones, but with some ooidal pack-ironstones. In the eastern pit [SH 6699 7256] this unit is cut through by quartz veins and is mineralised, with the zones of mineralisation now weathered. In the tips next to the exposures, fresh samples of sulphide mineralisation are found, which consist of 'balls' of pyrite replacing the pack-ironstone (Figure 2.12). The ooidal grain-ironstone from the central pit [SH 6693 7245] shows evidence of thin beds with differing ooid grain-size. Cleaved pale grey mudstones occur on the northern side of each pit. In the western pit the mudstones are seen in contact against the ooidal grain-ironstone, which is faulted and mineralised.

The Gorddinog ironstone [SH 6789 7294] is only a small working. The entrance exposes cleaved mudstones. At the end of the trial is the exposure of ironstone with abundant oncoids and stromatolitic crusts, but it is now extensively pyritised.

2.4.3 Northern Snowdonia [SH 6773 6496 to 6114 5801]

This ironstone is considered here as one horizon, although it is exposed intermittently along strike for approximately 10km. It always occurs at the top of the Nant Ffrancon Formation just below the base of the Llewellyn Volcanic Group and has been traditionally regarded as basal Caradoc (Howells *et al.* 1985). Evans (1968) considered the

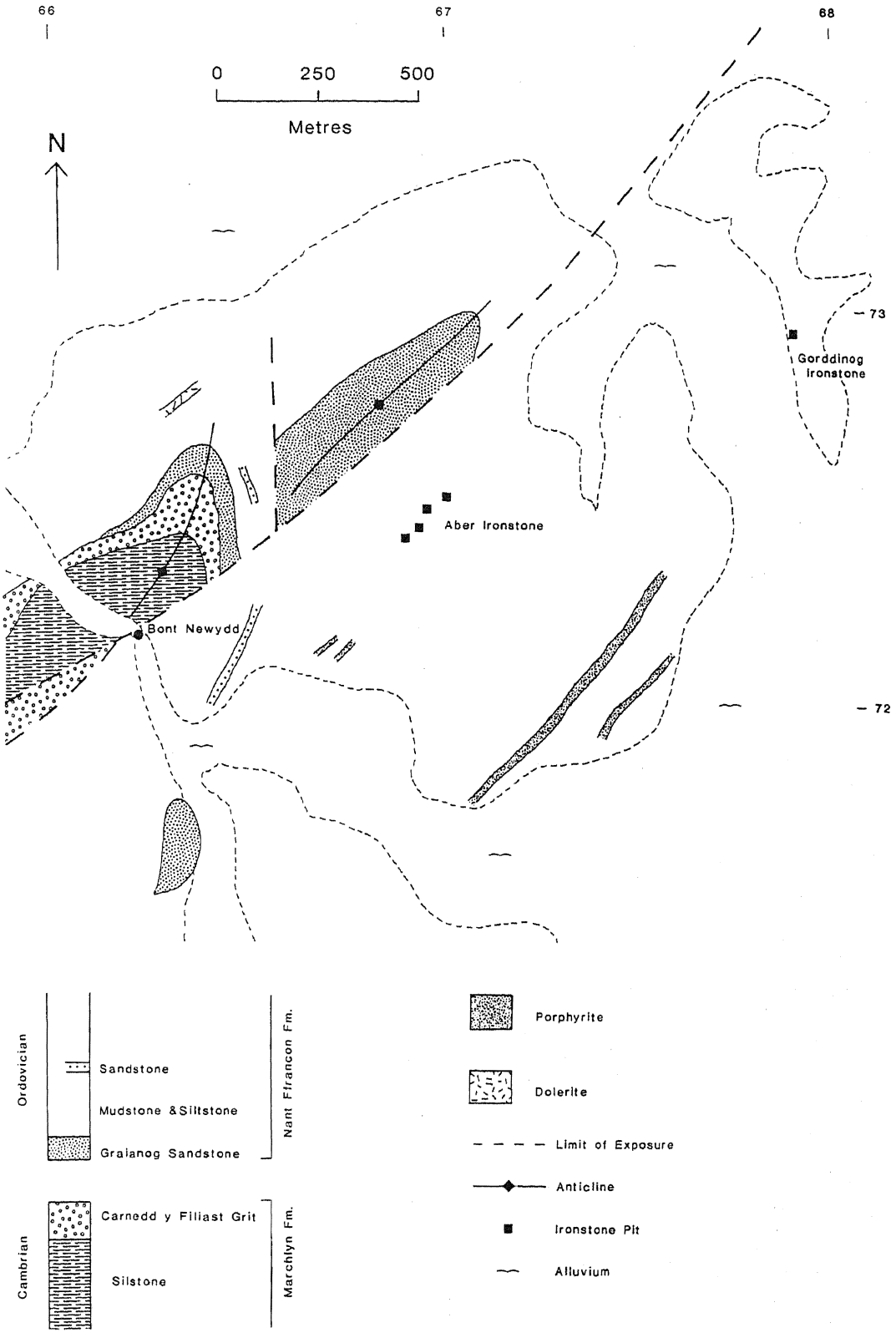

Figure 2.10 Geology of the Aber region (after BGS 1:10,000 field slips) showing the location of the Aber and Gorddinog ironstones.

a)

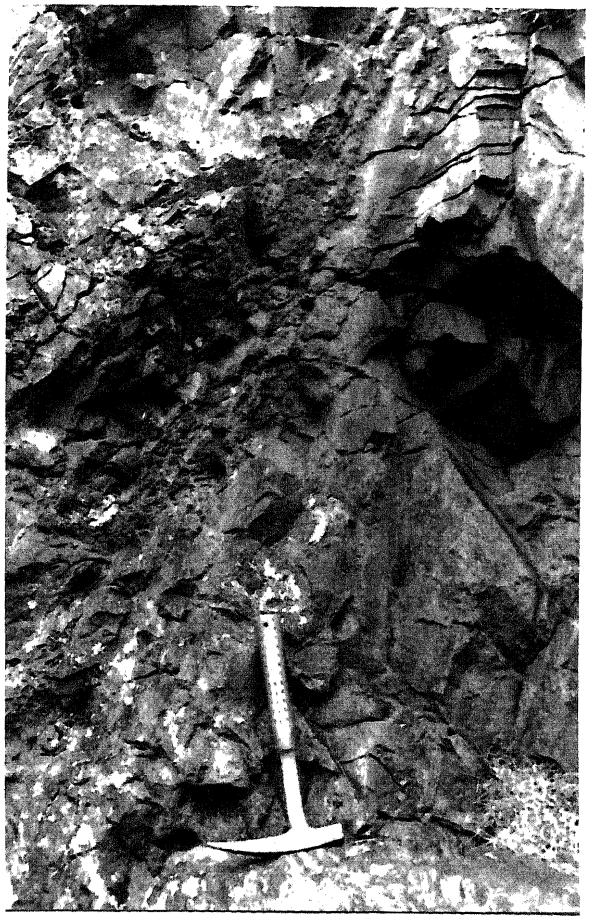

b)

Figure 2.11 Aber west pit [SH 6689 7243] a) photograph looking northeast showing the faulted nature of the contact between units. 1 cleaved mudstones with quartz injected along the cleavage, faulted against 2 ooidal wacke-ironstone, faulted against 3 ooidal grain-ironstone, this contact being mineralized (lower photograph) and weathered. The grain-ironstone is then faulted against 4 cleaved mudstones.

Figure 2.12 Pyrite 'balls' in the Aber ironstone. The rock is ooidal grain-ironstone and overgrowing this is massive pyrite, and faint traces of ooids can still be seen.

ironstones at Cwm Caseg [SH 6773 6496], Cwm Llafar [SH 6544 6424] and next to the A5 road [SH 6429 6224] all one horizon. The ironstone is oolitic, but also pyrite rich. At Cwm Caseg, sporadic ironstone exposures occur at the base of the back wall of the cwm, next to the lake, within intensively cleaved mudstones. At the A5, there is a cutting just to the east of the road, but the exposure is strongly weathered. Three metres of fresh pyrite-rich oolitic ironstone are exposed just to the west of the road. At Bwlch y Cywion [SH 6404 6125], chamositic mud-ironstone and ooidal pack-ironstone occur adjacent to the Bwlch y Cywion microgranite. The ooidal pack-ironstone is now partially replaced by magnetite. In the Llanberis valley, the BGS (1985a) record a magnetite-rich ironstone, adjacent to a rhyolite intrusion. Exposures of the ironstone [SH 6114 5801] show the features of a ferruginous debris flow.

2.4.4 Betws Garmon [SH 5318 5684 to 5453 5802]

Until recently, the Betws Garmon ironstone and adjacent sediments were thought to be of Cambrian age. However, Reedman et al. (1983) have shown that the sequence containing the ironstone is Ordovician (the Nant Ffrancon Formation). Acritarchs collected from the ironstone (Trythall et al. 1987) indicate a Lower or Middle Llandeilo age. The base of the Ordovician here is marked by the the Arenig Graianog Sandstone (Figure 2.13). Trythall et al. (1987) have suggested that a Llandeilo ironstone above Arenig sediments indicates the presence of a stratigraphic hiatus beneath the ironstone.

The principle feature of interest at Betws Garmon is the sedimentary thickening of the upper ooidal pack-ironstone toward the northeast, while toward the southwest the ironstone thins out entirely. The lower mud supported units are lithologically variable, but always grade up into the ooidal pack-ironstone, which is well sorted and contains no oncoids. The top of the ironstone is abrupt and marked either by cleaved mudstones, phosphatic oncoidal mudstones or intensely weathered shales (because of their high sulphide content). However, the ooidal pack-ironstone facies only now contains magnetite (Figure 2.14). Magnetite replacement does not occur in the pack-ironstone exposures to the south of the A4085 road. Subsequently the ironstone has also undergone hydrothermal alteration, indicated by quartz, siderite and pyrite veins, the pyrite veins now strongly weathered.

At locality 1 (Figure 2.13), just beyond Ystrad Farm, the bedding

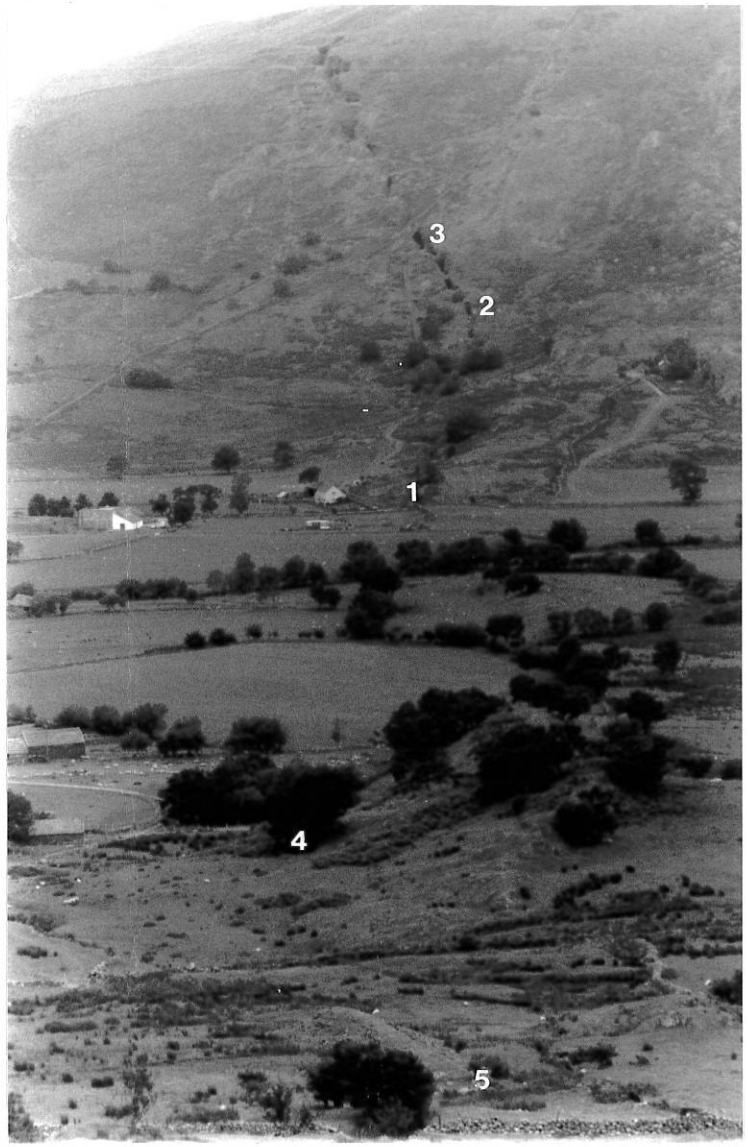

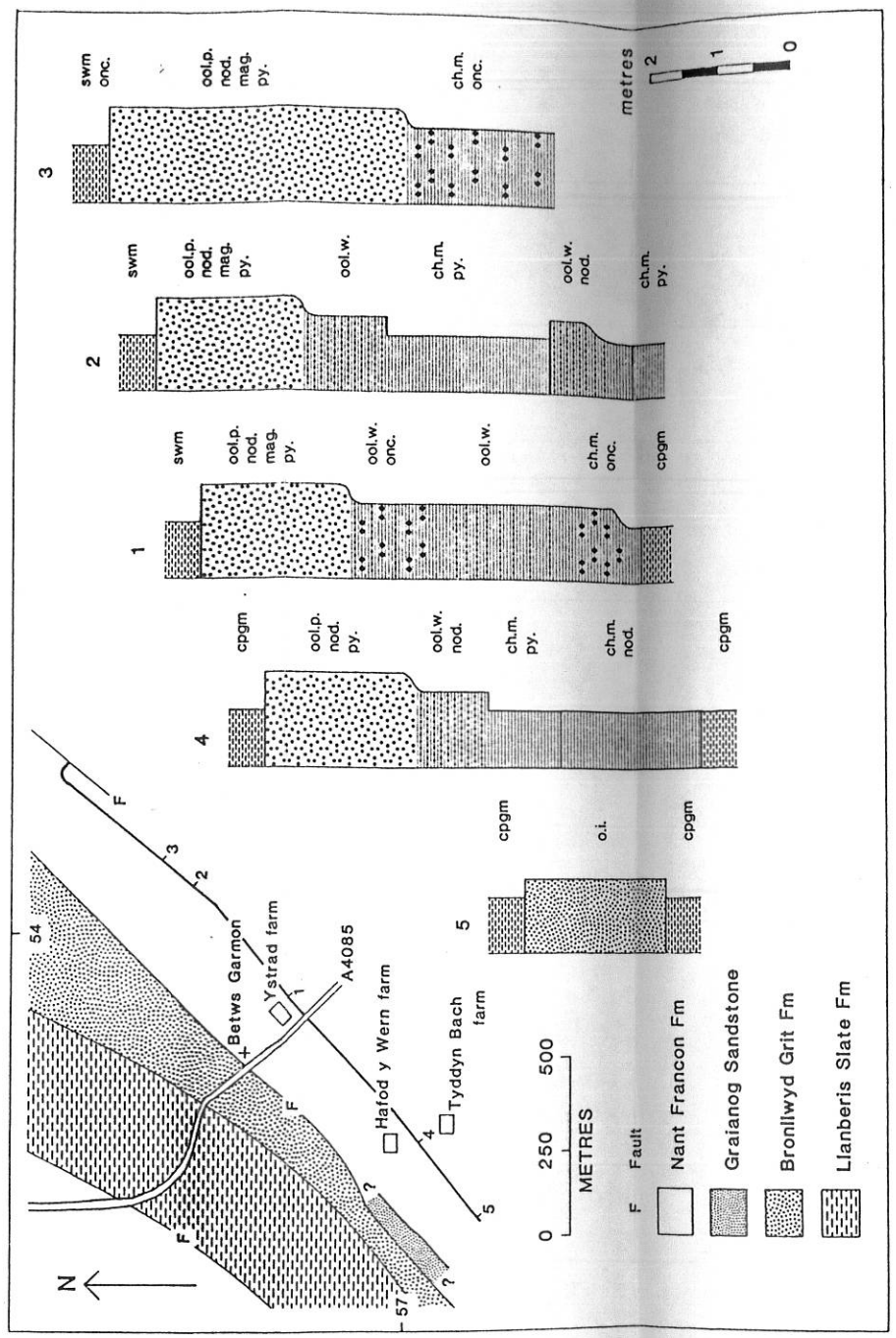

Figure 2.13 Lithological logs along the Betws Garmon ironstone exposure and geology of the Betws Garmon region (after BGS 1:10,000 field slips).

Figure 2.14 Magnetite ooidal pack-ironstone, locality 1 Figure 2.14, Betws Garmon.

strikes 256° and dips 44°E. A full ironstone sequence is exposed, being abruptly succeeded by strongly weathered mudstones. Bedding at locality 2 (Figure 2.13) is vertical. Pyrite replacement is much stronger at this locality, both in the ooidal pack-ironstone and the underlying muddier units. At locality 3 (Figure 2.13) the bedding dips steeply to the southeast where the ooidal pack-ironstone has increased in thickness from 2m to 4m. Further up the hill the bedding becomes less steep, to about 45° southeast, and the ooidal pack-ironstone continues to thicken to 5-6m (Figure 2.15).

At locality 4 to the south of the A4085 (Figure 2.13), just south of the track between Hafod y Wern and Tyddyn Bach Farms, bedding is vertical. The ooidal pack-ironstone contains no magnetite and is strongly sideritic due to hydrothermal alteration, with associated pyrite. Locality 5 (Figure 2.13), 200m further to the southwest, is the last ironstone exposure; further up the hillside the ironstone cannot be traced.

2.4.5 Tremadog [SH 5442 4099 to SH 5680 3929]

In the Tremadog region, the ironstone occurs intermittently along strike for 3km as a series of small workings from Tyddyn Deucwm [SH 5442 4099] to Ynys Galch [SH 5680 3929], with the principle iron mine at Tremadog [SH 5527 4028] (Figure 2.16), which is of basal Caradoc age (Trythall *et al.* 1987). In this region Cambrian sediments crop out to the south of the ironstone and it was originally thought (Fearnsides 1910) that thrusting had carried Caradoc sediments, with the ironstone near the base, over the Cambrian strata. However, Smith (1987) has shown that no thrusting has occurred, and that the tectonic features noted by Fearnsides (1910) can be explained by slumping of semi-lithified sediment induced by tectonic disturbance.

The general dip of the rocks in this region is 20°-30° to the north west. The lowest rocks are exposed on the southern side of the Tremadog mine. They comprise cleaved pale grey mudstones that show small-scale slump folding, overlain by 'disturbed' float-ironstones in ooidal wacke-ironstones (Figure 2.17.a). The latter contain rip-up clasts (Figure 2.18.a) and lenses of reworked phosphate nodules, which are rounded and elongate parallel with bedding (Figure 2.18.b). Oncoids (Figure 2.17.b) and reworked chamositic stromatolites are common in this facies. *In situ* stromatolites are seen 250m away at Pensyflog [SH 5619 3958].

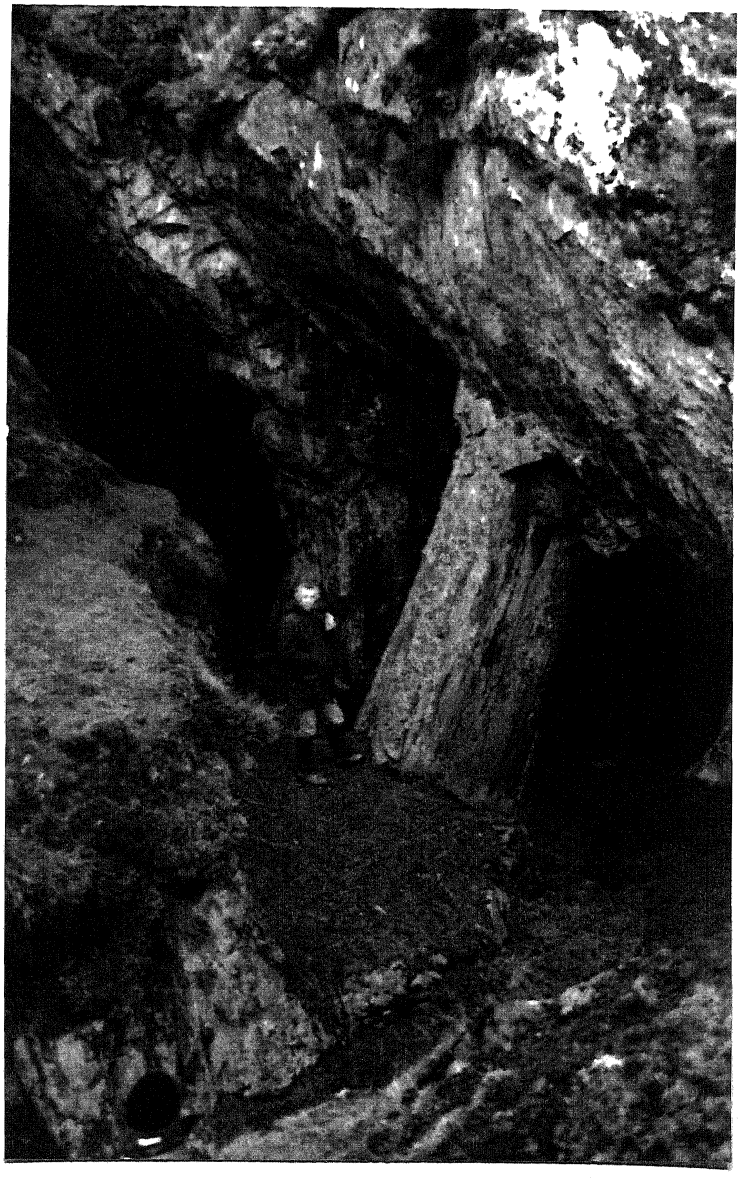

Figure 2.15 Ironstone pillar, Betws Garmon, showing the thickest development of the pack-ironstone in the northeast exposures of Betws Garmon. The ore mined is magnetite ooidal pack-ironstone, and the ore was hard enough to be left as support pillars for the stope. Above the pack-ironstone (hangingwall) is strongly weathered mudstone and below (footwall) are wacke-ironstones and mud-ironstones.

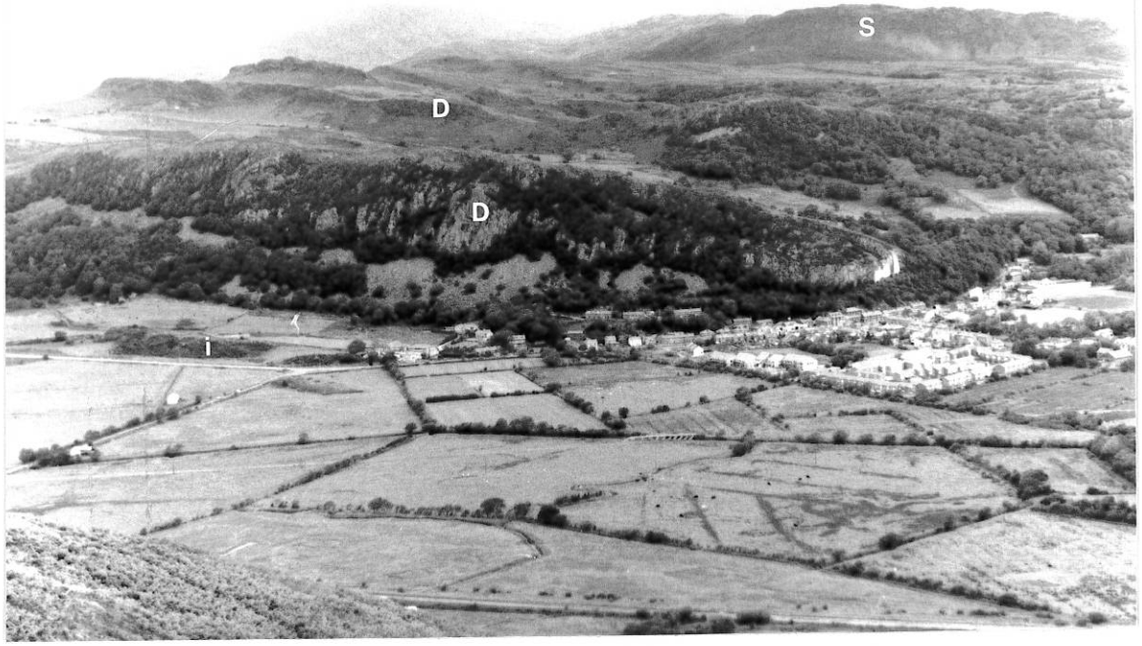

b)

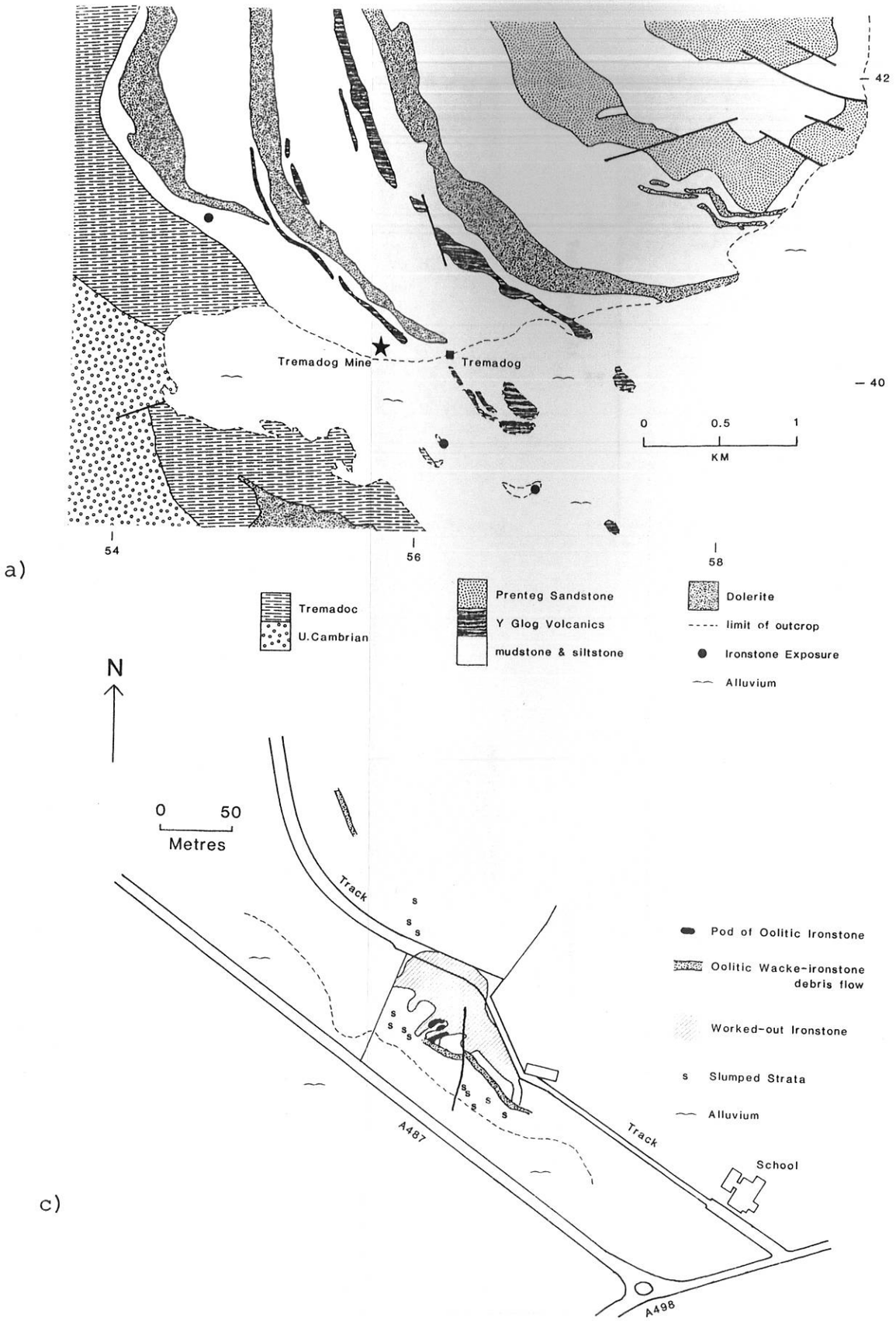

c)

Figure 2.16 The Tremadog ironstone. a) Geology of the Tremadog region. b) Photograph of the Tremadog region showing the Tremadog ironstone (i) and then up sequence dolerites (d) and sandstone (s) (from a). c) Sketch map of the Tremadog ironstone mine (after Martin Smith pers comm).

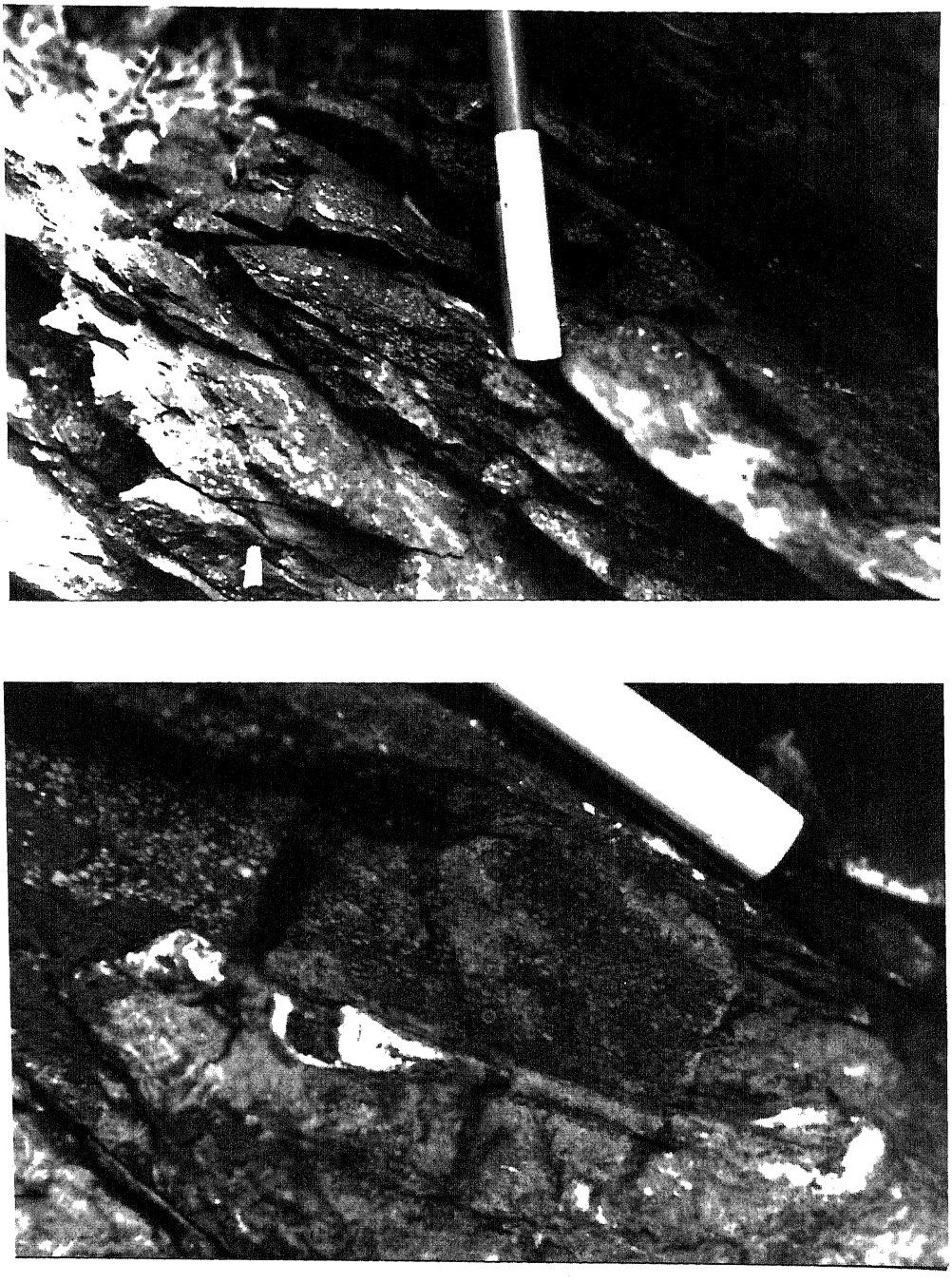

Figure 2.17 Tremadog [SH 5527 4028]. a) ooidal wacke-ironstone showing chamosite ooids in a darker muddy and silty matrix. b) large dumbell shaped oncoid in ooidal wacke-ironstone composed of alternating laminae of chamosite (dark) and phosphate (white).

Figure 2.18 Tremadog [SH 5527 4028]. Disturbed silicic phosphatic float-ironstones in ooidal wacke-ironstones showing a) lenses of reworked phosphate nodules and b) reworked clasts, nodules and oncoids.

The upper ooidal pack-ironstone, now virtually mined out, has been broken and rotated into 'pods' during slumping (Figure 2.19), with mudstone injected in between the pods. This pack-ironstone has been extensively replaced by magnetite, with some pyrite. Large quartz and dolomite veins, with strongly weathered veins of pyrite, cut the mudstones between the 'pods' (Figure 2.19). However, at Pensyflog an ooidal grain-ironstone is exposed, which has not been partially replaced by magnetite.

2.4.6 Rhyd [SH 6285 4093 to SH 6306 4118]

The Rhyd ironstone (Pen yr Allt - Weinberg 1973, Pulfrey 1933a) is similar to Tremadog in that it is caught up in a sedimentary melange (Smith 1987). The age of the Rhyd ironstone is uncertain, although it is possible that it is at the same stratigraphic level as the Tremadog ironstone. The Rhyd ironstone occurs within the metamorphic aureole of the Tan y Grisiau microgranite, which has caused spotting of sediments adjacent to the ironstone (Bromley 1969, 1963).

Two ironstone pits are exposed 300m along strike from each other [SH 6285 4093 & SH 6306 4118]. The pits [SH 6285 4093] are either faulted blocks or ironstone 'pods' in the melange. The entrance to the more western pit exposes hornfelsed shales, followed by a volcaniclastic debris flow, occurring just below the ironstone. Within both pits on the south wall are ooidal wacke-ironstones, which in the eastern pit are spotted, followed by approximately 4m of ooidal pack-ironstone. In the eastern pit towards the top of this unit the ironstone becomes strongly weathered, and was originally sulphide-rich. The north Wall of both pits exposes cleaved pale grey mudstones occurring above the ironstone.

Figure 2.19 The main ironstone exposure at Tremadog facing south [SH 5527 4028]. The ooidal pack-ironstone was broken and rotated into pods which are now mined out and three such pods are shown (p). Mudstones were injected in between the pods and were also mineralised and weathered.

2.5 CADAIR IDRIS AND THE ARANS

The geology of the Cadair Idris area has been outlined by Cox (1925) and Ridgway (1976). The age of the ironstone is uncertain as no acritarchs have been found (Trythall et al. 1987) but is thought to be of Lower Llandeilo age (Cox 1925). The ironstone is exposed on the northern slopes of Cadair Idris within a sequence of cleaved pale grey mudstones (the Llyn y Gadair Mudstones) which overlie a thick sequence of spilitic pillow lavas and ashes (Figure 2.20). The ironstone varies markedly in thickness across the Cadair Idris range (Figure 2.20), thickest in the east where no oncoids occur and average ooid size is small, and thinnest in the west where oncoids are abundant and detrital quartz grains occur. This is complemented by the Llyn y Gadair Mudstones which thin eastwards towards Cross Foxes (Davies 1956). Further west, the ironstone is absent until the Llanegryn Fault where on its west side some 50ft of 'oolitic and nodular' beds occur, at the same stratigraphic level as the Cadair Idris ironstones (Jones 1933).

2.5.1 Ffordd Ddu [SH 6477 1283]

The base of the sequence at Ffordd Ddu is exposed on the hillside above the pit, where cleaved pale grey mudstones rest on spilitic lavas (Figure 2.20; Figure 2.21). Bedding strikes 068^{o} and dips 36^{o}S. Above these mudstones are oncoidal chamositic mud-ironstones (Figure 2.22) containing detrital (2-3mm) quartz grains, lateral equivalents of the ooidal pack-ironstone exposed within the pit (Figure 2.20). Due to a small fault parallel to the strike, the spilitic lavas are repeated just above the ironstone pit, and the majority of the exposure within the pit is of cleaved pale grey mudstones, gradually darkening upwards into chamositic mud-ironstones. Thin beds of ooidal pack-ironstone are exposed at the top of the sequence on the west side of the pit.

2.5.2 Foxes Path [SH 7104 1378]

Here a large thickness of nodular chamositic mudstones occur below a sulphide-rich ooidal ironstone, now strongly weathered (Figure 2.20). This alteration of the ironstone may be due to the intrusion of the granophyre above the ironstone (Figure 2.23).

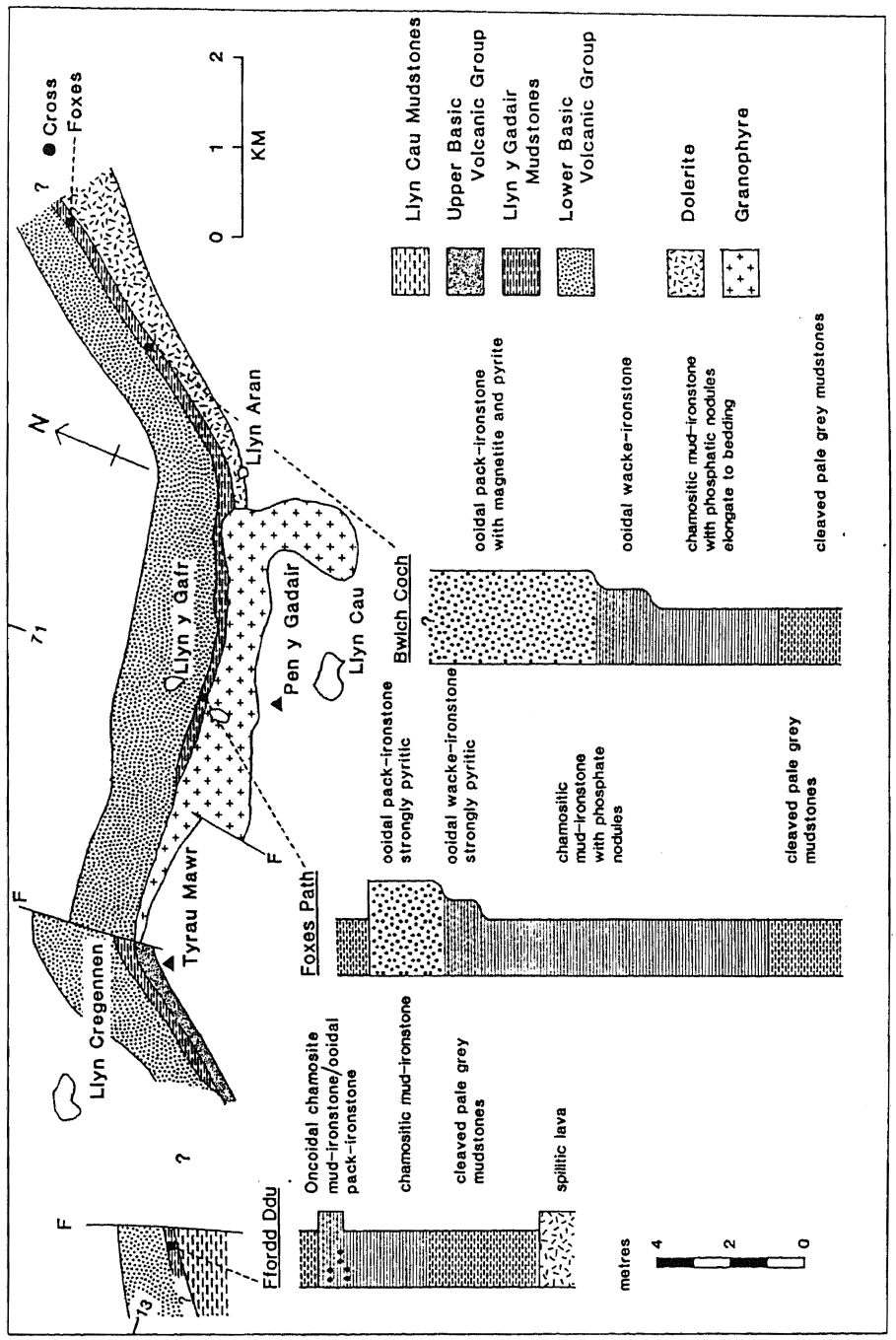

Figure 2.20 Geology of the Cadair Idris region (after Cox & Wells 1927) and lithological logs of the Ffordd Ddu [SH 6477 1283] Foxes Path [SH 7104 1378] and Bwlch Coch [SH 7495 1557] ironstones.

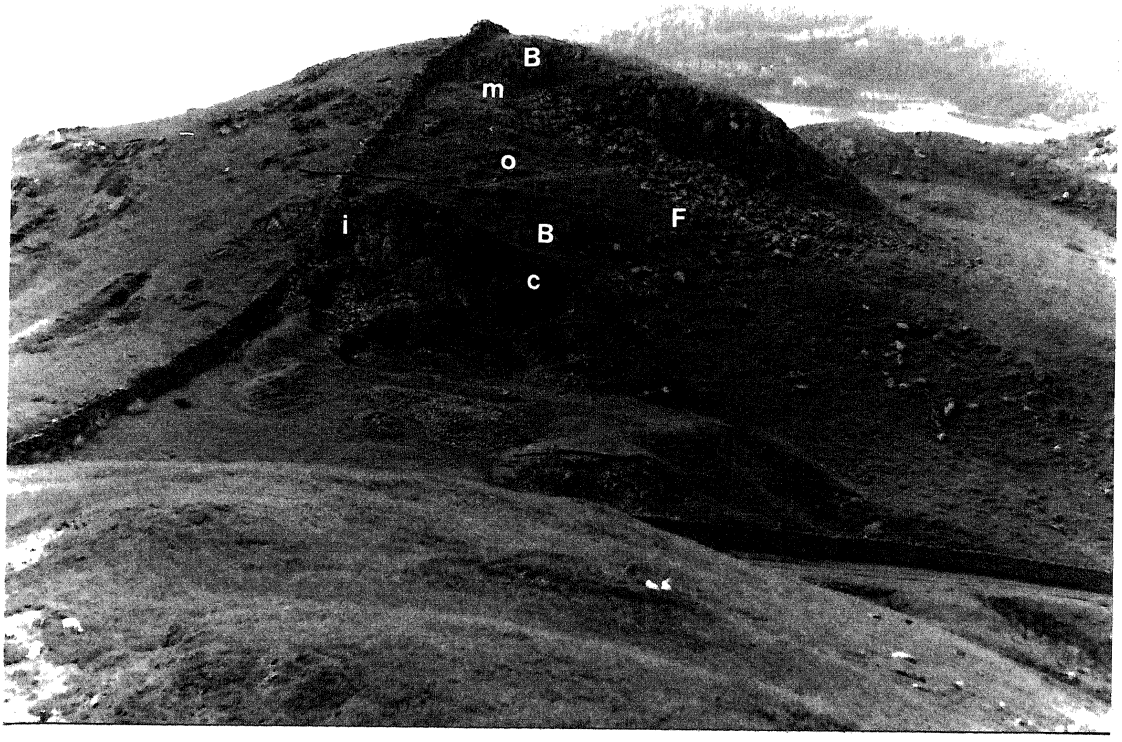

Figure 2.21 The Ffordd Ddu ironstone exposure [SH 6477 1283]. The top of the hill is spilitic lavas (b) and just below is the contact with the cleaved pale grey mudstones (m); below again are oncoidal mud-ironstones (o). The strike of the rocks is left to right with the dip toward the camera (south). A strike fault just above the ironstone pit repeats the sequence with spilitic lavas occurring just above the pit. The exposure within the pit is mostly of cleaved mudstones, which darken upward into chamosite mud-ironstone (c). Ooidal pack-ironstone (i) is exposed on the very left of the pit.

Figure 2.22 Oncoidal chamositic mud-ironstone, Ffordd Ddu [SH 6477 1283]. Large irregular oncoids in mud-ironstone, the oncoids are composed of interlaminated chamosite (dark) and phosphate (light).

Figure 2.23 The Foxes Path [SH 7104 1378] exposure, the rocks strike from left to right and dip away from the camera (south). The hummocky terrain in the centre is the spilitic lavas below the ironstones (s). To the left of the terminal moraine is exposure of oolitic ironstone (i) followed by cleaved mudstones. The escarpment behind is a large granophyre intrusion (g). At the top just to the left in cloud is the summit of Cadair Idris - Pen y Gadair (893m).

2.5.3 Bwlch Coch [SH 7495 1557] and Cross Foxes [SH 7597 1639]

In the eastern part of the Cadair Idris range, the ironstone is exposed intermittently from 600m west of Bwlch Coch [SH 7451 1517] to Cross Foxes. The section for this eastern region is taken from Bwlch Coch, where the exposure is most complete (Figure 2.20). The feature of interest at Bwlch Coch is the cleaved chamositic mud-ironstones just above the pit which contain phosphate nodules elongate to bedding at an angle to the cleavage (Figure 2.24). At Cross Foxes the bedding dips at 50-70^{o} towards the southeast. Strongly weathered shales just above spilitic lavas lie below approximately 7m of fine-grained oolitic pack-ironstone (average ooid size 0.25mm). Oncoids and detrital quartz grains are absent. In the eastern part of Cadair Idris a dolerite sill has metasomatised adjacent sediments (Davies 1956) including the Cross Foxes and Bwlch Coch ironstones. The upper ooidal pack-ironstone only now contains magnetite.

2.5.4 Llanegryn [SH 5791 0389 to 2947 2731]

The geology of the Llanegryn area has been outlined by Jones (1933), who described the ironstones as the 'oolitic and nodular beds'. Exposure of the ironstone is very poor, (limited to sporadic outcrops from [SH 5791 0389] to [SH 2947 2731]) and restricted to fine-grained ooidal wacke-ironstone with phosphate nodules.

2.5.5 Tyllau Mwn [SH 8441 2054]

The geology of the Aran mountains has been described by Dunkley (1978). The age is uncertain, although on lithological correlations with the Cadair Idris region it is placed in the U.Llanvirn (Dunkley 1978). The ironstone at Tyllau Mwn is exposed in three pits along strike and is a magnetite-rich ooidal pack-ironstone with limited exposures of other ferruginous beds lying adjacent to volcanic deposits.

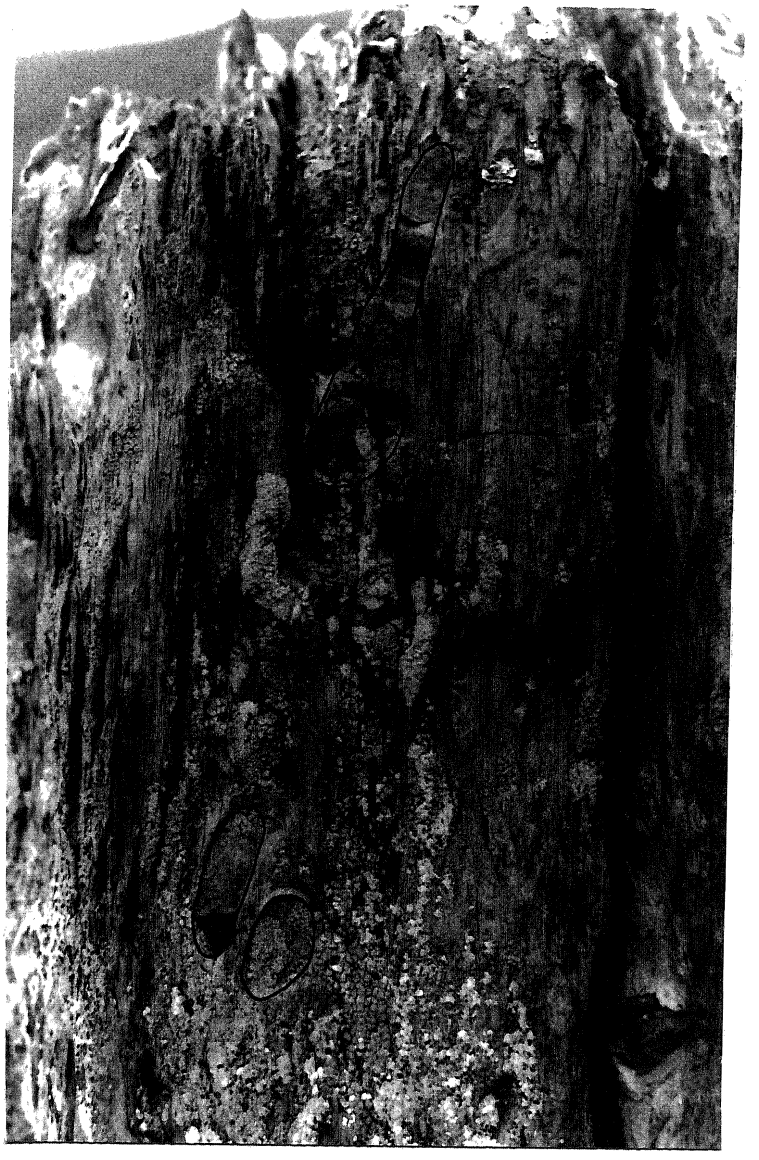

Figure 2.24 Nodular chamositic mud-ironstone, Bwlch Coch [SH 7495 1557]. Bedding dips steeply to the left (southeast) and the phosphate nodules are elongate parallel to bedding. Cleavage is vertical but does not cut through the nodules, because of their rigidity.

3 SEDIMENTARY CHARACTERISTICS OF THE IRONSTONES

Despite low-grade regional metamorphism and development of a penetrative cleavage, numerous sedimentary features of the ironstones can be observed or inferred. Previous ideas on the sedimentation of the North Wales Ironstones have been published by Weinberg (1973) and Pulfrey (1933). This chapter seeks to expand upon a discussion of the depositional controls of the mid-Ordovician North Wales Ironstones which has already been published (Trythall et al. 1987).

3.1 GRAIN TYPES OF THE IRONSTONES

The mid-Ordovician North Wales Ironstones are typical of Phanerozoic Ironstones, being mostly composed of berthieroid (chamosite) ooids. Ancillary types of ferruginous allochems in the ironstones are peloids, oncoids and stromatolites. Ooids and oncoids are divided purely on morphological grounds (Section 1.5.2) although by implication oncoids are of algal/bacterial/fungal origin. Despite the overwhelming abundance of ferruginous allochems in the ironstones, there are also other grain-types of significance present, principally quartz grains. In thin section ooids, oncoids and peloids are predominantly green in colour, indicating ferrous chamosite. Some laminae or all of the ooids may now be a brown colour, indicating oxidation to a more ferric chamosite. The original mineralogy of all ooids in the North Wales Ironstones was chamosite (berthierine). Now they may be partially or wholly replaced by silica, siderite, magnetite, pyrite, haematite and goethite, which will be detailed in Chapters 4 and 5. Additionally, EPMA analyses have detected traces of quartz and apatite within ooids and these phases were most likely mobilized during diagenesis (Chapter 4).

3.1.1 Peloids

Peloids occur most commonly as nuclei to ooids (Figure 3.1) at all ironstone localities, although they may be found as grains in the matrix (Figure 3.6), and vary from 0.1mm to 0.3mm in size. They are composed of green fine-grained chamosite. The chamosite in peloids has

a)

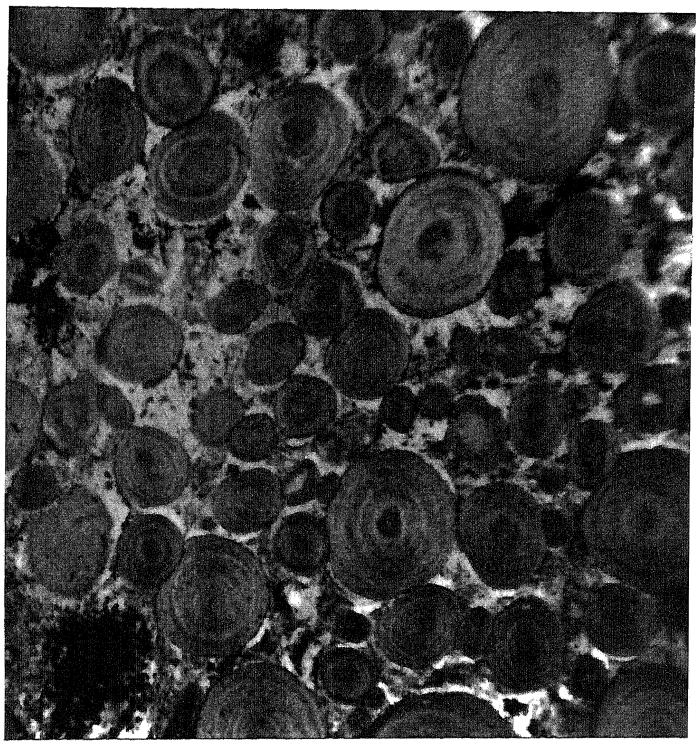

b)

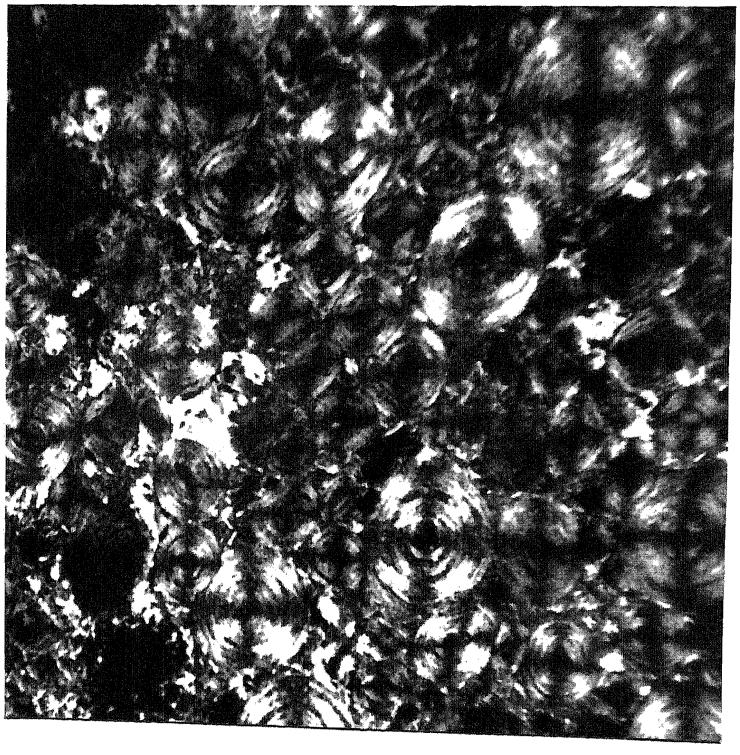

Figure 3.1 Photomicrograph a) plane polarised light b) crossed polarised light, chamosite ooidal chamositic pack-ironstone, Cadair Idris [SH 7606 1652]. Typical chamosite ooids showing concentric laminations around a peloidal nucleus. In crossed nic ols the extinction cross shown by the ooids indicates the tangential orientation of the chamosite. Peloidal nuclei show up as having no orientation. Scale bar = 1mm.

no preferred orientation as it does not show an extinction cross.

3.1.2 Ooids

Ooids in the mid-Ordovician North Wales Ironstones are composed of a nucleus surrounded by chamosite laminae. The most common nuclei are chamosite peloids. Detrital quartz grains are also common as nuclei. These are usually angular quartz grains showing undulose extinction (Section 3.1.6), but within a well-rounded ooid. Detrital quartz grains are present as nuclei only when they are also present in the matrix. The exception is in reworked ironstones (eg Pen Y Gaer) where quartz grains form the nuclei to ooids but do not occur in the matrix. Other more rare nuclei are pelletal phosphate, phosphate fragments, broken ooids, and sponge spicules. The latter two are coated by laminae of chamosite, but this coating has not rounded the grain (Figure 3.2). These other types of nuclei are more commonly found in the Anglesey and Llŷn ironstones.

The laminae of the ooids are fine-grained green chamosite. All ooids show an extinction cross in crossed nic ols (Figure 3.1), indicating tangential orientation of the clay flakes around the nucleus. The ooid chamosite laminae are defined by thin dark layers (Figure 3.2). This is best seen at Ffordd Ddu where ooids have been partially dissolved and the dark layers concentrated along solution seams (a microstylolite). The most likely suggestion for this material is that it is organic carbon. Weinberg (1973) has shown that the North Wales Ironstones contain an average of 0.3% non-carbonate carbon. It is most probable that this carbon would define the chamosite laminae of ferruginous ooids. Organic material defining laminae is common for calcareous ooids (Bathurst 1975). Hughes (1989) has now suggested the same for ferruginous ooids.

Most ooids are spherical or subspherical in shape although ooids may be deformed or broken. Deformed ooids (spastoliths) occur either around diagenetic phosphate nodules or in the wacke-ironstones and mud-ironstones. Deformed ooids that occur around diagenetic phosphate nodules are described in Section 4.2. Spastolithisation in the wacke-ironstones and mud-ironstones occurs as flattening of ooids parallel with bedding, indicating burial compaction (Figure 3.3). Broken ooids occur in slumped semi-lithified material (eg Pen y Gaer), where the two most common ways that ooids break are along laminae or by breaking up into wedge shaped pieces (Figure 3.4). They may also

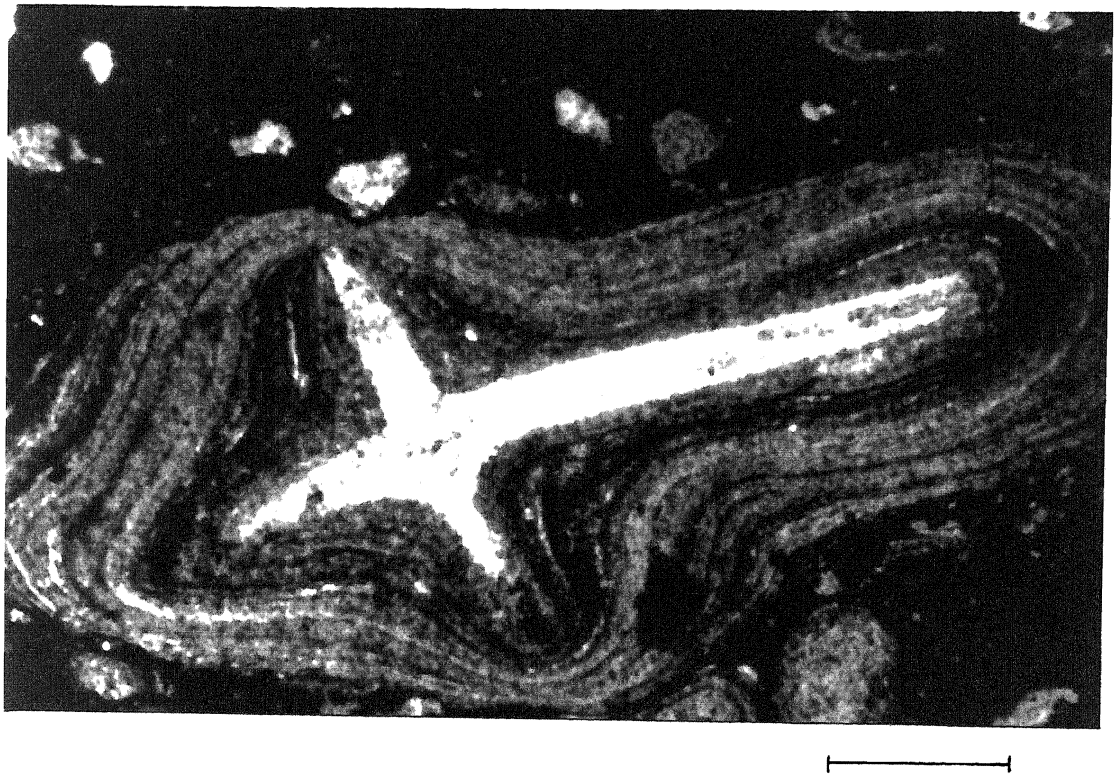

Figure 3.2 Photomicrograph, ooidal pack-ironstone, LP22A Pen y Gaer, [SH 2990 2821]. Sponge spicule coated by chamosite laminae demonstrating the rounding effect by the laminae. The central canal of the spicule on the right hand side can be shown to be infilled by chamosite mud before the spicule was coated. The darker thin layers defining the chamosite laminae are most likely organic carbon. Scale bar = 1mm.

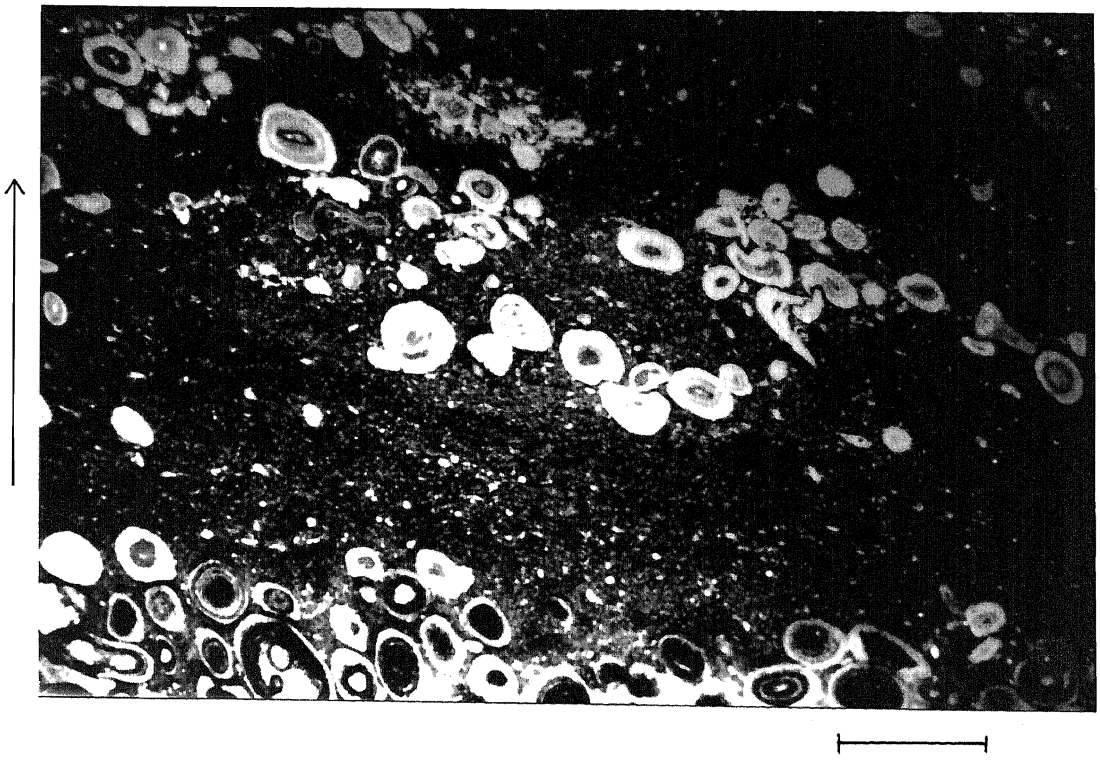

Figure 3.3 Photomicrograph, ooidal pack-ironstone, YF-X Betws Garmon (loose grab sample). Spastoliths within muddy lenses of the pack-ironstone. These ooids were deformed during burial compaction and their shape and their indentation on one another indicate their plastic nature. Scale bar = 1mm.

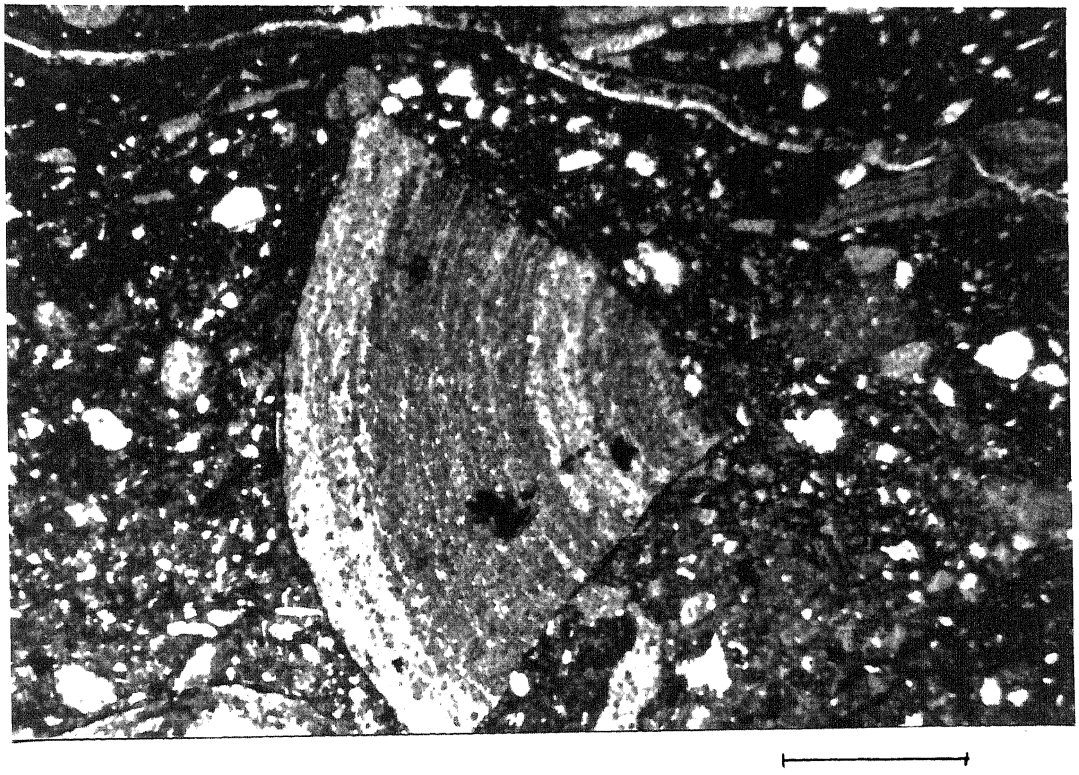

Figure 3.4 Photomicrograph, disturbed bed, LP20A Pen y Gaer [SH 2984 2829]. Broken ooid in a disturbed bed (Figure 3.18) showing brittle breakage of the ooid during slumping of the sediment, in a muddy silty matrix. Within the matrix also occur thin strips of chamosite lamellae that have broken off other ooids. Scale bar = 0·1mm.

occur in pack-ironstones, where in the Anglesey and Llŷn ironstones they may be subsequently recoated by chamosite laminae. Ooids in the grain-ironstone from Pensyflog (near Tremadog) show splay textures (Figure 4.12.a), where ooids have been broken during compaction of the grain-supported sediment.

These features indicate that the ooids some mechanical cohesion during deposition and burial. Spastolithisation in muddy sediments indicate that the ooids were originally in a plastic state. This was due to the high water content in the original clay mineral within the ooid, which could not rapidly dewater in a muddy sediment. Broken ooids indicate that with maturation (dewatering) the ooids became more brittle and in a high energy environment can become broken, either in slumped material or during strong water agitation. Broken ooids are found in disturbed beds and pack-ironstones. Broken ooids have been found in the Frodingham ironstone, interpreted as occurring in a barrier bar environment (Knox & Fletcher 1989).

Generally ooids are larger (average ooid size 0.5mm) than the associated quartz grains (average size 0.2mm). This indicates they were hydrodynamically lighter than quartz grains, even though chamosite is the denser of the two minerals. This implies that ooids had a high initial water content. A similar disparity in size between goethite ooids and quartz grains has been recognised from Miocene oolitic ironstones from northeastern Colombia (James & Van Houten 1979).

3.1.3 Oncoids

The presence of ferruginous oncoids are an important and distinctive feature of the mid-Ordovician North Wales Ironstones. These oncoids have previously been recognised as organic structures (Hallimond 1925; Cullis in Pulfrey 1933a; Jones in Pulfrey 1933a). Ferruginous oncoids have only been recorded from one other British Phanerozoic Ironstone, the Frodingham Ironstone (Knox & Fletcher 1989). However, within the Ordovician North Wales Basin, oncoids are not restricted to the ironstones. Morphologically identical structures (Bolopora undosa - Hoffman 1975) are found in the basal beds of the Arenig. These are predominantly phosphatic, but with some chloritic (?chamositic) laminae.

The oncoids in the North Wales Ironstones are morphologically distinct from ooids. They grow to much larger sizes, the laminae are

Figure 3.5 Top - Photograph of thin section, oncoidal rud-ironstone in ooidal pack-ironstone, LP73A Trefor [SH 3672 4739]. Chamositic oncoids from the oncolite bed, now showing partial replacement by haematite (dark). Scale in mm. Bottom - Photomicrograph, oncoidal wacke-ironstone, YF-B Betws Garmon (loose grab sample). Chamositic (dark) and phosphatic (white) oncoid, showing growth around a previous oncoid. This is within a phosphate nodule where the groundmass is phosphate but opaques are sulphides and iron oxides. Scale bar = 0.5mm.

commonly mammilated and discontinuous, and some oncoids show a multiphase growth history. The nuclei for oncoids are either chamosite, phosphate or an earlier oncoidal structure. There is a range of mineralogical compositions of the oncoids, from purely chamositic to interlaminated chamosite and phosphate (Figure 3.5). Purely phosphatic oncoids have not been found, although some are predominantly phosphatic with only minor chamosite.

The majority of the oncoids have a concentrically laminated spongiostromate fabric with only minor porostromate fabric. The thickness of the spongiostromate laminae are relatively uniform around the oncoid (Figure 3.5). Some oncoids have both spongiostromate and porostromate fabrics and these have more uneven laminae thicknesses around the oncoid. Fenestrae within the porostromate fabric are now mineral infilled (siderite, silica, phosphate, chamosite). Oncoids with a predominantly spongiostromate fabric have a maximum size of approximately 2cm and are spherical/subspherical to elongate in shape. Those oncoids with both spongiostromate and porostromate fabrics are larger (up to 10cm in size), show more irregular shapes (including dumb-bell shaped - Figure 2.17), and can have a 'cauliflower' structure or have 'buds' growing from them (Figures 3.6, 3.7).

Oncoids are found at virtually all ironstone localities, usually within the mud-supported ferruginous facies. However, the Anglesey and Llŷn upper grain-supported ironstone facies also contain oncoids. Oncoids which are spongiostromate and subspherical to elongate predominantly occur in pack-ironstones, float-ironstones and pack-ironstone lenses in mud-ironstone (Figures 3.6, 2.8.a). Those which are both spongiostromate and porostromate with more irregular shapes predominantly occur within mud-ironstones (Figures 3.6, 2.17), disturbed beds and within or adjacent to stromatolites.

3.1.4 Stromatolites

Stromatolites are much less common. They are distinguished from oncoids in that they are found as *in situ* mat-like crusts, or as endolithic encrustations on allochems. Their laminae are morphologically identical to oncoids, they are composed mostly of porostromate fabric, and they are predominantly chamositic, although some *in situ* stromatolitic crusts are also phosphatic. *In situ* stromatolitic crusts have only been found at Gorddinog (Aber) (Figure 3.8) and Pensyflog (Tremadog). Ooids and oncoids are commonly trapped

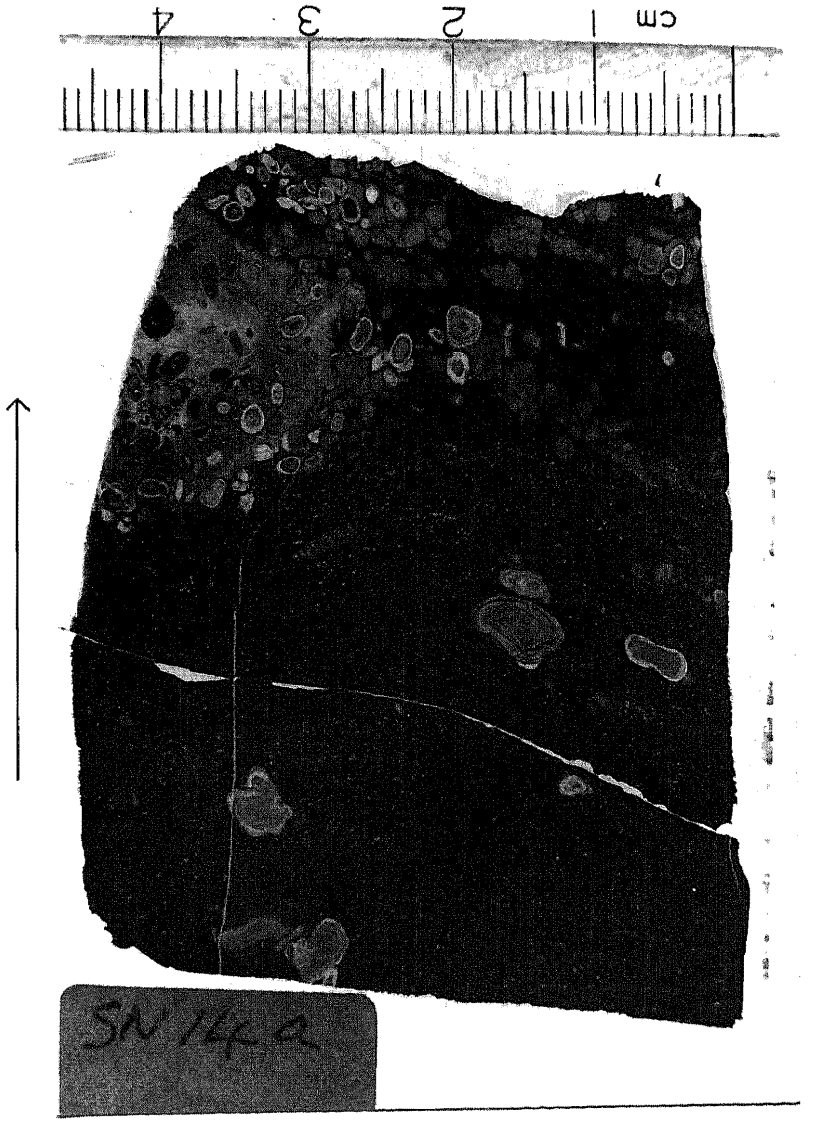

Figure 3.6 Photograph of thin section, ooidal oncoidal wacke-ironstone lense in an oncoidal chamositic mud-ironstone, SN14a Betws Garmon [SH 5433 5778]. Oncoidal lense in a chamositic mud-ironstone. Oncoids are both phosphatic (white) and chamositic (dark). Also present are ooids and peloids in the lense. There is a strong difference of oncoid type with facies. Oncoids in the lense are small, subspherical and regular. The oncoids in the chamositic mud-ironstone beneath are larger and irregular.

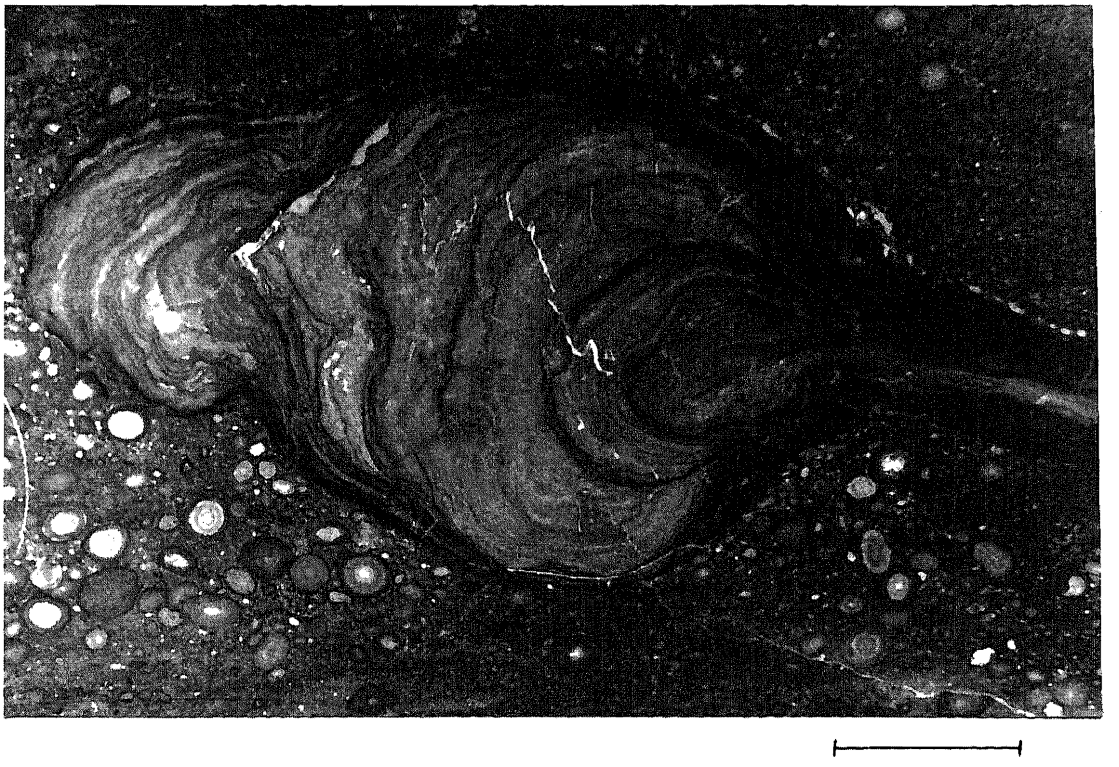

Figure 3.7 Photograph of thin section, oncoidal ooidal wacke-ironstone Tremadog [SH 5527 4028]. Detail of a dumbell shape oncoid (figure 2.17), with chasmositic laminae defined by darker organic carbon. Some fenestrae are present within the porostromate fabric. Scale bar = 5mm.

Figure 3.8 Photograph of thin section, Bind-ironstone, SN20A Gorddinog (Aber) [SH 6789 7294]. The bottom half of the photograph is a chamositic and phosphatic stromatolite, the opaque parts are mineralised by pyrite. The upper half is a more chamositic muddy encrustation, trapping irregularly shaped chamositic oncoids, which show 'budding' and 'cauliflower' structures.

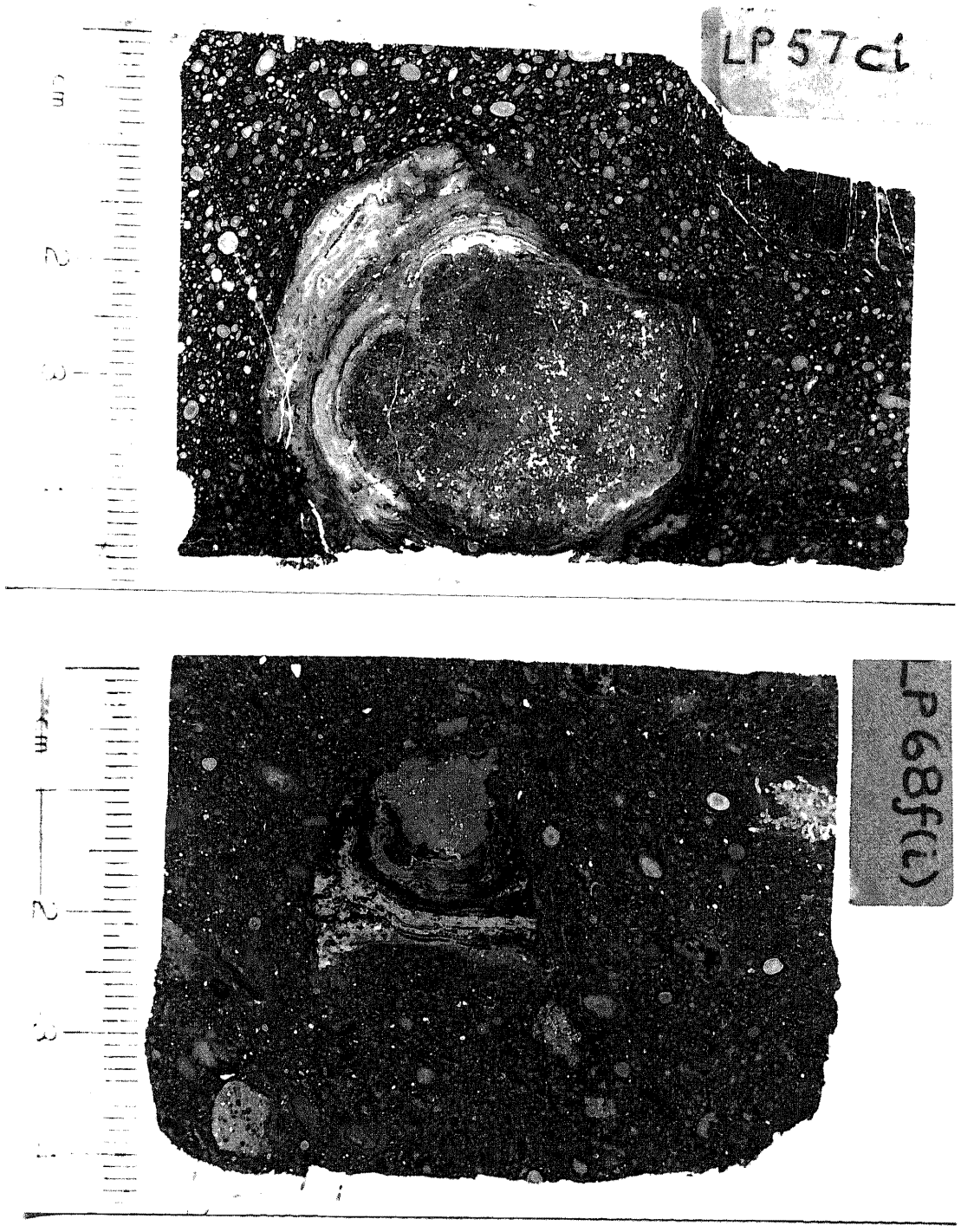

Figure 3.9 Top - Photograph of thin section, float-ironstone in an ooidal wacke-ironstone, LP57C Hen dy Capel [SH 3002 2714]. Stromatolitic encrustation around a ?sponge. The stromatolite is chamositic with abundant fenestrae. Bottom - Photograph of thin section, oncoidal ooidal float-ironstone in an oncoidal ooidal pack-ironstone, LP68F Trefor [SH 3715 4747]. Stromatolitic encrustation of a clast of chamositic mud. The stromatolite is both phosphatic and chamositic and is now partially haematised (black).

within these structures, which tend to be fenestral. Endolithic encrusting stromatolites are particularly evident in the Llŷn ironstones, forming around sponges, broken phosphate nodules and other clasts (Figure 3.9), but are also found at Ffordd Ddu. Ripped-up stromatolite crusts are seen in the disturbed Llŷn ironstones and Aber pack-ironstones.

3.1.5 Other Algal Structures

Other algal structures have been seen in some ironstones. Rod and tube structures, of probable organic origin composed of chamosite and silica, occur in the Ffordd Ddu ironstone. Girvanella tubes have been identified in the Pen y Gaer ironstone (St. Tudwals) within phosphatic nodules, and also from the Llandegai ironstone (Pulfrey 1933a). Hallimond (1925) identified algal borings in ooids from the Llandegai ironstone.

3.1.6 Detrital Quartz

The Bryn Poeth, Trefor, St. Tudwals, Tremadog and Ffordd Ddu localities all contain detrital quartz grains in the ironstone sequence (Appendix 2). At Bryn Poeth, Trefor and St. Tudwals detrital quartz also occurs in the upper pack-ironstones or float-ironstones. Detrital quartz grains found within the ironstone sequences very commonly show strongly developed undulose extinction in crossed nicols. They are most commonly angular silt- fine sand-sized grains. However, well rounded quartz grains with no undulose extinction are also seen, and may occur adjacent to deformed quartz grains. This indicates that deformation of quartz grains did not occur within the ironstones; they are detrital eroded from a metamorphic or possibly acid plutonic terrane.

Visible detrital rutile grains (identified by EPMA) only occur within ooids at Bryn Poeth. Visible detrital zircon grains have only been identified from within the nuclei of a chamosite ooid from Bryn Poeth. The Bryn Poeth ironstone also has a high detrital feldspar content, which from XRF analyses shows it to be a sodic feldspar (albitic).

3.2 SEDIMENTARY TEXTURES AND STRUCTURES

In the previous chapter the sedimentary features of the North Wales Ironstones seen in the field were detailed. In this section sedimentary textures and structures seen in thin section are described in relation to those features already mentioned. The bulk of observations are from the Bryn Poeth locality, where a pervasive cleavage has not affected the original sedimentary structures. These observations are supported by similar textures seen at other localities. A discussion of these sedimentary textures and structures is given at the end of this chapter.

3.2.1 Sorting of the Ironstones

The grain-size distribution of the ferruginous allochems (peloids, ooids and oncoids) in the North Wales Ironstones is presented on a 'box and whisker' plot (Figure 3.10). The measurements, from 30 thin sections, were taken using an eyepiece graticule with a point counter. The data is presented in Appendix 2. The longest length of each grain was measured, although deformed grains were ignored. Some spread of the data must be expected as two dimensional slices through three dimensional objects were taken. However, there is a large variation between samples that can be described and related to the sorting of the ironstones. All facies types of the ironstones, grain-ironstones pack-ironstones, float-ironstones, wacke-ironstones and mud-ironstones, were analysed (Figure 3.10).

The one grain-size analysis of a grain-ironstone (Bryn Poeth) shows a negatively skewed distribution. The majority of the ooids are 0.6-1.0mm in size. This indicates that the grain-ironstones are well sorted with no anomalously large (>1.5mm) ooids, but a wide range of smaller ooids (Figure 4.12.b). Lenses of two different ooid grain-sizes are recognised in the Aber and Pensyflog grain-ironstones. The grain-size of these two different lenses has not been accurately measured. However there is approximately 1 phi grain-size difference between the two (Figure 3.11).

The pack-ironstones, float-ironstones, wacke-ironstones and mud-ironstones are described together in the context of their regional variation. In general the Anglesey and Llŷn ironstones are poorly sorted. They have positively skewed grain-size distributions, large interquartile ranges, and large allochems (oncoids) within them

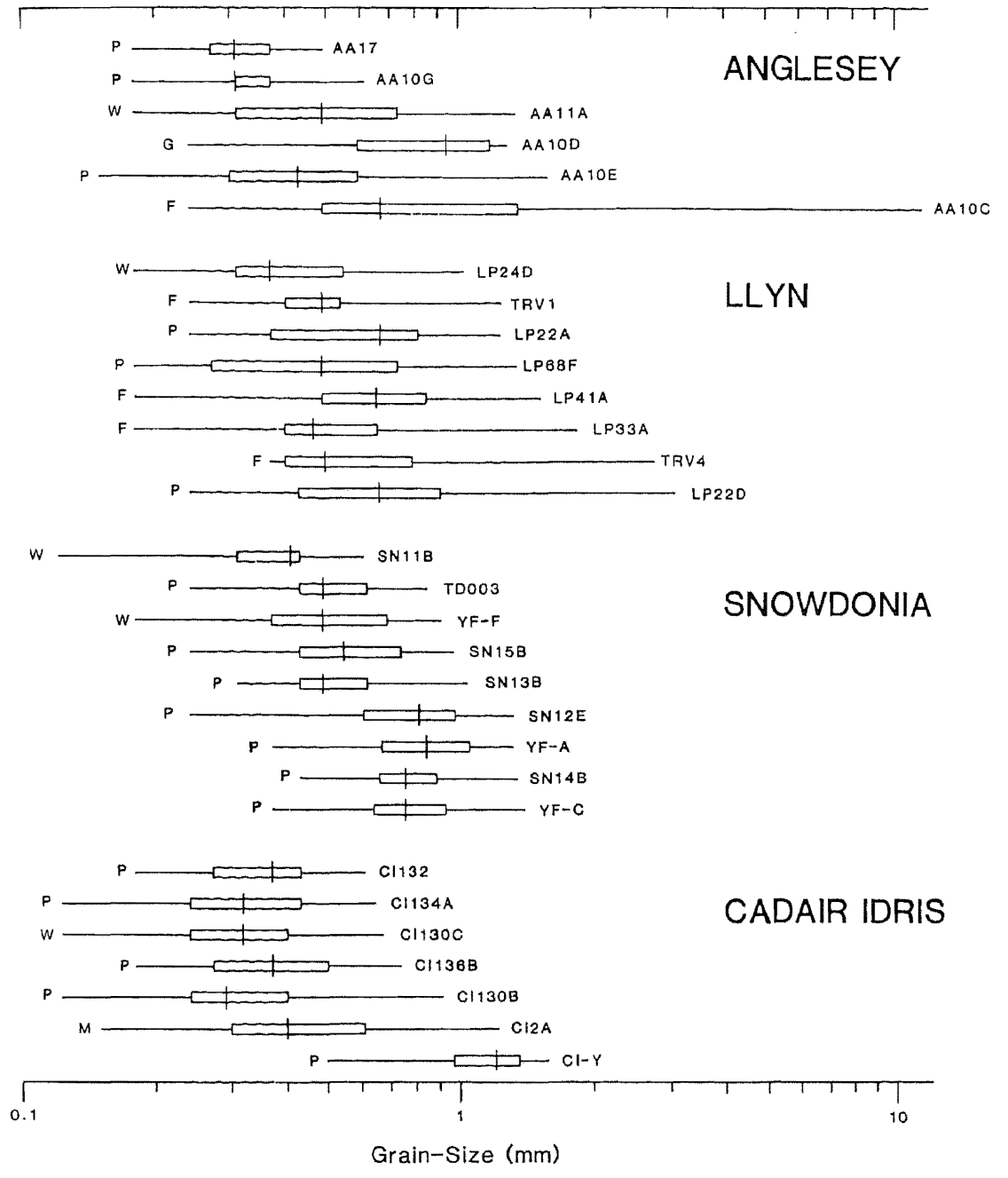

Figure 3.10 'Box and whisker' plot of the grain size analysis of the North Wales Ironstones, showing minimum, maximum, interquartile range and median. Data is presented in Appendix 2, grain-ironstone (G), pack-ironstone (P), float-ironstone (F), wacke-ironstone (W) and mud-ironstone (M). Anglesey - all samples are from Bryn Poeth except AA11A, Llŷn - all St. Tudwals except for TRV1, LP68F, TRV4 Trefor, Snowdonia all Betws Garmon except SN11B and TD003 (Tremadog), Cadair Idris all east except for CI2A and CI-Y (Ffordd Ddu). Thin section numbers are detailed in Appendix 1.

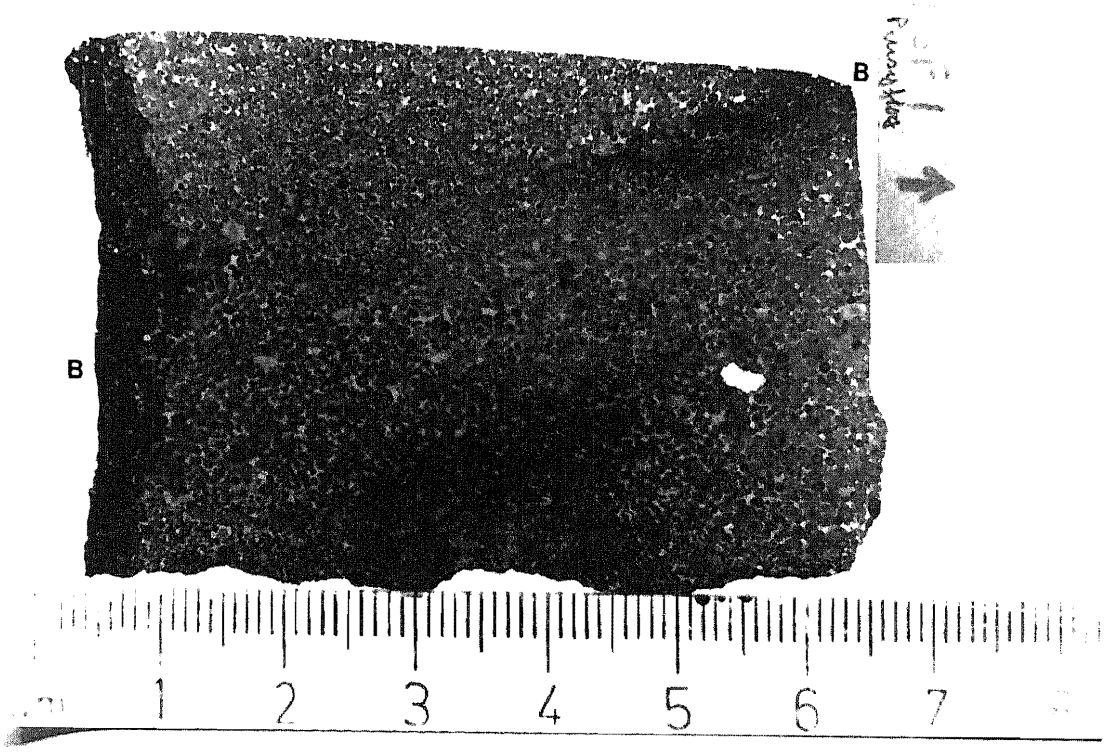

Figure 3.11 Photograph of thin section, chamosite ooidal sideritic grain-ironstone, PSF1 Pensyflog (Tremadog) [SH 5619 3958]. Ooidal grain-ironstone showing current sorting of ooids into finer and coarser beds with approximately one phi grain size difference between the two. Dark patches within the thin section and along the left hand edge are due to weathering of siderite to goethite. Arrow on the thin section indicates vertical orientation in the field. Letter b) indicates bedding.

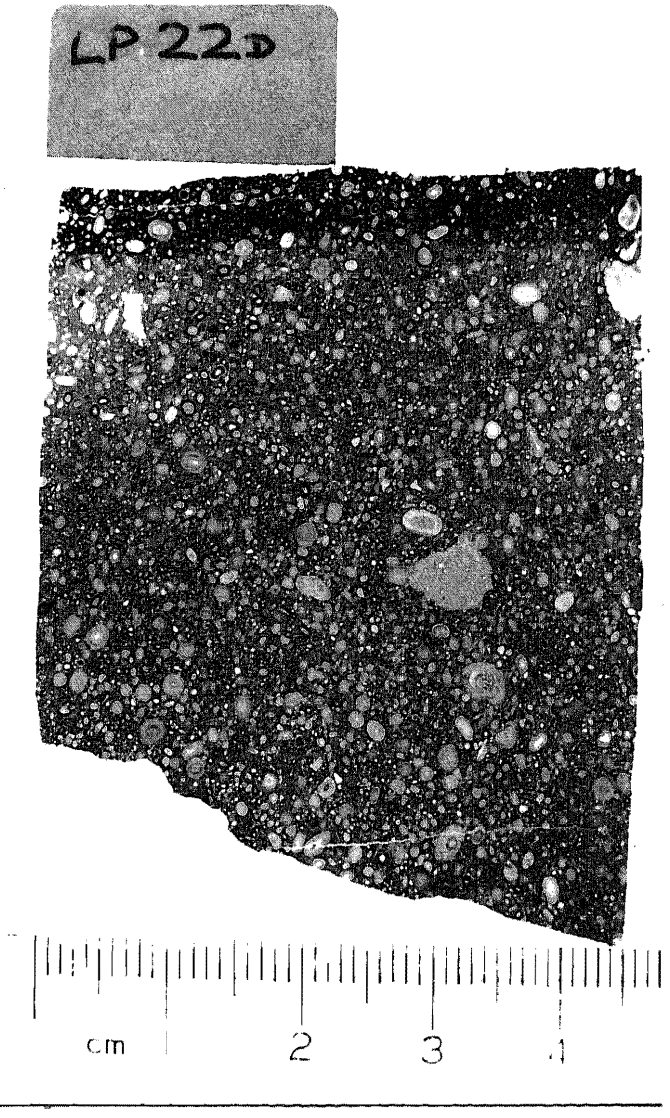

Figure 3.12 Photograph of thin section, oncoidal ooidal pack-ironstone LP22D Pen y Gaer [SH 2990 2821]. A poorly sorted pack-ironstone with a negatively skewed grain-size distribution (Figure 3.10). The poor sorting is due to larger oncoids within the ironstone. Also present are reworked phosphate nodules (centre right) with embayed edges, marking the site of plucked ooids. The dark layer at the top is a weathering rim of goethite.

(Figures 3.12, 3.14.b). By comparison, the Snowdonia and Cadair Idris ironstones are better sorted. They show only a small skewed distribution, have a smaller interquartile range, with no large allochems (oncoids) present (Figure 3.13). However, there are exceptions to this generalisation. Samples AA17 and AA10G (Bryn Poeth) are thin beds of fine-grained ooidal pack-ironstone with a high (3-5%) detrital quartz content (Figure 3.14.a), within an otherwise poorly sorted pack-ironstone. Texturally, their sorting is similar to the Cadair Idris East ooidal pack-ironstones, which are well sorted and a small mean ooid size. The Cadair Idris ironstones show a strong variation in sorting along strike. The Cadair Idris West (CI2A & CI-Y) ironstones are coarse-grained with a wide variation in allochem grain-size (and include oncoids). Those from Cadair Idris East are fine-grained and well sorted, and do not contain oncoids.

3.2.2 Current Structures

One characteristic feature of the North Wales Ironstones is that they do not show cross-bedding or other obvious current structures, which are common in other oolitic ironstones (Van Houten & Purucker 1984; Van Houten & Bhattacharyya 1982). Despite this lack of current structures, a number of features of the ironstones imply current reworking. The typical appearance of an ironstone sequence is as follows, using Bryn Poeth as the example.

Laminated silty chamositic mud-ironstones in the lower part of the Bryn Poeth sequence (Figure 2.4) grade upwards from parallel-laminated muddy siltstone at the base to silty chamositic mud-ironstone within 10cm. This sequence grades up through chamositic mud-ironstone and wacke-ironstone (or pack-ironstone lenses in mud-ironstone) into pack-ironstone and capped by a thin grain-ironstone. Ooids in the wacke-ironstone are concentrated into centimetre thick lenses (Figure 3.15) which are laterally impersistent, poorly sorted, do not have sharp bases and show a strong variation in thickness. These ooid lenses have a high fine-sand/silt-sized grade quartz grain content. This concentration of quartz grains with ooids in lenses indicates that ooids were reworked. Chamositic mud drapes devoid of any silt occur directly over these ooid lenses, although the chamositic muddy matrix between lenses of ooids does contain some silt and ooids. Within this sequence occur small scour and fill structures (Figure 2.5), cutting into the wacke-ironstones or pack-ironstone lenses, and

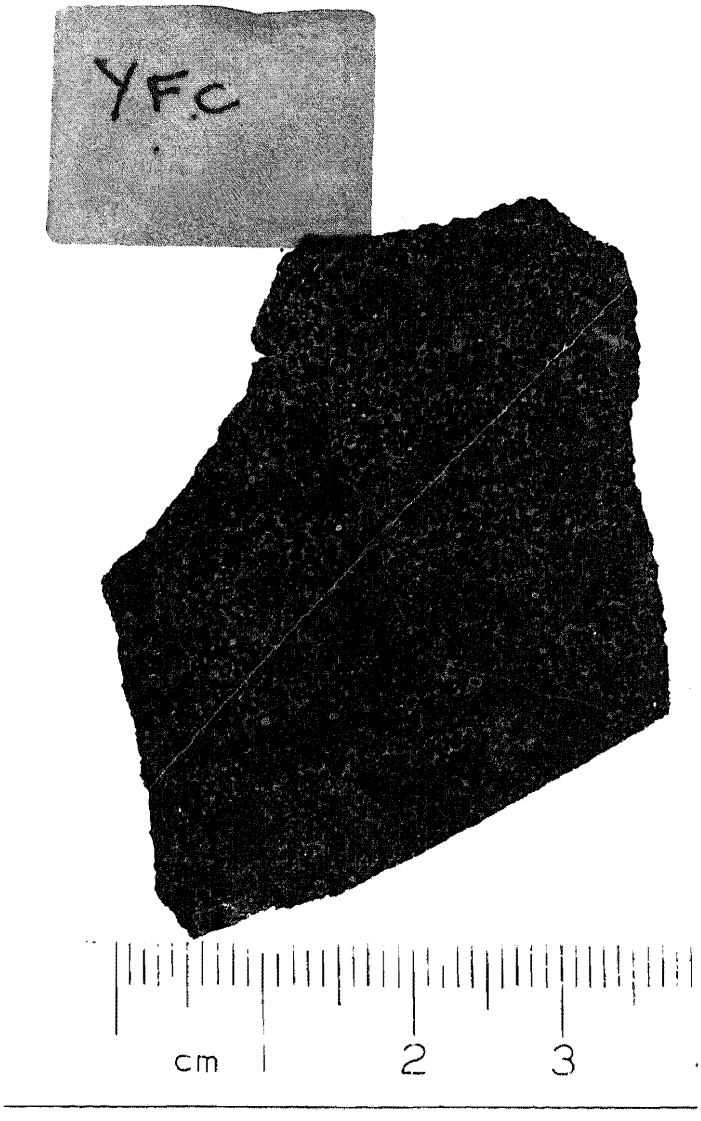

Figure 3.13 Photograph of thin section, magnetite ooidal chamositic pack-ironstone, YF-C Betws Garmon (loose grab sample). This is a well sorted ooidal pack-ironstone with a non-skewed grain-size distribution. The ironstone is now partially replaced by magnetite (Chapter 5), with magnetite ooids (black) in a muddy matrix. Note the uneven distribution of mud in the matrix.

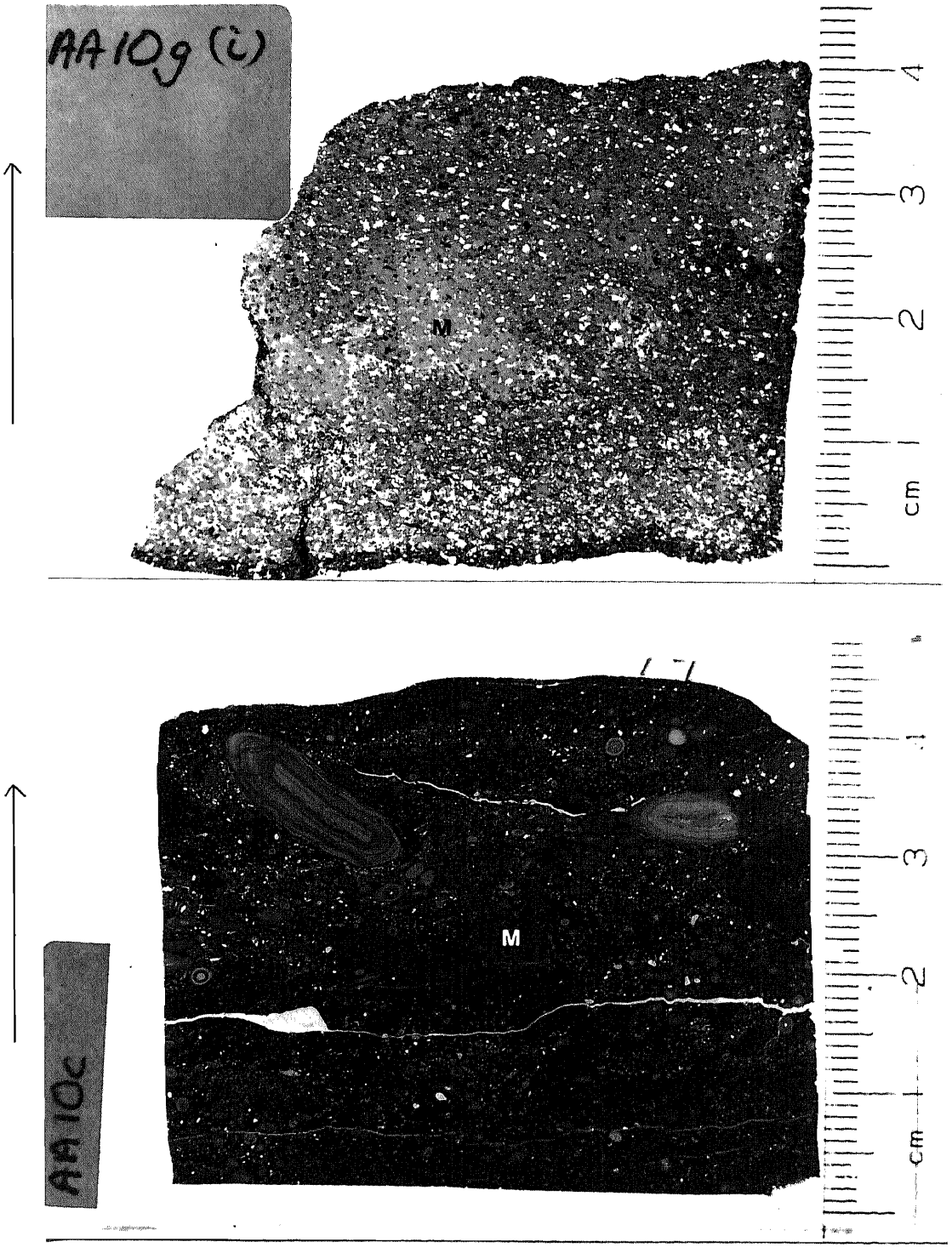

Figure 3.14 Top - photograph of thin section, ooidal pack-ironstone, AA10G Bryn Poeth [SH 6016 7958]. A fine-grained pack-ironstone from within the main pack-ironstone (Figure 2.4 section A) showing a high detrital quartz content decreasing upward. Bottom - Photograph of thin section, oncoidal float-ironstone in an ooidal wacke-ironstone, AA10C Bryn Poeth (Figure 2.4 section B) [SH 6016 7958]. Poorly sorted wacke-ironstone containing very large oncoids, spastoliths and burrow mottling in the centre of the photograph. Burrow mottling in both ironstones (M) is indicated by the uneven mud distribution.

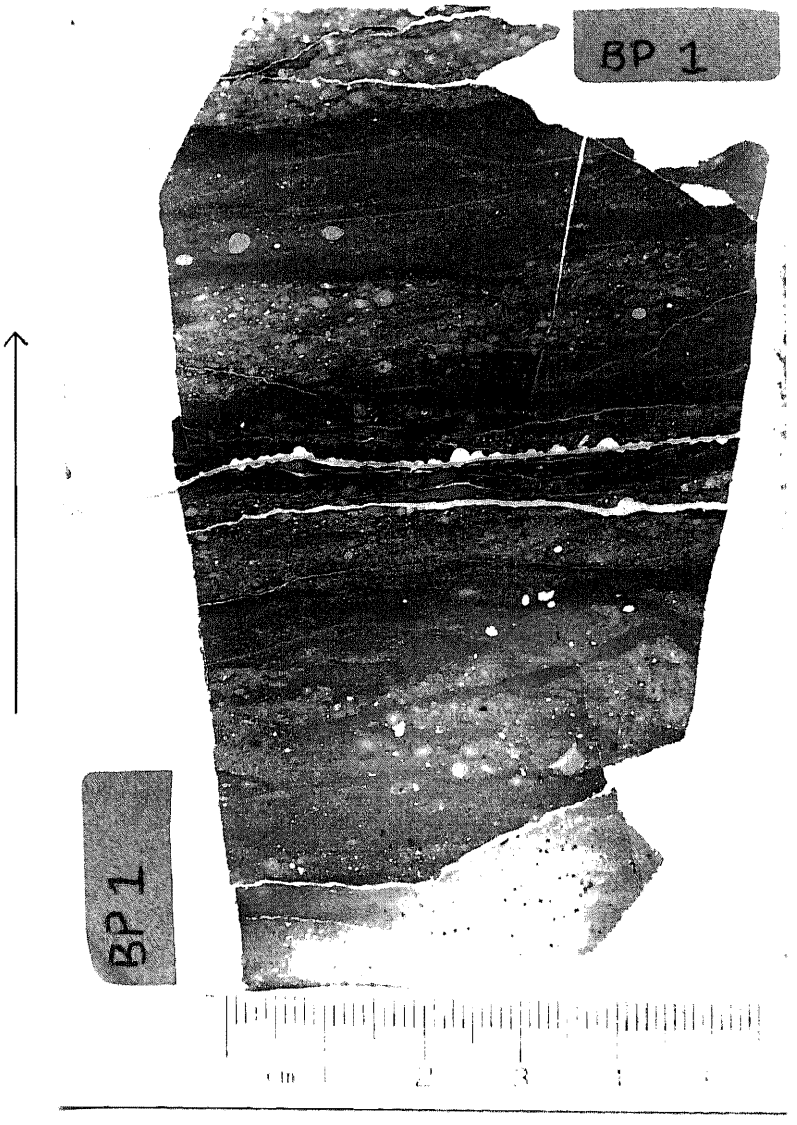

Figure 3.15 Photograph of thin section, ooidal pack-ironstone lenses in chamositic mud-ironstone, BP1 Bryn Poeth (Figure 2.4 section B) [SH 6016 7958]. The ooidal lenses also contain detrital quartz and feldspar, and mud drapes devoid of detritus occur above these lenses. Spastoliths are present in the middle of the thin section showing deformation of ooids with compaction.

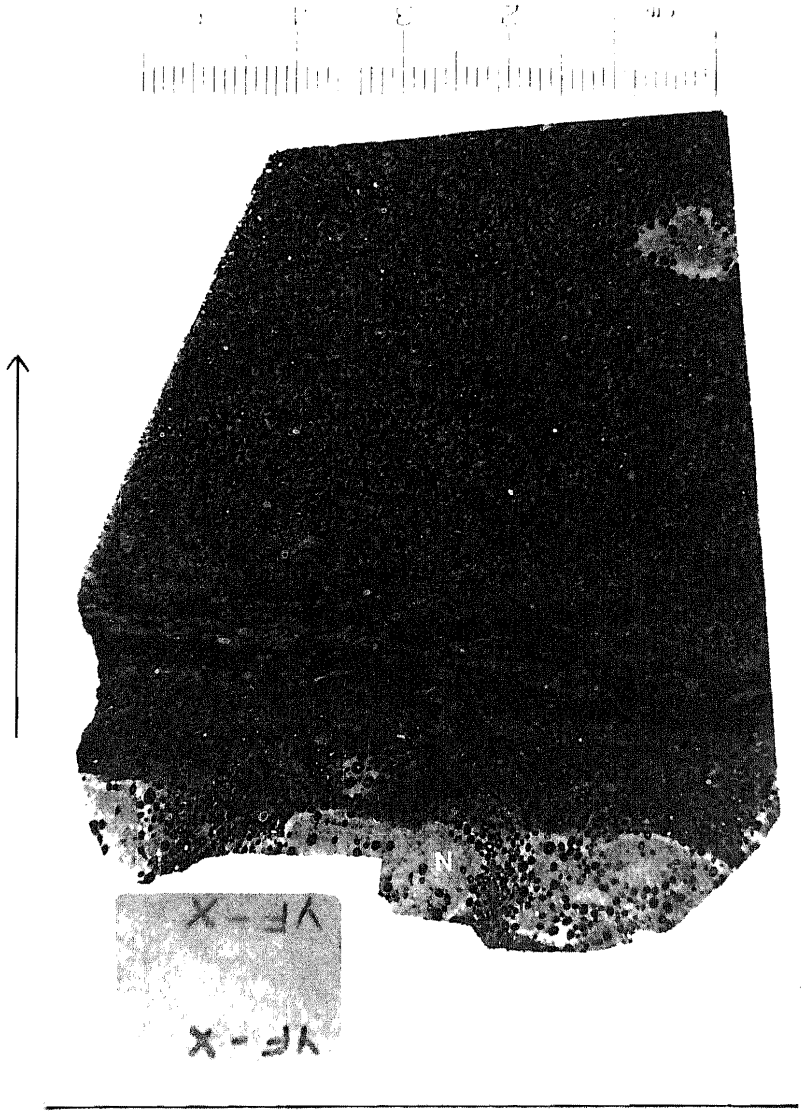

Figure 3.16 Photograph of thin section, magnetite ooidal chamositic pack-ironstone, YF-X Betws Garmon (loose grab sample). Chamosite mud lense in a pack-ironstone. Note the concentration of phosphate nodules below the mud lense, which may represent a more intensively bioturbated horizon. Ooids are now replaced by magnetite (black) in a chamositic matrix except for those ooids in the mud lense. There is also deformation of the ooids in the mud lense (see Figure 3.3).

contain fining-up sequences. No other ironstones contain facies sequences which are capped by thin grain-ironstones. Description of ooid lenses of different sizes in grain-ironstones has been given in the previous section.

All other ironstone localities show a similar trend of increasing ooid content and decreasing mud content. A number of other ironstone localities show lenses of ooids and/or oncoids, which may be devoid of detrital quartz, within mud-ironstones (Chapter 2) and so is not a feature unique to the Bryn Poeth ironstone. Mud lenses have only been seen at Betws Garmon (Figure 3.16), but mud patches are a common feature of all pack-ironstones, with a mottled texture of dark muddy patches and bright green chamosite mud patches (Figure 3.14), discussed below (Section 3.2.4).

3.2.3 Diamictic Structures

Ferruginous debris flows, found within the ironstone sequences at Trefor, St. Tudwals, Llanberis Valley and Tremadog, have been described in Chapter 2. Texturally they consist of broken ooids, reworked phosphate nodules with sharp or embayed edges (marking the sites of plucked ooids), ripped up rafts of chamosite mud, and clasts of laminated siltstones in a muddy silty matrix (Figure 3.17). The flaking and folding of the siltstone laminae and the diffuse nature of the margins of some clasts, showing mixing with the surrounding matrix, all indicate that the clasts were derived from incoherent break-up of intermittently slumped masses, and so are not storm reworked deposits. At Pen y Gaer sub-angular volcanic fragments (up to 10cm) also occur in the silty muddy matrix (Figure 3.18).

3.2.4 Bioturbation Structures

There is a lack of obvious faunal activity within the ironstones, as ooid lenses and siltstone laminae are preserved. This is despite the evidence of the presence of some macrofauna within the ironstones (sponge spicules and inarticulate brachiopods). However, there are two lines of evidence to indicate bioturbation of the ironstones. Firstly, burrow mottling has been identified in the Bryn Poeth ironstone (Figure 3.13). Similarly this can be implied for other ironstone localities. The theoretical ooid content for pack-ironstones is approximately 70%. A large number of pack-ironstones show considerably

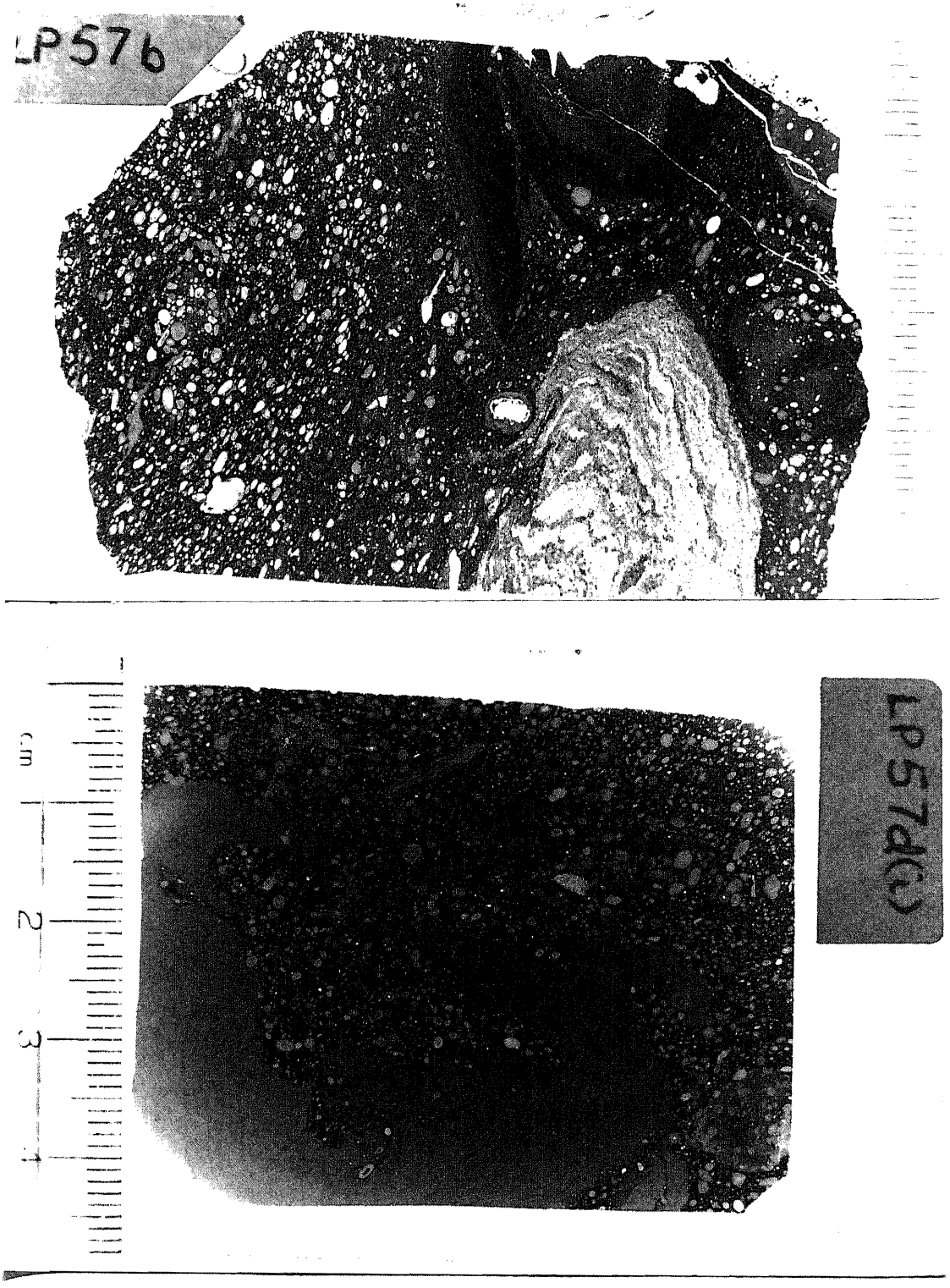

Figure 3.17 Top - Photograph of thin section, phosphatic silicic float-ironstone in an ooidal wacke-ironstone, LP57B Hen dy Capel [SH 3002 2714]. Disturbed bed showing ripped-up and deformed clast of laminated siltstone, ripped-up lenses of dark mudstone and broken phosphate nodules. Bottom - Photograph of thin section, phosphatic chamositic float-ironstone in an ooidal wacke-ironstone, LP57D Hen dy Capel [SH 3002 2714]. Disturbed bed containing ripped-up and deformed raft of chamosite mud within a wacke-ironstone. Its unusual shape indicates that it must have been transported only a short distance.

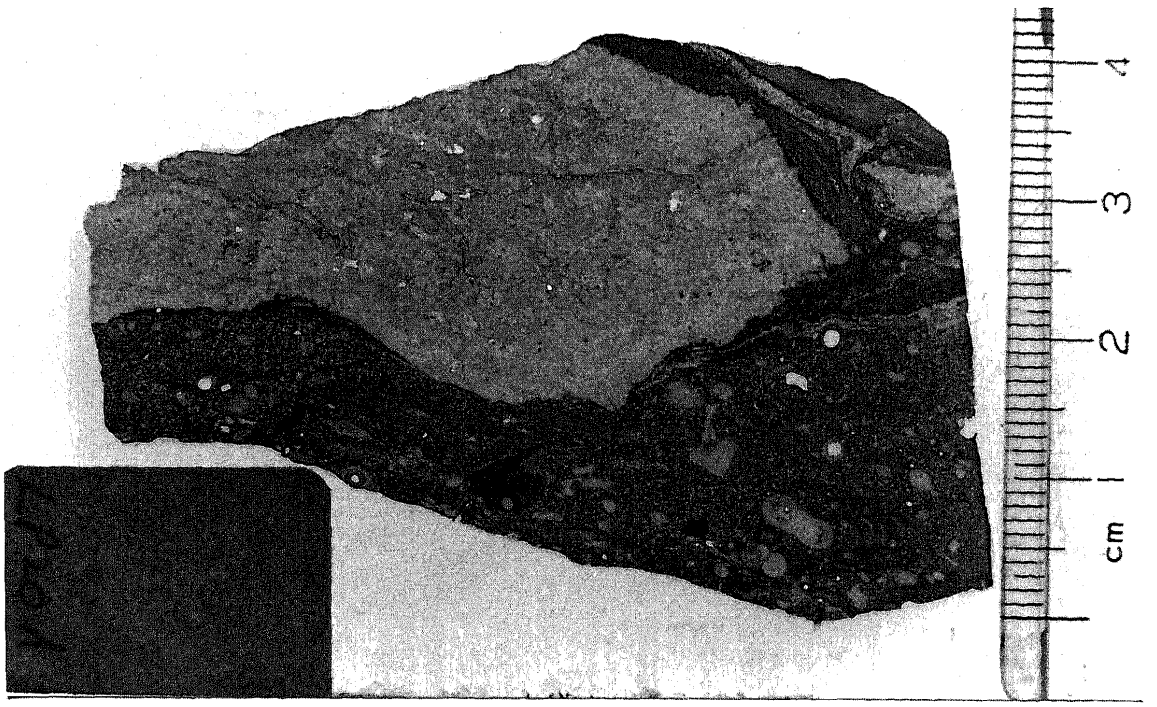

Figure 3.18 Photograph of thin section, debris flow, LP20A Pen y Gaer [SH 2984 2829]. Volcanic clast in disturbed bed in silty muddy matrix containing broken and fragments of ooids (Figure 3.4).

less than this maximum value (Appendix 2). On closer examination of the thin sections it is seen that these pack-ironstones are inhomogenous; they contain muddy patches with ooids that are mud-supported. Some wacke-ironstones listed in Appendix 2 have the appearance of a pack-ironstone but have a low ooid content. For example sample YF-F is a wacke-ironstone, but occurs within the upper pack-ironstone facies at Betws Garmon, which is predominantly a grain-supported sediment. This muddy matrix most commonly occurs as a dark organic-rich chamosite mud, but patches of bright green featureless chamosite mud also occur. This variation is described in further in Chapter 4 where the difference in mud distribution has had a marked effect on diagenesis.

Secondly, some evidence of bioturbation is present in the pack-ironstones. Diagenetic phosphate nodules in pack-ironstones preserve a much looser ooid packing than that within the pack-ironstone. Either this looser packing texture represents the original state of all the sediment, with later compaction forming a grain-supported sediment, or that the original sediment was grain supported with areas of looser packing within it, later phosphatised. The difference between pack-ironstones and grain-ironstones is that the latter show some sedimentary structures, do not have a muddy matrix and do not contain nodules. Therefore the mottling of pack-ironstones and the presence of phosphate nodules would suggest that pack-ironstones are most likely bioturbated grain-ironstones.

3.3 GEOCHEMISTRY OF THE IRONSTONES

Previous chemical analyses of the North Wales Ironstones (Strahan et al. 1920; Hallimond 1925; Pulfrey 1933a; and Groves 1952), were undertaken mainly to determine the iron content of the ore, except for Pulfrey (1933a) who analysed the rock for it's chlorite composition. Weinberg (1973) analysed 31 ironstone samples by atomic absorption spectromphotometry (AAS) for major elements and 6 trace elements (Ba Co Cr Ni Sr V). Weinberg's (1973) results have been compared with this present study as a cross-reference check. Weinberg (1973) used the geochemistry of the North Wales Ironstones to infer lateritic weathering as the source of iron.

There is little background information on the geochemistry of oolitic ironstones. James (1966) classified ironstones on the basis of their geochemical characteristics. Siehl & Thein (1978) implied a lateritic weathering origin for the Minette ironstone on the basis of it's geochemical variation. Myers (1989) analysed, by portable gamma ray spectrometry for potassium, thorium and uranium, the Cleveland Ironstone Formation to show that it was derived from lateritic weathering.

The processes of sedimentation, diagenesis and alteration should be reflected in the geochemistry of the ironstones. In this section, the overall geochemical variation of the ironstones is described and interpreted in terms of the above processes. The sedimentary geochemical variation and rare earth elements are then described in more detail. The localities of the samples analysed are given in Appendix 1, and the results for both XRF and ICP are given in Appendix 5.

3.3.1 Major Element Variation

The three most abundant oxides present are $Fe_2O_3(T)$, SiO_2 and Al_2O_3, indicating that the mid-Ordovician North Wales Ironstones are predominantly composed of chamosite. The variation in the proportion of these three oxides is shown in Figure 3.19. Most of the ironstone bulk geochemical compositions lie close to that of chamosite (an average value from EPMA). Analyses trending towards SiO_2 and $Fe_2O_3(T)$ are attributable to the presence of detrital quartz in the wacke-ironstones, and the presence of magnetite or siderite in the pack-ironstones respectively. Grain-ironstones (from Aber) lie close

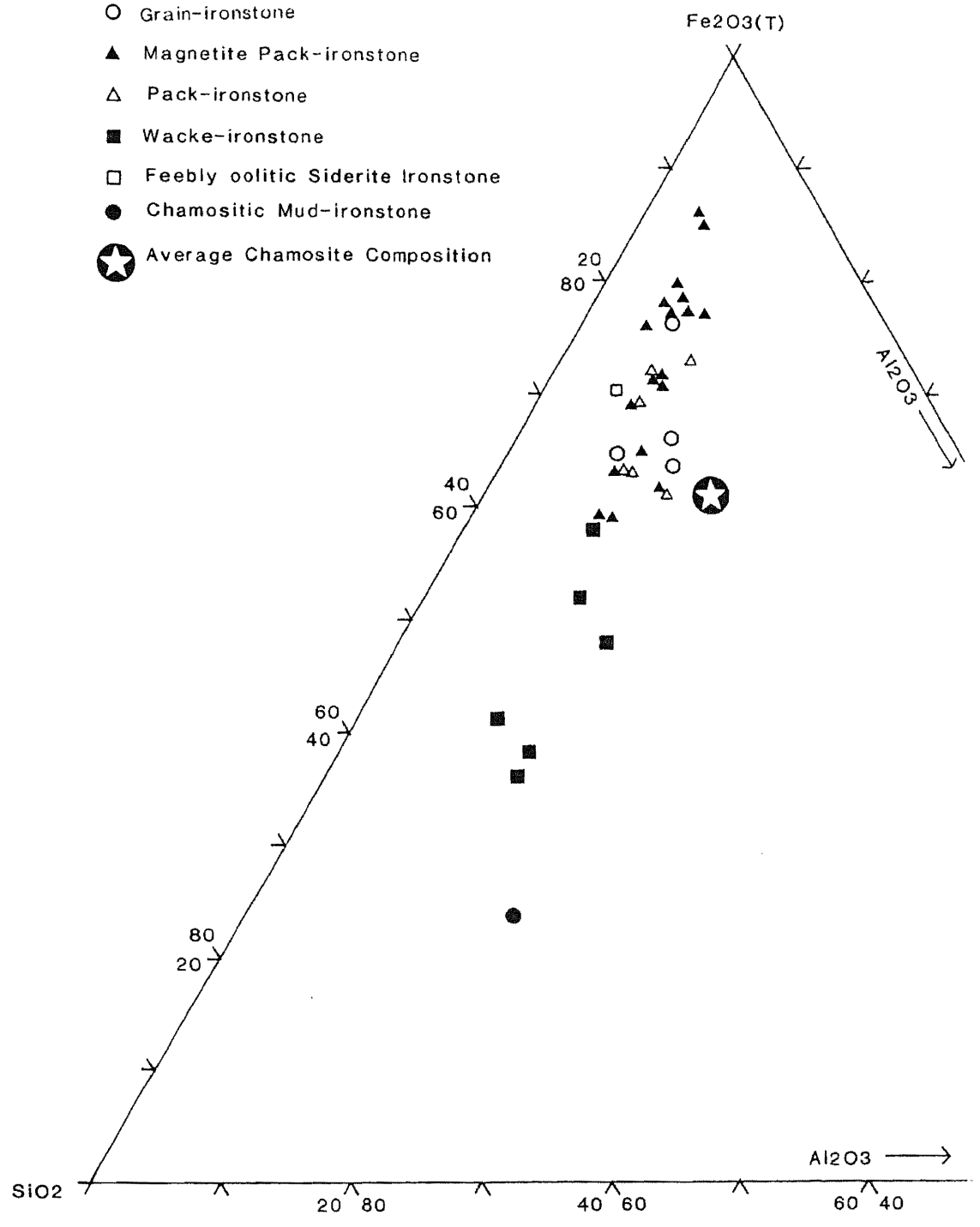

Figure 3.19 Triangular Fe2O3(T), SiO2, Al2O3 plot of the XRF data showing the distribution in composition of the different ironstones facies types, and also distinguishing between magnetite-bearing and non magnetite-bearing pack-ironstones. Average chamosite composition is calculated from the EPMA data.

to the average value of chamosite, except for one which has a higher $Fe_2O_3(T)$ content, due to surficial weathering. The one chamositic mud-ironstone analysed plots away from the mixing line between chamosite and quartz, and indicates excess Al_2O_3 and SiO_2 than can be accounted for by chamosite and quartz. The high potassium content of this rock indicates the presence of other clays (illite).

The oxidation state of iron in the ironstones is very variable. The ratios are shown in the geochemical data (Appendix 5) as the oxidation-reduction index (ORI - $Fe^{2+}/[Fe^{2+} + Fe^{3+}]$). High values are ferrous and low values are ferric. This variation in oxidation state naturally falls into three groups: predominantly ferrous (ORI>0.6), both ferrous and ferric (0.6>ORI>0.4) and predominantly ferric (ORI<0.4). This variation is represented in Table 3.1.

	MIDDLE OF INTERVAL OF ORI	NUMBER OF OBSERVATIONS		
	0.1000	1	*	
FERRIC	0.1500	0		
	0.2000	1	*	Group iii
	0.2500	0		
	0.3000	2	**	
	0.3500	0		———
	0.4000	0		
	0.4500	5	*****	
	0.5000	4	****	Group ii
	0.5500	3	***	
	0.6000	0		———
	0.6500	3	***	
	0.7000	5	*****	Group i
FERROUS	0.7500	5	*****	
	0.8000	6	******	

Table 3.1 A histogram of the distribution of the ORI for the North Wales Ironstones (see text for details).

Group i comprises the majority of the ironstone samples, and are dominantly ferrous in nature. This group includes all those ironstones which contain siderite, but also includes those magnetite-bearing ironstones (Figure 3.19) which only contain a small quantity of magnetite (001, 002, 003, 008 - Betws Garmon and 011, 013 - Cadair Idris). The ferric component in this group is either contained in

magnetite or as iron oxides formed by surficial weathering of the ironstones which was not removed during sampling.

Group ii comprises the majority of the magnetite-bearing ironstones, plus two other samples, which all contain roughly equal amounts of ferrous and ferric iron. The two exceptions are 017 (N. Anglesey) a weathered siderite ironstone, and 030 (Pen y Gaer) a weathered siderite chamosite oolitic ironstone.

Group iii is only a small group of ironstones dominated by ferric iron. Two of the four samples are weathered magnetite-rich ironstones (026 & 027 Tremadog). The remaining two are strongly weathered siderite-rich ironstones (015 Bryn Poeth, 033 Betws Garmon).

The effect of surficial weathering can be demonstrated in Figure 3.20, a plot of ORI against Fe_2O_3. This shows a trend of decreasing ORI with increasing Fe_2O_3. All samples have been affected to some degree by weathering. Only those ironstones that are strongly weathered fall off the trend, where the increase in oxidation is not accompanied by an overall increase in iron content (015 Bryn Poeth, 033 Betws Garmon). The total iron content of the ironstones shows a positive correlation with ferric iron (r=0.681) indicating that total iron increased with the addition of ferric iron. It is considered that the iron was deposited originally as Fe^{II}, with later magnetite replacement (Section 5.1.4)(and to a lesser extent weathering) increasing the Fe^{III} content.

Magnesium occurs in small amounts (less than 2% MgO) in the ironstones, as a minor constituent of chamosite, siderite and stilpnomelane. The calcium and phosphorus contents are controlled by diagenetic phosphate (apatite). The average values for all the ironstones are 4.1% CaO and 2.9% P_2O_5, although maximum values of 13.4% CaO and 9.2% P_2O_5, in nodule-rich ironstones (025 - debris flow Tremadog, 040 - Bwlch y Cywion). The grain-ironstones from Aber have the lowest phosphorus contents, even though there are no nodules present they still contain an average 1.16% P_2O_5.

The ironstones are extremely low in both potassium and sodium, most values falling below the detection limit of the XRF. The only clay mineral in the ironstones is chamosite, explaining the absence of the alkali metals which are normally present in other clay minerals in the surrounding mudstones. The small amounts of potassium in some of the Pen y Gaer and Bryn Poeth ironstones is due to the presence of detrital illite, detected by EPMA. However, there are two exceptions to the low alkali content. Those ironstones with a significant

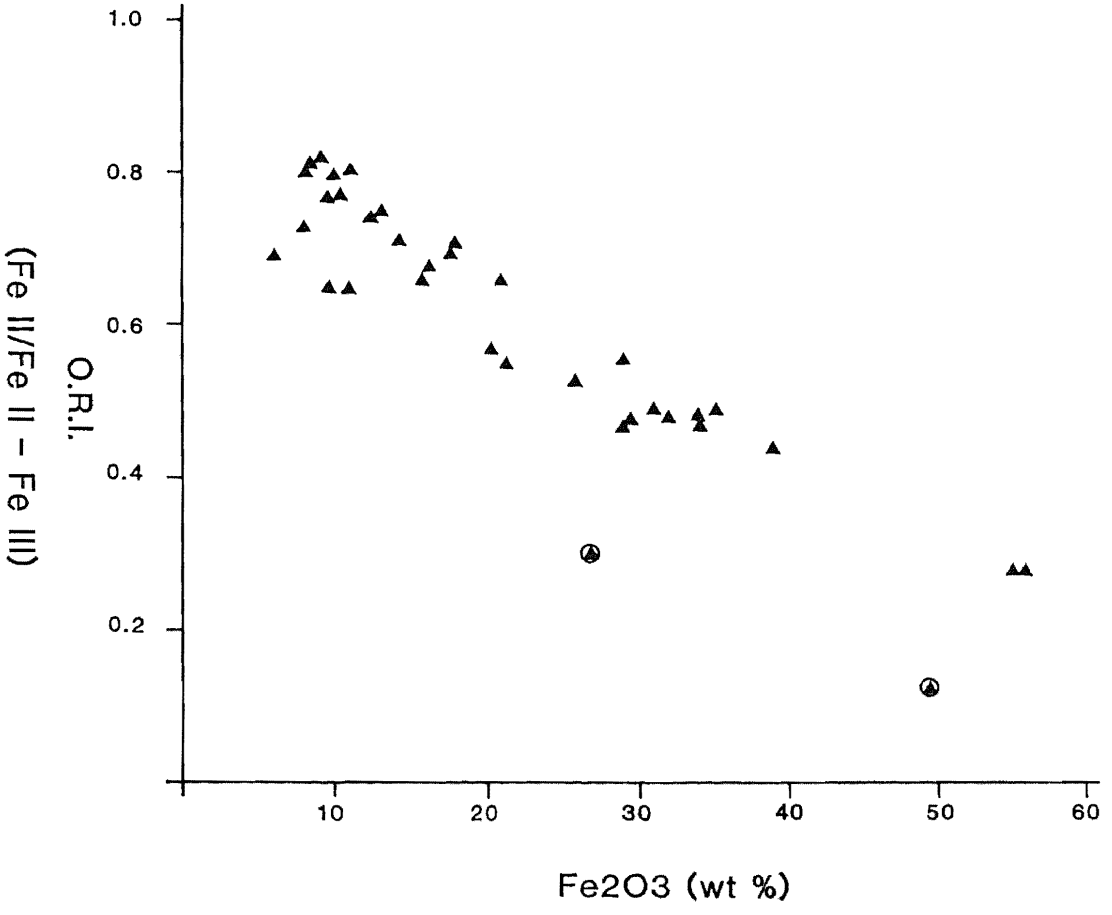

Figure 3.20 Plot of ORI against Fe2O3. This indicates the trend of a decrease in the index with increasing ferric iron. The two ironstones, encircled, that are strongly weathered (015 Bryn Poeth, 033 Betws Garmon) fall off the trend indicating an increase in ferric iron (due to surficial weathering) not accompanied by an increase in iron content.

potassium content, up to 0.71% K_2O, (Samples 011-014 Cadair Idris, 022 Tyllau Mwn, 023 024 Rhyd, and 040 Bwlch y Cywion) show the presence of stilpnomelane (Chapter 5). The one chamositic mud-ironstone also has a high (2.4% K_2O) potassium content, due to the presence of illite. Those ironstones with high levels of sodium, up to 0.47% Na_2O, contain detrital feldspar (Bryn Poeth), although two Rhyd samples (023 024) and two Aber samples (018 021) may contain sodic micas formed during hydrothermal alteration.

3.3.2 Statistical Analysis

Multivariate statistical analyses of the North Wales Ironstones helped to identify natural geochemical groupings of elements within the data set. This gives an unbiased description of the variation in geochemistry, and so give the best interpretation of inter element relationships and their possible mineralogical controls. Siehl & Thein (1978) showed stratigraphic and regional geochemical trends in connection with the genesis of the Minette Ironstones using Hierarchical Cluster Analysis. Jarvis (1980) was able to identify chemical changes which occur during the lithification and mineralisation of Cretaceous phosphatic chalks and hardgrounds using Principle Component Factor Analysis. Multivariate statistics is not used to replace interpretation of the geochemical data, but merely assembles it into a more readily interpretable form.

In this study two different methods were used, hierarchical cluster analysis and principal component factor analysis (Heley 1980). Hierarchical cluster analysis is a technique used mainly for classification purposes. The usual application is to find groups (or clusters) of samples whose members are very similar to other members in the cluster but which have much lower similarity with members of other clusters. Similarity is defined by the 'distance' between samples, which is the root mean square of differences between points taken over all variates. However, there are a wide variety of different clustering methods that can be used (Jones 1988). The Vax mainframe system has 7 different clustering techniques (Heley 1980). These clustering methods were tried, some could be ignored as they produced a chained dendrogram (Jones 1988). Of these, simple average clustering of the data set was used. This is because it manipulates the data the least.

Factor analysis reduces complex relationships between large numbers

of variables to a small number of relationships and identify mechanisms that are working within the system, which explain most of the variance in the original data. Variables are grouped on the basis of their intercorrelation into factors, which are associations of highly correlated variables. These factors, which are statistically the dominant features of the data variation, are derived from the Pearson Correlation Matrix.

Simple average cluster analysis of the geochemical data (Figure 3.21) identified five main groups of elements and two isolated elements, differentiated at a similarity level of 1.25. Group 1 was further subdivided to produce two geochemically distinct subgroups, at a similarity level of 1.0. These groups are briefly described here and dealt with in more detail in the appropriate chapters.

Group 1a - includes the major elements SiO_2, Al_2O_3, TiO_2, MgO, Na_2O and MnO and trace elements Zr, Nb Sc. These are described as detrital (Section 3.3.3), but also include magnesium and manganese which are also contained in diagenetic siderite (Section 4.3) and metasomatic stilpnomelane (Section 5.2).

Group 1b - are the three alkali metals associated with stilpnomelane, K_2O, Ba and Rb (Section 5.2).

Group 2 - is Cu and S which are of hydrothermal origin in chalcopyrite (Section 5.4).

Group 3 - are Fe_2O_3(T) and Fe_2O_3, with a poor association with Ce, and related to magnetite development within the ironstones (Section 5.1).

Group 4 - is a group with little internal association (except Co and Ni) made up of trace elements.

Group 5 - is dominated by the very close association between CaO and P_2O_5 (apatite) and relates to diagenetic phosphate within the ironstones (Section 4.2). Within this group Y is associated with apatite, Cr and V are closely associated together and with Sr are included in this group.

Factor analysis shows many similarities with cluster analysis, but allows interpretation on the major controls of the variation within the data set. Five factors control the majority of the variation within the data (Table 3.2) and since the eigen vectors are mutually perpendicular these mechanisms are statistically independant of one another.

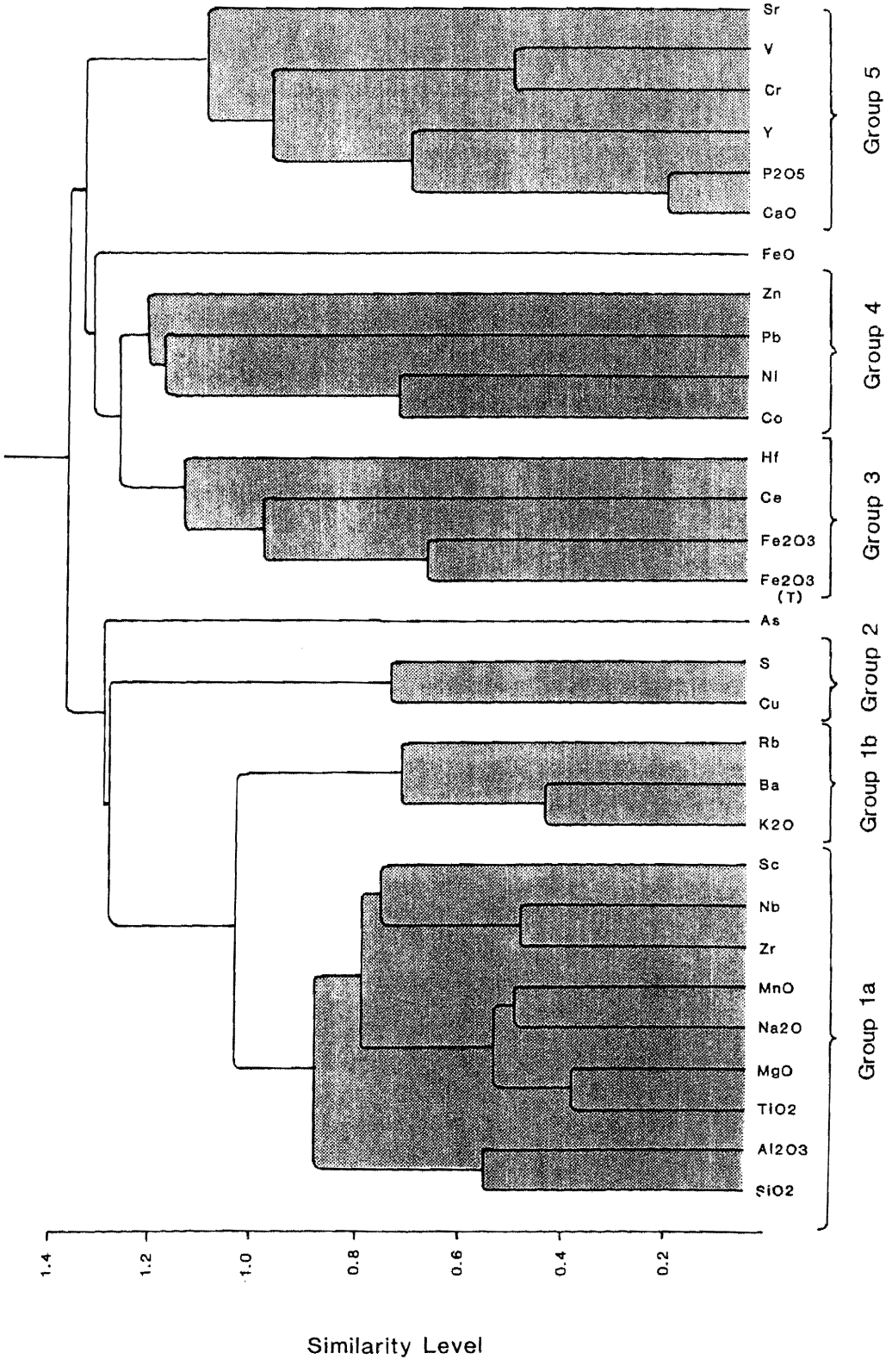

Figure 3.21 Simple average hierarchical cluster analysis of the XRF data set. The groups are divided at a similarity level of 1.25. Also separated are two elements (FeO & As) which do not associate with any group. Group 1 is further subdivided at a similarity level of 1.0. The six groups are highlighted by shading.

Element	Factor 1	Factor 2	Factor 3	Factor 4	Factor 5	Mean	St. Dev.
SiO2	0.626	-.552	0.205	0.172	-.022	20.28	8.94
Al2O3	0.842	-.254	0.282	0.094	-.281	7.50	2.76
TiO2	0.915	-.042	-.006	-.027	-.196	0.38	0.16
Fe2O3(T)	-.607	0.628	-.364	0.175	0.073	52.30	12.80
FeO	-.103	0.177	-.468	-.485	-.190	27.26	8.26
Fe2O3	-.474	0.510	-.020	0.547	0.201	22.30	13.60
MgO	0.528	-.258	0.131	-.311	0.199	1.28	0.53
CaO	-.334	-.628	0.493	-.233	-.098	4.59	2.39
NaO	0.280	0.582	0.578	0.174	0.161	0.05	0.10
K2O	0.490	-.432	-.124	0.669	-.044	0.15	0.43
MnO	0.522	0.578	0.230	-.301	0.111	0.33	0.45
P2O5	-.393	-.628	0.510	-.124	-.126	3.21	1.70
As	0.118	-.175	0.207	-.012	-.362	52.0	146.0
Ba	0.445	-.411	-.022	0.603	-.250	236.0	898.0
Ce	-.285	0.442	0.531	0.381	0.016	210.2	78.1
Co	0.143	0.671	0.289	0.216	0.254	41.1	23.2
Cr	-.652	0.096	0.154	0.121	-.494	220.9	82.5
Cu	0.003	-.117	0.224	-.112	0.737	34.1	19.3
Hf	-.043	0.353	-.209	0.103	0.133	5.4	4.7
Ni	0.435	0.514	0.416	-.014	0.001	58.9	67.2
Nb	0.858	0.219	0.009	-.005	-.092	9.8	4.6
Pb	0.026	0.229	0.687	0.112	0.107	19.9	15.2
Rb	0.395	-.281	-.278	0.640	0.173	19.6	18.6
S	-.028	-.461	0.157	-.148	0.711	12794.0	23234.0
Sc	0.527	0.507	-.009	-.388	-.197	17.5	10.0
Sr	-.577	-.309	0.208	-.141	0.039	241.0	185.0
V	-.803	0.144	0.256	0.151	-.307	355.0	119.0
Y	-.373	-.157	0.719	-.040	-.337	84.5	23.4
Zn	0.180	0.383	0.187	0.000	-.212	129.7	79.0
Zr	0.885	0.226	0.108	-.172	-.204	86.5	33.2
Eigen Values	7.713	5.014	3.342	2.602	2.260		
%-age of Variation	25.71	16.71	11.14	8.67	7.53		
Cumulative %-age of variation	25.71	42.42	53.56	62.23	69.77		

Table 3.2 Principal component factor analysis of the North Wales Ironstones XRF data.

Factor 1 - Geographical Distribution This factor controls 25.7% of the variation within the ironstones. The detrital group of elements (Group 1a above) have high positive loadings, plus positive loadings for the stilpnomelane group elements (Group 1b). The Group 3 elements (Fe_2O_3(T) and Fe_2O_3) plus Cr, V and Sr of Group 5 all have high negative loadings. This opposite nature is also shown by the cluster analysis which shows that the positive (Group 1) and negative loadings (Groups 3 & %) have the least similarity. This factor distinguishes the fact that different ironstone localities, because of their localised nature, have undergone differing post-depositional alterations. It distinguishes those ironstones with a high detrital content, plus those with stilpnomelane, from the magnetite ironstones, where the increase in iron has a diluting effect on the immobile elements (Section 5.1).

Factor 2 - Magnetite Replacement This factor controls 16.7% of the variation in the data set. Fe_2O_3(T), Fe_2O_3 (Group 3), Co, Ni (Group 4) and MnO all have positive loadings and can be related to the formation of magnetite within the ironstones. Apatite (CaO, P_2O_5 - Group 5) and stilpnomelane (K_2O, Ba, Rb - Group 1b) have negative loadings. The opposite nature between magnetite and stilpnomelane replacement is confirmed by the fact that magnetite and stilpnomelane have an antipathetic relationship (Chapter 5).

Factor 3 - Diagenetic Phosphate Growth controls 11.1% of the variation, with high positive loadings for Y, CaO and P_2O_5, corresponding to Group 5 of the cluster analysis.

Factor 4 - Metasomatic Stilpnomelane Replacement controls 8.7% of the variation with positive loadings for K_2O, Ba and Rb corresponding to Group 1b of cluster analysis.

Factor 5 - Hydrothermal Alteration controls 7.5% of the variation with positive loadings for Cu and S, indicating the presence of chalcopyrite, corresponding to Group 2 of cluster analysis.

These groups identified by statistical analysis reflect diagenetic and metasomatic processes and are dealt with in the appropriate chapter. The one group which represent sedimentary processes is dealt with next.

3.3.3 The Immobile Elements

The correlation of the elements within Group 1a are shown in Table 3.3.

	SiO2	Al2O3	TiO2	MgO	Na2O	MnO	Nb	Sc	Zr
SiO2	-								
Al2O3	0.787	-							
TiO2	0.592	0.876	-						
MgO	0.266	0.445	0.436	-					
Na2O	-.060	0.170	0.163	0.010	-				
MnO	-.143	0.268	0.435	0.398	0.607	-			
Nb	0.464	0.706	0.759	0.380	0.331	0.513	-		
Sc	-.077	0.335	0.542	0.273	0.328	0.752	0.619	-	
Zr	0.459	0.795	0.894	0.419	0.314	0.591	0.866	0.711	-

Table 3.3 Correlation matrix table between the Group 1a elements.

Magnesium and manganese are poorly associated with this group and are contained within chamosite or siderite (Chapter 4), which occur within the more detrital-rich ironstones. Sodium occurs within detrital feldspar and silicon in detrital quartz. The closest association is between the remaining elements (Al_2O_3, TiO_2, Zr, Nb and Sc) and it is this close association which indicates the overall detrital nature of this group.

Detrital rutile has been visually identified within ooids only in the Bryn Poeth ironstone, otherwise any rutile that might be present is too fine-grained to be visible. Titanium detected on the EPMA in chamosite within ooids (found at most localities) most likely indicates detrital rutile. EPMA Analyses of recrystalised chamosite (cements and veins) show no titanium. Therefore titanium is not contained in the chamosite lattice, but in detrital minerals. Brindley (1982) and Rohrlich (1974) assigned titanium in berthierine analyses to detrital rutile. Detrital rutile and zircon have been found in the Northampton Sand Ironstone (Taylor 1949) along with detrital metamorphic minerals. Visible zircon has only been identified from the nucleus of an ooid from Bryn Poeth. Presumably, like rutile, zircon is too fine-grained to be visible. Zirconium is present in the mineral

zircon, which can resist more than one cycle of weathering and sedimentation, and is also resistant to metamorphism up to moderate to high grades (Deer et al. 1962a). That titanium and aluminium correlate very well with zirconium (Table 3.3) indicates that they were of detrital origin. The regression line of the plots between these elements passes very close to the origin, suggesting that the titanium and aluminium contents have not been affected by low grade regional metamorphism. Niobium either substitutes for zirconium in the zircon lattice, or occurs as a niobium bearing phase, either as an independant mineral or as inclusions in rutile and zircon (Deer et al. 1962a). Scandium correlates with titanium, manganese, niobium and zirconium (Table 3.3). However, the behaviour and mineral control of scandium is poorly understood. It would be expected that hafnium would show a correlation with this detrital group as there is always some hafnium in zircon (Deer et al. 1962a). However the hafnium content of the ironstone bears no relationship to zirconium, although the values for hafnium are low and some analyses are below detection limits. Likewise yttrium, which occurs in the mineral xenotime (YPO_4) and can show isostructural replacement of $ZrSiO_4$ in the zircon lattice, would be expected to show some correlation with this group. Yttrium also shows no correlation with zirconium.

3.3.4 The Rare Earth Elements

A selected number of the XRF samples were subsequently analysed for the rare earth elements (REE) by ICP. Published data on the REE content of Phanerozoic Ironstones is extremely limited (Timofeeva & Balashov 1972; Bhattacharyya 1986). The REE results of the mid-Ordovician North Wales Ironstones are:

1) normalised to chondrite values (Boynton 1984), to show the basic REE pattern of the ironstones, and to normalize to average shale values (Cody Shale - Jarvis & Jarvis 1986) for comparative purposes.

2) correlated to the major and trace elements of the ironstones, to study the controls on the variation of the REE.

3) compared to ironstone REE, to other ferruginous sediments REE (glauconites and BIF) other sediments and volcanics REE.

The plots of the REE for the ironstones normalised to chondrite values are shown in Figure 3.22. The samples are from Betws Garmon (5 samples), Cadair Idris East (4), Pen y Gaer (3), Aber (2), Bryn Poeth (2), and individual samples from Rhyd and Cadair Idris west. Within analyses from one ironstone locality, the similarity of the plots is readily apparent. The main variation is the absolute values of the REE. All samples have a negative europium anomaly and some samples have a positive cerium anomaly (Bryn Poeth, Rhyd, Cadair Idris west). The other difference in the ironstone REE patterns is the notable enrichment of the heavy rare earth elements (HREE) in some ironstones (Aber, Bryn Poeth, 032-Pen y Gaer, Rhyd, Cadair Idris west).

The ironstones have been normalised to average shale values to compare similarities and differences between 'normal' marine sediments and ironstones. Cody Shale values, analysed by ICP, are used to normalise the data (Jarvis & Jarvis 1986). When the chondrite normalised ironstone plots are compared to the chondrite normalised plots for the Cody Shale a number of differences are apparent. The Cody Shale has only a small europium anomaly ($Eu/Eu^* = 0.83$) whereas the ironstones have a much larger anomaly (average = 0.64). The overall gradient and light rare earth element (LREE) gradients for the Cody Shale are markedly steeper than those of the ironstones (La/Lu Cody Shale = 102, average ironstone = 47; La/Sm Cody Shale = 6.28, average ironstone = 3.06). The Cody Shale has a flat HREE profile while the HREE profile for the ironstones is variable. These features are demonstrated by normalising the ironstone values to the Cody Shale (Figure 3.23). All ironstone samples have a similar overall concave pattern, with the inflexion point lying around terbium-dysprosium. Those ironstones with an anomalous HREE concentration show up clearly, as do those with a cerium anomaly.

The REE and their ratios have been correlated with the XRF major and trace element data. This shows a number of relationships that can help to explain the variation between the REE samples in relation to the major and trace elements, and therefore to processes acting upon the ironstones. There are three groupings of major and trace elements that can be shown to influence the REE:

1) Immobile elements (TiO_2 Zr Nb Sc),
2) Ferric iron and related transition metals (Fe_2O_3 MnO Co Ni V),
3) Apatite (CaO P_2O_5).

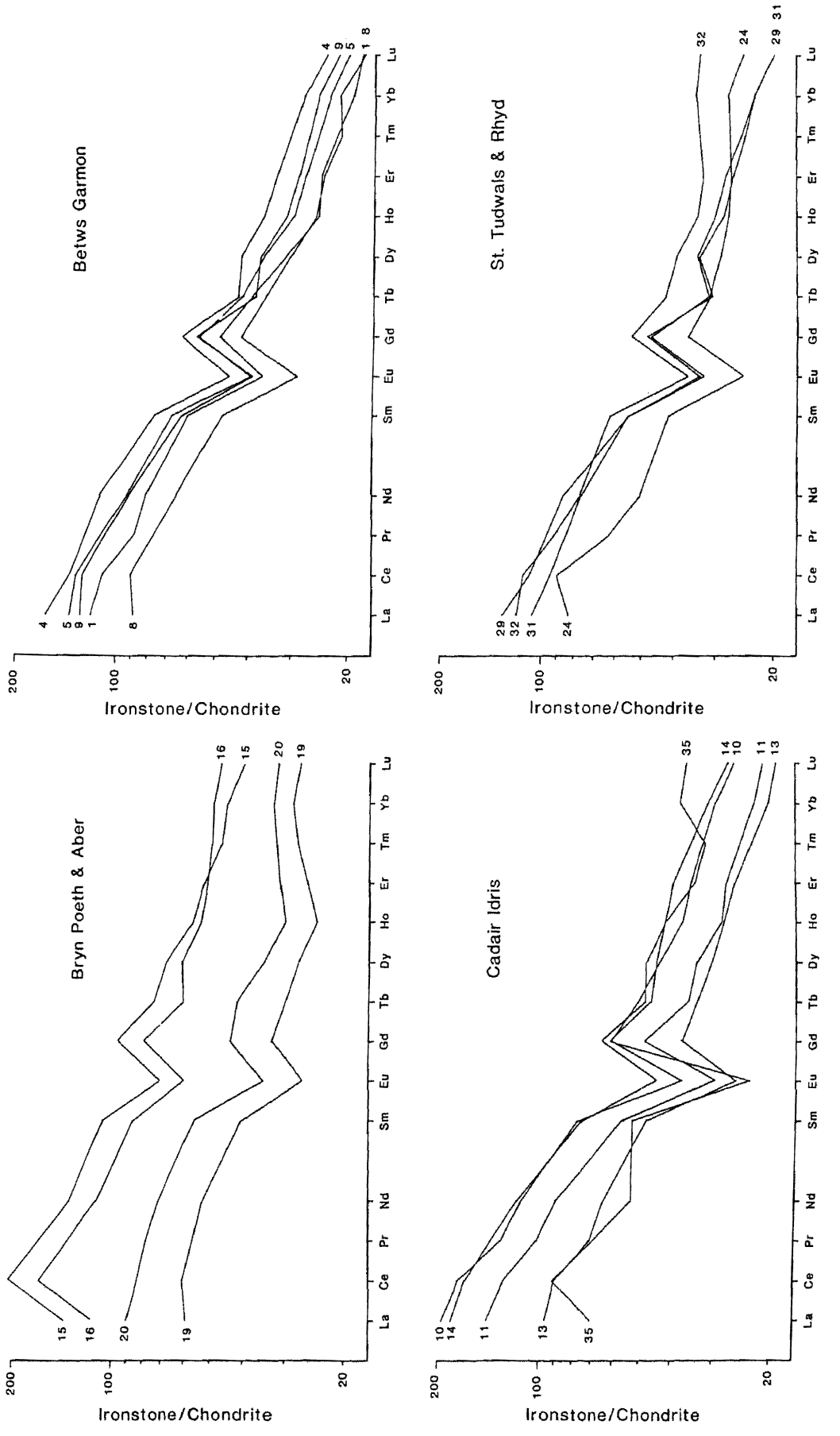

Figure 3.22 Chondrite (Boynton 1984) normalised REE data for the North Wales Ironstones. Numbers refer to XRF sample No.s in Appendix 5.

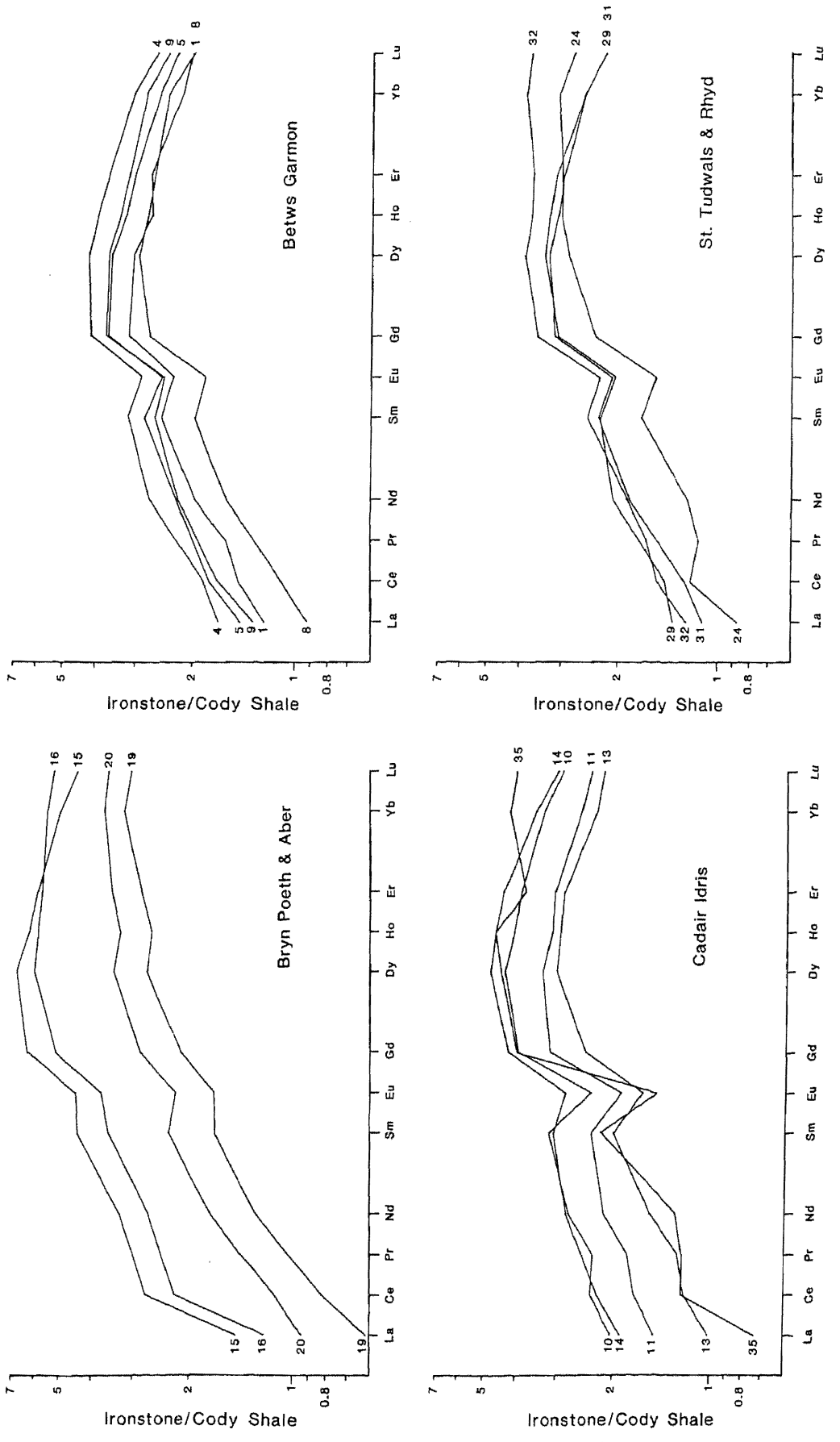

Figure 3.23 REE data for the North Wales Ironstones normalised to Cody Shale values (Jarvis & Jarvis 1986). Numbers refer to XRF sample No.s in Appendix 5.

The elements within these three groupings all show strong correlations with certain REE and ratios.

The immobile elements (Group 1a above) show a strong correlation with the HREE (Table 3.4)

	TiO_2	Zr	Nb	Sc
Lu	0.494	0.695	0.626	0.616
La/Lu	-0.653	-0.765	-0.773	-0.872
Gd/Lu	-0.806	-0.797	-0.885	-0.861
Ho/Lu	-0.767	-0.803	-0.853	-0.910

Table 3.4 Correlation table between the immobile elements, and Lutetium and the HREE ratios.

The samples with high immobile element values show an anoma ly in HREE distribution, in that their HREE increase rather than decrease (Figures 3.22; 3.23). This is indicated by the good negative correlation between increasing titanium, zirconium, niobium and scandium and decreasing La/Lu Gd/Lu and Ho/Lu (Table 3.4). This is best demonstrated by the chondrite normalised plot (Figure 3.22) for sample 019 (Aber) where from holmium onwards the HREE increase. Its chondrite normalised plot shows an enrichment in HREE and depletion in lanthanum. One St.Tudwals ironstone sample with some hydrothermal alteration also shows anomalous HREE enrichment and lanthanum depletion, as does the sample from Rhyd. It is uncertain why hydrothermally altered ironstones should show a relative enrichment in the HREE plus scandium and a depletion in lanthanum, as this has not been documented from other ironstones.

The REE are also affected by ferric iron and related transition metals (MnO, Co, Ni, V). However, this group of elements do not behave in such a coherent fashion as the other two, the influence of these elements is more varied. The first influence by this group is on the total rare earth element (TREE) content. Ferric iron, cobalt and vanadium all show a positive correlation (r= 0.5-0.6) with the TREE content. Additionally ferric iron and vanadium also show a positive correlation with the LREE (La/Sm r=0.5), indicating that the probable

control of the LREE (being more abundant will influence the TREE more) is by the ferric iron content. Manganese, cobalt and nickel also show a positive correlation with the cerium anomaly (Ce/Ce*:Co r=0.710 Ni r=0.735 MnO r=0.526). These results roughly agree with the XRF data for Ce, which shows a positive correlation with ferric iron (Ce/Fe_2O_3 r=0.538), suggesting that ferric iron (diagenetic and/or metasomatic and/or weathering) had a large control on the LREE of the ironstones.

Apatite has only a limited influence on the REE pattern. Both calcium and phosphorus show a positive correlation with lanthanum (La/CaO r=0.496; La/P_2O_5 r=0.480). The XRF data for the relationship between yttrium and apatite indicate that yttrium shows a good correlation with apatite (Y/CaO r=0.683 Y/P_2O_5 r=0.651). This suggests that yttrium is associated with this phase. However the regression line for this correlation cuts the yttrium axis at 55ppm, suggesting an additional primary yttrium phase; as xenotime substituting in the zircon lattice.

The North Wales Ironstone REE patterns are compared to other REE patterns (Figure 3.24). The North Wales Ironstones have a very dissimilar pattern to BIF, to East Pacific Rise crest metalliferous sediments and to glauconites. This indicates no genetic link between oolitic ironstones and other iron-rich deposits. The REE patterns for various North Wales volcanics (acid, intermediate and basic) are dissimilar to the North Wales Ironstones, indicating no genetic link. Likewise the ironstones are not comparable to average shales or upper crustal values (equivalent to average basement). The North Wales Ironstones do show similarities to phosphate rocks (Jarvis & Jarvis 1986) and also to Russian ironstone REE patterns (Timofeeva & Balashov 1972). These similarities and differences allow constraints to be placed on the significance of the North Wales Ironstones pattern, which is discussed in the next section.

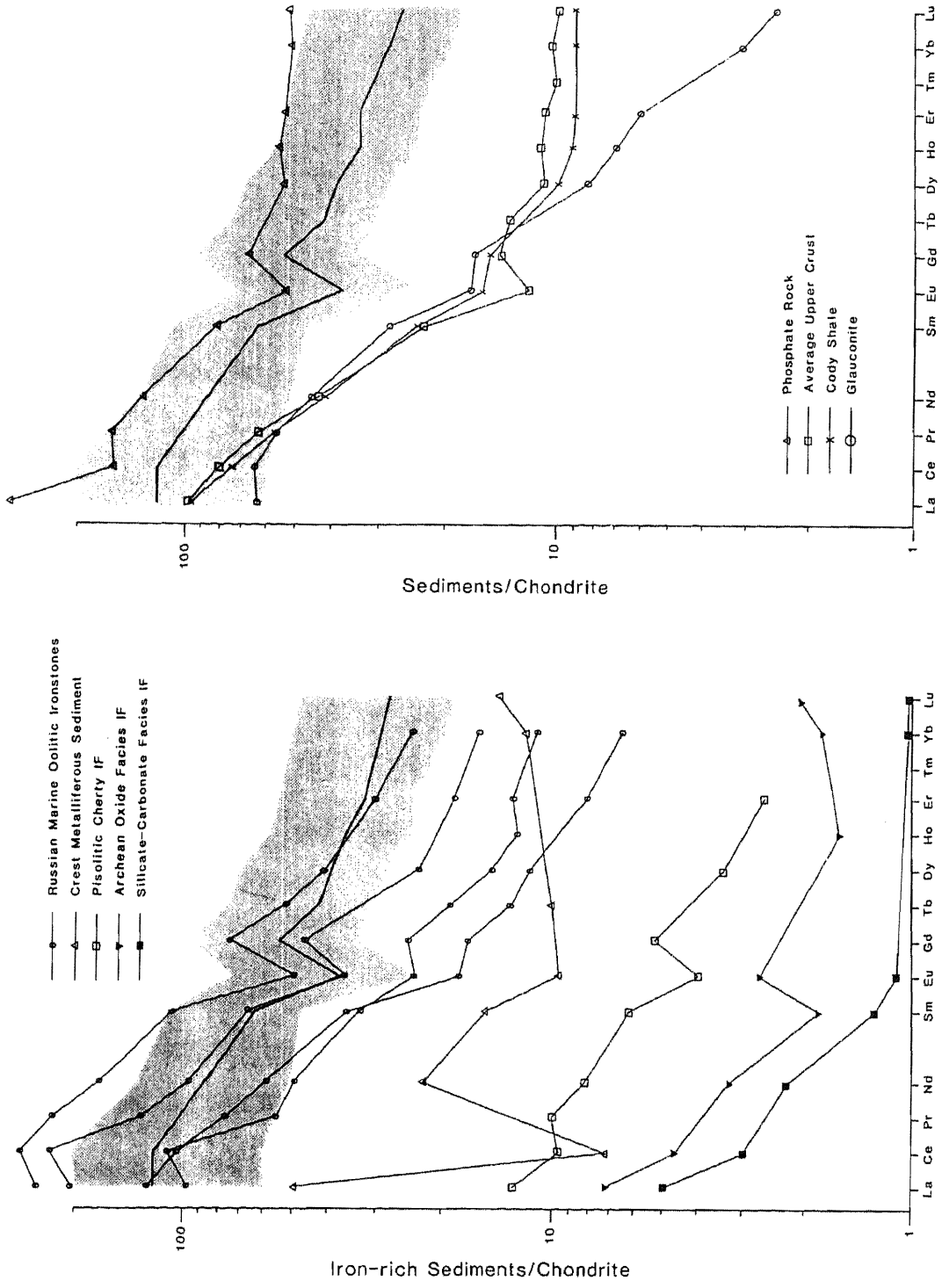

Figure 3.24 Comparison of the North Wales Ironstones REE to other sediments, all normalised to chondrite (Boynton 1984). Shaded area is extent of North Wales Ironstones and the thick black line is average REE values. Source for other REE values: Phosphate Rock, Cody Shale, Glauconite (Jarvis & Jarvis 1986), Average Upper Crust (Taylor & McLennan 1985), Russian Marine Oolitic Ironstones (Timofeeva & Balshov 1972), Crest Metalliferous Sediment, Pisolitic Cherty Iron Formation, Archean Oxide Facies Iron Formation, Silicate-Carbonate Facies Iron-Formation (Fryer 1983).

3.4 DISCUSSION

Trythall et al. (1987) have accounted for the depositional controls of the mid-Ordovician North Wales Ironstones. In this section the ideas are justified in greater detail and expanded upon.

3.4.1 Source of the Ironstone

A number of possible sources of iron for oolitic ironstones have been suggested (Maynard 1983). A volcanic source for iron for the North Wales ironstones would at first seem to be likely. Volcanic activity is abundant within the Ordovician of North Wales and has also formed the source for other ironstones (Quade 1976; Dreesen 1989). However there are a number of arguments against a volcanic source for the North Wales Ironstones:

1) The ironstones are older than the main volcanic event in North Wales, and volcanic sediments and the oolitic ironstones are not associated with each other.
2) The one occurrence of a volcanic-associated ferruginous deposit in North Wales is a massive sulphide deposit (Ball & Bland 1985).
3) Volcanic associated ironstones are oxide and sulphide dominated, the North Wales Ironstones are silicate dominated, plus a REE pattern that does not resemble any of the North Wales volcanics.

The geochemistry of the ironstones indicates that the original sediment was Fe-Si-Al dominated, with no alkali metal bearing clays present. The most likely mechanism to produce this pattern is lateritic weathering of an adjacent landmass. This process generates kaolinite and iron oxide complexes, as colloids or organic complexes, which are then eroded and transported into the basin (Maynard 1983; Carroll 1958).

Oolitic ironstones commonly form close to shorelines (Bayer 1989). The detrital content of the Anglesey and Llŷn ironstones, and the presence of feebly oolitic ferruginous grits forming part of the basal beds of the Caradocian transgression on Anglesey, indicate that the shoreline lay close to the northwest. This was the Irish Sea Landmass (George 1963) or Mona terrane (Gibbons & Gayer 1985). The

presence of detrital quartz in the Anglesey and Llŷn ironstones indicate a metamorphic or acid plutonic provenance. This is consistent with the exposures of Precambrian metamorphic and plutonic rocks on Anglesey and the Llŷn.

The geochemistry of the ironstones adds support to the argument of lateritic weathering. For each ironstone locality the REE patterns are remarkably similar and overall the REE patterns are similar. Any differences are accounted for by post-depositional changes. The anomalous HREE patterns are associated with hydrothermal alteration, and the LREE patterns are affected by metasomatism and weathering. The immobile elements (Al, Ti, Zr, Nb, Sc) all have a constant relationship which, combined with the original relatively uniform REE pattern, suggests the same source for all the ironstones despite their geographically widespread nature.

The North Wales Ironstones REE pattern is dissimilar to patterns of other ferruginous deposits, average sediments and average continental crust. Therefore the two most likely explanations for the ironstone REE patterns are either derivation from a terrane with an overall REE pattern similar to the ironstones, or that they reflect a fractionation process that is characteristic of ironstone formation. REE data for Russian oolitic ironstones (Timofeeva & Balashov 1972) are broadly similar to the North Wales Ironstones. The likelihood of Russian oolitic ironstones being derived from a terrane with the same REE pattern as the North Wales Ironstones is low . Therefore the REE patterns of ironstones suggests that they reflect a common process formation, and not an inherited pattern.

If the source for the ironstone was by lateritic weathering then this must be reflected by the REE composition, as the REE are not immobile under chemical weathering conditions (Fleet 1984). The detrital behaviour of the immobile elements (plus HREE) suggest that these phases survived lateritic weathering. This has been shown for modern laterites, where the immobile elements are present as residual minerals (Isaac 1983; Nair & Mathai 1981; Kronberg et al. 1979). This is also the case for the Northampton Sand Ironstone (Taylor 1949). Gromet et al. (1984) have shown that a significant proportion of the HREE in shales are contained in detrital resistate minerals, especially zircon. However, the LREE tend to be enriched in modern laterites and occur adsorbed onto clays and iron oxides (Isaac 1983; Nair & Mathai 1981), and can be transported in this state. In the North Wales Ironstones the LREE are modified by post-burial processes,

indicating that the LREE adsorbed onto clays and iron oxides were released during diagenesis of the ironstones. The North Wales Ironstones do not contain a negative cerium anomaly, indicating that phases containing the LREE were not precipitated from seawater (Fleet 1984). However, the North Wales Ironstones do have a large negative europium anomaly when compared to average shale (Cody Shale). The europium anomaly in shales is inherited from the continental crust from which they were derived (Taylor & McLennan 1985). It is unlikely that the crustal material from which the North Wales Ironstones were derived had a similarly large negative europium anomaly, as Ashgillian mudstones from North Wales (A. Kearsley unpublished data) do not have a similarly large negative europium anomaly. Therefore it is most likely that this anomaly reflects fractionation processes during lateritic weathering. For the significance of the North Wales Ironstones REE to be fully understood, much more REE data of other Phanerozoic Oolitic Ironstones is needed.

Supporting geochemical evidence of a laterite weathering source for ironstones comes from a study of Thorium and Uranium (similar in behaviour to the REE) in the Cleveland Ironstone Formation (Myers 1989). Thorium is an immobile phase while uranium can be oxidized and is then soluble. The Cleveland ironstones have a high Th/U ratio (are relatively depleted in uranium) indicating highly oxidizing conditions under which uranium had been leached. Thorium enrichment in the Cleveland ironstones is a primary and not diagenetic feature, and thorium is enriched in laterites with a close association with kaolinite. The thorium content of the Cleveland ironstones reflect a transported detrital component, enriched in thorium and depleted in uranium (Myers 1989).

3.4.2 Controls on the localisation of the ironstones

A number of constraints can be placed on the environmental conditions under which the North Wales Ironstones must have been deposited:

1) They are geographically widespread but sporadic deposits.
2) They occur above stratigraphic hiatuses, and their lateral equivalents are thicker siliciclastic sequences.
3) Some ironstones contain slump structures and debris flow deposits.

4) They must be the site for the formation of ooids.

5) They are reworked and current sorted before final deposition.

6) They contain stromatolites and oncoids.

The first two constraints imply some control(s) which produce localised deposits with lateral facies changes. The third constraint implies topographic or tectonic instability. The last two constraints imply relatively shallow water and reworking by currents. Within the Welsh Basin this environmental milieu could be provided either by volcanic rises, or by topographic highs produced by fault control. It has already been established that there is no association with volcanism. Therefore the evidence for fault control on ironstone deposition is investigated (Figure A).

At Bryn Poeth the N-S trending Garth Ferry fault is exposed just to the west of the Ironstone, and also a stratigraphic gap occurs beneath the ironstone of the bifidus Biozone. Bates (1974) noted that the majority of N-S faults on Anglesey had some movement in the Ordovician.

The Mid-Ordovician ironstones on the Llŷn peninsula (Trefor and St. Tudwals) may both be related to a single fault. In the St. Tudwals peninsula a major N-S fault (Figure 2.9) is known to have been active in the Cambrian (Nicholas 1915). The St. Tudwals ironstone only occurs on the west side of this fault. Further to the north there are differences in the Caradocian sequences either side of the same fault (Roberts 1979, p63-66). Blenkinsop et al. (1986) have noted that this fault trends toward the epicentre of the North Wales 1984 earthquake (Turbitt et al. 1985), which was formed on a N-S oriented basement fault. The Trefor ironstone occurs just to the east of this fault. The Llanvirn is missing from beneath the St. Tudwals ironstone and there may be a stratigraphic hiatus beneath the Trefor ironstone (Section 2.3.1). Both localities contain disturbed ironstones and debris flows, indicating tectonic disturbance, which become more persistent towards the fault at St. Tudwals.

In Snowdonia, the ferruginous debris flow in the Llanberis valley terminates against the Llanberis Valley Fracture Zone (Wilkinson & Smith 1988), a NW-SE oriented structure. At Betws Garmon the ironstone occurs near a major NE-SW fault, which has been shown to have been active in Cambrian times (Webb 1983). A hiatus beneath the ironstone has been proposed (Section 2.4.4). The Tremadog ironstone has been shown (Smith 1987) to have been affected by contemporaneous tectonic

activity, slumping on a NW dipping palaeoslope away from the Harlech Horst. A large stratigraphic gap occurs beneath the Tremadog ironstone (Section 2.4.5).

In the Cadair Idris region the ironstone shows the thickest development in the east while the Llyn y Gader mudstones are the thinnest (Davies 1956). Westwards the ironstone sequence becomes thinner, more detrital quartz rich, more poorly developed and the adjacent mudstone sequence thicker. West of Ffordd Ddu there is no ironstone, and only a thick clastic sequence is developed, up to the Llanegryn Fault (Jones 1933). Across the fault is 50ft of oolitic and nodular beds, above a stratigraphic hiatus (Jones 1933). To the east of Cross Foxes the ironstone abruptly disappears. The synsedimentary faults prevalent at this time have been shown by Fitches & Campbell (1987); to the east of Cross Foxes is the junction between the Harlech & Aran horsts and the Aran Graben. This is also the connection between the Tal y Llyn and Bala faults, all indicating further synsedimentary faulting terminating the ironstone. Contemporaneous tectonic slumping of sediments and ironstones can also be seen in the Arenig of North Wales (Beckley 1987,1986; Kokelaar 1979).

This fault control on the ironstones would have the effect of producing short-lived shallow water shoals. Fault scarps would not propagate in the predominantly muddy sediments but would form shoals instead (Kokelaar et al. 1984). Fault scarps are relatively rare in Ordovician North Wales, the most significant being in Central Anglesey (Bates 1972). The formation of shoals would account for the localised distribution of the ironstones, their occurrence above a hiatus, lack of clastic dilution and a lateral correlation with thicker clastic sequences. Ironstones forming on shallow water shoals are seen in the Jurassic (Hallam 1975; Sellwood & Jenkyns 1975).

3.4.3 Formation of the Ferruginous Allochems

Berthierine today occurs as peloids, largely faecal in origin, on sediment-starved continental shelves (Van Houten & Purucker 1984), although these peloids may also form as inorganic floccules (Bhattacharyya 1989). The shallow water shoals in the North Wales Basin would therefore supply a similar environment for berthierine accumulation. Peloids supply the necessary reducing microenvironment to form berthierine from kaolinite/iron oxides (Velde 1989, 1985). Berthierine may also have formed by trapping of kaolinite/iron oxides

by stromatolites or other microbiota, both of which also produce a reducing microenvironment. The initial stage in the formation of ooids is the formation of nuclei, which are predominantly peloids. The presence of sponge spicules and quartz grains as nuclei indicate that the ooids formed in the marine environment and so are not reworked laterite soil ooids (Siehl & Thein 1978). Ooids then formed by successive coating of the nucleus by chamosite laminae. Mechanical accretion of chamosite laminae is shown by detrital rutile grains within the laminae, and by the rounding effect on the ooids by the successive accretion of laminae. The presence of organic carbon defining laminae indicates that although there was no direct biogenic influence on ooid formation there was an indirect influence. An analogy with recent calcareous ooids can be made. These contain organic carbon defining laminae, where the organic mucilage was sticky enough to allow accretion to occur (Bathurst 1975). Bacterial activity within this mucilage could provide the reducing conditions necessary to form and preserve berthierine. This would therefore explain the paradox of chamosite preserved in ooids as a ferrous mineral in an oxidizing depositional environment.

The site of ooid formation in the ironstones is problematic. Ooids are restricted to the ironstones, do not occur in the underlying and overlying beds and laterally pass into clastic mudstones. Clearly the shoals must have been both the site of ooid formation and of final deposition. The grain-ironstones, pack-ironstones and float-ironstones are all reworked sediments and so do not represent the original site of formation. However, chamositic mud-ironstones are very rare in oolitic ironstones, and are best seen in the North Wales Ironstones (Hallimond 1925). This mud-ironstone may have been the substrate upon which the allochems were rolled to form ooids. This and the presence of stromatolites (see below) may represent the original site of formation of the ooids.

Bhattacharyya (1989) has advocated ooid formation in 'lean muddy oolites', which are thin and laterally extensive. These are reworked, the ooids transported like sand grains, into 'concentrated oolites' which are lense like deposits. Within the 'lean muddy oolites' the initial stage of ooid formation is by forming a peloid, which is subsequently coated by laminae by snowball accretion. This two phase growth of ooids, an initial peloid stage subsequently coated by laminae by snowball accretion, has also been advocated for a number of Phanerozoic Oolitic Ironstones (Chauvel & Guerrak 1989; Van Houten &

Purucker 1984).

Accounting for the formation of the oncoids is more difficult as similar biogenic structures in other ironstones are rare. Their interpretation must be made solely by analogy with carbonate oncoids within the Lower Palaeozoic Welsh Basin and by comparison with published data on biogenic structures in other ironstones.

Phosphatic oncoids within the Arenig of North Wales (Bolopora undosa, Hoffman 1975) occur within grits and conglomerates of the basal beds of the Arenig transgression. Their formation has been attributed to growth above an unconformity within coarse clastic sediments, but with periodic cessation of sediment influx (Roberts 1979; Bates 1969).

Within the North Wales Ironstones two types of oncoids were found; small, concentrically laminated, with spongiostromate fabric, and larger, irregularly or discontinuously laminated, with both spongiostromate and porostromate fabrics. These correlate with Type A and Type B oncoids, respectively, of the Much Wenlock Limestone. Oncoids in this limestone have been used as environmental indicators (Ratcliffe 1988). Oncoids are constructed by algae and therefore only form in conditions suitable to growth; one condition being that optimum growth is within the photic zone (although deep water oncoids are known) and generally less than 50m water depth (Ratcliffe 1988).

Type A oncoids, being concentrically laminated, were formed by rolling in a continuous high energy environment. By contrast Type B oncoids, because of their irregular or discontinuous lamination, were intermittently rolled and therefore indicate a more intermittent turbulent environment. In the North Wales ironstones Type B oncoids predominantly occur in mud-ironstones, but also debris flows, while Type A oncoids occur in pack-ironstone lenses in mud-ironstone, and Anglesey and Llŷn pack-ironstones and float-ironstones. This facies control on different oncoid types suggests that oncoids were not formed at the same location as ooids, but were formed during reworking of the sediments. However, oncoids are also particularly abundant at Gorddinog (Aber), where they occur above stromatolitic crusts. This is interpreted as an environment particularly favourable for algal activity, and indicates very limited transport of oncoids, as they are not found at the main Aber ironstone, 1km away.

Stromatolites differ from oncoids in that they represent in situ growth, although with the same constraining factors for oncoid growth. Their presence at Gorddinog and Pensyflog, where they are partially

phosphatised, represent hardgrounds on the shoal where they had the effect of initially binding the muddy sediment. The fact that these in situ stromatolites are not found at the site of main deposition indicates the nature of reworking and local transport of allochems before final deposition. The presence of ripped up stromatolite crusts in the Llŷn ironstones debris flows and Aber ironstone further supports this hypothesis.

Dahanayake & Krumbein (1986) state that micro-oncoids are more common in oolitic ironstones than previously realised. They advocate formation of ooids and micro-oncoids within microbial mats, which would produce the necessary reducing microenvironment for chamosite formation. Microbial mats would stabilize the sediment surface to an extent that resistance to suspension is up to 10 times higher than in areas where no mat is forming (Dahanayake & Krumbein 1986). The to and fro motion of grains within the slimy gel-like mat due to current action during their formation is one way of forming ooids.

3.4.4 Sedimentation

The North Wales ironstones differ from other oolitic ironstones in not showing cyclic sedimentation and cross bedding (Van Houten & Purucker 1984; Teyssen 1984). However, the sedimentation of the ironstones can be discussed by interpreting the sedimentary features that can be seen and then comparing these features to other oolitic ironstones.

The North Wales ironstones have been reworked and winnowed before final deposition. The overall upward increasing ooid content and decreasing mud content suggest progressive current winnowing. None of the ironstones show more than one 'cycle' of sedimentation, apart from Bryn Poeth where half metre thick cycles are present. Within each cycle is an increasing ooid content and decreasing mud content, capped by a thin grain-ironstone, reflecting on a small scale the overall ironstone sequence (except for the grain-ironstone). This small scale cyclicity reflects local (autocyclic) controls on sedimentation.

The lens -like nature of the Betws Garmon pack-ironstone suggests a winnowed bar deposit over muddier sediments, which is also suggested by the 'pod' like nature of the other ironstones. However, the lack of cross bedding is a conspicuous feature of the North Wales ironstones, which distinguishes them from other, otherwise similar, oolitic ironstones. The two occurrences of thick grain-ironstones (excluding

Bryn Poeth) both occur in tectonised localities and no sedimentary structures in outcrop are seen. In thin section a bimodal grain-size difference is apparent, with approximately one phi grain-size difference between the two. The Minette ironstone, which is tidal current deposited (Teyssen 1984), show a one phi difference in ooid size from deposition from flood currents to deposition from ebb currents. This suggests that the North Wales grain-ironstones were winnowed and deposited by tidal currents. Even though the pack-ironstones show the form of a bar deposit, they do not show this grain-size difference, have an uneven mud distribution and contain phosphate nodules. By analogy with limestone oolites, active ooid shoals are grainstones, and when abandoned form packstones by colonizing fauna which bioturbate the sediment, with an uneven mud distribution in the lime packstone (Halley et al. 1983). Ancient carbonate oolite bodies may have their sedimentary structures removed by homogenization by burrowers (Halley et al. 1983). Therefore pack-ironstones may represent bioturbated grain-ironstones, which destroys sedimentary structures (including cross bedding), infills the spaces between grains with an uneven mud distribution and nodules may represent burrows within the sediment that are infilled by phosphate, the random loose packing of ooids representing later infil of the burrow. Therefore the ironstones represent a shoaling up sequence with an upper tidal bar deposit, which represents shallow water conditions (several metres deep - Teyssen 1984; Halley et al. 1983) in a marine basin.

Bayer (1989) noted a grain-size difference between ironstones nearest a shoreline containing large 'onkolite like ooids' and those further offshore which are finer grained. This is related to winnowing of smaller ooids into the more distal environment. Although the North Wales Ironstones show the same general pattern of proximal ironstones with oncoids not seen in the distal ones, this cannot be related to winnowing into a more distal environment as the ironstones are isolated deposits. The poorer sorting of the Anglesey and Llŷn pack-ironstones, reflected by the presence of oncoids, indicates conditions more favourable for oncoid formation in these ironstones. This is most likely due to increased algal activity at these localities.

4 DIAGENESIS OF THE IRONSTONES

Diagenesis has affected the textures, mineralogy and geochemistry of the ironstones, the main minerals formed are apatite, siderite and chamosite. These are common diagenetic phases in other ironstones (Maynard 1986). This chapter describes the field relationships, textures, mineralogy and geochemistry of each diagenetic phase occurring in the North Wales Ironstones. Maynard (1986) described ironstone formation and ironstone diagenesis, based on observations of compositional variations of primary and diagenetic minerals in ironstones. A similar approach is adopted here. Diagenesis in sediments has been defined by a number of authors (eg. Fairbridge 1983) and for ironstones (Maynard 1986; Bubenicek 1983; Dimroth 1977, 1975). Diagenesis in this work is taken as beginning after the final deposition of the ironstones (although berthierine formation and phosphate nodule formation may pre-date the final deposition of the ironstone) and includes burial metamorphism. The ironstones have not undergone any significant changes during burial metamorphism (ranging from diagenetic to low greenschist facies, Figure 1.4), and so is included in this chapter. Metasomatic and hydrothermal alterations of the ironstones are described in Chapter 5.

Diagenetic pyrite as an alteration of berthierine-rich oolitic ironstones is common, as berthierine is unstable even at low sulphide activity (Maynard 1983; Young 1989a). However, diagenetic pyrite is not seen in the North Wales Ironstones. Pyrite occurs particularly in the uppermost parts of Ironstone Formations developed in mudstone sequences, and these sulphide bearing excursions in the ironstone facies often correlate laterally with intervals of resumed or accelerated sediment accumulation (Young 1989a). Although pyrite is a common phase in some of the North Wales Ironstones, its textural relationships show it to be associated with metasomatism and hydrothermal alteration (Chapter 5). Therefore diagenetic pyrite was not formed in the North Wales Ironstones, the reasons for which will be presented at the end of this chapter.

4.1 PHOSPHATE DIAGENESIS

Phosphate is not unique to the Mid-Ordovician North Wales Ironstones. It occurs within other North Wales sediments and other Ordovician Ironstones as Arenig phosphatic oncoids (Hoffman 1975), as Arenig phosphatic nodules (Beckley 1987), as Caradoc phosphatic nodules (Cave 1965), and in European Ordovician Ironstones and associated sediments (Young 1988, 1989b). In the North Wales Ironstones phosphate occurs either within chamositic and phosphatic oncoids, or as phosphatic nodules. In the oncoids the phosphate is most likely to be of sedimentary origin (Chapter 3). However, nodules represent concretionary growth of phosphate in the ironstones. They are important since they are critical in understanding diagenetic processes in the ironstones, because they preserve textures otherwise not seen within the ironstones. Phosphate nodules occur in all the Mid-Ordovician North Wales Ironstones except for the ferrified grits of central Anglesey (Fferam Uchaf, Figure 2.2) and in all ferruginous facies except grain-ironstones. The occurrence and general description of phosphate nodules has been given in Chapter 2. This section gives detailed descriptions of the textures and mineralogy of the nodules, and discusses possible origins of formation.

4.1.1 Textures and Mineralogy

Although nodules occur in all ironstone facies types, excepting grain-ironstones, there are differences in nodule morphology between different facies types. There is a distinction between nodules in pack-ironstones and wacke-ironstones, and nodules in float-ironstones and rud-ironstones, which have been disturbed prior to burial (especially at Trefor, St. Tudwals and Tremadog). In the former, nodules have diffuse margins, because the collophane (material forming the nodule) merges with the grain-supported ooids (Figure 4.1). There is strong deformation of ooids above and below these nodules (Figure 4.1), and also between nodules when they occur close together (Figure 3.16). In contrast nodules in float-ironstones and rud-ironstones have either sharp or eroded margins (Figure 4.2). They may also have embayed edges marking the site of former ooids plucked out during reworking (Figure 4.3). Nodules with dissimilar internal texture, one full of ooids and spicules another barren, may occur adjacent to one another. Deformation of ooids around these nodules is not as intense

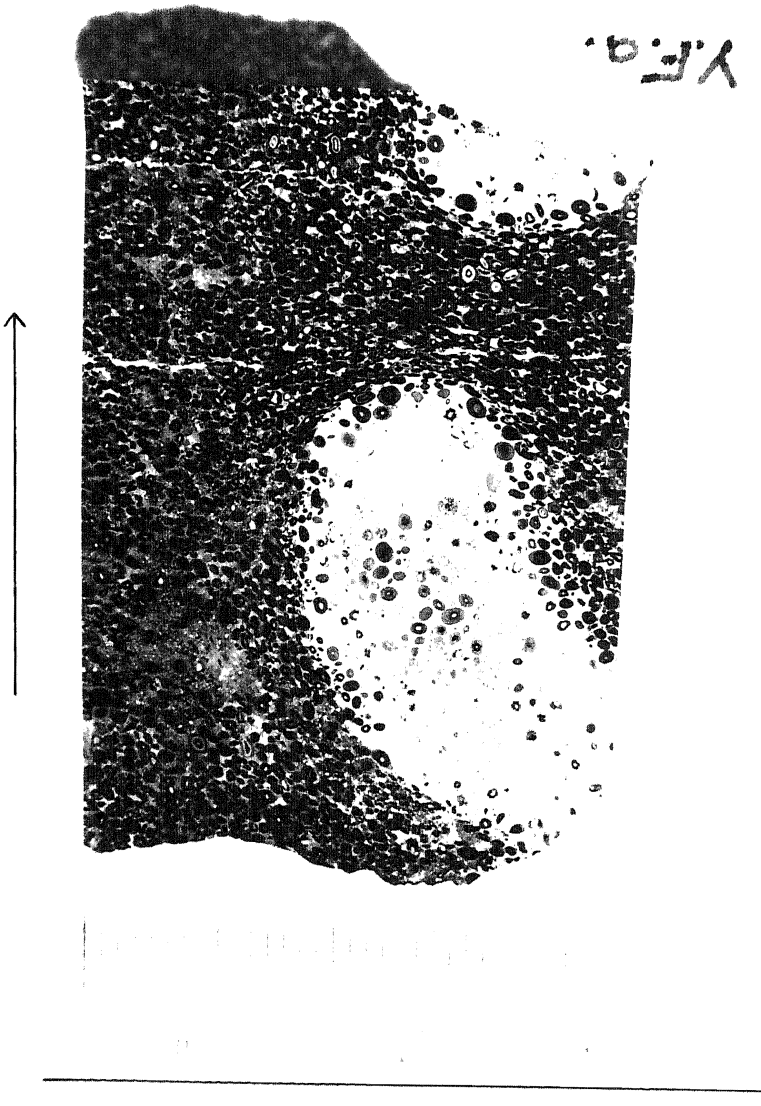

Figure 4.1 Photograph of thin section, magnetite ooidal chamositic pack-ironstone, YF-A Betws Garmon (loose grab sample). In situ phosphate nodules in ooidal pack-ironstone (showing magnetite (opaque) replacement). Note the diffuse margins of the nodules with the surrounding pack-ironstone, strong deformation of ooids around, especially above and below, the nodules, the random distribution of ooids within the nodules. Ooids within the nodules are not replaced by magnetite.

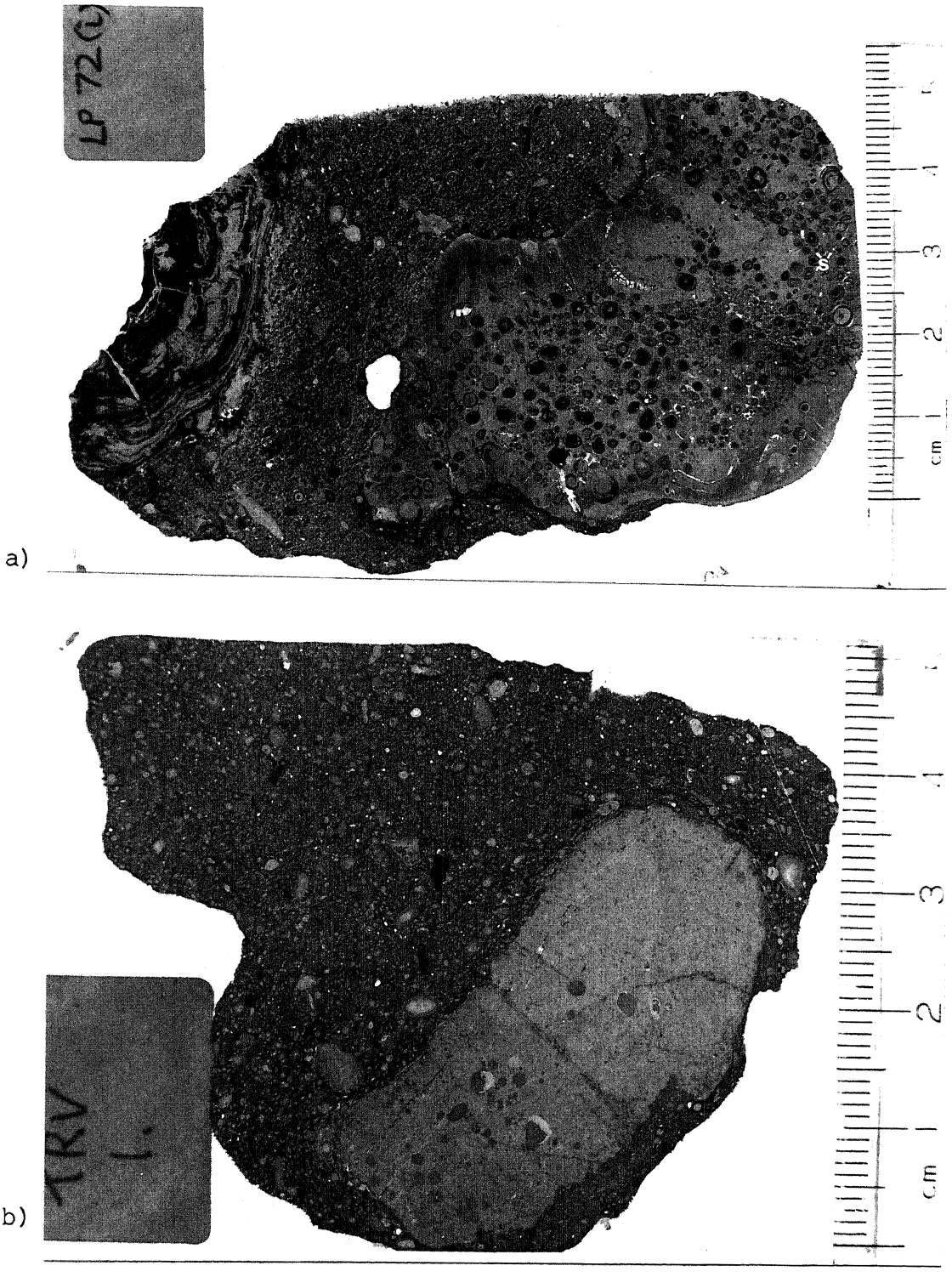

Figure 4.2 Photographs of thin sections, a) stromatolitic phosphatic float-ironstone in an oncoidal ooidal pack-ironstone matrix, LP72A Trefor [SH 3676 4739], b) phosphatic float-ironstone in an oncoidal ooidal pack-ironstone matrix, TRV1 Trefor [SH 3715 4747]. Very large pebble/small cobble-sized reworked phosphatic nodules in 'disturbed' pack-ironstone. Note the sharp or broken margins to the nodules and only minor uniform deformation around the nodules. a) note random distribution of ooids and oncoids within the nodule and shrinkage cracks, S, (white) around the ooids and oncoids when close together.

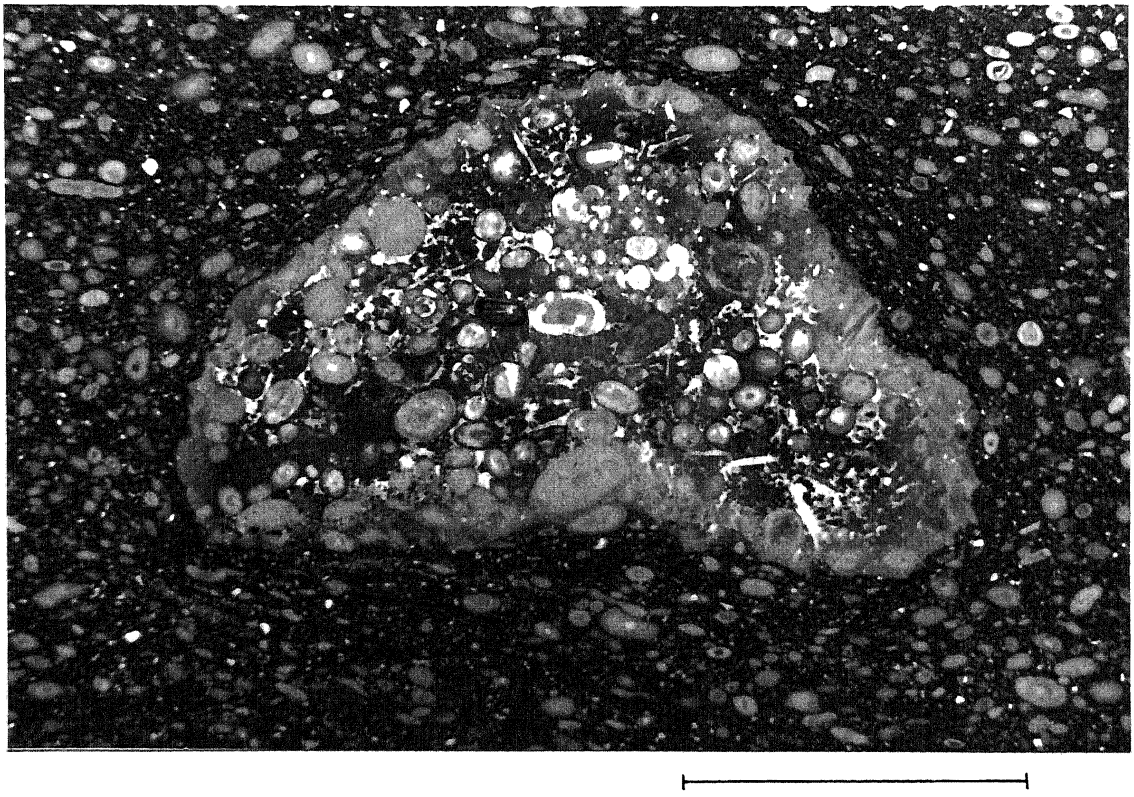

Figure 4.3 Photomicrograph, phosphatic float-ironstone in an ooidal wacke-ironstone matrix, LP33 Creigir Uchaf (St. Tudwals) [SH 2989 2806]. Large pebble-sized reworked phosphatic nodule in a 'disturbed' wacke-ironstone. The edge of the nodule is broken and embayed, marking the sites of former ooids. Deformation is only minor and uniform around the nodule. White patches in the nodule are due to abundant sponge spicules and shrinkage cracks, now infilled by secondary cements. Scale bar = 1cm.

and occurs all the way around the nodule (Figure 4.2). These nodules may show a crude bedding alignment, or be reworked and concentrated into beds (Tremadog, Figure 2.19). Very rarely stromatolite coated nodules are seen (Bryn Poeth, Trefor, St. Tudwals, Ffordd Ddu). Within mud-ironstones nodules are rounded, show both elongation parallel with bedding (Bwlch Coch, Figure 2.25), and deformation of the mud around the nodule. Nodules in mud-ironstones do not contain ooids but may contain fossil fragments.

Fossils are not a common feature of the ironstones, although fossil fragments are seen within the phosphate nodules. The most common fossil fragments within the nodules are sponge spicules (Pulfrey 1933b) (Figure 4.4), although brachiopod fragments (Figure 4.5), Girvanella tubes and chitinozoa are also present. Spicules are so abundant in some nodules that they appear to form a framework for the nodule to grow around and infill. The central canal of some spicules has been filled by chamosite mud before the formation of the nodules. The nodules contain variable amounts of ooids (and oncoids), although there is no pattern to their distribution within the nodules, which is entirely random. Nodules do not contain deformed ooids, which are found immediately around the nodules. When ooids occur close together in the nodules then vugs occur in between the ooids. Usually a thin rim of collophane is left atta ched to the ooids (Figure 4.6). These vugs are subsequently infilled by a variety of cements. Usually the cement is either a rim of apatite needles and then infilled by chamosite and quartz, or infilled by siderite. Later cements are either calcite or pyrite (St. Tudwals) or stilpnomelane and pyrite (Cadair Idris east).

The material forming the nodules is cream/brown in colour and is very fine-grained. This material is referred to as collophane, and generally has a homogenous texture. In the St. Tudwals ironstone can be seen to be pelletal. Between crossed nichols the collophane is isotropic, but in XRD is highly reflective, indicating that it is cryptocrystalline. The principle component of the collophane material is apatite. XRD analysis of one nodule which contains no ooids shows that the collophane is a fine-grained mixture of apatite with some chamosite and silica. XRD shows that it is carbonate fluorapatite (Francolite) (Appendix 3) and EPMA shows the CaO/P_2O_5 ratio to be 1.27 (Appendix 4), which is low compared to to normal francolite (McClellan 1980). A regression line for calcium and phosphorus from the XRF data set has a good correlation (r=0.968) and runs through the origin

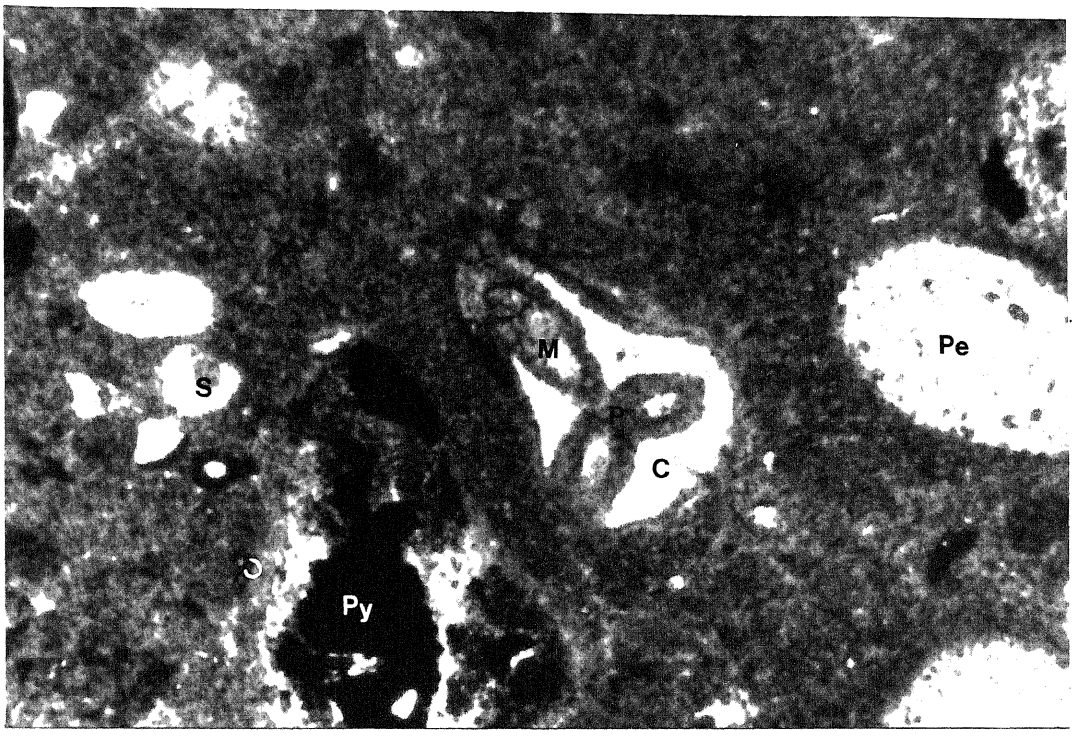

a)

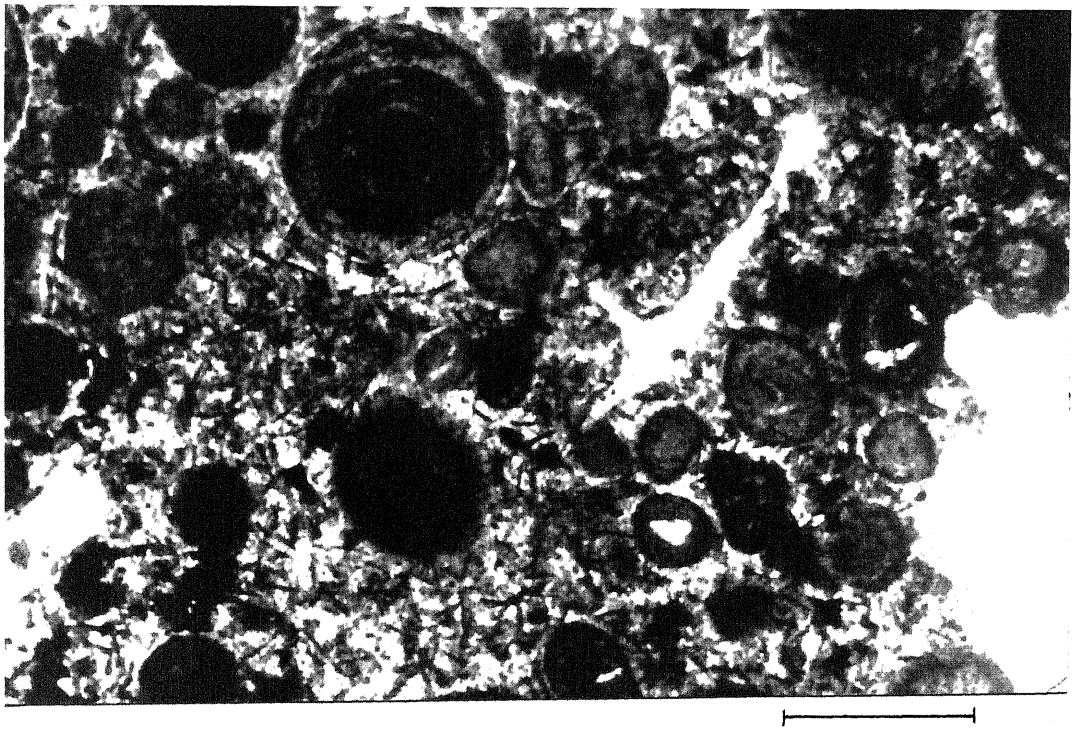

b)

Figure 4.4 Photomicrographs a) phosphate nodule within an ooidal wacke-ironstone, LP19a Pen y Gaer [SH 2982 2832], b) phosphate nodule within an ooidal magnetite pack-ironstone, CI137 Cross Foxes [SH 7606 1652]. Sponge spicules preserved in phosphate nodules. a) cross section of a spicule showing chamosite mud infilling the central canal (M) then collophane (P) then later cements (C) in a nodule also preserving fragments of spicules (S) chamosite peloids (P) and pyrite (P). b) length section of sponge spicule now infilled by later cements. Ooids and peloids in this nodule show some replacment by fine-grained magnetite and the matrix of the nodule contains disseminated flakes of stilpnomelane. Scale bar = 1mm.

Figure 4.5 Photomicrograph, nodule in ooidal wacke-ironstone, LP19A Pen y Gaer [SH 2982 2832]. Brachiopod valve preserved within a phosphatic nodule.

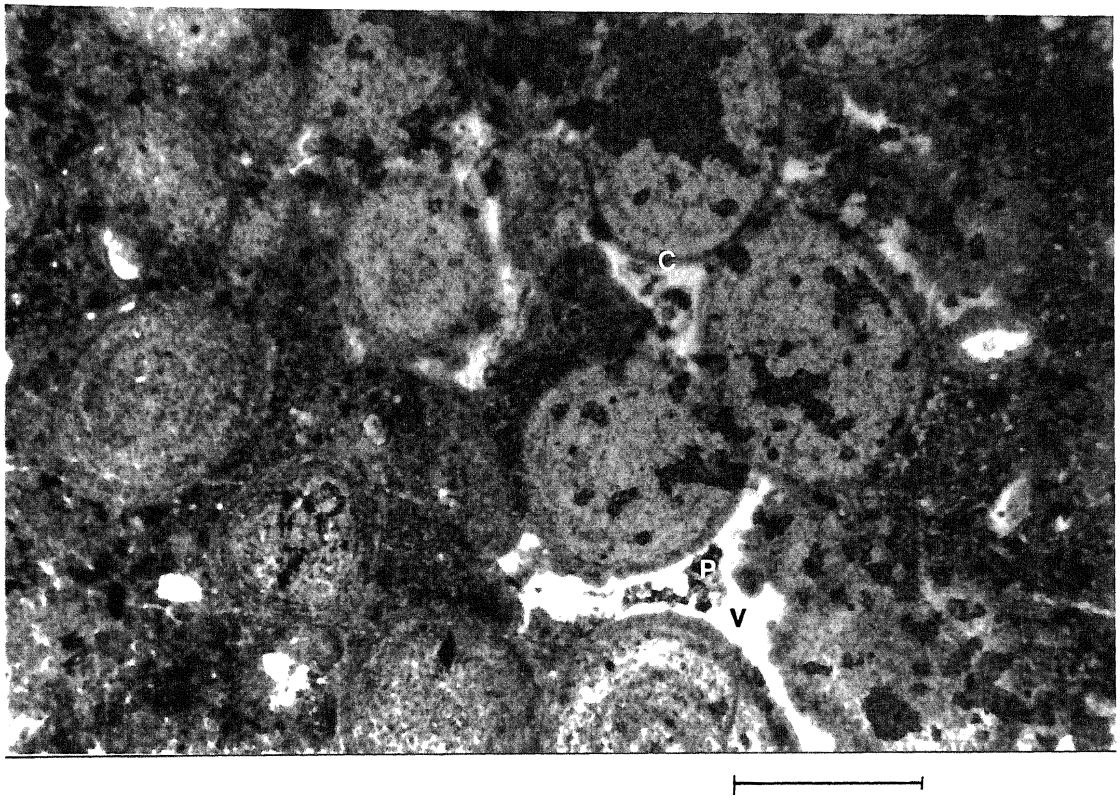

Figure 4.6 Photomicrograph, phosphatic nodule in ooidal pack-ironstone, LP24A Llanengan (St. Tudwals) [SH 2947 2731]. Shrinkage cracks in phosphatic nodules around ooids. A thin rim of darker collophane (C) is left attatched to the rim of the chamosite ooid, and the vug (V) is now infilled by secondary cements (see text for details) including late pyrite (P). Patchy appearance of some ooids is due to the thin sectioning of the sample. Scale bar = 1mm.

(Figure 4.7). This indicates that in the ironstones both these elements are controlled in one phase. The carbon dioxide content of the carbonate fluorapatite was determined using the peak-pair method of Gulbrandsen (1970) from XRD data, the results show 1.5 wt% CO_2. Carbonate fluorapatite is common in primary phosphatic rocks (Swett & Crowder 1982) and also in ironstones (Maynard 1986; Deans 1938).

Statistical analysis (Section 3.3.2) shows the control of phosphate formation on the trace element composition of the ironstones. Heirarchical cluster analysis groups yttrium, chromium, vanadium and strontium with apatite. For chromium and vandium this is a geographical effect as the Betws Garmon ironstone (10 samples) has both a high apatite content, but also a high chromium and vanadium content, due to magnetite formation (Section 5.1). However, a relationship between apatite and yttrium and strontium would be expected as they are both enriched in phosphorites (Altschuler 1980). Yttrium shows a good correlation with apatite (Y/CaO = 0.683, Y/P_2O_5 = 0.651). Yttrium either substitutes for calcium in the apatite lattice or occurs as the mineral xenotime (Clark 1984), identified within the ironstones by SEM with EDAX. Strontium can substitute for calcium, although not in the rhombohedral carbonate lattice (calcite and siderite). It would be expected to see a good correlation between apatite and strontium, but no such correlation is seen (Sr/CaO r=0.369 Sr/P_2O_5 r=0.408). Examination of the XRF data shows that two individual ironstone samples with anomalously high apatite contents (025 Tremadog, 040 Bwlch y Cywion) have anomalously low strontium values. Not including those two samples strontium then shows a good correlation with apatite (Sr/CaO and Sr/P_2O_5 r=0.698), suggesting that it occurs mainly in this phase. The effect of diagenetic apatite on the REE content of the ironstones has been discussed in Chapter 3.

4.1.2 Interpretation

Nodules within pack-ironstones and wacke-ironstones represent *in situ* growth. This growth was controlled by the original texture of the sediment, indicated by the loose packing of ooids (and oncoids) within the nodule, the cessation of nodule growth against the grain-supported matrix, and by the diffuse nature of the nodule margins. Therefore they result from passive growth in more loosely packed and porous areas within the pack-ironstones, below the sediment/sea water interface. The most likely suggestion for the presence of these more

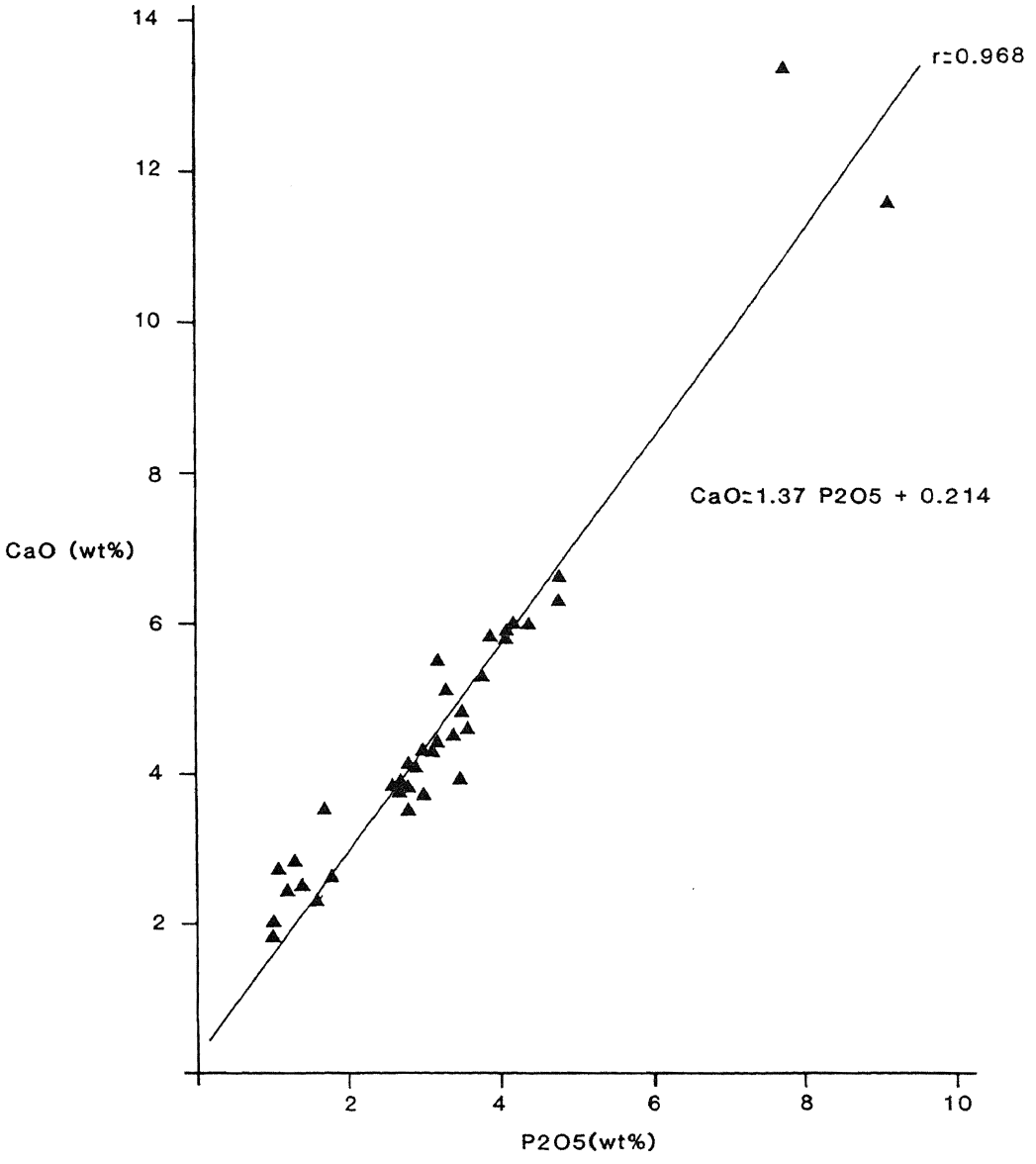

Figure 4.7 Plot of CaO against P2O5 for the ironstones from the geochemical data. This shows a strong correlation between the two (r=0.968), the regression line for which passes close to the origin, indicating that all calcium and phosphorus virtually occur in one phase (apatite). Note two samples (025 Tremadog, 040 Bwlch y Cywion) with anomalously high apatite contents.

loosely packed areas within pack-ironstones is that they are formed by burrowing (Section 3.3.4), a higher phosphate content and organic activity associated with bioturbation may have been the nucleating point for nodule growth. The textural features of nodules in float-ironstones and rud-ironstones indicate that they are reworked and eroded sedimentary clasts in 'disturbed' ironstones. This is also indicated by the algal coating of some nodules, formed initially below the sediment/sea water interface, reworked and then coated by stromatolites. Deformation of ooids around nodules, especially above and below in situ nodules, indicate deformation of still plastic ooids around rigid nodules during burial compaction. As nodules do not contain deformed ooids this indicates that all deformation took place after nodule formation. In the mud-ironstones, deformation of chamosite mud around the nodule indicate that in these sediments too growth occurred before burial compaction.

The presence of fossil fragments, especially sponge spicules and brachiopod fragments, within the nodules, not seen in the ironstones, suggest that these fragments were present throughout the ironstone. Spicule moulds would form in the nodules after solution of the siliceous spicule material. However, in the in the ironstone records of spicules would be completely removed, unless the spicule was originally coated by chamosite laminae (Section 3.1). Vugs formed around ooids in the nodules are shrinkage cracks. Rims of collophane left attatched to the ooids, and the occurrence of vugs only when ooids are close together indicate that these are shrinkage cracks and not shelter cavities. These shrinkage cracks indicate that the ooids have reduced in size during diagenesis. The most probable mechanism for this was by dewatering of chamosite in the ooids (Section 4.5). These vugs were subsequently infilled by cements, giving an indication of the timing of the various diagenetic phases (Section 4.6).

4.2 SIDERITE DIAGENESIS

Thermodynamics dictate that siderite is not a primary phase in marine sediments (Krauskopf 1979; Berner 1971), although it can occur as a primary phase in freshwater environments as bog iron ores (Maynard 1983; Krauskopf 1979). Siderite does occur in marine sediments as a diagenetic phase (Curtis & Coleman 1986; Berner 1981; Matsumoto & Iijima 1981), and siderite is a common diagenetic phase in oolitic ironstones (Maynard 1986,1983). Until recently little detailed work on its petrography or paragenesis had been undertaken (Kearsley 1989; Spears 1989). Both diagenetic and hydrothermal siderite occur within the North Wales Ironstones. However the two can be easily distinguished as diagenetic siderite occurs at virtually all localities, as primary cements and replacing matrix and ooids (Section 4.2.1), while hydrothermal siderite is found at only a few localities, its replacement textures are different to diagenetic siderite, and is always accompanied by some Fe-Cu±Zn±As mineralisation (Section 5.3).

4.2.1 Textures and Mineralogy

Diagenetic siderite occurs only in the upper pack-ironstone, wacke-ironstone or float-ironstone facies and in all grain-ironstones. Intense siderite replacement occurs in the Porth Padrig ironstone (feebly oolitic siderite ironstone), and although textures are quite different (see next section) it is still included in the diagenetic section.

There are five different modes of siderite in the ironstones:

1) primary cementation,
2) secondary alteration of matrix,
3) secondary alteration of ooids,
4) secondary infil of pore spaces,
5) overgrowth of the oolitic texture.

Primary cements only occur in the grain-ironstones, as equant, clear, non-rhombic 'drusy' or sparry siderite (Figure 4.8). This siderite does not show a clear epitaxial relationship to the ooid substrate. Neither does it show coarsening of crystals into the spaces between ooids.

a)

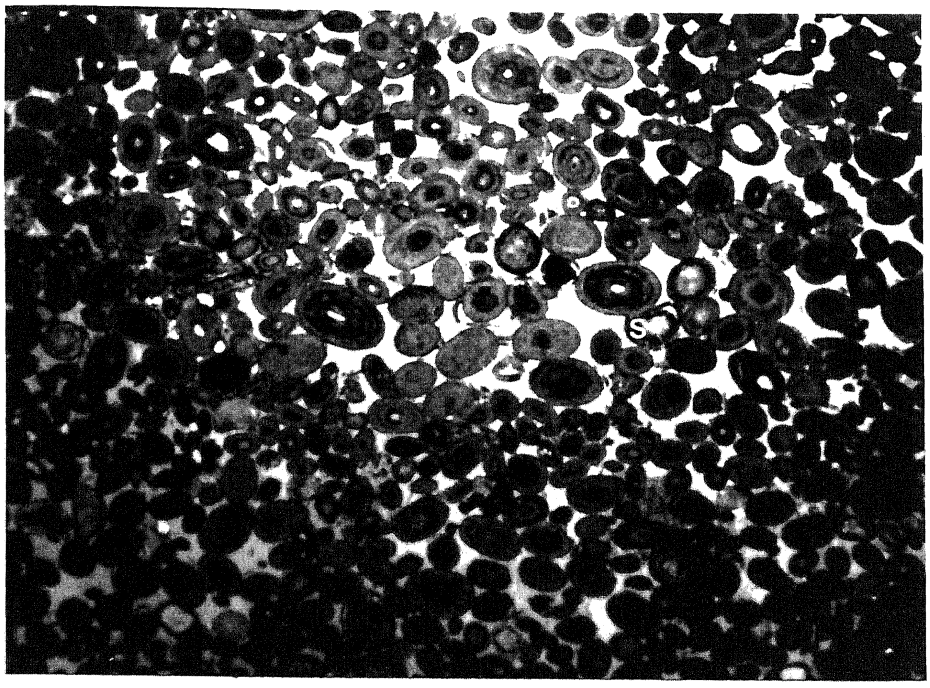

b)

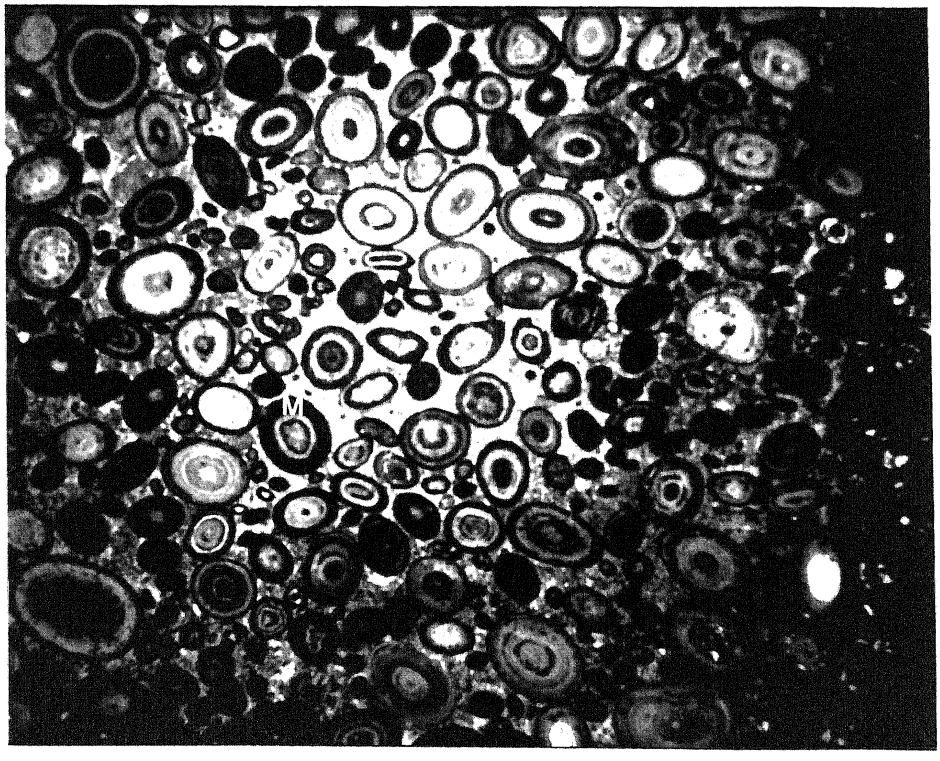

Figure 4.8 Photomicrographs a) chamosite ooidal sideritic grain-ironstone, PSF1 Pensyflog (Tremadog) [SH 5619 3958], b) chamosite ooidal sideritic grain-ironstone, AA10D Bryn Poeth [SH 6016 7958]. Sparry siderite cemented ooidal grain-ironstones, a) with ooids showing splay textures (S) indicating burial compaction before cementation and b) dark micritic siderite replacement (M) of chamosite ooid laminae, mostly of the outer laminae of the oids. The dark outer parts of the photomicrographs are goethite replaced, as siderite is especially vulnerable to surficial weathering. Scale bar = 5mm.

The most common form for siderite to take is as secondary alteration of the matrix. This takes the form of siderite rhombs, on average 100μm in size, within the matrix of the upper pack-ironstones, wacke-ironstones or float-ironstones facies, either as disseminated rhombs or as a cluster of rhombs entirely replacing matrix (Figure 4.9). There is a gradation in the matrix between microcrystalline cemented green chamosite mud with no rhombs to darker organic-rich muds with abundant rhombs, this uneven mud distribution having been discussed in Chapter 3. With more intensive siderite development rhombs also occur disseminated around the edges of phosphate nodules. With very intensive siderite development (Pen y Gaer, St. Tudwals), siderite also occurs disseminated throughout the nodules but also as clusters of rhombs replacing a patch of nodule (Figure 4.10). Siderite rhombs in some of the Snowdonia and Cadair Idris ironstones are now pseudomorphed by chamosite (Subsection 4.3.1).

With this increasing sideritisation there is associated secondary alteration of the ooids, which also occurs in the grain-ironstones associated with cement growth. Initially the first replacement is of the ooid rim by dark (possibly due to weathering) micritic siderite (Figure 4.8). Further alteration of the ooid is by replacement of chamosite laminae by micritic siderite. There is a variation in the upper ironstone facies between ooids in green chamosite mud and dark organic-rich mud. The former have no siderite rhombs and no replacement of ooids by siderite. The latter have siderite rhombs and show extensive replacement by micritic siderite.

With intensive sideritisation secondary pore spaces in nodules, shrinkage vugs and fossil cavities, are also cemented by siderite instead of apatite and chamosite (Section 4.1). Finally the Porth Padrig ironstone (feebly oolitic siderite ironstones) is now almost totally replaced by interlocking rhombs of siderite overgrowing both the ooids and the matrix. The ooids, originally chamosite, are now composed of a mosaic of silica.

Deer et al. (1962c) have shown that there is a complete solid solution series between siderite ($FeCO_3$) and rhodochrosite ($MnCO_3$), siderite ($FeCO_3$) and magnesite ($MgCO_3$), but only limited substitution between siderite ($FeCO_3$) and calcite ($CaCO_3$) of up to 10-15% calcite. This is due to the size difference between the Fe^{2+} and Ca^{2+} ions (Table 4.1). XRD data for siderites is shown in Appendix 3, a composite of all siderites. As the largest siderite peak $d_{(10\bar{1}4)}$ overlaps with the $d_{(005)}$ chamosite peak, the relative intensities of

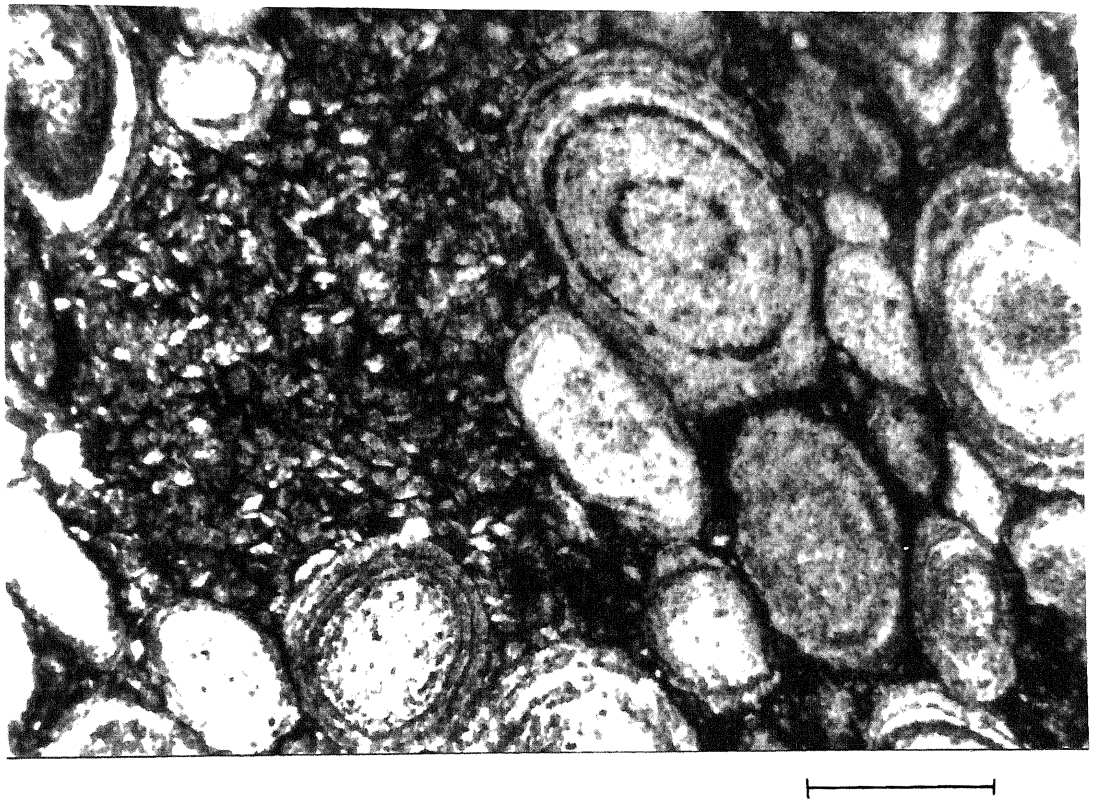

Figure 4.9 Photomicrograph, ooidal wacke-ironstone, LP24D Llanengan (St. Tudwals) [SH 2947 2731]. Siderite rhomb replacement of chamositic matrix. Pleochroic rhombs of siderite replacing a patch of dark organic-rich chamositic muddy matrix. This darker matrix can be seen between ooids to the right, where one or two siderite rhombs occur. Scale bar = 1mm.

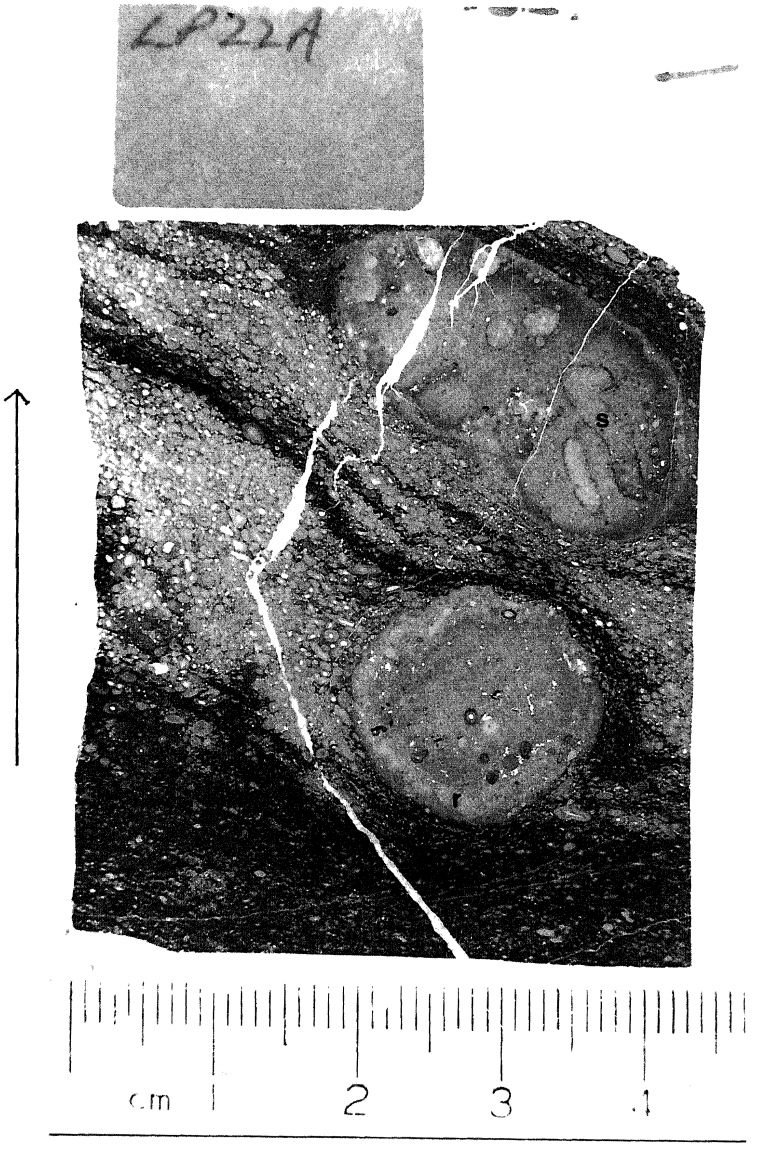

Figure 4.10 Photograph of thin section, ooidal pack-ironstone with mud-ironstone lenses, LP22A Pen y Gaer [SH 2990 2821]. Diagenetic siderite replacement of phosphatic nodules. Both nodules show a pale reaction rim (R) of disseminated siderite rhombs, and the upper nodule shows patches within the nodule entirely replaced by siderite (S). Note deformation of ooids above and below the nodules and especially in between the two, but with little or no deformation to the side of the rhomb. The darker lenses within the section are very organic-rich chamositic mud. The cross-cutting veins contain mostly coarsely crystalline chamosite with some quartz.

the siderite peaks cannot be determined. However, Curtis et al. (1975) have shown that the $d_{(10\bar{1}4)}$ peak for siderite can vary with ionic substitution. This depends on the size of the ion substituting for Fe^{2+} and therefore expands or contracts the cell dimensions. End member $d_{(10\bar{1}4)}$ peaks and ion sizes of the rhombohedral carbonates are shown in Table 4.1.

IONIC RADII		CARBONATE $d_{(10\bar{1}4)}$ SPACINGS	
Mg^{2+}	0.066nm	Magnesite	0.274nm
Fe^{2+}	0.074nm	Siderite	0.279nm
Mn^{2+}	0.080nm	Rhodochrosite	0.284nm
Ca^{2+}	0.099nm	Calcite	0.3035nm

Table 4.1 Ion sizes and $d(10\bar{1}4)$ spacings for the end members of the siderite-magnesite-rhodochrosite-calcite series.

Examination of the XRD data shows that for the St. Tudwals siderites $d_{(10\bar{1}4)}$ = 0.279nm and for the Bryn Poeth siderites $d_{(10\bar{1}4)}$ = 0.280-0.281nm. The St. Tudwals siderites usually show Mg and [Ca+Mn] in the same proportion (see below) so the unit cell does not change. However, the Bryn Poeth siderites show high [Ca+Mn] and low Mg substitution (see below) so an expansion of the unit cell is seen.

EPMA analyses of siderites from the Bryn Poeth (1 PTS), Trefor (1 PTS) and St. Tudwals (3 PTS) ironstones are given in Appendix 4. Analyses are plotted on a triangular diagram $[Fe+Mn]CO_3$, $CaCO_3$, $MgCO_3$ (Figure 4.11). There is a clear distinction between the Bryn Poeth siderites and Llŷn peninsula siderites in that although both roughly have the same magnesium content, Bryn Poeth siderites have much higher substitution by calcium (plus a higher manganese substitution not shown on Figure 4.11).

Different siderite modes have been analysed by EPMA. These are siderite rhombs, siderite cements and micrite replacing ooids (Appendix 4), although analyses are only available for the latter from Bryn Poeth. For the Trefor and St. Tudwals ironstones there is little difference between rhomb and cement compositions. The overall trend of

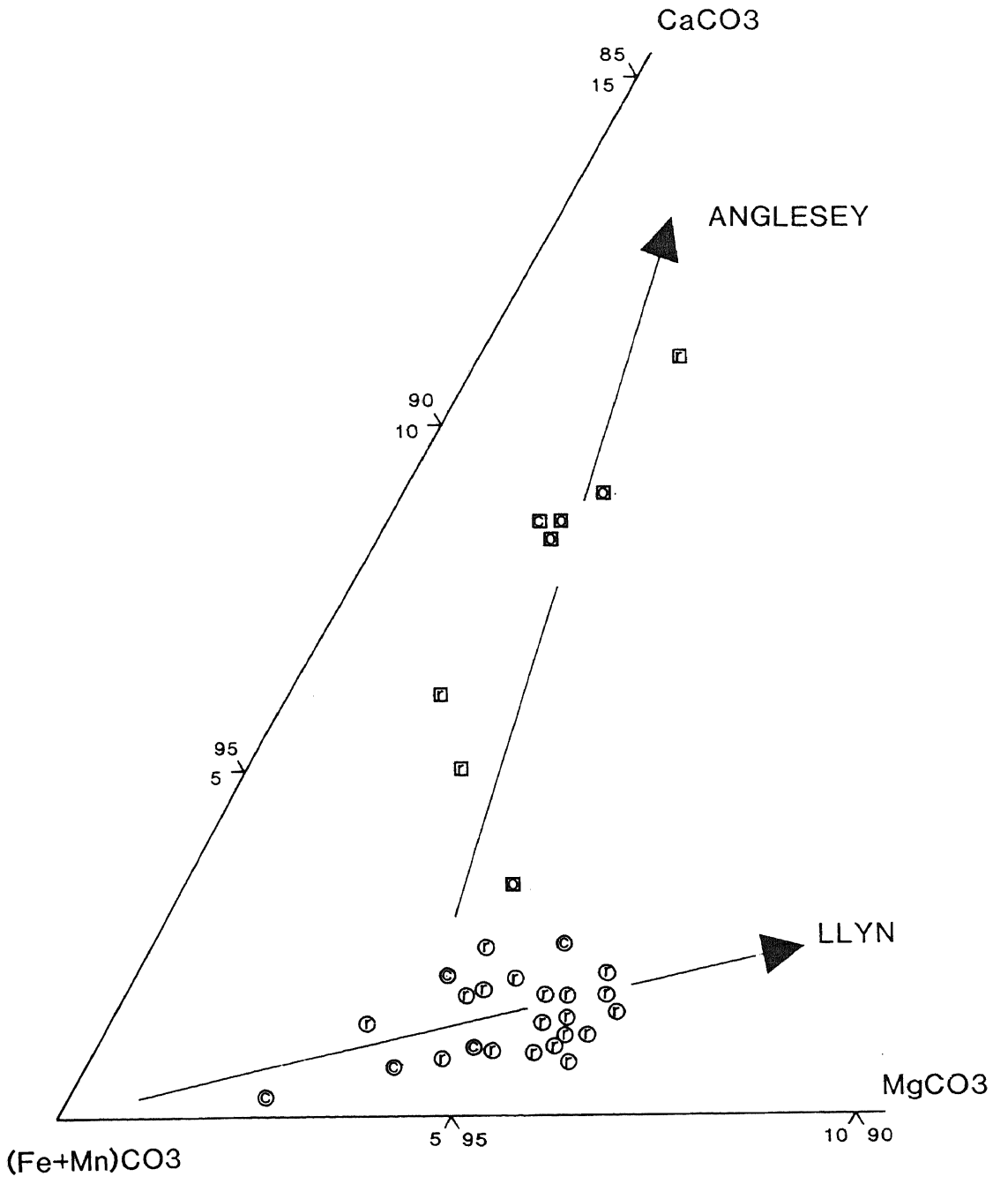

Figure 4.11 EPMA analyses of diagenetic siderite from Anglesey (squares) and the Llŷn Peninsula (circles). The siderites show no compositional variation with morphology, r=rhomb, c=cement, o=ooid. Instead the Llŷn siderites show a compositional trend toward a more magnesian-rich composition. The Anglesey siderites show a trend away from the Llŷn siderites toward a more calcium-rich composition (see text for further details).

changing siderite composition is unaffected by the mode the siderite takes. However, for the Bryn Poeth ironstone there is a marked difference (based on only a small number of analyses) between rhombs and secondary cements and micrite replacements. Siderite rhombs have a much higher Mn content than secondary cements or micritic siderite.

4.2.2 Interpretation

Siderite cementation and alteration is a fabric selective feature; the main control on the distribution of siderite is the porosity of the ironstones. The porosity of the ironstones allowed the movement of diagentic pore waters which, to precipitate siderite, must have been iron-rich, alkaline and reducing. The composition of siderite also gives an indication of the diagenetic history of the ironstones, as mineral composition reflects pore water composition (Curtis et al. 1975, Matsumoto & Iijima 1981).

For a sparry cement to form in grain-ironstones mud was clearly absent. Large equant siderite grains with no preferred orientation indicate slow formation of these cements from low levels of supersaturation (Berner 1980). The uneven distribution of siderite rhombs in the matrix of the ironstones is primarily a porosity control. However, the darker muds where rhombs are abundant are also rich in organics, the reduction of which would provide bicarbonate ions for siderite formation. In these darker muddy patches ooids also show secondary alteration by micritic siderite. With more reduction of organic matter there would be increased activity of bicarbonate ions in the pore waters. These bicarbonate-rich pore waters are highly corrosive to silicates (Burley et al. 1985) and so are capable of reacting with the matrix to form siderite rhombs, and with the rims of ooids (the part of the ooid first in contact with the pore waters) to form a micritic replacement. These pore waters are the most likely mechanism for the solution of siliceous spicule material. The formation of moulds in nodules implies that this occurred after nodule formation. With further bicarbonate activity there is selective replacement of ooid laminae by micritic siderite, reflecting different microfabrics between ooid laminae. More porous and coarsely crystalline phyllosilicate laminae are very susceptible to reaction to pore fluids (Kearsley 1989). EPMA analyses of siderites rhombs and micrite from the Bryn Poeth ironstone indicate that rhombs formed before micrite. Analyses of rhombs and micrites indicate that rhombs

have a much higher manganese content than micrite. Siderite scavenges any available manganese suggesting that rhombs were the first mode to form.

The composition of siderites reflect the composition of the pore waters at the time of their formation. Curtis et al. (1975) and Matsumoto & Iijima (1981) have shown that early formed siderites have a high Fe and Mn and low Ca and Mg content, and later siderites have a lower Fe and Mn and higher Ca and Mg content, as if at the Fe-rich end of a mixing line between siderite and dolomite. Analysis of the North Wales Ironstones siderites do not show this trend. All siderites have approximately the same magnesium content, and the manganese content most likely represents scavenging of available manganese by siderite. The high values of calcium for the Bryn Poeth siderites are therefore enigmatic. They do not represent surficial weathering, a process which would leach magnesium and therefore relatively enrich iron and calcium. Either it represents higher pore water contents of calcium at the time of diagenesis or a later enrichment by calcium. The St. Tudwals ironstone was originally contained some calcite, as calcite Girvanella tubes and late ferroan calcite cements are present. However, this is not reflected by the siderite compositions, which are calcium poor. Therefore the Bryn Poeth siderite compositions most likely reflect later enrichment by calcite. As Carboniferous Limestone occurs approximately 60m above the Bryn Poeth ironstone (Greenly 1919) this is the most probable mechanism.

4.3 CHAMOSITE DIAGENESIS

All berthieroid material in the ironstone is now present as chamosite (sensu AIPEA 1980). No berthierine has been detected in any of the North Wales Ironstones. Petrographic observations of secondary cements give an indication of the remobilisation of chamosite during diagenesis. Mineralogical analysis of compositional and structural changes detail mineralogical changes undergone by chamosite during burial diagenesis and metamorphism. Throughout this thesis it is assumed, as there is no direct evidence, that at the time of deposition and diagenesis the berthieroid material was present as berthierine, and was subsequently converted to chamosite during burial metamorphism (Hughes 1989; Maynard 1986; Velde 1985; Van Houten & Purucker 1984; and references therein).

4.3.1 Petrography

Chamosite occurs in the ironstones in five different modes:

1) Allochems,
2) Mud matrix,
3) Secondary cements,
4) Siderite pseudomorphs,
5) Veins,

Allochems and mud matrix are both sedimentary in origin and were converted from berthierine to chamosite during burial metamorphism, discussed in more detail later in this chapter. The petrographic description of the chamosite allochems and mud matrix is given in Chapter 3. The last three modes of chamosite are demonstrably diagenetic in origin. It will be later shown that secondary cements and siderite pseudomorphs were formed as berthierine, and were also later converted to chamosite (Section 4.5).

Chamosite secondary cements are most commonly seen in the phosphate nodules, but also more rarely occur as void infills in the matrix. Within the nodules chamosite cements occur within shrinkage cracks and fossil cavities. Unless these vugs are filled by siderite (Section 4.2) the first phase is a rim of apatite needles, followed by either blades of chamosite infilling the vug, or intergrowths of chamosite and quartz. Secondary cements are seen at all localities but secondary

cements in the matrix are only seen at Betws Garmon and Cadair Idris east. The vugs in the matrix are the result of the dissolution of ooids. Chamosite in these vugs occurs with pyrite, stilpnomelane and quartz. Chamosite pseudomorphing siderite is seen at Trefor, Betws Garmon and Cadair Idris, where former rhombs of siderite are now infilled by interlocking blades of chamosite. Chamosite in cross cutting veins is seen at Trefor and St. Tudwals, and as chamosite rims of quartz veins at Aber (Figure 4.12).

4.3.2 Mineralogy

The mineralogy of chamosite in the North Wales Ironstones has been studied using XRD and EPMA techniques. The location of the 25 samples analysed by XRD are shown in Appendix 1 and the results in Appendix 3. The location of the 16 samples analysed by EPMA are shown in Appendix 1. The EPMA analyses, with 5 to 15 spot analyses of chamosite from each polished thin section, is given in Appendix 4. This also includes methodology to ensure that mixed mineral spot analyses are excluded.

XRD analysis shows the only iron-rich sheet silicate in the ironstones (excluding metasomatic stilpnomelane) to be chamosite. EPMA analysis confirms that they are iron-rich aluminous chlorites. As is typical for iron-rich chlorites, the $d_{(001)}$ and $d_{(003)}$ peaks are very weak and the $d_{(002)}$ and $d_{(004)}$ peaks very strong. Identification of the chlorite polytypes (Brindley & Brown 1980; Hayes 1970) indicates that virtually all samples are the Ib ($B=90^{\circ}$) polytype, characterised by a large $d_{(202)}$ peak at approximately 0.25nm (Figure 4.13). Only two samples (AB002, Aber and CI104, Foxes Path) showed the IIb chlorite polytype (Figure 4.13), which differ from the Ib ($B=90^{\circ}$) chlorite polytype in the 0.21-0.28nm region.

Appendix 4 shows different modes of chamosite analysed by EPMA (ooids, ooids in nodules, deformed ooids, cements, veins). However, the variation in chamosite composition is not related to these different modes. The variation in chamosite composition is best presented by plotting tetrahedral substitution of silicon by aluminium against octahedral substitution between iron and magnesium (Hayes 1970; Curtis *et al.* 1985). Figure 4.14 defines the main fields of the different sedimentary chlorite polytypes and their evolutinary pathways (Curtis *et al.* 1985). The North Wales chamosites have little variation in octahedral substitution of iron by magnesium but a large variation in tetrahedral substitution of silicon by aluminium. North

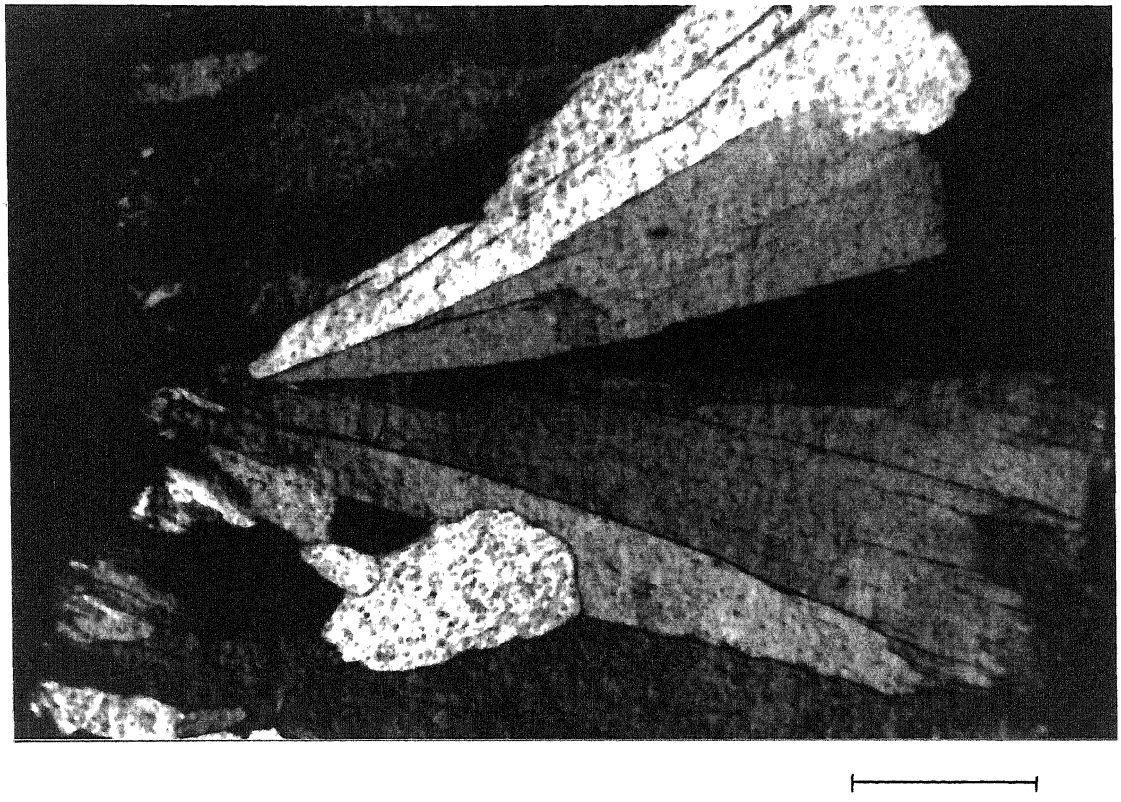

Figure 4.12 Photomicrograph crossed polarised light, vein material, AB002 Aber [SH 6699 7296]. Large blades of chamosite forming a rim to the quartz vein from the edge of the ironstone, and showing a IIb chlorite polytype XRD trace (Figure 4.13).

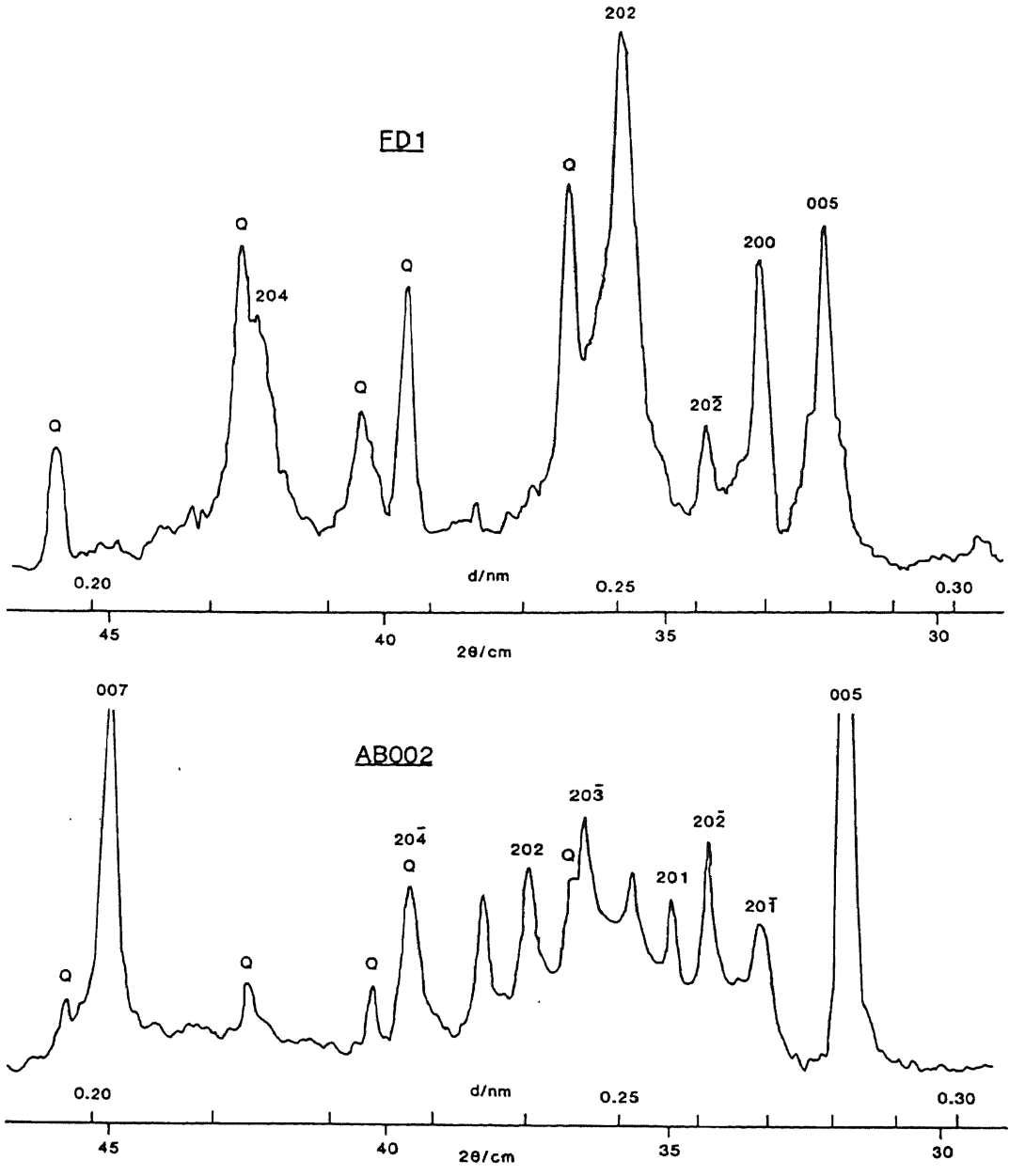

Figure 4.13 XRD traces showing the two different chlorite polytypes for the ironstones. Top (FD1 Ffordd Ddu) showing a Ib(B=90°) chlorite polytype and bottom (AB002 Aber) showing a IIb polytype. See Appendix 3 for details of XRD data.

Wales chamosites from all localities plot on the Fe-rich end of Figure 4.14 and are shown in Figure 4.15.

The composition of the North Wales chamosites vary from an initial 'berthierine-like' composition to a 'IIb-like' composition when compared to the compositional fields defined by Curtis et al. (1985). This variation in composition can be related to trace element content and variation in chamosite crystallinity. An indication of the crystallinity of chamosite can be achieved by measuring $\Delta 2\theta$ half height peak width of the $d_{(002)}$ peak. This gives a semi-quantitative value of chamosite crystallinity to confirm empirical observations from XRD traces. The only samples with a 'berthierine-like' composition are from Cadair Idris (Figure 4.15). This includes both samples from Cadair Idris west (CI & CI1) and a magnetite-rich pack-ironstone from Cadair Idris east (CI137). These show no variation in octahedral substitution of magnesium by iron, but a large variation in tetrahedral substitution of silicon by aluminium over the berthierine compositional field. Overall they have low tetrahedral aluminium totals (average Al(T)=1.94). An average analysis of Cadair Idris chamosites shows high silicon and ferrous iron values, low aluminium values, the presence of vanadium, chromium, manganese and potassium within the chamosite lattice, and low (11.82) octahedral totals (Table 4.2). The chamosites have a poor crystallinity ($\Delta 2\theta$=0.6) and the $d_{(001)}$ peak is absent, the presence of an $d_{(003)}$ peak indicating it is chamosite and not berthierine.

Some samples have a composition transitional between a 'berthierine--like' and 'IIb-like' composition. These are a stilpnomelane-rich wacke-ironstone from Cadair Idris east (CI130c), an oncoidal float-ironstone in ooidal wack-ironstone lenses within a mud-ironstone from Bryn Poeth (AA10C), a magnetite-rich pack-ironstone (YF-A) and an oncoidal wacke-ironstone (YF-B) both from Betws Garmon (Figure 4.15). These all show little variation in octahedral substitution of magnesium by iron (although YF-A has a high Fe content) but some variation in tetrahedral substitution of silicon by aluminium (average Al(T)=2.45). Compared to the other Cadair Idris chamosites they are more crystalline ($\Delta 2\theta$=0.5), trace elements analysed for are absent (apart from some Mn) and have lower silicon and ferrous iron values, higher aluminium values and higher octahedral totals (Table 4.2).

The rest of the samples have a 'IIb-like' composition, although they are all Ib($B=90^{\circ}$) chlorite polytypes. The exception to this is the chamosite vein material from Aber (Figure 4.12) which has a IIb

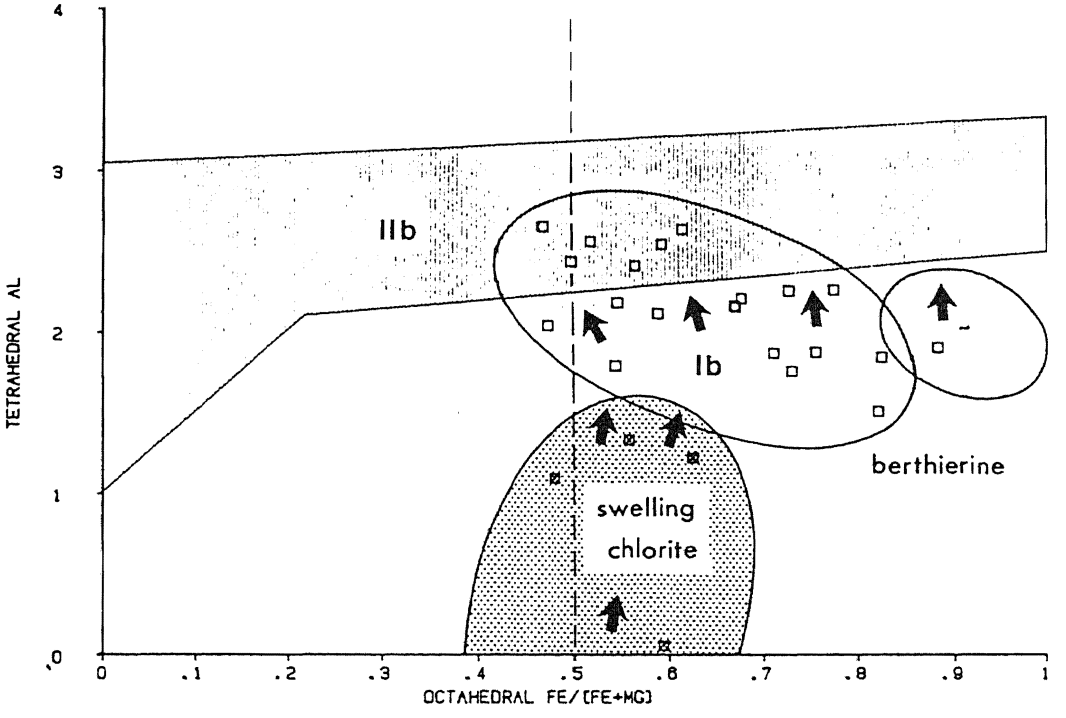

Figure 4.14 Evolution of the sedimentary chlorites by compositional changes, after Curtis et al. (1985).

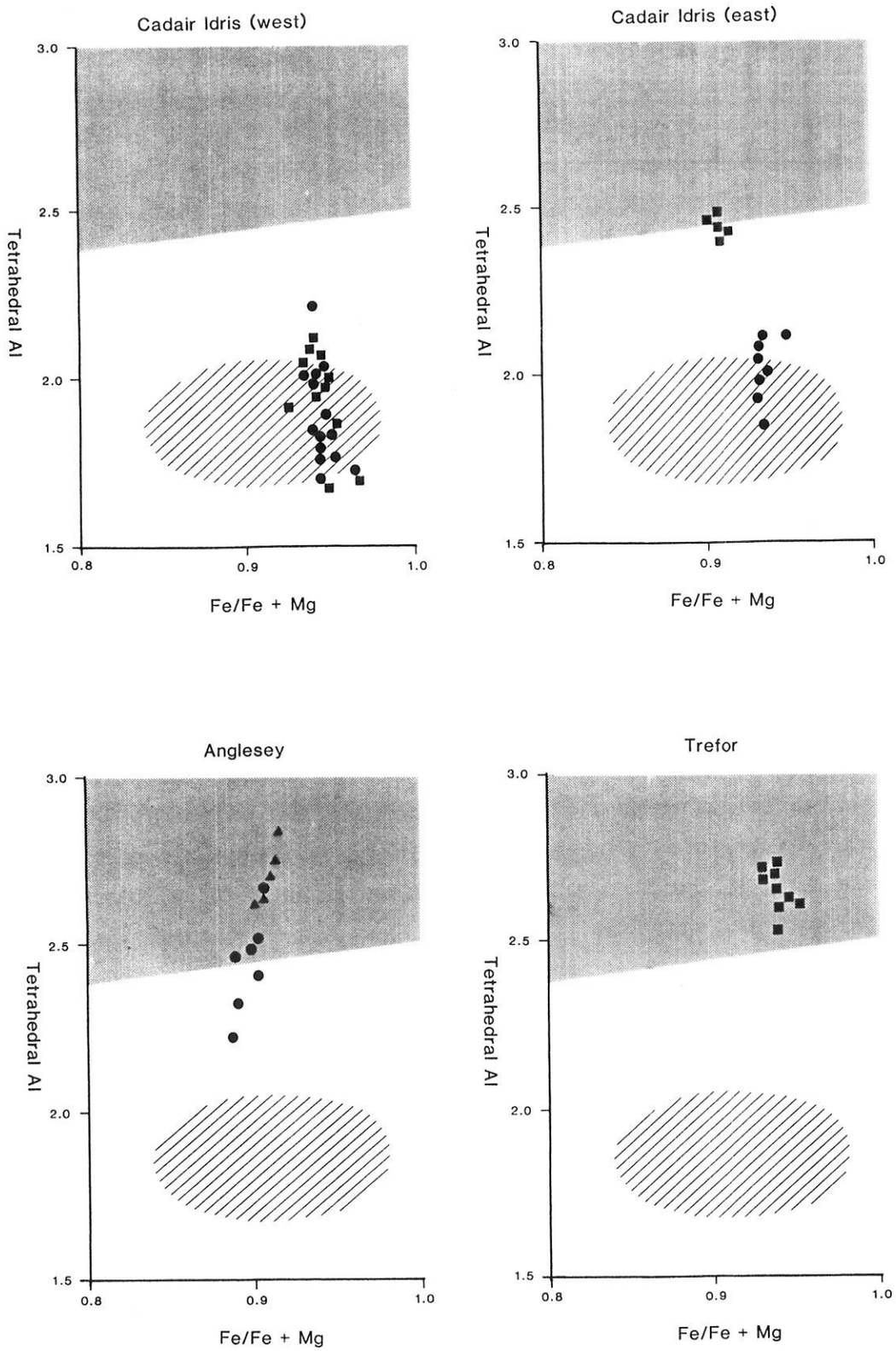

Figure 4.15 Plot of chamosite EPMA analyses on the Fe-rich end of Figure 4.14. Stippled area - IIb compositional field, shaded area - berthierine compositional field (after Curtis et al. 1985). Cadair Idris west, squares CI1, circles CI. Cadair Idris east, squares CI130C, circles CI137. Anglesey, circles AA10C, triangles AA10E. Trefor, squares LP72.

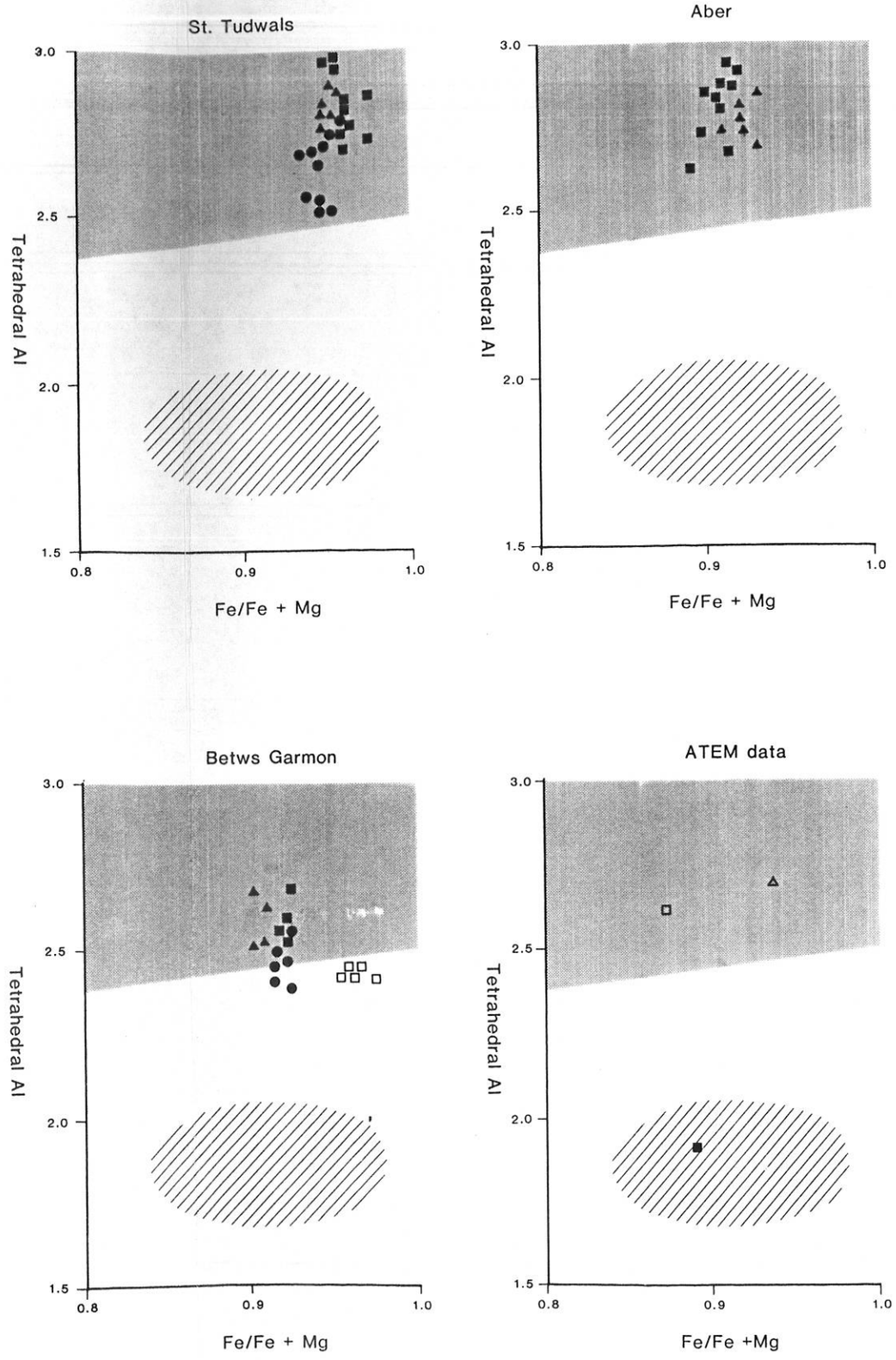

St. Tudwals, squares LP19A, circles LP22A, triangles LP22D. Aber, squares AB-A, triangles AB002. Betws Garmon, open squares YF-A, circles YF-B, triangles YF-G, filled squares SN15C. ATEM data (after Hughes 1989) filled square - berthierine, Cleveland Ironstone, open square Betws Garmon, triangle Tremadog.

chlorite polytype XRD trace (Figure 4.13). Although there is some variation in octahedral substitution, the main variation is still in tetrahedral substitution of silicon by aluminium (average Al(T)=2.72). These chamosites are the most crystalline ($\Delta 2\theta$=0.4), trace elements analysed for are absent (apart from some Mn), have aluminium and silicon values almost equal to each other and have high octahedral totals (Table 4.2).

Hughes (1989) has studied berthierines from Jurassic ironstones and Ordovician chamosites from Betws Garmon and Tremadog by analytical transmission electron microscopy (ATEM). He has shown that the North Wales chamosites are crystalline with much larger crystallites than berthierine. The crystallite grain sizes for chamosite are from 0.1 X 1.5 μm to 0.5 X 2.0 μm. Plotted on Figure 4.15 the ATEM results of Hughes (1989) agree closely with the EPMA analyses in this study.

4.3.3 Discussion

All chamosites are Ib(B=90^{o}) polytype, except for two samples AB002 (Aber) and CI104 (Foxes Path), which are IIb chlorite polytypes. Sample AB002 is a chamosite rim to a hydrothermal quartz vein. Therefore the chamosite was precipitated at high temperatures and so directly formed a IIb polytype. This chamosite vein material has the same composition as chamosite from the ironstone, indicating that the vein material formed in chemical equilibrium with the surrounding rock. The IIb chamosite polytype from Foxes Path, an ooidal wacke-ironstone, is more problematic. The ironstone occurs below a granophyric intrusion which, by contact metamorphism, may have formed a IIb polytype (Section 5.5).

The compositional and structural variation in the chamosites is from an initial 'berthierine-like' composition, with low tetrahedral aluminium values, low octahedral totals, high silicon and ferrous iron contents, contain appreciable potassium, chromium and vanadium in the chamosite lattice, and with poor crystallinity. With maturation the chamosites evolve toward a 'IIb-like' composition, with high tetrahedral aluminium contents, high octahedral totals, silicon and aluminium values equal, no trace elements in the chamosite lattice, and with high crystallinity. The compositional and structural changes described above can be related to the maturation of chamosite with burial diagenesis and metamorphism (Section 4.6). Only at two ironstone localities, Cadair Idris and Bryn Poeth, can the variation

	Ffordd Ddu CI1	Bryn Poeth AA10C	Bryn Poeth AA10E	Aber AB002
n	11	6	4	6
MgO	1.557	2.757	2.462	2.088
Al2O3	15.553	19.486	20.382	21.247
SiO2	26.109	24.362	23.422	23.327
K2O	0.164	-	-	-
V2O3	0.102	-	-	-
Cr2O3	0.126	-	-	-
MnO	0.199	-	0.193	0.150
FeO	46.430	43.187	43.358	44.458
Si	6.021	5.527	5.333	5.240
Al(T)	1.979	2.473	2.667	2.760
Al(O)	2.249	2.740	2.803	2.867
Al	4.228	5.213	5.470	5.627
K	0.048	-	-	-
Mg	0.535	0.933	0.836	0.699
V	0.019	-	-	-
Cr	0.023	-	-	-
Mn	0.039	-	0.037	0.029
Fe	8.955	8.195	8.257	8.352
OCT	11.820	11.868	11.933	11.947
TOT	19.820	19.868	19.933	19.947
y	0.944	0.898	0.908	0.923

Table 4.2 Average analyses of chamosites from Ffordd Ddu, Bryn Poeth (wacke-ironstone), Bryn Poeth (Pack-ironstone) and Aber showing averaged EPMA analyses (n = number of analyses) and mineral formula calculations (based on 36 oxygens), octahedral total, mineral total and $Fe/_{[Fe+Mg]}$ ratio (y).

in composition and structure be shown to be controlled by additional factors to burial metamorphism.

At Cadair Idris the majority of the chamosite analyses have a berthierine-like composition. These are two samples from Ffordd Ddu (Cadair Idris west) and a magnetite-rich pack-ironstone from Cadair Idris east (Cross Foxes and Ffordd Ddu). The other sample is a stilpnomelane-rich wacke-ironstone from Cadair Idris east, and has a composition on the edge of the 'IIb-like' field. This difference in chamosite composition has been detailed in Chapter 5. The magnetite-rich sample shows magnetite replaces the matrix around the ooids. This substantially reduces its porosity. Therefore chamosite can undergo no further reaction once magnetite has replaced the matrix, and so retains an initial 'berthierine-like' composition. By contrast stilpnomelane reacts with chamosite during its formation. Therefore during the metasomatic reactions, due to the dolerite intrusion above the Cadair Idris east ironstone (Chapter 5), chamosite can mature.

The two chamosite samples from Bryn Poeth (AA10C & AA10E) show an evolution in composition towards a 'IIb-like' composition. Plotted on Figure 4.15 they show a strong positive correlation (r=0.906) between a large increase of tetrahedral aluminium substitution with a small octahedral iron substitution. The polished thin section containing chamosite with the lower tetrahedral aluminium values and lower octahedral totals is a mud-ironstone with ooidal and oncoidal lenses. By contrast the chamosite in the ploished thin section with the higher tetrahedral aluminium values and octahedral totals is from an ooidal pack-ironstone. Both samples are from the same locality, therefore it is unlikely that burial metamorphism alone would account for this difference in composition. The mud-ironstone with oncoidal and ooidal lenses would have a reduced porosity in comparison to the pack-ironstone. Therefore during burial metamorphism there would be less maturation of chamosite in the mud-ironstone.

The Ffordd Ddu chamosites do not show a correlation between chamosite maturity and conditions of metamorphism. The Ffordd Ddu chamosites show the lowest levels of maturation, but illite crystallinity studies (Robinson & Bevins 1986) place the Cadair Idris region in the highest grades of metamorphism (Epizone). This would either indicate that chamosite is not affected by burial metamorphism (Section 4.6) or that illite crystallinity values were misinterpreted, due to the effects of dolerite and granophyric intrusions in the area.

The question then raised is why porosity should affect the maturity of chamosite. It has been shown that sedimentary chlorites have higher Si and lower octahedral totals than those stable at higher temperatures (Curtis et al. 1985). It has been suggested that this change in composition is either by the elimination of residual smectite from chlorite, or by modifying the composition of the tetrahedral sheet by the incorporation of aluminium or elimination of silicon (Curtis et al. 1985). Despite the fact that immature North Wales chamosites are siliceous and contain minor potassium (Ffordd Ddu), it is unlikely that there are smectite interlayers in the chamosite structure. This is because berthierines and North Wales chamosites do not show any change in the basal spacing positions with heating (Brindley & Youell 1953; Weinberg 1973). Therefore the North Wales chamosites change composition by either loosing silicon or incorporating aluminium. Of these two processes it is most likely to be the elimination of silicon from the tetrahedral sheet, as geochemically aluminium is effectively immobile. Therefore it would be easier for chamosite to loose silicon (and iron - Table 4.2) than gain aluminium. This would explain why differences in porosity would control the variation in chamosite maturation.

4.4 SILICA DIAGENESIS

Quartz crystals occur in voids in the phosphate nodules, commonly intergrown with chamosite and therefore late diagenetic in origin. However, significant amounts of silica are present in the ironstone (from XRD data) despite the fact that no visible quartz is present in thin section. EPMA analyses of chamosite in ooids occasionally show some mixing with silica, indicating that quartz is present within the ooids, although it is too fine-grained to be visible. One unusual feature is the presence of quartz-rich ooids in some ironstones. They have the appearance of original chamositic ooids now replaced by silica. They occur only in the Ffordd Ddu and Tremadog ironstones.

4.5 DISCUSSION

The main control of diagenesis in the North Wales Ironstones is their porosity. This controls the distribution and maturation of the diagenetic phases, and the composition of the interstitial pore waters, which dictate the composition of the diagenetic phases formed. The compositions of carbonates, silicates and phosphates in oolitic ironstones are similar to those reported for early diagenetic minerals from other types of sedimentary rocks, indicating that ironstone formation does not require unusual chemical conditions other than a large supply of iron (Maynard 1986). The earliest diagenetic reactions in Phanerozoic Ironstones can involve phosphatisation of the components of the ironstones, and often the extensive generation of siderite (Young 1989a). Siderite generation occurs at various times from very soon after deposition until later burial diagenesis. Early siderite is often influenced by the presence of bioturbation (Young 1989a). Therefore the diagenetic reactions in the North Wales Ironstones are not unique but common to many other ironstones.

4.5.1 Controls of Phosphate Diagenesis

The main controls of phosphate formation are a supply of phosphorus, a low sedimentation rate and a low Mg^{2+} ion concentration, as magnesium inhibits the precipitation of phosphate (Martens & Harriss 1970). The lack of clastic dilution in the North Wales Ironstones indicates a low sedimentation rate. The sediment, predominantly iron, silicon and aluminium rich, had a low magnesium content. The source of the phosphorus is uncertain, the most frequently evoked model for phosphorites involves upwelling of deep oceanic water which is rich in phosphorus. However, Kram & Berner (1981) have noted that in the upper 10cm zone of fine-grained sediment, phosphorus is released from ferric hydroxides on the reduction of the iron. Marshall (1983) advocated that the source of phosphorus in offshore ferruginous sediments are the iron-rich sediments themselves. Soil iron oxides can adsorb phosphorus by ligand exchange reactions (Taylor 1987). Immediately below the sediment/sea water interface the reducing conditions established would reduce the iron and so release phosphorus. Another form of phosphorus release may be by algae (Slansky 1986), which were abundant in the ironstones (Section 3.1). An indication of this source of phosphorus in the North Wales Ironstones is given by the chemical

composition of the grain-ironstones from Aber. The average phosphorus content of the grain-ironstones is 1.2% P_2O_5 compared to an average of 3.5% P_2O_5 for the ironstones. This indicates that the grain-ironstones contain some phosphorus, originally as adsorbed phosphorus on iron oxide/kaolinite complexes, even though they contain no nodules.

The most favourable site for phosphorite formation lies just below the sediment/sea water interface and in slightly reducing to oxidizing conditions, near the boundary of the O_2 minimum layer. In these conditions apatite can precipitate directly from interstitial waters (Slansky 1986). The nodules in the North Wales ironstones also formed just below the sediment/sea water interface, indicated by the ease with which they can be reworked. Other mechanisms for apatite formation are by direct replacement of carbonate material and by pelletal phosphate. The former is unlikely as little carbonate material is present within the ironstones. Pelletal phosphate plays only a minor role in the formation of phosphorites (Slansky 1986), although some of the nodules (particularly the St. Tudwals) do have a pelletal appearance.

Slansky (1986) has also shown the importance of humic acids in the formation of phosphates. Humic acids coating quartz and clay surfaces can trigger apatite precipitation from pore water solutions. The nodules in the North Wales Ironstones are a fine-grained intermix of apatite, chamosite and quartz. This may indicate the importance of this process in nodule formation. It has been shown that nodule formation is also related to bioturbation. This would naturally be accompanied by a higher organic content, and would result in higher humic acid activity.

4.5.2 Controls of Siderite Formation

From thermodynamic considerations, the diagenetic conditions necessary for the formation of siderite are a supply of Fe^{2+}, high HCO_3^- activity, low Eh (reducing) activity and zero S^{2-} activity (Berner 1971). Additionally, siderite cannot form in waters rich in calcium, for siderite to be stable the concentration of Fe^{2+} must be 5% greater than that of Ca^{2+}. However, siderite is stable in the presence of low amounts of sulphide if, in the thermodynamic equilibrium reaction, $Fe(OH)_3$ and FeS phases are used instead of haematite and pyrite (Maynard 1983).

Iron oxides become unstable in the reducing environment beneath the

sediment/sea water interface, and siderite develops mostly from these hydrated iron oxides in the sediment detrital fraction (Oertel & Curtis 1972). The mechanism for this reduction of goethite or hydrated iron oxides is given below (Curtis 1985; Curtis et al. 1985):

$$2Fe_2O_3 + C + 4H_2O \rightarrow 4Fe^{2+} + HCO_3^- + 7OH^-$$

Reduced iron (from above) forms in alkaline conditions with high bicarbonate activity, ideal conditions for siderite formation. Therefore increased organic content would continue iron reduction and bicarbonate generation and would therefore form more siderite. Those North Wales Ironstones with intensive siderite replacement (eg Pen y Gaer) therefore had a greater original organic content. Evidence of algal activity in these ironstones indicate a higher organic content.

Siderite diagenesis in the North Wales ironstones does not occur immediately after burial as it has been shown that siderite forms later than apatite. The major problem of interpreting siderite formation in sediments is that with organic bacterial reduction occurs sulphate reduction to form sulphide ions and pyrite (Berner 1981). Therefore some mechanism has to be proposed to form bicarbonate ions without the formation of sulphide ions. One mechanism evoked is that of rapid deposition removing the sediment from effective diffusive contact from sea water which contains the sulphate (Curtis et al. 1975; Weinberg 1973). This mechanism is unlikely in the ironstones as they had a slow deposition rate and were reworked.

Spears (1989) considers that during reworking of the ironstone considerable organic matter suitable for bacterial sulphate reduction is lost. Any remaining material may survive into the post-oxic zone (Berner 1981) and be suitable for fermentation. Stable isotope data (C^{13}) would help to clarify this situation by differentiating between oxidation processes which are isotopically light (C^{13}= -15) and fermentation processes which are isotopically heavy (C^{13}= +15) (Maynard 1983). From the above reactions it is clear that Fe^{2+} and HCO_3^- are produced during berthierine formation. However, siderite did not start to form until after burial, indicating that inhibition by sulphate/sulphide ions was removed by burial of the sediment and removal of pore water contact with sulphate-rich sea water. The muddy nature of the ironstones and the blanketing of the ironstones by muds, may have effectively prevented diffusion of sea water into the ironstones.

Once formed these carbonate-rich pore waters are highly corrosive to silicates (Burley et al. 1985). Therefore they are capable of reacting with the matrix and forming siderite rhombs, with ooids to form micritic cements, and are responsible for forming solution moulds in nodules by dissolving the siliceous material of spicules.

4.5.3 Controls of Berthierine/Chamosite Diagenesis

It is uncertain at what stage in the diagenetic sequence berthierine formed in the North Wales Ironstones, either after burial, before burial or before ooid formation. From discussions in Section 6.1.2, it is implied that berthierine formed before the formation of ooids. In the reducing conditions established in the ironstones below the sediment/sea water interface, berthierine would continue to be stable and would preserve its ferrous oxidation state. Much dewatering of the ironstones has occurred during early diagenesis, as muds have a high initial water content. The ooids, when formed, had a significantly lower water content as ooid formation ordered the chamosite so expelling much intergranular water. It is assumed here that berthierine initially had little change of composition, but much dispelling of intergranular and interstitial water (Maynard 1986). With this occurred increased ordering and crystallinity of berthierine. Dewatering of ooids in the North wales ironstones is indicated by the shrinkage cracks around ooids in nodules.

Maynard (1986) analysed the nuclei and cortices of berthierine ooids and showed that berthierine in the nucleus of the ooid had a higher water content and lower octahedral total than the berthierine in the cortex. The main control on dewatering (and therefore crystallinity) would therefore be porosity. The control of porosity on composition and structure of chamosite has been shown in the Bryn Poeth ironstone chamosite compositions. Similar controls are seen in other ironstones where other controls of porosity, such as magnetite, also take effect.

The presence of potassium in the berthieroid lattice (Hughes 1989; Maynard 1986) is problematic. It has been shown that minor amounts of smectite interlayering do not occur in berthierines and chamosites (Section 4.3). Therefore potassium must be accommodated in the chamosite lattice. Chlorites have a theoretical octahedral total of 12.0 (Deer et al. 1962b). Bethierines and the North Wales chamosites have octahedral totals less than 12.0 (Maynard 1986), indicating vacancies in the chamosite lattice. The presence of such vacancies in

the lattice, accompanied by charge imbalances poor crystallinity, would allow the incorporation of potassium in the interlayer sites. With increasing crystallinity and octahedral totals potassium can no longer be accommodated and so is expelled.

The presence of chamosite in shrinkage cracks and fossil vugs within the phosphate nodules indicate that the original bicarbonate-rich solutions later become more acidic, although still under reducing conditions, to produce berthierine cements. The presence in the St.Tudwals ironstones of siderite cements infilling pore spaces in the nodules may indicate one of two things. Either bicarbonate activity was high enough to penetrate the nodules associated with siderite rhombs at the edges to the nodules to infil the pore spaces. Or all nodule cavities had an original siderite cement, which were later removed by the more acidic pore waters. This latter texture is indicated by the stromatolite coated sponge at St.Tudwals (Figure 3.9), where the central part is infilled by siderite cement while the outer part is apatite, chamosite and silica cemented. Possibly both these processes occurred within the ironstones although it is more likely that with low levels of bicarbonate activity pore waters did not penetrate the nodules. The presence of chamosite pseudomorphing siderite indicates the action of later acidic pore waters dissolving out siderite.

The source for the later acidic silica-rich pore waters is also problematic. One source may be from the dissolution of chamosite by siderite precipitating pore waters. Another may be the release of Fe and Si during the changing composition of chamosite to a more tetrahedral aluminium rich composition. However, the cements formed before burial diagenesis, before the change in chamosite composition (Section 4.6). A more likely source is silicon-rich pore waters derived from the muds adjacent to and beneath the ironstones.

It has been shown (Iijima & Matsumoto 1982, Schoen 1964, Velde et al. 1974, Velde 1985, Curtis et al. 1985) that berthierine transforms to chamosite under late diagenetic conditions, at temperatures of 150°C (Schoen 1964), 130-160°C (Iijima & Matsumoto 1982) or 100°C (Velde 1985), under normal pressures and temperatures. The mechanism for this conversion is unknown, although one suggestion (Whittaker pers. comm. in Weinberg 1973 p169) is that firstly the basal layer of the hydroxyl sheet is deprotonated, and secondly the movement of a silicon atom, which only involves the breaking of one Si-O bond per tetrahedron. Chamosite only starts to change composition once it has

been converted to a 1.4nm chlorite. Therefore the compositional variation of chamosite reflects post-diagenetic changes only. The Ib($B=90^{o}$) polytype is the most stable of the Ib chlorite polytypes (Hayes 1970). This structure can persist in the burial environment until enough energy is available to cause convertion to a IIb polytype. This happens with the thermal energy usually associated with low-grade metamorphism, at 150-200^{o}C assuming normal temperatures and pressures (Hayes 1970).

4.6 TIMING OF DIAGENESIS

The main diagenetic phases in the North Wales Ironstones have been dsecribed and discussed in the previous sections. These phases have been presented in the order of their formation, although this order has not been previously justified. It is intended in this section to document the relationships between, and therefore the timing of, of the different diagenetic phases. These phases are divided into syndepositional, early postdepositional (diagenetic) and late postdepositional (burial metamorphic)(Figure 8).

Syndepositional changes involve the formation of phosphate nodules. Nodules start to form before the final deposition of the ironstone, as reworked nodules occur within the ironstone sequence. Nodules lithify very early as during reworking they show brittle fracture. The formation of berthierine also occurred at this time (Section 6.1), but no textural evidence of this is preserved in the ironstones.

Early postdepositional changes involve the dewatering of berthierine, both the plastic deformation and brittle breakage of ooids, the formation of siderite, and the formation of secondary chamosite cements. The dewatering of berthierine in oolitic ironstones is a continuous process (Maynard 1986). However, dewatering of berthierine ooids in the North Wales Ironstones occurred before the formation of siderite, as some shrinkage vugs around ooids in nodules are cemented by siderite. Dewatering of ooids continued after burial compaction, indicated by plastically deformed ooids around rigid phosphate nodules and in mud-ironstones. This plastic state of the ooids indicates that they still had a significantly high water content during burial compaction. By contrast ooids in grain-ironstones show brittle deformation (splay textures). However, there was no mud between ooids to prevent them from rapidly dewatering. Therefore during burial compaction these ooids show brittle fracture.

The generation of siderite in the ironstones post-dates nodule formation, dewatering of ooids and deformation of ooids during burial compaction. This is indicated by siderite rhombs which show a reaction rim around the edges of some nodules, and by undeformed siderite rhombs in the matrix between deformed ooids around nodules. The presence of splay textures in grain-ironstones indicate that siderite cementation post-dates burial compaction. The first siderite phase to form is rhombic in habit in the matrix of the ironstones, seen at all localities. With continuing generation of siderite, the rims of ooids

and the rims of nodules are replaced by micrite and rhombs respectively. With extensive generation of siderite, ooid laminae are replaced by micrite, rhombs occur within nodules, and solution vugs in nodules are infilled by cement. Secondary chamosite cements formed later than siderite as only those vugs within nodules which do not contain siderite contain chamosite. Chamosite pseudomorphs of siderite rhombs also indicate that chamosite cements postdate siderite cements.

Later post-depositional changes involved the conversion of berthierine to chamosite, and compositional changes to chamosite. At some time during late burial diagenesis berthierine converted to chamosite. It is uncertain at what time this occurred, as estimates for the temperature of conversion are uncertain, and there was a higher heat flow (ie not a normal P/T gradient) in the Welsh Basin. However, some indication can be given from relating chamosite cements to metasomatism of the ironstones. Textural and mineralogical evidence presented in Chapter 5 show that chamosite cements (originally precipitated as berthierine and later converted) predate igneous intrusive activity. These intrusives are related to Caradoc igneous activity, some 10Ma after the formation of the ironstones. Later, with burial metamorphism, chamosite compositions evolved toward a more stable 'IIb-like' composition.

5 METASOMATISM AND HYDROTHERMAL ALTERATION OF THE IRONSTONES

The North Wales Ironstones are the only ones in the British Isles to have undergone metamorphism (Hallimond in Pulfrey 1933a). Changes to the ironstones undergone by burial metamorphism have been discussed in Chapter 4. It will be shown in this chapter that further changes undergone by the ironstones are the result of the influence of igneous intrusions. This resulted in the formation of magnetite, stilpnomelane, siderite, pyrite and other sulphides within the ironstone. Magnetite and stilpnomelane of metamorphic origin have been previously described in the North Wales Ironstones (Matthews & Scoon 1964; Pulfrey 1933a; Hallimond 1925,1924). These minerals frequently occur in Banded Iron Formations, but are rare in Phanerozoic Oolitic Ironstones (Maynard 1983).

Metamorphic stilpnomelane has been recognized in ironstones in the Tertiary Himalayan orogenic belt (Garzanti et al. 1989) in the Alpine orogenic belt (Velde 1989) and the metamorphosed Arenig ironstones of Brittany (Chauvel 1974). By contrast, magnetite in oolitic ironstones has been variously described as metamorphic (related to dolerite intrusions - Guerrak & Chauvel 1985), diagenetic (in Upper Devonian Libyan ironstones, based on stable isotope data - Hangari et al. 1980), and authigenic (in the Arenig ironstones of Brittany - Chauvel (1974). Hydrothermal siderite has not been described from other oolitic ironstones. Diagenetic pyrite is a common constituent of many ironstones (Maynard 1983), but hydrothermal pyrite, or base metal sulphides (chalcopyrite, sphalerite arsenopyrite), have not been described from other Phanerozoic Ironstones.

These changes in the North Wales Ironstones are related to igneous intrusions. The sections in this chapter describe the distribution, textures, mineralogy and geochemistry of each mineral (magnetite, stilpnomelane, siderite and sulphide minerals). A discussion of the controls of formation is presented at the end of the chapter.

5.1 MAGNETITE

The Bwlch y Cywion, Llanberis Valley, Betws Garmon, Tremadog, Rhyd, Cadair Idris East and Tyllau Mwn ironstones all contain magnetite, which at Bwlch y Cywion, Rhyd, Cadair Idris East and Tyllau Mwn is associated with stilpnomelane (Section 5.2). At all these ironstone localities magnetite distribution is restricted to certain ironstone sedimentary facies, and at any one locality the magnetite distribution is laterally variable, the significance of which will be discussed later.

Magnetite only occurs within the upper ooidal pack-ironstone or wacke-ironstone facies. The one exception to this is the Llanberis Valley ironstone, a ferruginous debris flow. The magnetite is too fine-grained to be distinguished under a hand lens, but is shown to be present by the use of a hand held magnet (Figure 2.15). Magnetite distribution at Cadair Idris is limited to the eastern part of the range (Bwlch Coch to Cross Foxes) and at Betws garmon to those exposures to the north of the A4085 road (Figure 2.14). Here magnetite replacement becomes more intense to the northeast with increasing thickness of the upper ooidal pack-ironstone. The ironstone at Tremadog is replaced by magnetite, but the siderite cemented ooidal grain-ironstone at Pensyflog, only 250m away, shows no sign of replacement. The ironstones of Northern Snowdonia also show variation in the style of replacement along strike: the Llanberis Valley to Bwlch y Cywion ironstones have magnetite replacement, the A5 to Cwm Caseg ironstones have pyrite replacement.

5.1.1 Textures

Four different types of magnetite development can be recognised:

1) replacement of ooids by magnetite (Betws Garmon, Tremadog, Rhyd),
2) replacement of matrix by magnetite (Cadair Idris east),
3) overgrowth of the oolitic texture (Bwlch y Cywion, Tyllau Mwn),
4) growth of euhedral magnetite in a non-oolitic ironstone (Llanberis Valley).

Magnetite replacement of ooids is typified by replacement of the ooid nucleus and the majority of the laminae by fine-grained magnetite (Figure 5.1). The matrix between ooids is now recrystallised chamosite, but may also be siderite rhombs or chamosite pseudomorphing rhombs. However, there is a gradation which can be recognised in the extent of replacement; varying from no replacment to complete replacement by magnetite. This is controlled by the presence of phosphate nodules, chamosite mud patches and and chamosite mud lenses. Ooids within phosphate nodules only show minor magnetite replacement, while outside the nodules the ooids are extensively replaced (Figure 4.1). Ooids within chamosite mud patches only show partial replacement by magnetite, where the nucleus of the ooid but only some of the ooid laminae show magnetite replacement. Ooids within the chamosite mud lens in the Betws Garmon pack-ironstone show no magnetite replacement. Ooids at the margin of this mud lens are only partially replaced (Figures 3.3, 3.16), but away from the mud lense all ooids are replaced by magnetite. This style of replacement is texturally similar to magnetite replacement in the Brittany ironstones (Chauvel 1974).

The only example of replacement of the matrix by magnetite is at Cadair Idris east. Fine-grained magnetite occurs replacing the matrix around the ooids (Figure 5.1). With increasing magnetite development, this replacement also encroaches on the edges of the ooids (Figure 5.1). However, the chamosite ooids still retain their internal structure. Magnetite also occurs in vugs, both in the matrix and phosphate nodules, as euhedral intergrowths with pyrite and stilpnomelane. There is an antipathetic relationship in this ironstone between the occurrence of stilpnomelane and magnetite. There is a gradation between ironstones that are predominantly replaced by either magnetite or by stilpnomelane with pyrite. In the magnetite-rich ironstones, magnetite occurs as a fine-grained replacement of the groundmass. In both stilpnomelane-rich and magnetite-rich ironstones, magnetite occurs in vugs. In the centre of sponge spicules, the order of cements is 1) needles of apatite 2) blades of chamosite 3) interlocking crystals of pyrite and magnetite with blades of stilpnomelane.

Overgrowth of the ironstone texture by magnetite and stilpnomelane occurs by interlocking small (50-100um) subhedral crystals of magnetite which preferentially overgrow the matrix, with minor stilpnomelane. Stilpnomelane also ghosts the ooids with sparse

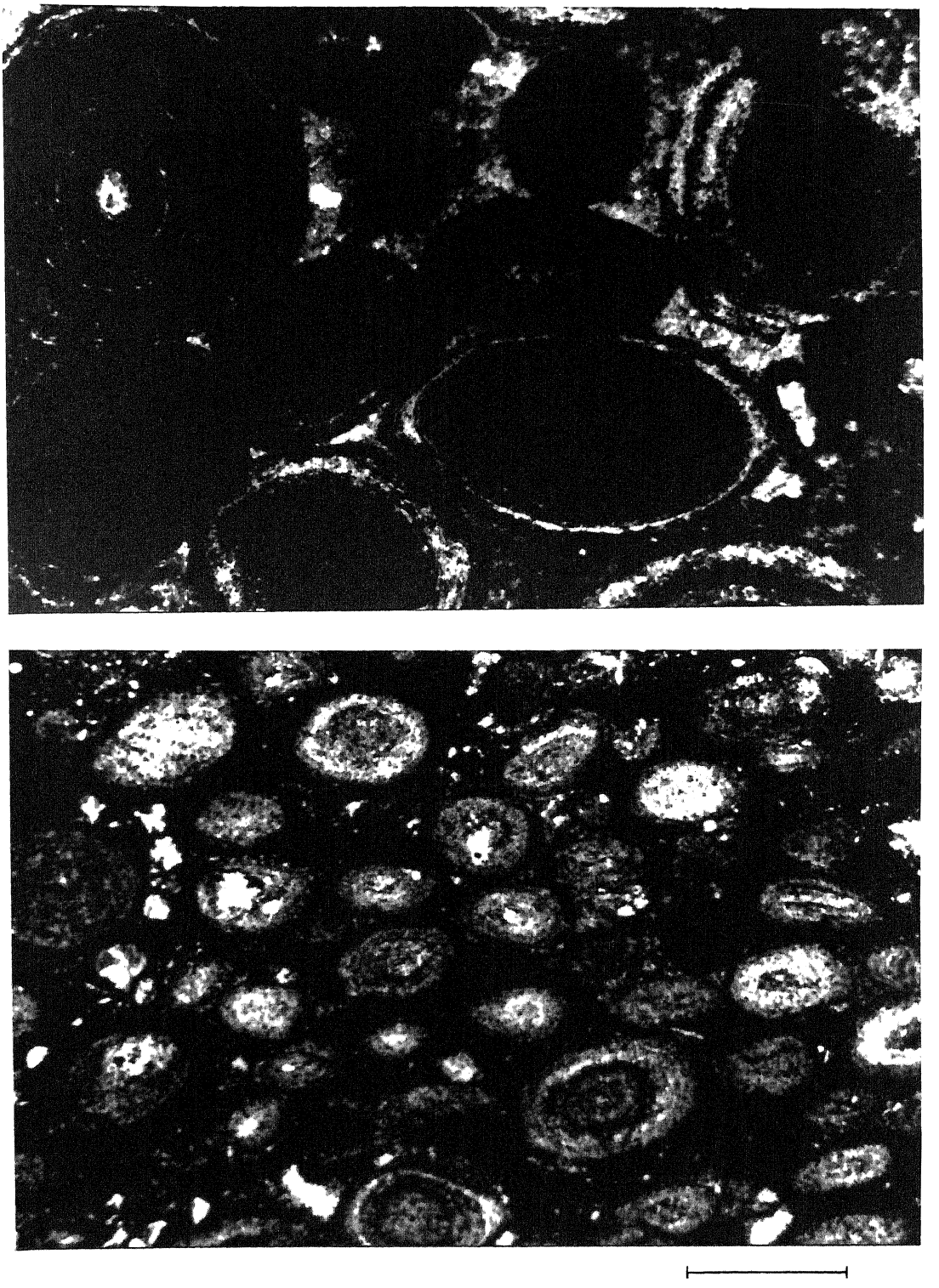

Figure 5.1 Photomicrographs, a) magnetite ooidal pack-ironstone, YF-X Betws Garmon (Loose Grab Sample), b) ooidal magnetite pack-ironstone, CI134 Cross Foxes, [SH 7595 1639]. Differing styles of magnetite replacement: a) fine-grained replacement of chamosite ooids, with some chamosite laminae still preserved, b) fine-grained magnetite replacement of chamosite matrix, but also encroaching on the edge of ooids. Scale bar = 1mm.

disseminated magnetite. The majority of the oolitic texture is now replaced, although remaining chamosite ooids still preserve an extinction cross. Lastly, the Llanberis Valley ironstone, a ferruginous debris flow deposit, has abundant euhedral grains of magnetite disseminated within the matrix. These grains are commonly 200μm in size, but may form aggregates up to 1mm in size.

Magnetite has been detected by XRD in samples from Betws Garmon, Tremadog and Cadair Idris east. All samples showed the same XRD pattern (Appendix 3), magnetite being characterised by its $d_{(311)}$=0.2532nm peak. Two polished thin sections from Cadair Idris east and three from Betws Garmon were analysed by EPMA for magnetite, but it was not possible to obtain pure analyses as the magnetite was too finely intermixed with chamosite and quartz.

5.1.2 Geochemistry

Statistical analysis of the XRF data set (Section 3.3.2) identified the elements related to magnetite development as total iron [Fe_2O_3(T)] and ferric iron (Fe_2O_3) (Group 3). In this section the relationship between the ferric component of the ironstones and the rest of the data set is considered. Special discussion of the geochemistry of the Cadair Idris east ironstone, which includes discussion of magnetite, is included with the geochemistry of stilpnomelane (Section 5.2.2). The major elements, when correlated against total iron, all show a negative linear correlation, particularly silicon (SiO_2/Fe_2O_3(T) r=-0.839) and aluminium (Al_2O_3/Fe_2O_3(T) r=-0.769). Those ironstones with high total iron contents (and therefore the high ferric iron) content are the magnetite rich ironstones. When total iron is correlated against the immobile elements, they all show a negative linear correlation, aluminium (above), titanium (TiO_2/Fe_2O_3(T) r=-0.588) and zirconium (Zr/Fe_2O_3(T) r=-0.467), indicating that dilution of the ironstone by ferric iron has occurred.

The total iron and ferric iron content of the ironstones show a positive linear correlation (Fe_2O_3/Fe_2O_3(T) r=0.753), but few trace elements correlate with these elements. However, chromium and vanadium both show a poor positive correlation with total iron (Cr/Fe_2O_3(T) r=0.447, V/Fe_2O_3(T) r=0.547), although they show a strong correlation between each other (r=0.876). Deer et al. (1962c) have shown that chromium and vanadium can substitute for ferric iron in magnetite and so would be expected to show a correlation. The Betws Garmon ironstone

XRF samples show a strong correlation of increasing total iron, ferric iron, vanadium and chromium indicating that these elements must have been introduced into the Betws Garmon ironstone during magnetite formation. The Cadair Idris east analyses (Section 5.2.2) show that zinc increases with magnetite formation, substituting for ferrous iron in the magnetite lattice (Deer et al. 1962c). They show no correlation with chromium or vanadium. This difference in trace element correlation with different localities (and therefore different modes of magnetite replacement) would suggest differing geochemical conditions for magnetite replacements.

5.2 STILPNOMELANE

Matthews & Scoon (1964) and Hallimond (1924) have previously identified stilpnomelane from the Tyllau Mwn and Rhyd ironstone localities respectively. They described, separated and analysed stilpnomelane from veins cross cutting these ironstones. In addition in this study stilpnomelane has found at Bwlch y Cywion and Cadair Idris east. Stilpnomelane has only been found in the upper ooidal pack-ironstone or wacke-ironstone facies, and is always associated with magnetite (Section 5.1). Textural and geochemical data is available for stilpnomelane from all four localities. Additionally, mineralogical analyses (XRD and EPMA) of stilpnomelane from the Cadair Idris east samples were undertaken.

5.2.1 Textures

Texturally stilpnomelane occurs in three ways:

1) replacing matrix and rimming ooids (Cadair Idris east),
2) overgrowing the oolitic texture (Bwlch y Cywion, Tyllau Mwn),
3) in cross cutting veins (Rhyd, Bwlch y Cywion, Tyllau Mwn).

Replacement of matrix and rimming of ooids occurs in the Cadair Idris (east) ironstone, where stilpnomelane replacement shows an antipathetic relationship with magnetite replacement. At this locality there is a gradation between stilpnomelane-rich ironstones and magnetite-rich ironstones. Within both types stilpnomelane occurs as randomly dispersed needles both in the matrix and in the phosphate nodules (Figures 5.2, 4.4.b). Stilpnomelane also occurs in vugs as larger interlocking bladed crystals with pyrite and magnetite. The difference between stilpnomelane-rich and magnetite-rich ironstones is in the extent of stilpnomelane replacement. In the stilpnomelane-rich ironstone virtually all the matrix is composed of stilpnomelane with only minor magnetite. This mode of replacement is similar to that found in Mesozoic ironstones in the Himalayan orogenic belt (Garzanti et al. 1989).

Where stilpnomelane overgrows the oolitic texture it is intimately associated with euhedral magnetite, seen at Bwlch y Cywion and Tyllau Mwn (Section 5.1). Where replacement by stilpnomelane and magnetite is not extensive, and some oolitic texture is preserved, stilpnomelane

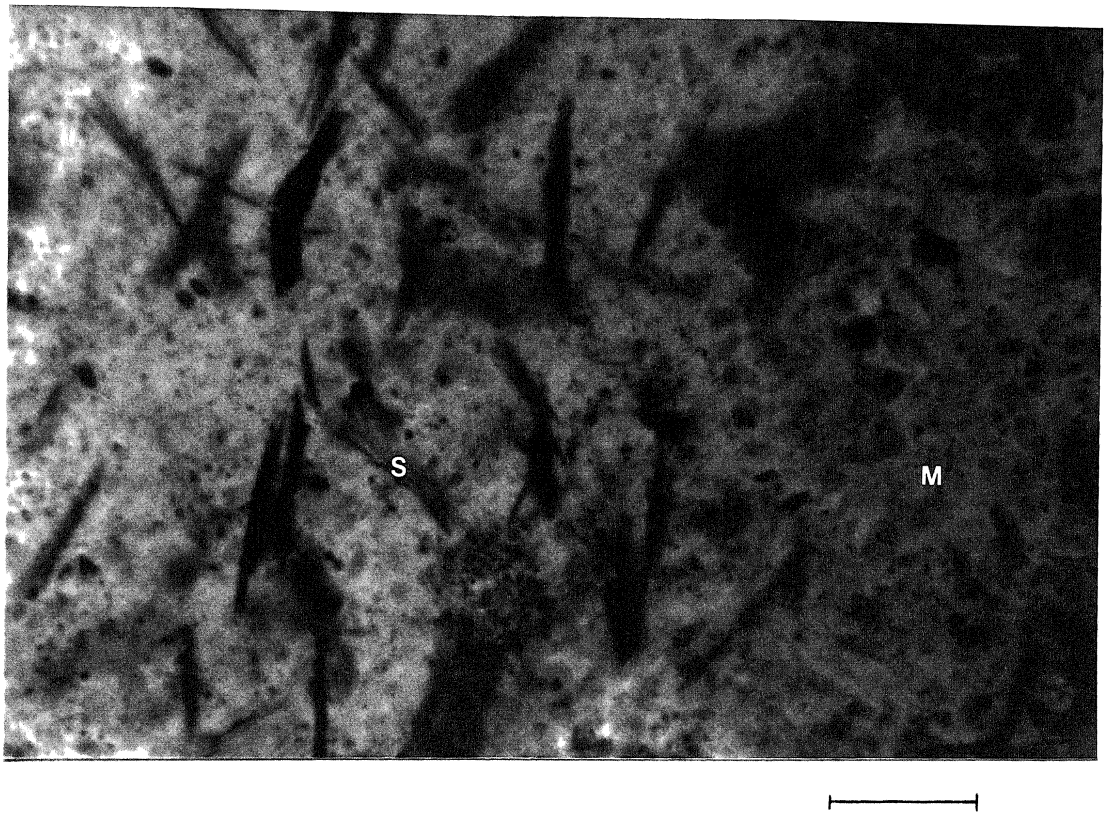

Figure 5.2 Photomicrograph, phosphate nodule in ooidal pack-ironstone, CI134 Cross Foxes [SH 7595 1639]. Disseminated flakes of stilpnomelane (s), within the collophane matrix (m) of a phosphate nodule. Stilpnomelane shows a strong pleochroism from pale/colourless (east-west) to dark brown (north-south). Scale bar = 500μm.

occurs infilling tension gashes both in the matrix and between ooid laminae. With intense replacement stilpnomelane preferentially occurs as large interlocking blades ghosting ooids. It may also be intergrown with magnetite, but is then much finer grained. Similar overgrowth of oolitic texture is seen in the Alpine Mesozoic ironstones (Velde 1989). At Rhyd neither of the above two replacement textures are seen as it contains only minor quantities of stilpnomelane. It mostly occurs in cross-cutting veins, intergrown with euhedral magnetite, or more rarely as interlocking bladed crystals infilling dissolved out ooids.

5.2.2 Mineralogy

EPMA and XRD data are available for two samples containing stilpnomelane from Cadair Idris (east), one from an ooidal stilpnomelane wacke-ironstone (CI130c, XRF sample No. 011) and the other from an ooidal magnetite pack-ironstone (CI137, XRF sample No. 014). Both samples show the same XRD pattern (Appendix 3), peaks identified after Eggleton (1972). The dominant feature is the large $d_{(001)}$=1.1946nm peak characteristic of stilpnomelane.

EPMA data for stilpnomelane in Appendix 4 represent four spot analyses from the stilpnomelane-rich ironstone and five from the magnetite-rich ironstone. The formula for stilpnomelane was based on 11 oxygens (Baker 1985) and the tetrahedral values made up to 4. The analyses show that stilpnomelane is composed mostly of iron and silicon and that the main alkali phase is potassium. However, compositional differences between the two are apparent, the analyses from the stilpnomelane-rich sample have higher potassium, manganese and magnesium values and lower ferrous iron and calcium values than the analyses from the magnetite-rich sample. The oxidation state of the iron is unknown, although an estimation can be made from XRF data on the assumption that stilpnomelane is in equilibrium with the whole rock (Velde 1989). Stilpnomelane has a complete range of compositions from totally ferrous to totally ferric (Deer *et al.* 1962b). Samples with more ferrous iron than ferric iron are ferrostilpnomelanes and those with more ferric iron are ferristilpnomelanes. The stilpnomelane-rich ironstone contains a ferrostilpnomelane (as the rock is dominantly ferrous, ORI=0.658) and the magnetite-rich sample a ferristilpnomelane (as the rock is dominantly ferric, ORI=0.492).

Statistical analysis of the XRF data set (Section 3.3.2) identified the elements related to stilpnomelane formation as potassium, barium and rubidium (Group 1b). The relationship between these three elements is discussed first. Then the five XRF samples from Cadair Idris east are considered together for the geochemical variation between stilpnomelane-rich and magnetite-rich ironstones.

The only ironstones to contain significant amounts of potassium (>0.07% K_2O) are those containing stilpnomelane. The one exception is the chamosite mud-ironstone from Cadair Idris, which contains illite (XRF sample No. 036). Potassium shows a strong positive linear correlation with rubidium (Rb/K_2O r=0.963). A plot of barium against rubidium (Figure 5.3) clearly distinguishes two different groups of ironstones. The first group with variable barium content and low rubidium content are the majority of the ironstones (ie samples with no stilpnomelane). The second are those with high rubidium content and variable barium content (Ba/Rb r=0.684) and are the stilpnomelane-rich ironstones. EPMA data indicates that manganese is a trace element occurring stilpnomelane. This may form up up to 0.5% MnO of the bulk rock ironstone sample. These relationships indicate that potassium rubidium and manganese have been introduced into the ironstone. Barium has not and instead has been redistributed. Rubidium and barium have the same ionic size as potassium and so can substitute in the stilpnomelane lattice. Manganese substitutes for ferrous iron in stilpnomelane (Deer et al. 1962b); indicated from EPMA analyses by the higher MnO contents of the ferrostilpnomelanes.

The Cadair Idris east ironstone has undergone differing geochemical changes with magnetite and stilpnomelane formation. Five samples were analysed by XRF from this area. These are plotted on Figure 5.4 arranged in order of increasing potassium content (equivalent to increasing stilpnomelane development). It can be seen that potassium, rubidium, barium, manganese and silicon all increase with increasing stilpnomelane. Conversely, total iron, ferric iron and zinc all increase with increasing magnetite (decreasing stilpnomelane). Aluminium, titanium and ferrous iron all remain unchanged. The fact that 'normal' ironstones do not contain potassium and have low ferric iron values indicates that potassium and iron (plus silicon, rubidium, manganese and zinc) have been added to the ironstone.

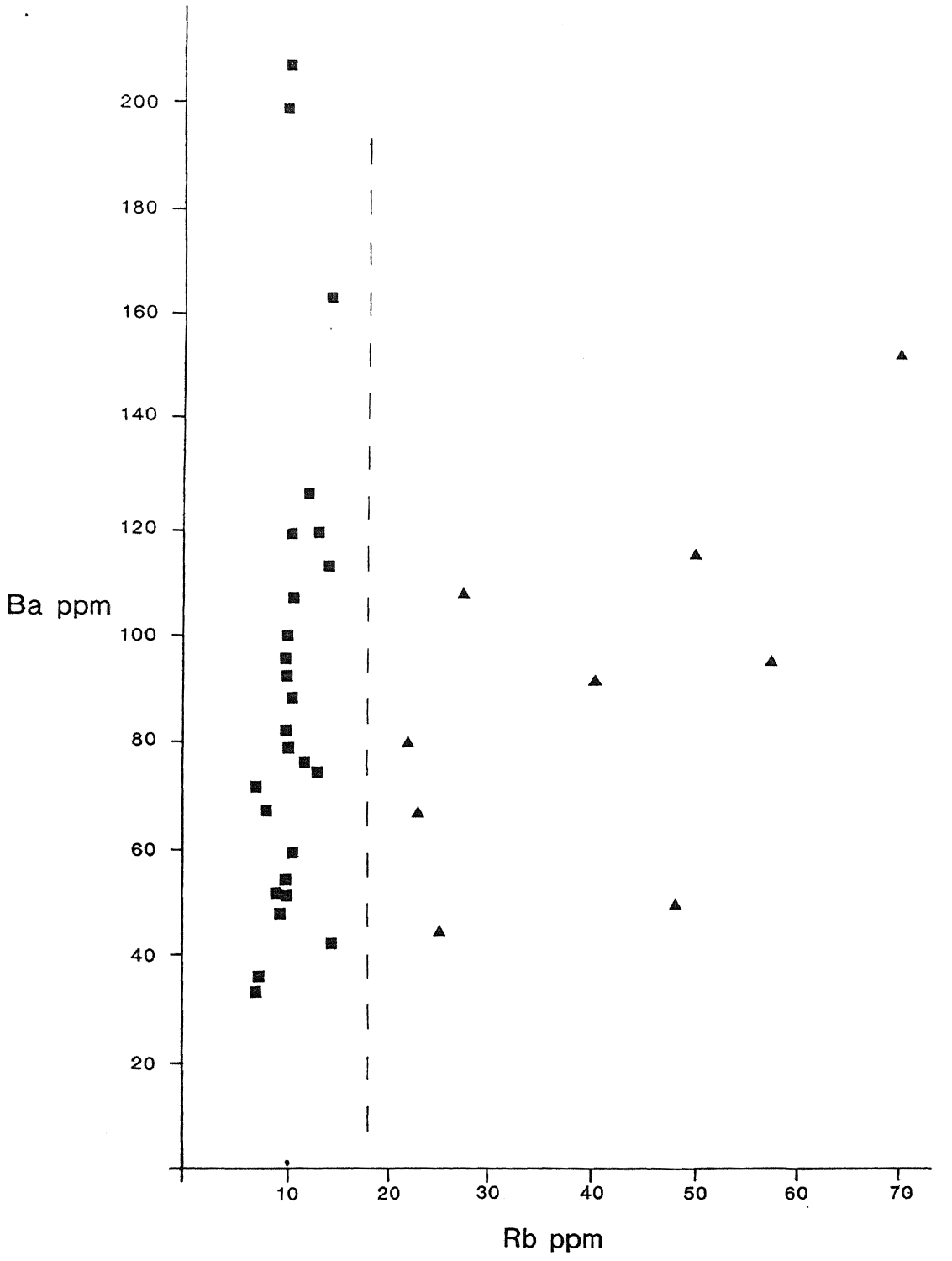

Figure 5.3 Plot of barium against rubidium from the XRF data set (excluding sample No.36), distinguishing between stilpnomelane bearing (triangles) and non-stilpnomelane bearing (squares) ironstones. Dashed vertical line is the approximate rubidium value distinguishing between the two sample types.

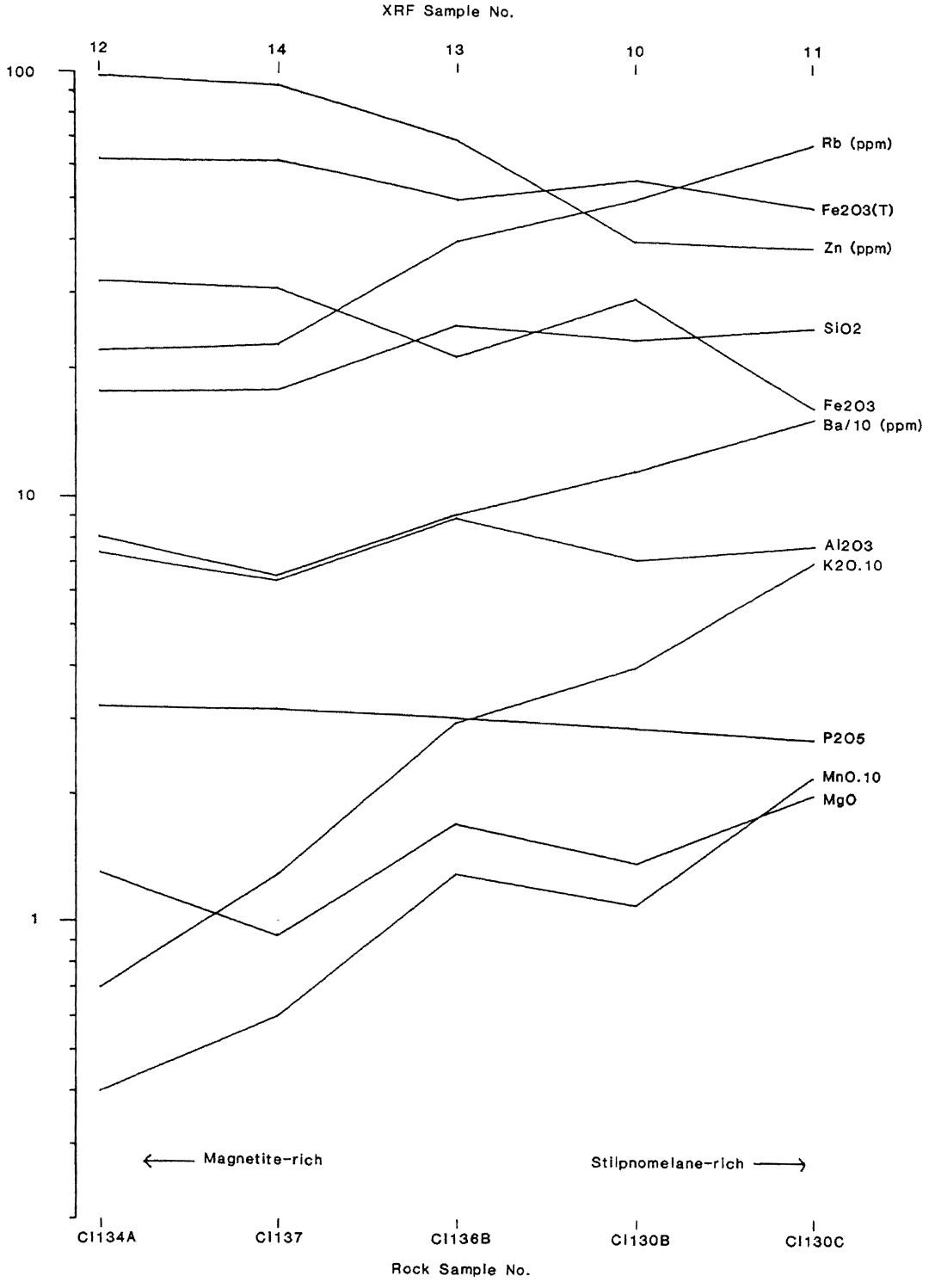

Figure 5.4 Major and trace element geochemical variation diagram for the five samples from Cadair Idris east. Samples are arranged in order of increasing K2O (equivalent to increasing stilpnomelane) and shows the geochemical variation between magnetite-rich and stilpnomelane-rich ironstone samples. All samples are actual values except for MnO, K2O (multiplied by 10) and Ba (divided by 10). This diagram shows increasing K2O, Ba, Rb, MnO and SiO2 with increasing stilpnomelane and increasing Fe2O3(T), Fe2O3 and Zn with increasing magnetite.

5.3 SIDERITE

Alteration of the ironstones by siderite, as distinguished from diagenetic siderite, has been identified at three localities, Aber, Betws Garmon and St.Tudwals. At each locality siderite is associated with sulphide mineralisation (Section 5.4). Alteration by siderite is distinguished from diagenetic siderite (Section 4.2) in that the former is a localised phenomenon, its replacement textures are different, as is associated with Fe-Cu±Zn±As mineralisation. At Aber, although the ironstone has been tectonised and mineralised (Section 2.4.2), only the grain-ironstone can be recognised as having been altered by siderite. Alteration by siderite at St. Tudwals only seen in isolated occurrences. At Betws Garmon alteration by siderite only occurs to the south of the A4085 road, where the ironstone is not replaced by magnetite. To the north of the A4085 minor alteration by siderite occurs, and will be shown to be later than magnetite replacement. At both localities alteration by siderite only occurs within the upper ooidal pack-ironstone facies.

5.3.1 Textures

A number of different modes of siderite are associated with alteration:

1) Void infills (Aber),
2) Reaction rim to voids (Aber),
3) Overgrowth of ooids (Aber),
4) Replacement of ooids (Betws Garmon, St. Tudwals),
5) Rhombs (Aber, Betws Garmon, St. Tudwals),
6) Cross Cutting Veins (Aber, Betws Garmon).

Void infills occur as epitaxial fibrous cements nucleated on, and in optical continuity with, micritic reaction rims to the voids (2 above) (Figure 5.5). The voids are either solution vugs in ?pack-ironstones or pore spaces between ooids in ?grain-ironstones. Reaction rims to voids occur either as micritic siderite replacing the outer laminae of ooids in ?grain-ironstones, or as micritic siderite replacing the edges of solution vugs in ?pack-ironstones (Figure 5.5). This micritic siderite is in optical continuity with 1 and 3 (above). Overgrowth of ooids occurs as epitaxial sparry siderite nucleated on,

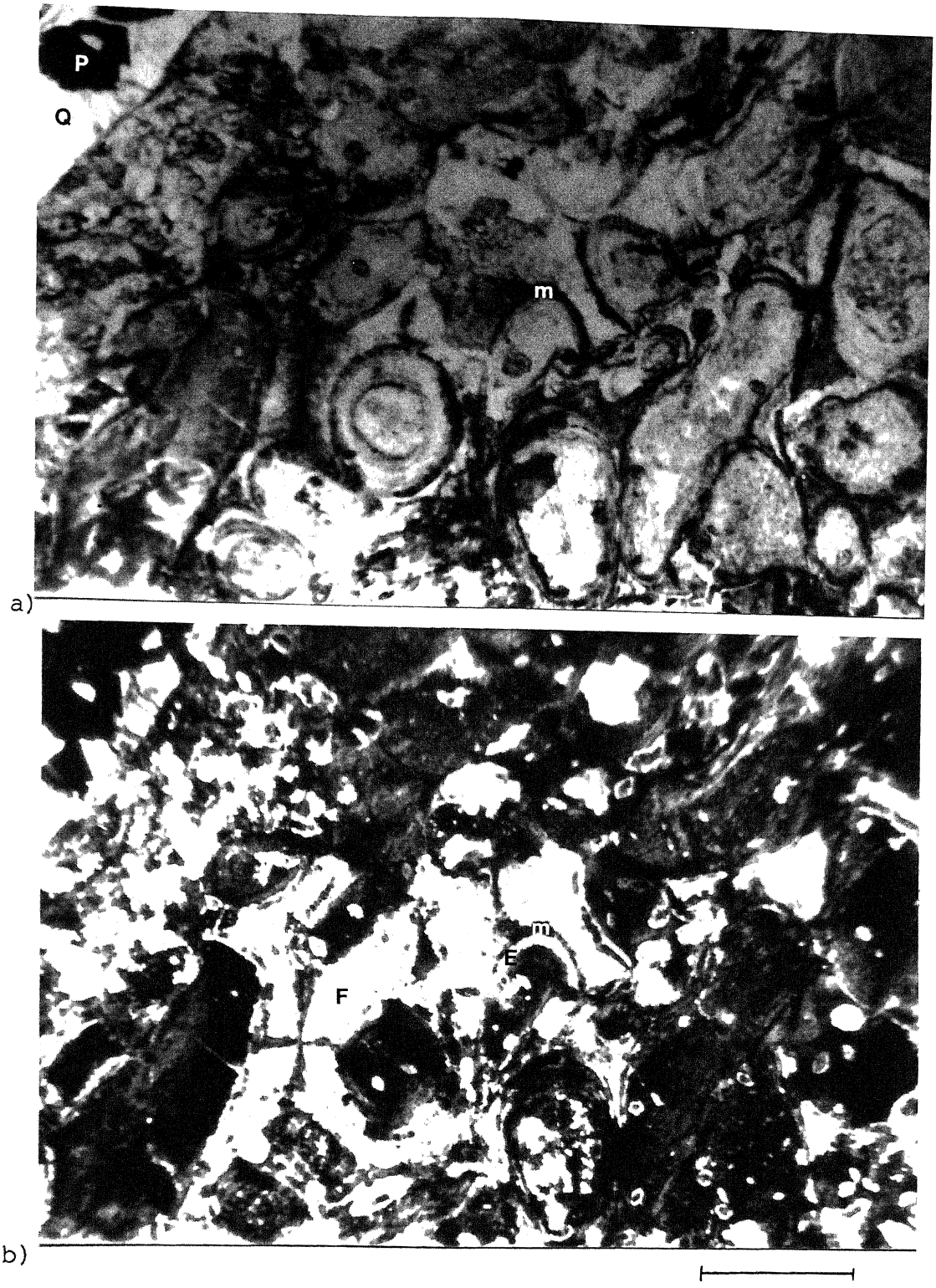

Figure 5.5 Photomicrograph, ooidal grain-ironstone, AB-A Aber [SH 6693 7245]. Sideritised ironstone a) plane polarised light b) crossed polarised light see text for detailed descriptions. a) micritic siderite rims to ooids (m) are distinguishable as dark rims. Cross cutting vein in top left corner contains quartz (Q) and pyrite (P). b) Chamosite (dark) and siderite light now clearly distinguishable, ooids no longer show an extinction cross. Four modes of siderite can be identified (see text): 1) micritic rims to ooids (m) 2) epitaxial sparry siderite overgrowing ooids (E) 3) fibrous epitaxial siderite infilling vugs (F) and showing an extinction cross 4) Disseminated siderite rhombs. Scale bar = 1mm.

and in optical continuity with, the micritic reaction rim (2 above) and overgrowing the ooid. In ?grain-ironstones there is only minor overgrowth by sparry siderite, and the oolitic texture and the tangential orientation of chamosite is preserved. In the ?pack-ironstones more of the ooid is overgrown by spar, and the oolitic texture is destroyed (Figure 5.5).

Replacement of ooids is by 'patchy' micritic siderite, with only minor chamosite laminae remaining. The matrix between ooids consists of microcrystalline chamosite. Within this matrix are disseminated siderite rhombs, which also occur in the chamosite matrix and ooids of 2 and 3 above (Figure 5.5). Finally, siderite occurs in cross-cutting veins intergrown with quartz; the veins also contain pyrite and base metal sulphides (Figures 5.7, 5.9).

At Aber and Betws Garmon there is a variation in the extent of siderite alteration. At Aber there are two differing styles of siderite alteration. The first is epitaxial fibrous siderite forming the cement between ooids, accompanied by micrite replacement of ooid rims and minor overgrowth by sparry siderite of the ooids. The second is epitaxial fibrous siderite infilling voids in chamosite matrix, accompanied by micritic reaction rims around these voids, extensive overgrowth by sparry siderite of the ooids, and disseminated siderite rhombs in the ooids and chamosite matrix (Figure 5.5). It is proposed here that these differences are due to primary differences in ironstone facies type. The first style of siderite alteration occurs in an ironstone with no chamosite mud matrix and with lenses of differing ooid grain-size (Section 3.2.1). It is most likely that this was originally a grain-ironstone. By contrast, the second style of alteration occurs in an ironstone with chamosite mud matrix, and no sorting of ooids, and was therefore originally a pack-ironstone.

At Betws Garmon to the south of the A4085 road, siderite alteration occurs as replacement of ooids by micritic siderite and disseminated siderite rhombs in a chamositic mud matrix. To the north of the A4085 siderite alteration was later than magnetite replacement. This is shown by quartz and siderite veins cross-cutting magnetite ooids (Figure 5.9). Replacement of magnetite ooids by pyrite occurred along the margins of these veins. Remaining chamosite ooids in phosphate nodules were altered by siderite (Figure 4.1), and disseminated siderite rhombs occur in the matrix. Diagenetic siderite can be shown to have been originally present by chamosite pseudomorphs of siderite rhombs at Betws Garmon, and siderite rhombs as inclusions within

pyrite from St. Tudwals.

5.3.2 Mineralogy

Siderite has been analysed by XRD and EPMA for the Aber and Betws Garmon ironstones. EPMA data for these siderites are given in Appendix 4 and plotted on Figure 5.6. This shows that the Betws Garmon siderites are Fe-rich, with only minor Mg. The Aber siderites are more Ca- and Mn-rich. This is reflected in the variation of the $d_{(10\bar{1}4)}$ peak (Section 4.2.1), for the Betws Garmon siderite $d_{(10\bar{1}4)}$=0.279nm as it is dominantly ferrous in nature. By contrast the Aber siderite has $d_{(10\bar{1}4)}$=0.280nm due to the higher Ca and Mn substitution in the siderite lattice.

Maynard (1986) distinguishes diagenetic and hydrothermal siderites by composition; hydrothermal siderites having little substitution by calcium and magnesium. Generally the North Wales hydrothermal siderites have less than 5% substitution by calcium and magnesium whereas the North Wales diagenetic siderites generally have more than 5%. However, three siderite analyses from Aber have high substitution by calcium and magnesium. It is not known what mode(s) of siderite was analysed to account for these differences.

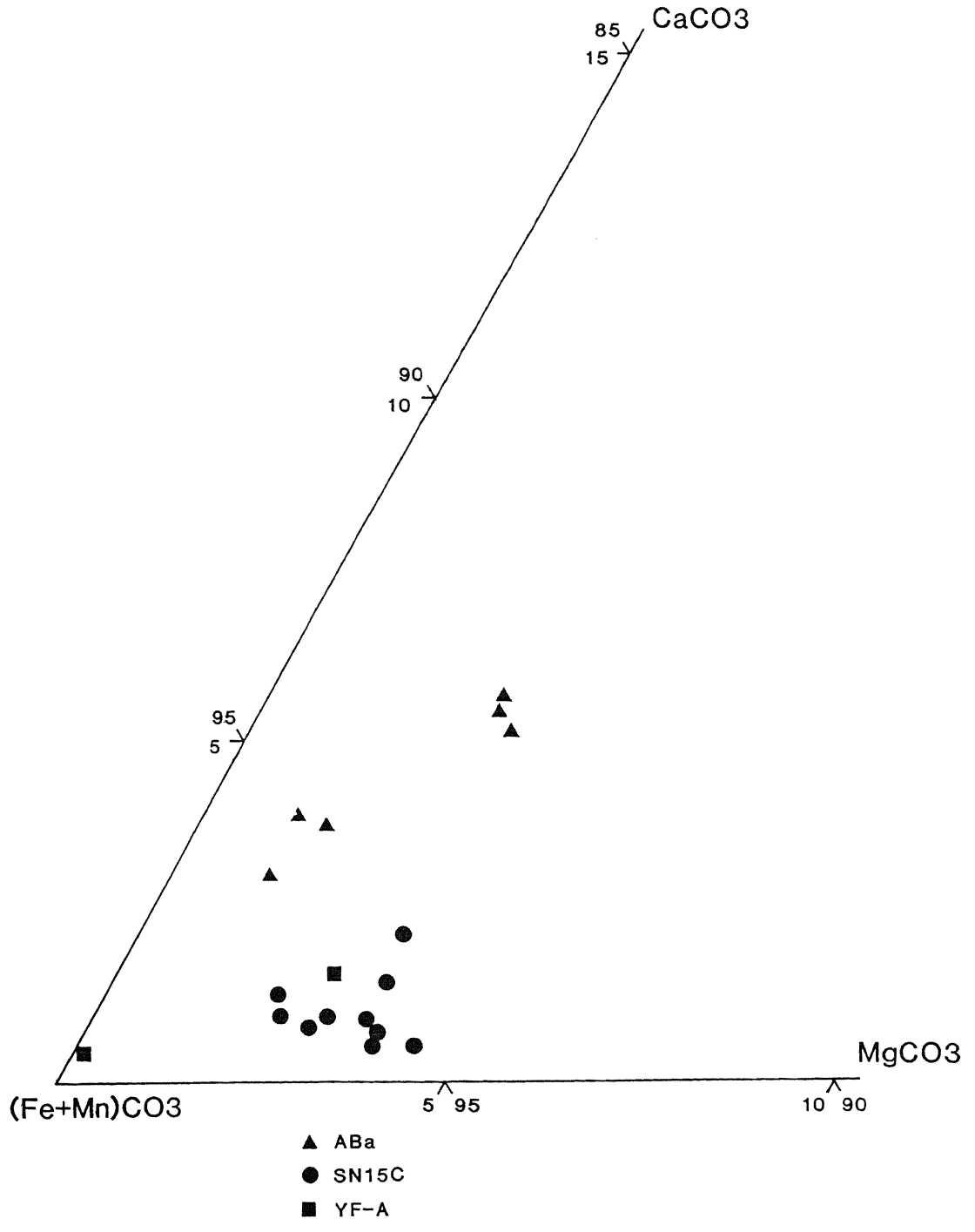

Figure 5.6 Plot of hydrothermal siderite compositions (from EPMA) on the same axes as diagenetic siderite (Section 4.2). Data from Appendix 4, see text for details. AB-A Aber, SN15C & YF-A Betws Garmon.

5.4 PYRITE & OTHER SULPHIDES

Some pyrite is found at virtually all ironstone localities. At any given locality more than one type of pyrite (plus base metal sulphides) can occur. At only a few localities is pyrite abundant. The distribution of pyrite at each locality is given in Chapter 2, and therefore is only summarised here. Likewise, a description of the textures associated with pyrite have mostly been described from the previous two sections and so are again only summarised here.

Pyrite occurs in five different forms in the ironstones:

1) in fault zones,
2) in veins,
3) in pyrite nodules,
4) disseminated throughout the ironstone,
5) massive replacment of the ironstone.

Tectonised ironstones (Trefor, Aber and Tremadog) have fault zones infilled by pyrite (Chapter 2), which at Tremadog are associated with quartz and dolomite. Veins containing pyrite are found in the Aber and Betws Garmon ironstones. At both these localities pyrite occurs in quartz and siderite veins, which at Betws Garmon also contain haematite. Similarly pyrite nodules (up to 6cm in size) are found at both these localities. At Aber pyrite nodules are restricted to the grain-ironstones, but at Betws Garmon are found in all the ferruginous facies. Pyrite nodules have also been recorded from the Llandegai ironstone (Strahan et al. 1920).

Disseminated pyrite, as euhedral cubes up to 2mm in size, is the most common occurence of pyrite in the ironstones. This occurs in all ironstone facies at Trefor, St. Tudwals, Aber, Gorddinog, Bwlch y Cywion, Betws Garmon, Tremadog, Rhyd, Cadair Idris east and Tyllau Mwn. Locally this form of replacement can become very intensive, as at St. Tudwals and Gorddinog. Finally massive replacement by pyrite is seen at Cwm Caseg and A5 localities (Northern Snowdonia), and at Foxes Path (Cadair Idris).

5.4.1 Textures

At Aber, cross-cutting quartz and siderite veins contain pyrite and minor chalcopyrite and sphalerite. The latter shows exsolution blebs

of chalcopyrite (Figure 5.7). Pyrite in these veins partially occurs overgrowing the chamositic and sideritic ironstone (Figure 5.8). The Betws Garmon ironstone also contains cross-cutting quartz and siderite veins. However, within these veins occurs intergrown pyrite and pyrrhotite (Figure 5.9), with minor chalcopyrite and arsenopyrite. Adjacent to these veins replacement of ooids by pyrite is very intense (Figure 5.9) and replacement decreases away from these veins. In contrast pyrite and base metal sulphides in the St. Tudwals ironstones occurs disseminated throughout the ironstone, and does not occur in cross-cutting veins.

Pyrite nodules in the Aber ironstone occurs as interlocking cubes of pyrite (up to 2mm) overgrowing the oolitic texture (Figure 5.7). The pyrite cubes have numerous inclusions of chamosite and siderite within them. At Cwm Caseg and A5 localities the original oolitic texture is now almost entirely replaced by pyrite. The mineralogy is now pyrite, quartz and siderite. Most of the ironstone is a mixture of quartz and siderite with rare disseminated pyrite. Some ghosts of ooids may be replaced by pyrite. Some areas of rock are completely replaced by pyrite. Here, pyrite first grows as euhedral cubes with siderite between grains, then a second phase of pyrite infills the spaces between cubes removing the siderite matrix.

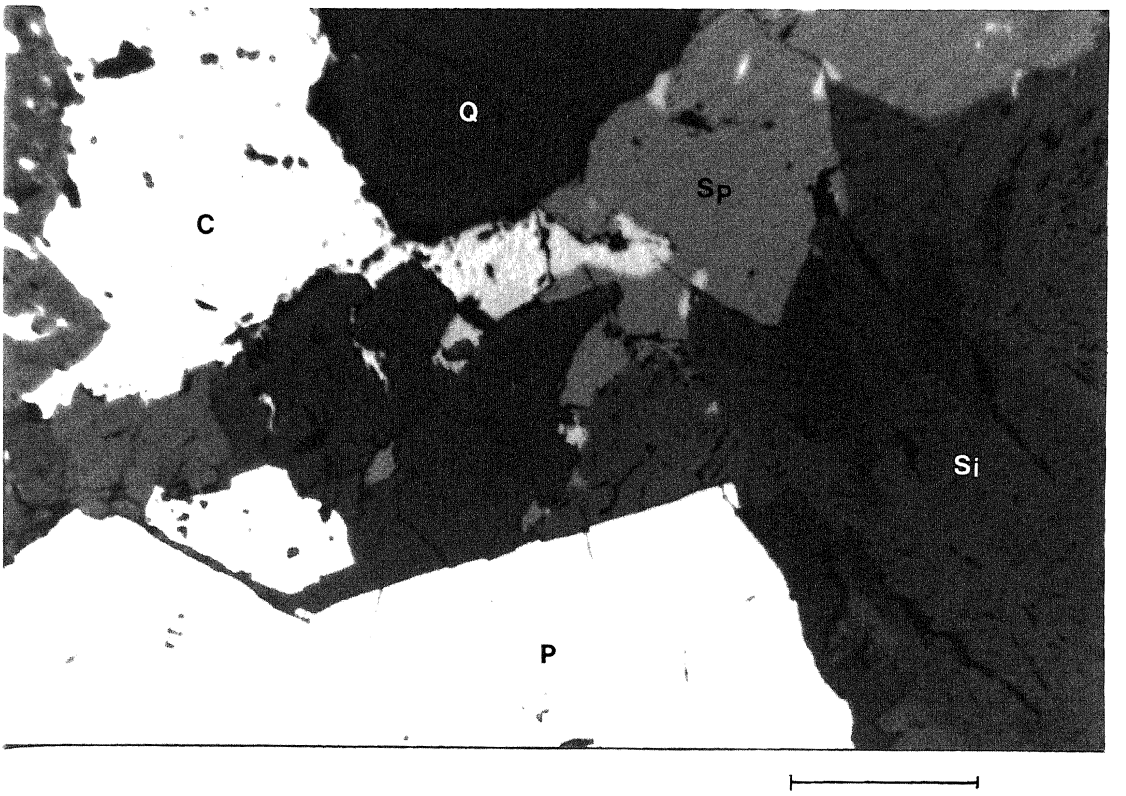

Figure 5.7 Photomicrograph, polished thin section, vein in ooidal grain-ironstone, AB-A Aber [SH 6693 7245]. Cross cutting vein through the ironstone containing, in order of reflectivity (bright to dark), pyrite (P), chalcopyrite (C), sphalerite (Sp) containing exsolution blebs of chalcopyrite, siderite (Si) showing bireflectance, and quartz (Q). Scale bar = 1mm.

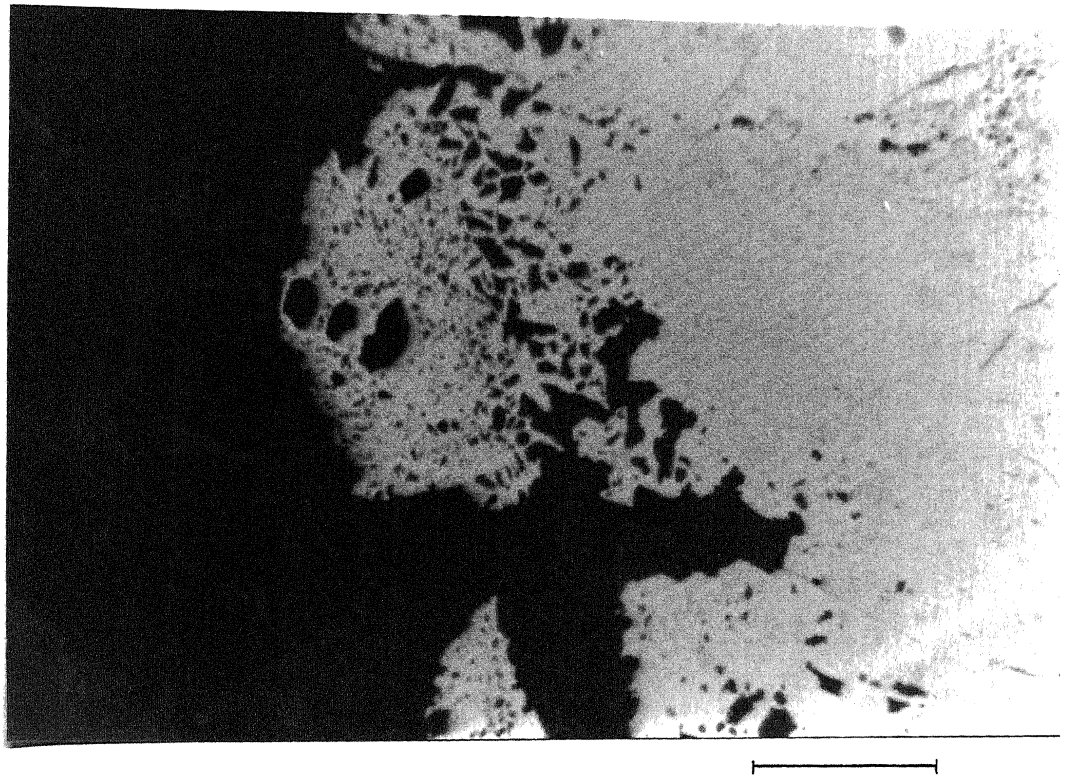

Figure 5.8 Photomicrograph, polished thin section, vein in ooidal grain-ironstone, AB-A Aber [SH 6693 7245]. The same pyrite grain as in Figure 5.7, which is also in contact with the ironstone (this figure). Here pyrite is overgrowing and including siderite (dark grey) and chamosite (darker grey). Scale bar = 1mm.

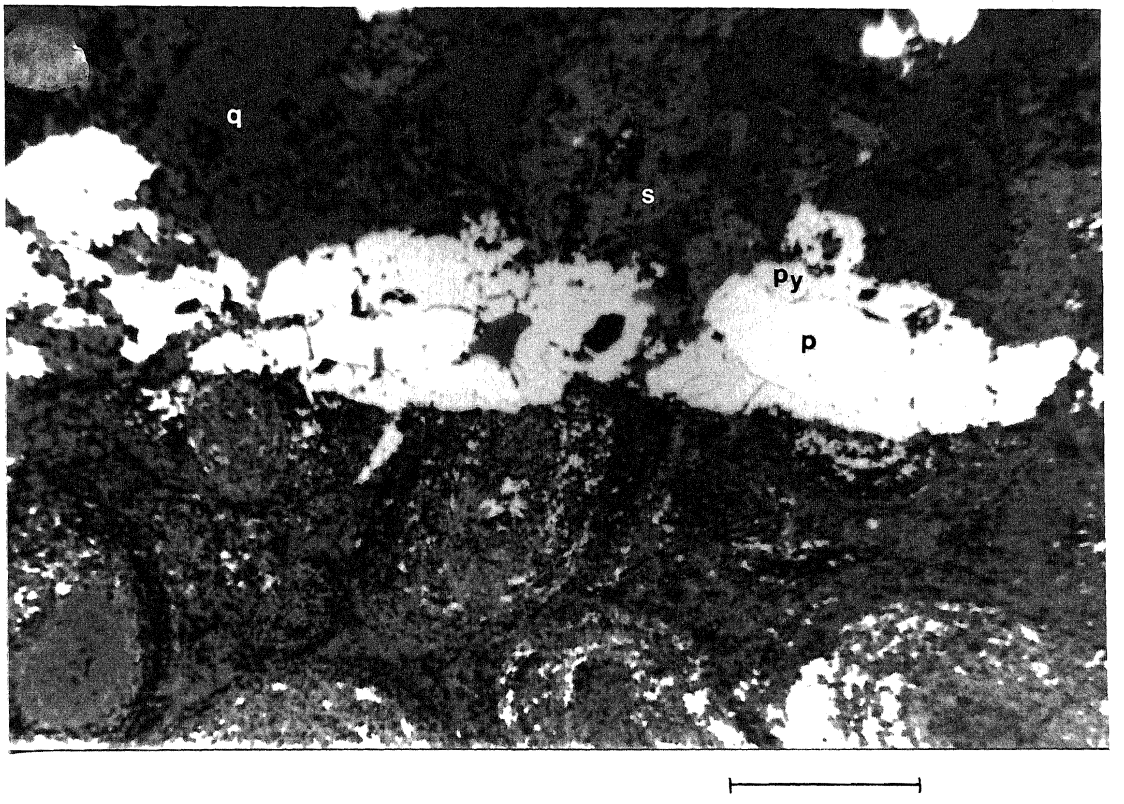

Figure 5.9 Photomicrograph, polished thin section, vein in ooidal pack-ironstone, YF-A Betws Garmon (loose grab sample). Edge of a quartz (Q) and siderite (S) vein cutting across the oolitic texture. Contained within the vein is pyrite (P) surrounded by slightly darker and bireflectant pyrrhotite (Py). Ooids are composed of magnetite but with some replacement by pyrite. Scale bar = 1mm.

5.5 DISCUSSION

All changes undergone by the ironstones described in this chapter, were caused by the proximity of some ironstones to igneous intrusions. It is proposed here that three different processes altered the ironstones. These resulted in the formation of magnetite plus stilpnomelane, the formation of siderite with pyrite plus base metal sulphides, and the formation of pyrite. These three processes can be related to different types of igneous intrusion.

The intimate association at some localities of magnetite and stilpnomelane suggest they are synchronous, and of the same origin. Magnetite and stilpnomelane formation within the ironstones is a porosity controlled feature. Alteration is restricted to the upper pack-ironstone facies only. Within the pack-ironstones phosphate nodules, chamosite mud patches and chamosite mud lenses are relatively unaltered, as are siderite cemented grain-ironstones (Pensyflog). All this indicates the strong control of porosity on pore fluid migration, which was responsible for altering the ironstones.

The composition of these pore fluids for magnetite to be stable is low Eh, high pH, and low sulphate, sulphide and bicarbonate activity (Maynard 1983; Curtis & Spears 1968). How these fluids reacted with the ironstones and formed magnetite is uncertain, as no published information is available for this process. At Cadair Idris east magnetite occurs as a fine-grained replacement of the chamosite matrix. The magnetite is a fine-grained mixture with chamosite and quartz. Magnetite is also less well developed in less porous areas. This would imply that magnetite replacement occurred by passive infilling of the more porous parts of the matrix. How magnetite replaced ooids is more problematic. This is also a porosity controlled feature, indicating that pore fluids reacted with ooids in the formation of magnetite. Either magnetite replacment occurred by reaction of the pore fluids with chamosite to form magnetite, or magnetite formed by the recrystalisation from an iron oxide/hydroxide precursor. This precursor must therefore have reacted with the chamosite ooids. Diagenetic siderite can be discounted as an iron precursor for magnetite, as magnetite would then have the same textural features as diagenetic siderite.

Deer et al. (1962b) give the following reaction for the formation of stilpnomelane:-

$$\text{Chamosite} + SiO_2 + K_2O \rightarrow \text{Stilpnomelane} + MgO + Al_2O_3$$

Aluminium behaves in an immobile fashion in the North Wales Ironstones (Section 3.3.3), and therefore is unaffected by alteration. This indicates that aluminium is neither added to nor lost from the overall ironstone system. Therefore for stilpnomelane to have formed it must have reacted with chamosite. XRD shows that there is no quartz present now in the Cadair Idris east ironstone. As all other ironstones analysed by XRD show some quartz, this must have been involved in the above reaction. At Cadair Idris, correlation can be made between chamosite maturity and porosity. The magnetite-rich ironstones have a chamosite composition that plots over the berthierine field (Section 4.3), whereas the stilpnomelane-rich ironstones have a chamosite composition that plots on the edge of the IIb field. The latter chamosite has reacted with pore fluids to form stilpnomelane. The aluminium released by the reaction is taken up by remaining chamosite in the rock, making it more tetrahedral aluminium rich. With increasing stilpnomelane formation the remaining chamosite becomes more aluminium rich. Magnetite replacement at Cadair Idris east does not react with chamosite, and reduces porosity so that no further maturation of chamosite can occur. Velde (1989) has shown that stilpnomelane formation in metamorphosed ironstones re-equilibrates with the surrounding rock, supporting the idea of more Al-rich chamosites in equilibrium with stilpnomelane.

These changes have resulted from the intrusion of igneous bodies near to some ironstones. These ironstones have undergone geochemical changes as a result of this alteration, principly the introduction of iron and potassium to the ironstones. In the Cadair Idris (east) region a dolerite sill (the Pen y Gader Dolerite - Davies 1956) intrudes into the Llyn y Gader Mudstones above the ironstone. Davies (1956) has shown that the dolerite has metasomatised the adjacent mudstones, introducing iron and potassium into sediments at least 30ft below the dolerite. This indicates that the ironstone has also been metasomatised by the overlying dolerite. However, this does not explain why some ironstones are stilpnomelane-rich and some magnetite-rich. One reason for this difference may be due to spatial distribution. The samples with the highest potassium (and therefore

highest stilpnomelane) values are both from Bwlch Coch, whilst the three more magnetite-rich samples are from Cross Foxes. This may reflect proximity to the dolerite, as the Cross Foxes locality is closer to the dolerite (Cox 1925).

There is a similar link for other ironstones and metasomatism. Other ironstones that contain magnetite and stilpnomelane have had iron and potassium introduced into the ironstone. The Tremadog ironstone occurs some 20m below a dolerite sill (Plate 2.13) just outside the limit of hornfels of the adjacent mudstones (Smith 1987). The Rhyd ironstone occurs partially within the aureole of the subsurface extension of the Tan y Grisiau microgranite (Bromley 1963; Smith 1987). Similar to the Rhyd ironstone the Bwlch y Cywion ironstone occurs adjacent to the Bwlch y Cywion microgranite. However, the Betws Garmon ironstone shows no such clear relationship between intrusion and metasomatism, although it may be in the aureole of the subsurface extension of the Mynydd Mawr microgranite (Wilkinson & Smith 1988, Figure 1). The formation of euhedral magnetite in the Llanberis Valley ironstone is most likely due to contact metamorphism of a ferruginous debris flow by an adjacent rhyolite intrusion (BGS 1985a). No chemical analyses are available to show any enrichment by iron.

Metasomatism by dolerites in North Wales clearly post-dates phosphate and siderite diagenesis, and compositions of chamosites from Cadair Idris east indicates that it pre-dates the transformation of berthierine to chamosite. This metasomatism occured in Caradocian times as shallow emplaced dolerite sills which reacted with still wet sediment (Smith 1987; Kokelaar et al. 1984). Similarly, metasomatism of the ironstones by microgranites occurred at this time, as these intrusions are spatially and genetically associated with the Caradocian volcanism (Reedman et al. 1985).

Alteration of the ironstones by siderite postdates the alteration by magnetite, and is associated with the formation of base metal sulphides. This would indicate hydrothermal alteration of the ironstones, with associated mineralisation. Hydrothermal alteration at Aber may be related to a number of smaller igneous intrusions nearby (BGS 1985b). Fluid inclusion studies on quartz veins from the Aber ironstone (W.E.G. Taylor pers. comm.) gives a poor definition for two fluid temperatures, one at approximately 190^{o}C and one at 110^{o}C. These fluids must have been bicarbonate-rich metal bearing brines to firstly form voids in the ironstone and react with the chamositic ooids, and secondly to precipitate not only siderite but also base metal

sulphides.

Reedman et al. (1985) describe mineralisation related to the Mynydd Mawr microgranite intrusion. The mineralisation associated with this microgranite is a late stage feature (Bromley 1969). It is probable that the hydrothermal alteration at Betws Garmon is due to the Mynydd Mawr intrusion, which is only approximately 2.5km away. This is supported by hydrothermal alteration of the Betws Garmon ironstone post-dating magnetite replacement. Minor hydrothermal alteration in the St. Tudwals ironstones is related to mineralisation in this region (Archer 1959); lead-zinc mines are found adjacent to the Hen dy Capel ironstone (Foster-Smith 1977a).

Pyrite replacement of the ironstones can be related to granophyric intrusions rather than microgranite intrusion. The Cwm Caseg and A5 localities (Northern Snowdonia) occur near the Aber-Drosgyl granophyric intrusion, and the Foxes Path locality (Cadair Idris) has a granophyric intrusion just above the ironstone (Section 2.4).

Bromley (1969) has described the acid intrusive complexes in North Wales and their aureoles. Metamorphism and spotting of sediments occurs much more widely around microgranite than granophyric intrusions (Bromley 1969). Granophyres do not show extensive large scale autometasomatism seen in the microgranites (Bromley 1969). The close association of granophyric intrusions and pyritisation of the ironstones, and microgranite intrusions and metasomatism and mineralisation, would indicate a close genetic link.

6 GENESIS OF PHANEROZOIC OOLITIC IRONSTONES AND THE SIGNIFICANCE OF THE NORTH WALES IRONSTONES

The previous chapters of this work have described and discussed the temporal and spatial distribution, deposition, diagenesis and alteration of the North Wales Ironstones. It is intended in this final chapter to review models of formation of Phanerozoic Oolitic Ironstones, and then compare and contrast the North Wales Ironstones within this context, with the intention of highlighting any significant similarities and differences. The three most important controls of ironstone genesis, source of iron plus ooid formation, depositional controls, and regional controls, will each be discussed in turn.

6.1 SOURCE OF IRON AND OOID FORMATION

The ferruginous components of Phanerozoic Oolitic Ironstones, for example berthierine peloids, are forming at the present day. This enables some analogies to be made between modern and ancient oolitic ironstone environments. However, berthieroid/iron oxide oolitic ironstones are not forming today, leading to poor understanding of their genesis due to the lack of modern analogues.

6.1.1 Source of Iron

A number of sources of iron for Phanerozoic Oolitic Ironstones have been quoted in the literature:

1) Clay leaching during burial (Kimberley 1979)
2) Oceanic upwelling (Maynard 1986)
3) Volcanic exhalation (Quade 1976)
4) Lateritic weathering (Maynard 1986; Van Houten & Purucker 1984; and references within)

Kimberley (1979) proposes that iron leaches downward from organic-rich muds during burial into carbonate oolites. This downward percolation of iron-rich groundwaters replaces the calcium carbonate but preserves the original tangential orientation of the aragonite ooids. This argument has now been dismissed (Maynard 1986; Bhattacharyya & Kakimoto 1983; Bradshaw et al. 1980), on the grounds of lack of association of ironstones with immediately overlying organic-rich muds, the lack of association of many ironstones with carbonates and the immobile nature of aluminium in the groundwater system. However, on a small scale, diagenetic berthieroid replacement of calcareous allochems can occur (Kearsley 1989), as does iron staining of calcareous allochems (Dreesen 1989). In the North Wales Ironstones, some diagenetic infilling of pore spaces by chamosite does occur, but is not a major source of iron.

Deep anoxic waters are capable of transporting large amounts of ferrous iron in solution (Maynard 1986, 1983). It has been proposed that upwelling of these waters onto the shelves and mixing with shelf aerobic waters would cause a large supply of iron at the mixing boundary. If this process of iron enrichment were to occur black shales would expected to be the deep water equivalents to ironstones (Maynard 1986). Ironstones and black shales in the Jurassic have been noted as occurring at the end of a regression and during a transgression respectively (Hallam & Bradshaw 1979). Van Houten & Arthur (1989) describe a much closer association between black shales and ironstones.

Black shales in the Lower Palaeozoic formed preferentially during transgressions, when the oxygen minimum zone intersected the sediment/sea water interface (Leggett 1980). They mostly correspond to 'G states' (polytaxic states) characterised by high sea level stands, higher marine temperatures, climatic amelioration, reduced oceanic circulation, extensive biotas and a large oxygen minimum zone (Leggett et al. 1981). However, it is uncertain if ironstones and black shales are coincident because they need the same background conditions of formation (transgressions, polytaxic conditions) or are formed by the same process, where ironstones are the shallow water equivalents of black shales. Within the North Wales Basin black shales occur in the Caradoc, related to high stands of sea level by eustatic transgression (Leggett 1980). The North Wales Ironstones are older then these black shales as they are mostly Llandeilo in age and coincide with the start of the transgression. There is a close setting relationship between

ironstones and black shales in the North Wales Basin as they both occur in a shelf environment, but do not show any close temporal association. In this respect the North Wales Ironstones and Caradoc black shales approximate more to the Jurassic, where ironstones mark the end of a regression and black shales the start of a transgression (Hallam & Bradshaw 1979). Thus an oceanic upwelling source for the North Wales Ironstones is unlikely.

The occurrence of volcano-sedimentary iron ore deposits (Lahn-Dill type ironstones) has been reviewed by Quade (1976). Typically these are volcanic or limestone hosted, haematite predominated, stratabound ore bodies at the top of volcanic rises of thick masses of spilitic tuffs and lavas. They are overlain by pelagic limestones and shales and may transgress onto nearby reef complexes. They are typical examples of metal precipitates, derived from active volcanism and deposited under marine conditions. There are accounts of some 'Lahn-Dill type' ironstones with chamosite, as a thin basal layer between the volcanic rocks below and the main iron ore above, and even one account of chamosite ooids, in a calcareous basin sequence adjacent to a typical volcano-sedimentary ore body (Quade 1976). These characteristic features of volcano-sedimentary iron ores are very different to the North Wales Ironstones, in that the latter are not associated with volcanics, do not contain primary haematite (or magnetite), and are chamosite and ooid predominated. This is further emphasized by geochemical comparisons; 'Lahn-Dill type' ironstones are iron and silicon dominated and depleted in aluminium and phosphorus compared to the North Wales Ironstones (Quade 1976).

Associated with 'Lahn-Dill type' ironstones is diagenetic mobilization of iron (as haematite) into associated limestones, indicated by ferruginised calcareous allochems. Similar ores, in areas with no obvious volcanic activity, are also seen (Dreesen 1989). These ores are thin, laterally extensive, ironstones containing ferruginised calcareous allochems, either iron stained probably from the surface waters of density-stratified evaporite pans, or iron chlorite impregnated from the diagenesis and halmyrolysis of volcanic ashes. These ironstones are time equivalents of 'Lahn-Dill type' ironstones elsewhere.

Phanerozoic Ironstones are built of two very common products of weathering, iron oxide and clay (Van Houten & Bhattacharyya 1982). Iron and Aluminium are insoluble in the oxide form and so can be concentrated in residual weathering (Clemmey 1985). Transport of

lateritic weathering material as kaolinite/iron hydroxide complexes (Carroll 1958) by rivers into the marine environment is the most frequently quoted source for Phanerozoic Ironstones (eg. Myers 1989; Van Houten & Purucker 1984; Maynard 1986, 1983; Hallam & Bradshaw 1979). The geochemical evidence discussed in Chapter 3 gives strong support for a lateritic weathering source for the North Wales Ironstones. Likewise, the temporal setting of the North Wales Ironstones is also favourable to this model, in that regressions allow for the exposure and leaching of landmasses. Reworking of this material during transgressions is the source of the ironstones. Despite the fact that in the literature lateritic weathering is the most frequently evoked model for the source of iron, other sources cannot be excluded and some ironstones may be polygenetic in origin.

6.1.2 Formation of Berthierine and Fixation of Iron

A major problem when considering ferruginous allochems in ironstones is that they now preserve a wide variety of mineralogies (Maynard 1983). However, only goethite and berthierine (limonite and chamosite in older literature) are the primary iron phases in ooid formation (Kearsley 1989; Maynard 1986; Chowns & Maynard 1986; Gehring 1985; Van Houten & Purucker 1984; Van Houten & Bhattacharyya 1982), which with post-depositional changes are particularly susceptible to mineralogical changes.

Berthierine especially is of interest in ironstones as not only is it the principle ferruginous component of the majority of Phanerozoic Oolitic Ironstones, but its formation, requiring reducing conditions but occurring in reworked and winnowed (and therefore oxidizing) environments, is also problematic. The two main types of ooids in marine ironstones, high sphericity goethite ooids and low sphericity berthierine ooids, strongly suggests that berthierine was the dominant phase in ooids before any significant compaction had occurred. This implies that it is unlikely that burial diagenesis could account for berthierine formation (Young 1989a). Therefore, regardless of how it forms, berthierine formation must occur at or near the sediment/sea water interface. This condition applies to ooids in the North Wales Ironstones, which are slightly subspherical in shape. The deformation of ooids around nodules and in mud lenses indicates the still plastic nature of berthierine ooids in the diagenetic environment.

Several models of berthierine genesis in ironstones have been put

forward (Young 1989a):

1) Direct precipitation from solution,
2) Precipitation from a gel,
3) Transformation of a kaolinite/iron oxide mixture.

Formation of berthierine by the precipitation from a fluid has been advocated for Jurassic Ironstones (Taylor 1951), and also more recently for other ironstones (Kearsley 1989; Gygi 1981). The first arguments against this were thermodynamic constraints (Curtis & Spears 1968), which precluded berthierine precipitation in seawater unless there was a markedly reduced salinity. More recently the role of organic matter in diagenetic reactions has been better understood; it gives rise to prolonged oxic and post-oxic reactions (Berner 1981). This allows for the authigenesis of iron-rich silicates in these environments (Spears 1989; Berner 1981). Kearsley (1989) has suggested ooid formation as precipitation of berthierine platelets around the edges of ooids. Subsequent 'tumbling' of the ooid would give a concentric laminar structure.

Precipitation of berthierine from a fluid does occur in the North Wales Ironstones as cements infilling secondary pore spaces, and as microcrystalline cements in chamosite mud-ironstones, both in the diagenetic environment. However, this postdates phosphate nodule formation and siderite rhomb formation. It is clearly late diagenetic and therefore is not a suitable method for iron fixation in the marine sedimentary environment. The geochemistry of the North Wales Ironstones further supports this. The immobile behaviour of aluminium would preclude its precipitation from an aqueous phase to form a large amount of berthierine. However, it has been shown that sedimentary chlorites do form in sandstones from pore waters, but at the expense of kaolinite and carbonate (Curtis et al. 1985).

The possibility of generating berthierine in the marine environment from a gel precursor has been proposed for oolitic ironstones (Harder 1989, 1978). Gels allow the preconcentration of iron, aluminium and silica in seawater. The formation of various minerals from such gels has been demonstrated experimentally. Pulfrey (1933a) suggested ooid formation in the North Wales Ironstones from gels. However, the role of gels in the formation of sediments has yet to be substantiated, and from later arguments it is most likely the North Wales Ironstones formed by another method.

The formation of berthierine from a mixture of kaolinite/iron oxides in reducing conditions is the most generally accepted model (Bhattacharyya 1989, 1983; Kearsley 1989; Velde 1989, 1985; Maynard 1986, 1983; Van Houten & Purucker 1984; Bhattacharyya & Kakimoto 1982), although organic matter may be involved in the reduction process (Curtis 1985; Curtis et al. 1985). The same process may also occur in pedogenic environments in the reducing parts of soil profiles (Siehl & Thein 1989). This type of berthierine formation is also consistent with the source for the iron, as kaolinite/iron oxide complexes and iron in colloids from lateritic weathering.

The modern day records of berthierine in the marine environment are as peloids, largely of faecal origin, forming on sediment starved shelves (Van Houten & Purucker 1984). Berthierine peloids and goethite proto-ooids are found along the Niger, Ogoone and Orinoco deltas. Goethite proto-ooids are found near the coast whereas berthierine peloids are found further offshore. In a study of Cretaceous Egyptian ironstones, Bhattacharyya (1989) noted peloid and ooid formation in 'lean muddy oolites' where peloids form as faecal pellets or flocculated peloids. However, the formation of peloids by precipitation, especially from gels within argillaceous sediments cannot be discounted.

However, one important aspect of the fixation of iron and berthierine formation is by microbiota, an aspect which has been neglected for Phanerozoic Ironstones. The major function of iron for all life forms is the transfer of electrons, as iron easily changes its valence state and is also readily abundant (Nealson 1982). Iron may also be used by magnetotactic bacteria (Frankel & Blakemore 1984). Numerous microbiota are known to fix or uptake iron, or oxidize or reduce iron for energy (Chemotrophs). Siderophores are a class of compounds synthesized by bacteria or fungi that are excreted into the growth medium to facilitate iron uptake (Nealson 1982). Iron fixing microorganisms would always be expected in an iron-rich environment (Dahanayake & Krumbein 1986).

Nealson (1982) has reviewed the bacterial oxidation and reduction of iron and related this to biomineralisation in Precambrian Banded Iron Formations. Bacteria either oxidize or reduce iron as part of their energy cycle. Iron oxidation is either direct, by enzymatic or cell associated processes, or indirect, by other processes through which environmental conditions are altered and lead to oxidation of iron. By contrast bacterial reduction of iron, although it is known to occur,

is a poorly understood process. In the Lower Gunflint Iron Formation abundant microfossils are found, similar in nature to the present day Metallogenium (a budding iron oxidizing bacteria). Similar microfossils are seen in other Precambrian iron ore deposits. Many Precambrian ore deposits, including iron, were probably directly or indirectly influenced by microbial and biogeochemical processes to concentrate the ore (Dexter-Dyer et al. 1984).

By contrast, the role of microbiota in the formation of Phanerozoic Ironstones has, until recently, been under-emphasized. Early studies this Century recognised the presence of organically formed ferruginous allochems in both Ordovician and Jurassic ironstones of Britain, and mentioned their possible significance (Hallimond 1951; discussion in Pulfrey 1933a). However, 'classic' Phanerozoic Ironstones are not suitable for the study of ferruginous microbiota. This is because oolites do not preserve any sign of organic activity as they are secondary accumulations and usually well sorted by winnowing (Bayer 1989). The only trace of organic activity is as fine organic laminae in ooids (Chapter 4) or algal/cyanobacterial borings (Hayes 1915; Hallimond 1925). This becomes more apparent when publications on ferruginous organic structures indicate that they do not form in high energy oolite bodies. Instead they occur in lower energy environments as mineralised encrustations on hardgrounds (Gehring 1986), as limonite concretions ('snuff boxes') in stratigraphically condensed limestones (Gatrall et al. 1972), as oncoids in nearshore lagoonal environments (Bayer 1989) or as goethite, berthierine and calcite oncoids in sublittoral, low-energy muddy facies (Knox & Fletcher 1989).

In this respect the North Wales Ironstones contribute significant new information about the role of microbiota in the fixation of iron and formation of ferruginous structures. Oncoids are found in the muddier facies, or in the poorly sorted grain-supported facies of the ironstones. In situ stromatolites, laterally equivalent to the final site of deposition of the oolite body, represent algal mats trapping the original sediment. Organic matter in ooids provided the material for reduction, allowing the preservation of berthierine in an oxidizing environment. Whatever the role microbes play in the fixation of iron and the formation of ironstones (eg Dahanayake & Krumbein 1986) it is much more significant than previously recognised.

6.1.3 Formation of Ooids

Ooids are a very important feature of Phanerozoic Ironstones as they are the principle iron bearing component. Many models for the formation of ferruginous ooids have been proposed, and these have been reviewed by Kearsley (1989) and Young (1989a). From the arguments in the previous section it is probable that berthierine and goethite, the primary components of ferruginous ooids, were deposited and formed before the formation of ooids. Therefore the most likely causes for the formation of ooids are (Young 1989a):

1) Derivation of terrestrial soils.
2) In situ growths as 'microconcretions'.
3) Fungal Mats.
4) Mechanical accretion.

It was originally thought that ooids were not reworked laterite soil ooids for a number of reasons. Bauxitic ooids have a radial and not tangential orientation (Bhattacharyya & Kakimoto 1982). Many nuclei to ooids are demonstrably marine in origin (Maynard 1983). Marine goethite has low aluminium substitution while soil goethite has high aluminium substitution (Maynard 1986). However, it has recently been shown that ferruginous ooids can form with a concentric orientation in pedogenic and hydromorphic environments. When these ooids are reworked they would form 'Minette type' ironstones (Siehl & Thein 1989, and Figure 6.1). However, it has been shown that the North Wales Ironstones have ooids with marine nuclei. Therefore this mechanism of ooid formation can be discounted for the North Wales Ironstones.

Intrasedimentary growth of ferruginous ooids in the soil environment has been proposed (Siehl & Thein 1989) and discussed above. In older literature the idea of in situ growth in the marine environment had great attractions, as it could account for the concentrically differing proportion of berthierine, goethite and apatite in ooids in marine ironstones (Hallimond 1951). Therefore the concentric variation of composition in ooids would reflect, at least in part, variations in the chemical environment of the formation of the ooid (Chauvel & Guerrak 1989). However, Kearsley (1989) suggests that much of the concentric variation in the mineralogy of ooids is due to the differential action of diagenetic processes in layers of the ooid with differing porosity. Therefore it is unlikely that this process would

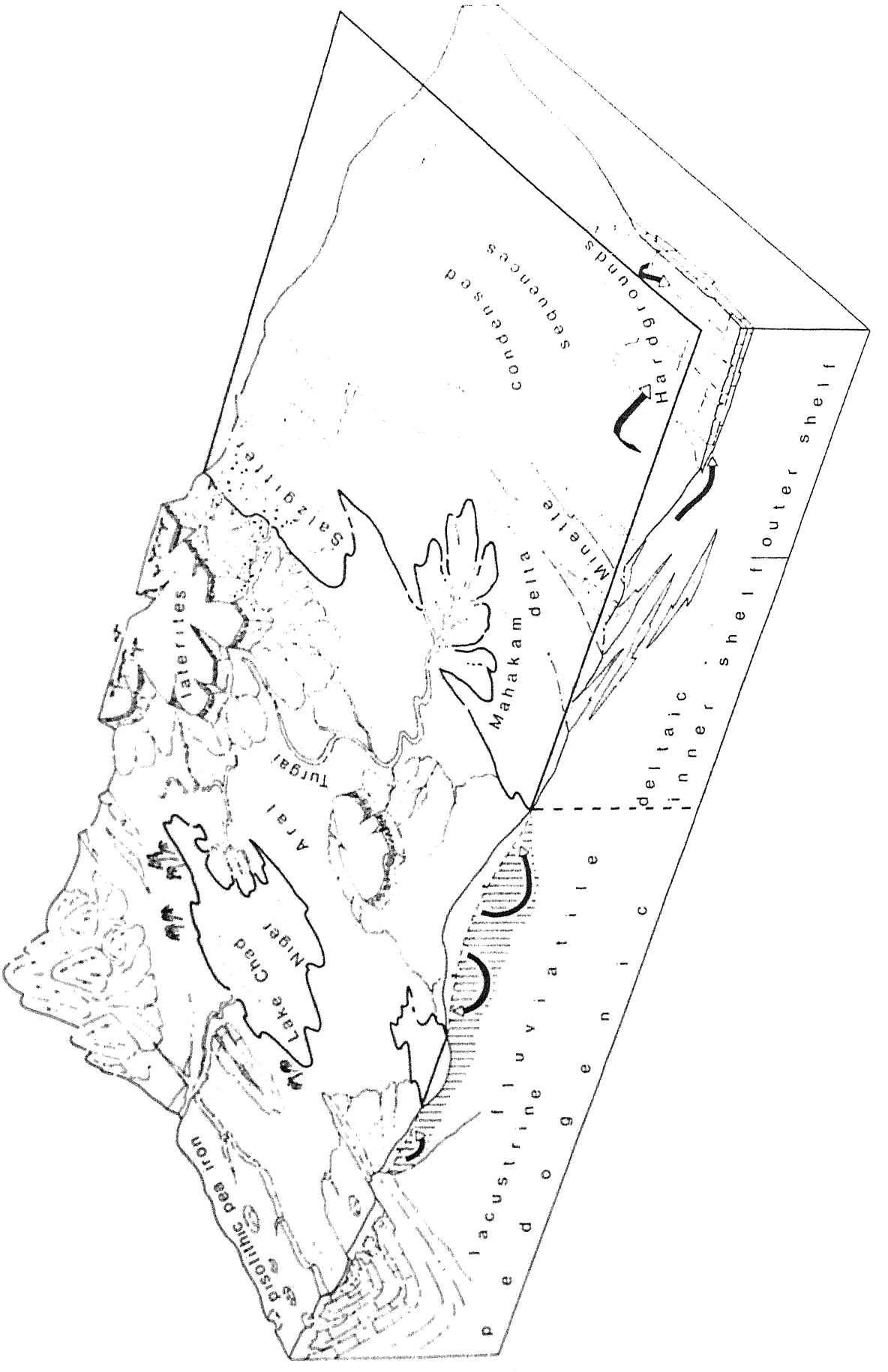

Figure 6.1 Pictorial summary of differing geological settings for 'Minette type' ironstones (after Siehl & Thein 1989) - ironstones that are derived from laterite soil ooids.

result in the formation of ooids. Any concentric variation in mineralogy of ooids in the North Wales Ironstones has been shown to be due to diagenesis/subsequent alteration.

A biological control of ooid formation has been proposed by Dahanayake & Krumbein (1986). Ooids are 'authigenically formed biogenic grains' within fungal mats, based on observations from the Minette ironstone of Lorraine. However, their descriptions do not match the sedimentological work of Teyssen (1984), who described in detail the tidal reworking of the ironstone. Siehl and Thein (1989) have provided alternative interpretations to Dahanayake & Krumbein's (1986) descriptions. However, as previously discussed, the biological control of the fixation of iron and formation of ooids in the North Wales Ironstones indicates that this process is under-emphasized and should be further investigated.

Mechanical accretion of berthierine or kaolinite/iron oxide complexes to form ooids is the most favoured model for ooid formation (Bhattacharyya 1989, 1983; Chauvel & Guerrak 1989; Van Houten & Purucker 1984; Van Houten & Bhattacharyya 1982). It has the advantage of being consistent with the lateritic weathering source model for ironstones, and consistent with the introduction of kaolinite/goethite complexes into the marine environment on sediment starved shelves. Chauvel & Guerrak (1989) have emphasized that one single process does not form ooids, and instead they suggest a two stage process. They advocate intrasedimentary accretion to form the inner part of an ooid and snowball (mechanical) accretion to form the laminae of ooids. Ironstones are most commonly nucleated around a peloid, but also nucleated around phosphatic or calcareous shell debris and quartz grains (Maynard 1983). Peloids may form by intrasedimentary accretion, flocculation or by faecal action.

The process of ooid formation is by mechanical accretion around a peloid or other nucleus. The most obvious mechanism is by direct analogy with carbonate ooids of snowball-type accretion (Van Houten & Purucker 1984). In this mechanism accretion is due to either adsorption onto ferric oxide/clay surfaces by 1) electrostatic interaction (Kearsley 1989; Gehring 1985), 2) ligand exchange reactions (Gehring 1985), 3) coating the grain with a sticky mucus and accreting (Kearsley 1989; Dahanayake & Krumbein 1986). This applies to both goethite ooids (Schiavon 1988; Gehring 1989,1985; Van Houten & Purucker 1984) and berthierine ooids (Bhattacharyya 1989; Chauvel & Guerrak 1989; Van Houten & Purucker 1984; Bhattacharyya & Kakimoto

1982). The differences between goethite and berthierine ooids may simply be due to thermodynamic control. Under normal seawater conditions (pH 8) and dissolved ions, goethite and kaolinite can convert to berthierine, and fluctuations of Eh can mean either berthierine or goethite and kaolinite are stable (Maynard 1986). Therefore goethite and berthierine ooids reflect differing physiochemical conditions in the environment of formation. Berthierine ooids were formed in muddy environments with weak currents whereas goethite ooids were formed in more aerated agitated waters (Van Houten & Purucker 1984).

However, there are ooids with a goethite nucleus but with berthierine laminae (Knox & Fletcher 1989), indicating an intimate link between the two environments. Goethite in marine ooids has a low aluminium substitution (and therefore is not soil derived); any aluminium in goethitic ooids is therefore due to the presence of clays (kaolinite) (Maynard 1986). Clearly there is no later alteration of goethite to berthierine as goethite ooids which contain kaolinite are preserved.

Ooids (and oncoids) in the North Wales Ironstones were formed and deposited in the marine environment on sediment starved shoals. Initially the lateritic weathering material was deposited and began forming berthierine, either as mud or flocculated peloids or faecal pellets. Algal or bacterial mats probaly had a trapping and then stabilizing influence on the sediment. Ooids were formed by mechanical accretion around peloidal, quartz grains and sponge spicule nuclei. This accretion process may have been helped by a sticky mucus from algal activity, bacterial reduction of which provided the conditions needed for berthierine formation and preservation. More intense algal activity also encouraged the formation of oncoids. Once formed ooids were reworked away from the site of formation, where intense algal activity was reflected by the presence of stromatolites and oncoids, to the site of final deposition.

6.2 FACIES MODEL

The sedimentary conditions under which ironstones form has recently attracted a great deal of research (Van Houten & Purucker 1984; Van Houten & Bhattacharyya 1982). Numerous authors have assigned sedimentary models to explain the formation of a particular ironstone (Bhattacharyya 1989; Knox & Fletcher 1989; Young 1989 b; Van Houten & Karasek 1981; Gygi 1981). However, to date only one general facies model for Phanerozoic marine berthieroid/iron oxide oolitic ironstones has been proposed (Van Houten & Purucker 1984; Van Houten & Bhattacharyya 1982).

In this section the facies model proposed for ironstones is summarised. The North Wales Ironstones are compared to this facies model and the similarities and differences discussed. Finally, some suggested modifications to this model are made.

6.2.1 Facies Models for Phanerozoic Oolitic Ironstones

This facies model is for Phanerozoic marine berthieroid/iron oxide oolitic ironstones, and therefore does not include glauconite iron ores (Hallam & Maynard 1987), fresh water oolitic ironstones (Davidson 1961), residual lateritic ironstones (see previous section and Siehl & Thein 1989) or bog iron ores (Spears 1989). The following characteristics are typical for Phanerozoic marine berthieroid/ iron oxide oolitic ironstones (Van Houten & Bhattacharyya 1982 and Figure 6.2):

i An Ironstone Formation may consist of a number of sandy or muddy shoaling up sequences. These asymmetric shoaling upward sequences are predominantly, but not exclusively, capped by an ironstone.

ii The base of the shoaling up sequence is characterised by mudstone with thin beds of silt and sand, commonly with hummocky cross stratification and bioturbated. This is followed by a variety of bioturbated sandstones. Away from this sandy input the upper part of the sequence is bioturbated muds with ooids. Where normal sedimentation waned, cross-bedded oolites developed.

iii Thin offshore ironstones laterally equivalent to the oolite bodies can occur and are distinctive in containing abundant intraclasts and bioclastic debris, subordinate ooids and both ferric oxide and calcite cements.

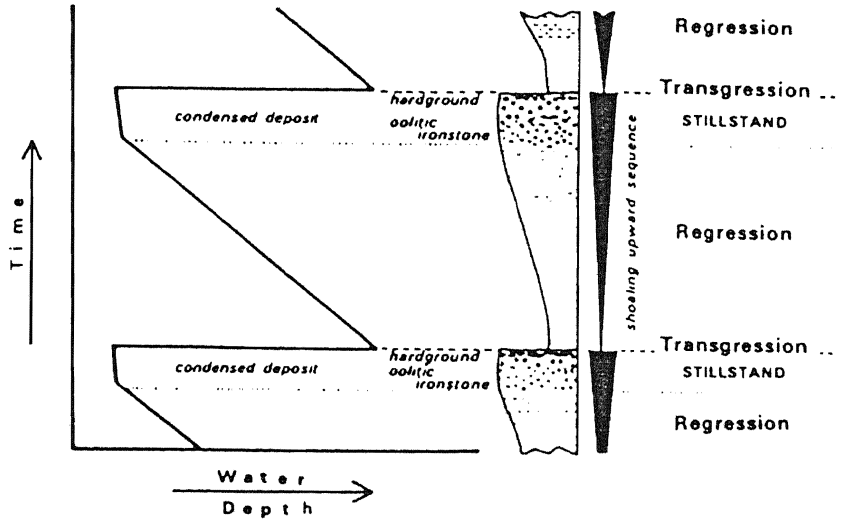

Figure 6.2 Facies model for Phanerozoic Oolitic ironstones contained in shoaling-up detrital sequences (after Van Houten & Bhattacharyya 1982). This emphasizes the relation of the ironstones to prolonged regression and relatively rapid transgression.

iv Oolitic ironstones are covered progressively by marine mud or a thin fine-grained basal sandstone. Many oolites are interrupted or succeeded by and laterally correlate with thin lenticular and nodular ferruginised hardgrounds. Some ironstones are covered by a thin ferruginous phosphatic sandy intraclast layer or lag deposit.

Oolitic ironstones are condensed deposits accumulated during the transition between a regression and transgression. They occur in detritus starved habitats , with a rarity of detrital grains in the oolite bodies or as nuclei to ooids. There is an absence of markedly asymmetric ooids (?oncoids), characteristic of very low energy environments, indicating repeated reworking of grains by currents and burrowers. Ironstones succeeded by hardgrounds represent a complete cessation of sediment influx. The barren sea floor was subject to submarine weathering, burrowing and mineralisation by ferric oxide and phosphate. Ironstones succeeded by lag deposits represent a local development when relatively high energy winnowing and transport by waves and currents of a renewed transgression spread across mudflats and crests of ooid bars.

Ironstones occur in a variety of shelf environments ranging from coastal/lagoonal to an offshore setting, but are predominantly associated with deltaic complexes. Some ironstones are contained in carbonate or mixed siliciclastic/carbonate sequences. The asymetric shoaling upward sequences commenced with muddy open shelf sediments settled from turbulent or colloidal suspension with thin sandy layers spread by storm surge currents. They were then bioturbated during fair weather sedimentation. The following sandstones accumulated at the front of a small prograding delta, characterised by deltaic distributary channel-mouth sands reworked by waves and littoral currents to form shoreface and delta front sandbodies, or a shoreline complex of bars and lagoons. More variable shoaling upward carbonate sequences commonly began with offshore fossiliferous calcareous mud with patches of shell debris and carbonate ooids, succeeded by shallow nearshore lime-rich mud. Some sequences ended with coastal oolitic and bioclastic deposits.

Most oolitic ironstones developed after the accumulation of a shoaling shoreline sequence, during delta lobe abandonment or other sediment starvation, allowing the formation of an ironstone. Some were formed in a late stage regression, for example during temporary waning of sediment influx along a prograding shoreline, or before the end of

a regression in areas remote from deltaic influx. Ooids were transported from their place of formation by coastal currents and concentrated in accreting cross-bedded bars. Interruptions in accumulation, probably due to shifting currents, permitted increased burrowing. Thin offshore intraclast-rich ironstones represent the seaward spreading of the ironstone by storms that swept across coastal ooid banks. Marine mud succeeding the ironstones indicate the advance of a renewed transgression developed on a discordance.

The two most important features of marine oolitic ironstones are their vertical shoaling upward sequences and their cyclic sedimentation (Figure 6.2; Van Houten & Purucker 1984). With this reconstruction of a model for an ironstone it is important to establish the controls of formation of these features, which vary between sedimentary basins (Van Houten & Purucker 1984). They may result from local autocyclic (intrabasinal) controls, such as the growth and abandonment of delta lobes or the migration of a tidal sandwave, or due to regional allocyclic (extrabasinal) controls, such as the tectonic control with intermittent subsidence or repeated eustatic rise in sea level.

6.2.2 Comparison with the North Wales Ironstones

The North Wales Ironstones show some marked differences to this generalised facies model. However, the two share many similarities as follows. The North Wales Ironstones occur in a muddy asymmetric shoaling upward sequence, the base of which is a mudstone which grades up into bioturbated mud-ironstones with ooids and oncoids and finally an oolite body. They are condensed deposits with thicker clastic sedimentation elsewhere, and they occur in detritus starved habitats, with a rarity of detrital grains in the oolite bodies or as nuclei to ooids. The North Wales Ironstones do contain ferruginised hardgrounds (stromatolites), as lateral equivalents to oolites, and phosphatic lag deposits, but within, not at the top of, the ironstone sequences. In the ironstones the ooids are transported from the place of origin and concentrated in accreting cross-bedded bars. Cessation of accumulation allowed for bioturbation and a subsequent covering by marine mud. These similarities are significant as they indicate that the North Wales Ironstones share the same general sedimentation pattern to the facies model.

The North Wales Ironstones do show some significant differences.

They are only a single asymmetric shoaling upward sequence, and they show no association with a deltaic complex, coastal barrier bar or lagoonal setting. Instead they occur offshore, but are not thin offshore storm reworked beds of coastal ooid bars.

These differences from the ironstones facies model demonstrates the importance of synsedimentary faulting on the control of sedimentation of the North Wales Ironstones. Although sedimentation at the time of ironstone deposition was predominantly fine-grained, the North Wales Basin was still tectonically active (Fitches & Woodcock 1987). The parochial nature of ironstone deposition on stratigraphic hiatuses indicates that syn-sedimentary faulting had a strong control on ironstone deposition, and is also known to have had a major control on the sedimentation and volcanicity within the North Wales Basin (Fitches & Campbell 1987; Kokelaar et al. 1984). The occurrence of debris flows within the ironstones further substantiates the significance of contemporaneous fault control. Condensed ironstone sequences, deposited above a stratigraphic hiatus, with phosphatic enrichment and lack of clastic dilution, formed at different times and in different places on short-lived shallow water shoals within the North Wales Basin, as is the case with similar deposits in the Jurassic (Hallam 1975; Sellwood & Jenkyns 1975). Eustatic falls of sea level would have tended to emphasize the significance of such shoals (Hallam & Bradshaw 1979).

Other Ordovician Ironstones may have a hardground beneath, either phosphatic or sideritic, on which the ironstones form (Young 1989b). Clearly the presence of a stratigraphic hiatus beneath the North Wales Ironstones indicates non-deposition or erosion. No siderite or phosphatic hardgrounds have been found beneath the North Wales Ironstones. The association of algae/bacteria with the ironstones and the presence of stromatolitic hardgrounds, which may originally have had a binding effect of sediment on the shoal, were the most probable causes for stabilizing chamositic mud-ironstone (Dahanayake & Krumbein 1986) on the shoal, which are the basal beds of the North Wales Ironstones.

Cyclic sedimentation is a common feature of oolitic ironstones, which for individual shoaling-up sequences is an autocyclic control, for example the Cleveland Ironstone Formation (Rawson et al. 1983), the Minette Ironstone (Teyssen 1984) and the Devonian Libyan ironstones (Van Houten & Karasek 1981). Small-scale (autocyclic) sedimentation is seen at Bryn Poeth, with 0.5m thick ironstone cycles

capped by a thin grain-ironstone, comparable to coquina beds at the top of other ironstone cycles (Teyssen 1984). The fact that the majority of the North Wales Ironstones preserve only one 'cycle' of sedimentation, a vertical shoaling-up sequence, indicate the short lived nature of the shoals upon which the ironstones were formed. The association of oolitic ironstones with shorelines (Bayer 1989; Van Houten & Purucker 1984; Van Houten & Bhattacharyya 1982) is seen for the Anglesey ironstones in North Wales. The ironstones of Central Anglesey, occurring in the basal beds of the gracilis transgression, have been shown to be shoreline related.

The North Wales Ironstones do not fit the standard model proposed for marine oolitic ironstones (Van Houten & Purucker 1984; Van Houten & Bhattacharyya 1982). However there are enough similarities to indicate a genetic link between the North Wales Ironstones and the Phanerozoic Ironstone facies model.

6.2.3 Suggested Revisions to the Ironstone Facies Model

This comparison of the North Wales Ironstones with the Phanerozoic Ironstones facies model has revealed some shortcomings. For example some ironstones have formed on offshore shoals, as in the Jurassic (Hallam 1975; Sellwood & Jenkyns 1975). Although these ironstones have some features in common, they also have many differing sedimentary features. It is not within the scope of this thesis to propose a new facies model for Phanerozoic Ironstones. However, from what has been discussed in this chapter and also reviewed by Young (1989a), the following four broad models for the formation of marine oolitic ironstones can be suggested.

1) The generation of ooids in lagoons or nearshore environment, and their subsequent reworking into ooid bars and offshore storm reworked deposits (Bayer 1989; Van Houten & Purucker 1984; Van Houten & Bhattacharyya 1982).

2) The generation of ooids and the development of oolitic ironstones on offshore swells which receive little clastic sediment, but upon which the sediments may be intensively reworked (This work; Trythall et al. 1987; Hallam 1975; Sellwood & Jenkyns 1975).

3) The *in situ* development of ooids on marine shelves during phases of sediment starvation, such as that produced by rising sea-level (Young 1989b).

4) The generation of ooids in the lateritic soil environment (Siehl & Thein 1989; Nahon *et al.* 1980). These ooids may be reworked by a transgression into the marine environment and deposited by tidal currents to form 'Minette type' ironstones (Siehl & Thein 1989; Teyssen 1989, 1984).

6.3 GLOBAL CONTROLS ON PHANEROZOIC IRONSTONE FORMATION & DISTRIBUTION

The temporal distribution of Phanerozoic Oolitic Ironstones is variable throughout the Phanerozoic. However, there is a pattern to the temporal and spatial occurrence of the Phanerozoic Ironstones. The three major controls on the distribution and formation of ironstones are palaeoclimate, regional/global changes and tectonic setting, and these controls are now well documented for Phanerozoic Ironstones. However, some major paradoxes arise when comparing the formation and distribution of the North Wales Ironstones to the general ironstone model. These are discussed below.

6.3.1 Palaeoclimate and Lateritic Weathering

Phanerozoic Ironstones were predominantly formed in two 170 Ma periods, earliest Ordovician to latest Devonian and earliest Jurassic to middle Cenozoic (Van Houten & Bhattacharyya 1982). These two congenial periods are essentially 'greenhouse' stages of Phanerozoic history, marked by a mild climate and a generation of prolific organic matter (Van Houten & Bhattacharyya 1982). They correspond to high partial pressures of CO_2, possibly produced by mantle outgassing (Van Houten 1985) and by increasing the rate of chemical weathering (Van Houten & Arthur 1989). There is also a correlation of general ironstone distribution on flooded landmasses adjacent to crudely outlined east-west trending seaways, allowing enhanced ocean circulation around the cratonic blocks on which the ironstones formed (Van Houten & Bhattacharyya 1982).

The evidence for a lateritic weathering source for the North Wales Ironstones has been discussed in Chapter 3 and Section 6.1.1. Lateritic weathering for Mesozoic Ironstones, associated with deeply weathered, well vegetated, low-lying landmasses, has been well established (Hallam 1975). However, if lateritic weathering is a source not only for the North Wales Ironstones but the majority of Ordovician Ironstones (Young 1989a), then two factors do not agree with this. Firstly, the majority of Ordovician Ironstones (including the North Wales Ironstones) accumulated at mid to high lat itudes. Either around the northern edge of Gondwana (Young 1989b; Van Houten 1985), which lay over the south pole, or as a separate Avalonia plate separated from Gondwana by the Rheic Ocean (McKerrow & Cocks 1986). This is based on cold water faunal associations (Fortey & Cocks 1986;

Cocks & Fortey 1982) and with no evidence of warm humid climates (red beds, carbonates or lateritic horizons - Van Houten in Boucot & Gray 1986). Secondly vascular land plants, needed to help in the process of weathering, had not evolved by Ordovician times (Van Houten 1985), although Bryophytes (eg mosses) may have been present (Boucot & Gray 1986).

Despite the restriction of cold climate and absence of land plants, the North Wales Ironstones have typical characteristics of an ironstone derived from lateritic weathering. One suggestion is that a higher partial pressure of carbon dioxide in the Ordovician atmosphere may have produced more acidic groundwaters at high la titudes (Van Houten 1985), which may have been capable of producing chemical weathering similar to that seen in well vegetated tropical la titudes today (Young 1989a). It is difficult to envisage a process to generate lateritic weathering in these conditions, and the problem remains unresolved.

Myers (1989) has shown that detrital kaolinite (now berthierine) occurs in the clastic mudstones within the Cleveland Ironstone Formation, indicating a continuous supply of lateritic material onto the shelf that was concentrated into an ironstone only at specific times. Similarly, examination of published XRD and EPMA data for Arenig to Caradoc clastic mudstones in the North Wales Basin (Merriman & Roberts 1985) indicate that sedimentary chamosite (originally berthierine and therefore ?kaolinite) is present throughout this mudstone dominated sequence. This would therefore indicate a small but continuous supply of lateritic material (kaolinite/iron oxide complexes) into the North Wales Basin, also indicated by the presence of the Bryn Poeth and Tremadog ironstones. However, only other favourable factors allowed the formation of an ironstone. The source of iron increases to form ironstones only when a major regression exposes land for weathering.

6.3.2 Regional Controls

The Phanerozoic Ironstone record suggests temporal cyclic patterns of distribution within sedimentary sequences on several different scales, and within this pattern Phanerozoic Ironstones are developed repeatedly in about 15 major sedimentary successions preserved in about 10 major sedimentary basins (Van Houten & Arthur 1989). The first scale of cyclicity is two 170 Ma episodes, earliest Ordovician

to latest Devonian and earliest Jurassic to middle Cenozoic, in which ironstones are abundant (Van Houten & Bhattacharyya 1982). These episodes are charaterised by high stands of sea level (Figure 6.3), with cratonic basins flooded by a general rise of sea level (Van Houten & Bhattacharyya 1982). Within these episodes, there are long enduring or reoccurring conditions for ironstone deposition which prevailed for a few to several tens of millions of years (Van Houten & Arthur 1989). Within these basins at relatively high stands of sea level, repeated ironstone development is related to eustatic changes of sea level, either at the end of regression, during a still stand or at the start of a transgression (Young 1989b; Hallam & Bradshaw 1979). Ironstones can also repeat on the several hundred thousand year time scale (Van Houten & Arthur 1989), with one explanation relating this repetition to Milankovitch cycles (Van Houten 1986), although much care is needed in distinguishing autogenic (local) controls from allogenic (regional) controls.

Within the Ordovician three stratigraphic levels have a particularly widespread and abundant distribution of ironstones, in the Lower Llanvirn, the Lower Caradoc and the Lower Ashgill, which correspond to global eustatic rises of sea level (Young 1989b). Ironstones particular to these stratigraphic levels are thin but persistent, even in relatively offshore areas, and are remarkably similar between the different stratigraphic levels. The repeat for this variation is 10-15 Ma (Young 1989b). However, the ironstones do not correspond to the end of a regression/beginning of a transgression or the stillstand as do the majority of Phanerozoic Ironstones, but instead occur well within the transgression at high stands of sea level. It has been suggested that the transgression was reworking into the marine environment lateritic weathering material formed by the exposure of land during the previous regression (Young 1989b).

McKerrow (1979), Fortey (1984) and Fortey & Cocks (1986) have shown the Upper Arenig (hirundo Biozone) and Llandeilo (teretiusculus Biozone) to be times of major eustatic regression. The Upper Arenig ironstones in North Wales all coincide with the hirundo regression or the initial phase of the subsequent transgression. The majority of the Mid-Ordovician ironstones likewise coincide with the teretiusculus regression or gracilis transgression. However, the Bryn Poeth (Upper Llanvirn) and Tremadog (basal Caradoc) ironstones, forming at high sea level, indicate that eustatic changes alone do not account for the formation and distribution of the North Wales Ironstones.

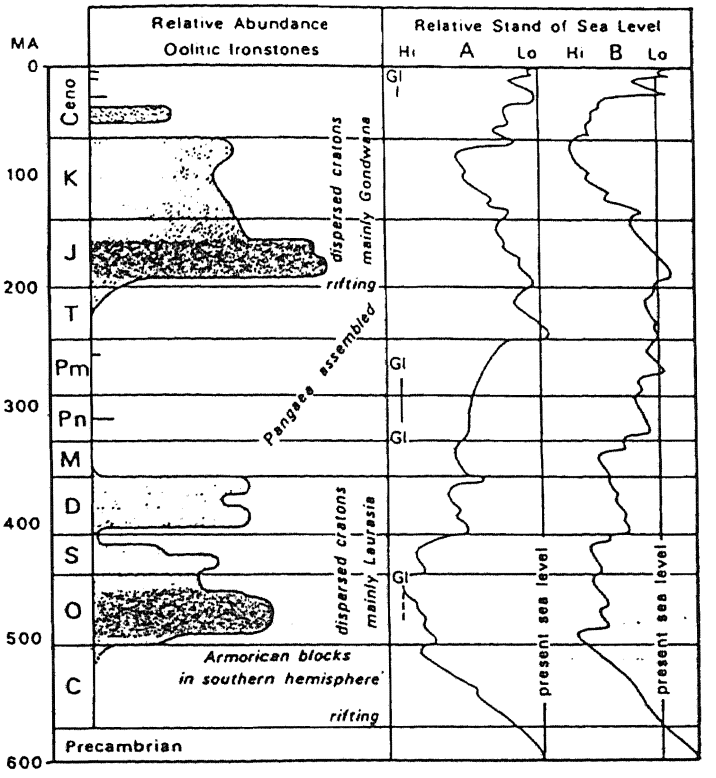

Figure 6.3 Phanerozoic record of berthieroid/iron oxide oolitic ironstones, with estimated sea level curves, Gl - widespread glaciation (after Van Houten 1985).

6.3.3 Tectonic Controls

It has been proposed that Phanerozoic Oolitic Ironstones occur in three different basin frameworks (Van Houten & Bhattacharyya 1982):

1) Along cratonic margins at times of divergence or initial convergence of lithospheric plates. Many of this type were later deformed by orogeny (eg Garzanti *et al.* 1989).

2) Intracratonic basins generally dominated by prolonged stability. The widespread middle and late Mesozoic ironstones of northwest Europe were deposited in a complex intracratonic setting in the northwest transgression of Tethys across faulted Caledonian & Variscan terranes.

3) Foredeeps along the interior side of mobile belts at times of diminished deformation and curtailed detrital influx.

The third setting for ironstones is rare in comparison to the other two settings (Figure 6.4).

The distribution of Phanerozoic Ironstones through time reflect a change in basin framework (Van Houten & Bhattacharyya 1982). Palaeozoic ironstones predominantly formed on the cratonic margins of drifting blocks of Laurasia & Gondwana in the southern hemisphere, whereas Mesozoic ironstones formed on intracratonic flooded blocks of Laurasia and Gondwana in the northern hemisphere (Figure 6.5).

Despite these different settings both were characterized by broad shelves and general tectonic stability or subdued orogeny (Van Houten 1985) and landmasses with low relief flooded by shallow epeirogenic seas, which therefore had a high potential for the formation of extended shallow bays and lagoonal environments needed for the formation of ironstones (Bayer 1989). This indicates that different tectonic settings still give the same local controls of ironstone formation.

The most likely source for the North Wales Ironstones was the emergence of the Irish Sea Landmass (George 1963) to the northwest of the North Wales Basin, which is also coincident with the occurrence of a widespread hiatus throughout Southern Ireland during the Llandeilo (Williams *et al.* 1972; Bruck *et al.* 1979). This is substantiated by the feebly oolitic ferrified grits of Anglesey which form part of the basal beds of the *gracilis* transgression over rocks of Monian,

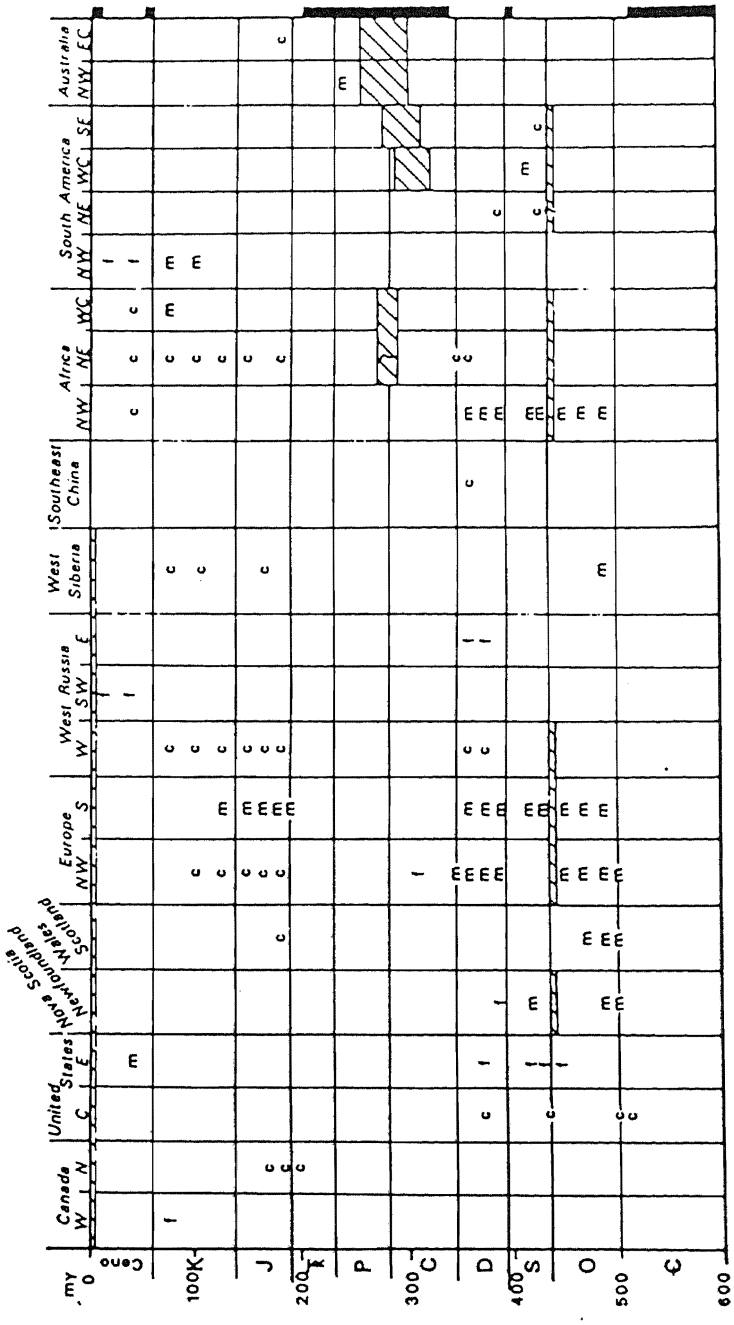

Figure 6.4 Geographic distribution of Phanerozoic Oolitic Ironstones on cratonic masses: c - intracratonic basin, f - foredeep, m - cratonic margin (after Van Houten & Bhattacharyya 1982). Unfavourable episodes and intervals - thick line along the right side of the chart. Diagonal pattern - continental glaciation.

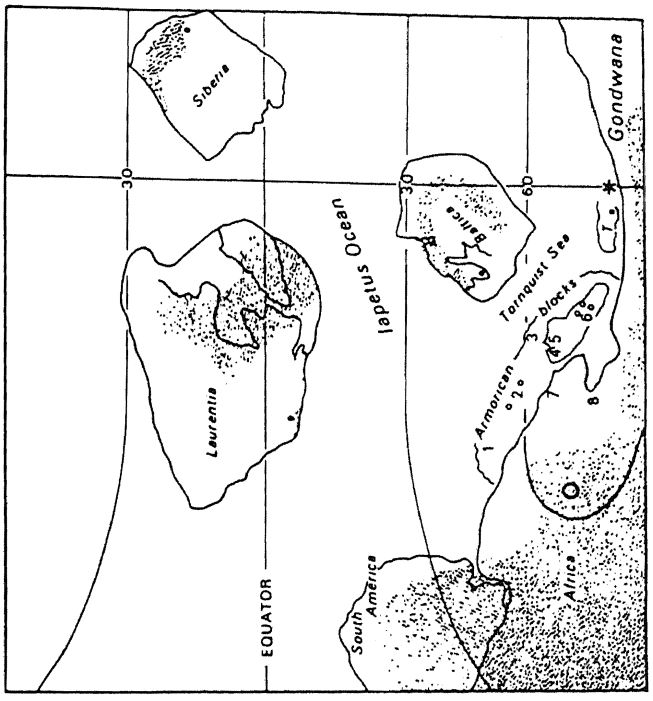

a) Ordovician

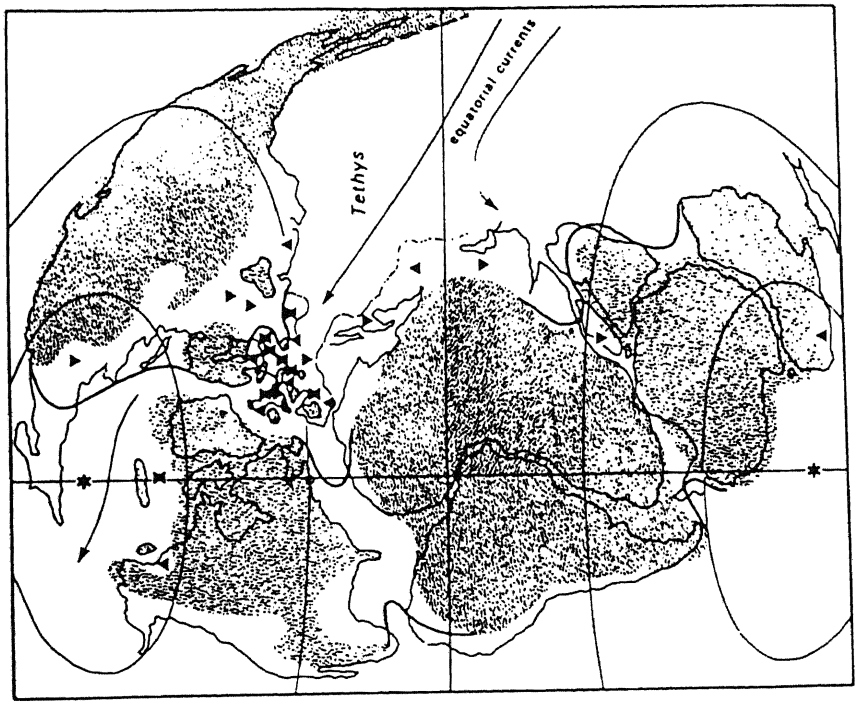

b) Jurassic

Figure 6.5 Distribution of Early to early Late Jurassic (b) and Early to early Late Ordovician (a) oolitic ironstones on palaeocontinental reconstructions (after Van Houten 1985). b) Jurassic - shorelines border patterned landmasses except where modified with thick lines for early Jurassic positions. Asterisks - poles; upright triangles Early Jurassic ironstones; hourglasses - Early and Middle Jurassic ironstones; inverted triangles - Middle Jurassic only. a) Ordovician - pattern indicates land areas; asterisk Middle Ordovician south pole; large circle - south pole at end of Ordovician; numbers - ironstones on Armorica and Gondwana; dots ironstones on other landmasses.

Cambrian and Ordovician age. The probable metamorphic nature of the adjacent landmass is indicated by the deformed quartz and feldspar grains in the Bryn Poeth ironstone and deformed quartz grains in other Anglesey and Llŷn ironstones.

A major paradox for this source for the ironstones is that the Irish Sea Landmass (Mona Terrane), a suspect terrane accreted onto the Welsh Basin at the start of the Cambrian (Gibbons & Gayer 1985), is now only a thin strip between the Welsh Basin and the Leinster-Lake District Basin. It is unlikely that this could have supported lateritic weathering on a large enough scale to supply the material for ironstone formation, or even as a major source of sediments in the Welsh Basin (Kokelaar et al. 1984; George 1963). However, strike slip faulting has recently been recognized as a major process in the Southern Caledonides (Gibbons & Gayer 1985; Woodcock 1984) and so the possibility of a terrane now removed by strike slip faulting cannot be ruled out, especially as major displacements of Ordovician or even later age through or northwest of Anglesey cannot be discounted (Fitches & Woodcock 1987).

6.4 SUMMARY AND SUGGESTIONS FOR FURTHER WORK

This comparison of the North Wales Ironstones to other Phanerozoic Oolitic Ironstones has highlighted a number of significant features, which are summarized below. One of the most significant questions raised by the North Wales Ironstones is the role of microbiota/organic matter in the formation of Phanerozoic Ironstones. The initial effect of algae/bacteria was to trap iron-rich sediment on sediment starved offshore shoals, sometimes forming algal stromatolites (hardgrounds). Once the sediment had been stabilised it allowed for the formation of ferruginous allochems and reduction of iron to form berthierine. The role of microbiota/organic matter on ooid formation was indirect, although the formation of oncoids and stromatolites was a direct result of microbial activity.

The significance of the North Wales Ironstones to the North Wales Basin is that they provide sedimentological information during a period when the sedimentary sequence was predominantly fine-grained. The ironstones demonstrate that synsedimentary faulting, which was a major control of volcanism and sedimentation in the North Wales Basin, was active during this period and was one of the main controls on the distribution and formation of the ironstones. The ironstones also give further information of the status of the Irish Sea Landmass to sedimentation. It must have been an extensive low-lying metamorphic terrane undergoing some form of lateritic weathering at least throughout the Lower and Middle Ordovician. However, a major eustatic regression further exposed land for deep chemical weathering to form the source of the ironstones.

A comparison of the depositional model of the North Wales Ironstones with a proposed facies model for Phanerozoic marine berthieroid/iron oxide oolitic ironstone has made further enlightenment on the controls of deposition of ironstones. The facies model advocates their deposition in a deltaic/nearshore/lagoonal environment. The North Wales Ironstones indicate a basic similarity to the facies model: a shoaling up sequence capped by an ironstone, formed from lateritic weathering material, secondary accumulations in cross-bedded oolites. However, the differences between the two indicate that more than one sedimentary setting can produce the factors necessary for the formation of ironstones.

This thesis has covered all aspects of the North Wales Ironstones. With this background suggestions for further work on the North Wales

Ironstones can be suggested. The role of microbiota within the ironstones has shown to be highly significant; this role could be studied further for both the North Wales Ironstones and other Phanerozoic Oolitic Ironstones. A detailed BSEI study of the ironstone textures (after Kearlsey 1989), would give much further information on sedimentary and diagenetic micro-textures. A study of the major, trace and REE geochemistry of other Phanerozoic Oolitic Ironstones would bring out the significance of the North Wales Ironstones geochemistry. In particular the REE content of ironstones would indicate similar fractionation processes forming the source of ironstones. Finally, the use of stable isotopes of the diagenetic phases in the ironstones, for example C^{13} of siderite, would give much further information on the source and processes of diagenesis.

REFERENCES

AIPEA 1980. Summary of the recommendations of AIPEA nomenclature committee. Clays & Clay Minerals, 28, 73-78.

Allen,P.M. Cooper,D.C. Fuge,R. & Rea,W.J. 1976. Geochemistry and relationships to mineralization of some igneous rocks from the Harlech Dome, Wales. Transactions of the Institute of Mining and Metallurgy, 85, Section B, B100-B108.

Altschuler,Z.S. 1980. The geochemistry of trace elements in marine phosphorites Part 1. Characteristic abundances and enrichment. Society of Economic Palaeontologists and Mineralogists, Special Publication No. 29, 19-30.

Archer,A.A. 1959. The distribution of non-ferrous ores in the Lower Palaeozoic rocks of North Wales. in: Future of Non-Ferrous Mining in Great Britain, Institute of Mining and Metallurgy, 259-276.

Baker,J.H. 1985. Greenalite, Mg-rich minnesotaite and stilpnomelane from the Osjoberg and Sirsjoberg iron-ore mines, Hjulso, W. Bergslagen, Sweden. Mineralogical Magazine, 49, 611-613.

Ball,T.K. & Bland,D.J. 1985. The Cae Coch volcanogenic massive sulphide deposit, Trefriw, North Wales. Journal of the Geological Society of London, 142, 889-898.

Bates,D.E.B. 1969. Some aspects of the Arenig faunas of Wales. in Wood,A. (ed) Precambrian and Lower Palaeozoic Rocks of Wales. University of Wales Press, Cardiff, 155-159.

Bates,D.E.B. 1972. The stratigraphy of the Ordovician rocks of Anglesey. Geological Journal, 8, 29-58.

Bates,D.E.B. 1974. The structure of the Lower Palaeozoic rocks of Anglesey, with special reference to faulting. Geological Journal, 9, 39-60.

Bates,D.E.B. & Davies,J.R. 1981. Geologists Association Excursion Guide No.40, Anglesey.

Bathurst,R.G.C. 1975. Carbonate sediments and their diagenesis. Developments in Sedimentology, 12, Elsevier, Amsterdam.

Bayer,U. (in press). Stratigraphic and environmental patterns of ironstone deposits. in: Young,T.P. & Taylor,W.E.G. (eds) Phanerozoic Ironstones. Special Publication of the Geological Society of London,

Beckley,A.J. 1986. The Arenig series in North Wales. Unpublished Ph.D. Thesis, University of London.

Beckley,A.J. 1987. Basin development in North Wales during the Arenig. Geological Journal Thematic Issue, 22, 19-30.

Bennett,M.A. 1987. Genesis and diagenesis of the Cambrian manganese deposits, Harlech, North Wales. Geological Journal Thematic Issue, 22, 7-18.

Berner,R.A. 1971. Principles of Chemical Sedimentology. McGraw Hill, New York.

Berner,R.A. 1980. Early Diagenesis - a Theoretical Approach. Princeton University Press.

Berner,R.A. 1981. A new geochemical classification of sedimentary environments. Journal of Sedimentary Geology, 51, 359-365.

Bevins,R.E. Kokelaar,B.P. & Dunkley,P.N. 1984. Petrology and geochemistry of Lower to Middle Ordovician igneous rocks in Wales: a volcanic arc to marginal basin transition. Proceedings of the Geologists Association, 95, 337-347.

Bevins,R.E. & Robinson,D. 1988. Low grade metamorphism of the Welsh Basin Lower Palaeozoic succession: an example of diastathermal metamorphism? Journal of the Geological Society, 145, 363-366.

Bevins,R.E. & Rowbotham,G. 1983. Low-grade metamorphism within the Welsh sector of the Paratectonic Caledonides. Geological Journal, 18, 141-167.

Bhattacharyya,D.P. 1983. Origin of berthierines in ironstones. Clays and Clay Minerals, 31, 173-182.

Bhattacharyya,D.P. 1986. Geochemistry of the Phanerozoic oolitic ironstones - genetic implications (abstract). American Association of Petroleum Geologists Bulletin, 70, 562.

Bhattacharyya,D.P. (in press). Concentrated and lean oolites: examples from the Nubia Formation at Aswan, Egypt, and the significance of oolite types in ironstone genesis. in: Young,T.P. & Taylor,W.E.G. (eds) Phanerozoic Ironstones. Special Publication of the Geological Society of London,

Bhattacharyya,D.P. & Kakimoto,P.K. 1982. Origin of ferriferous ooids: an SEM study of ironstone ooids and bauxite pisoids. Journal of Sedimentary Petrology, 52, 849-857.

Blenkinsop,T.G. Long,R.E. Kuznir,N.J. & Smith,M.J. 1986. Seismicity and tectonics in Wales. Journal of the Geological Society London, 143, 327-334.

Bottrell,S.H. Shepherd,T.J. Yardley,B.W.D. & Dubessy,J. 1988. A fluid inclusion model for the genesis of the ores of the Dolgellau Gold Belt, North Wales. Journal of the Geological Society of London, 145, 139-145.

Boucot,A.J. & Gray,J. 1986. Comment and reply on "Oolitic ironstones and contrasting Ordovician and Jurassic palaeogeography". Geology, 14, 634-635.

Boynton,W.V. 1984. Cosmochemistry of the Rare Earth Elements: meteorite studies. in Henderson,P. (ed) Rare Earth Element Geochemistry, Developments in Geochemistry, 2, Elsevier, Amsterdam, 63-114.

Bradshaw,M.J. James,S.S. & Turner,P. 1980. Origin of oolitic ironstones - Discussion and reply. Journal of Sedimentary Petrology, 50, 295-302.

Brindley,G.W. 1982. Chemical compositions of berthierines - a review. Clays and Clay Minerals, 30, 153-155.

Brindley,G.W. & Brown,G. 1980. Crystal structures of clay minerals and their x-ray identification. Mineralogical Society Monograph No.5.

Brindley,G.W. & Youell,R.F. 1953. Ferrous chamosite and ferric chamosite. Mineralogical Magazine, 30, 57-70.

British Geological Survey 1985a. 1:25,000, Passes of Nant Ffrancon and Llanberis, Parts of Sheets SH65 and SH66.

British Geological Survey 1985b. 1:50,000 sheet, Bangor, 106.

Bromley,A.V. 1963. The geology of the Blaenau Ffestiniog area, Merionethshire. Unpublished Ph.D. Thesis, University of Wales.

Bromley,A.V. 1969. Acid plutonic igneous activity in the Ordovician of North Wales. in Wood,A. (ed.) Precambrian and Lower Palaeozoic Rocks of Wales. University of Wales Press, Cardiff, 305-335.

Bruck,P.M. Colthurst,J.R.J. Feely,M. Gardiner,P.R.R. Penney,S.R. Reeves,T.J. Shannon,P.M. Smith,D.G. Vanguestaine,M. 1979. South East Ireland: Lower Palaeozoic stratigraphy and depositional history. in Harris,A.L. Holland,C.H. & Leake,B.E. (eds) The Caledonides of the British Isles-reviewed. Special Publication of the Geological Society of London, 8, Scottish Academic Press, 533-544.

Bubenicek,L. 1983. Diagenesis in iron-rich rocks. in Larsen,G. & Chilingar,G.V.(eds.) Diagenesis in Sediments and Sedimentary Rocks (2). Developments in Sedimentology, 25B, Elsevier, 495-551.

Burley,S.D. Kantorowicz,J.D. & Waugh,D. 1985. Clastic Diagenesis. in: Brenchley,P.J. & Williams,B.P.J. (eds) Sedimentology: Recent Developments and Applied Aspects. The Geological Society, Blackwells, 189-226.

Campbell,S.D.G. Howells,M.F. Smith,M. & Reedman,A.J. 1988. A Caradoc failed-rift within the Ordovician marginal basin of Wales. Geological Magazine, 125, 257-266.

Campbell,S.D.G. Reedman,A.J. & Howells,M.F. 1985. Regional variations in cleavage and fold development in North Wales. Geological Journal, 20, 43-52.

Carroll,D. 1958. Role of clay minerals in the transportation of iron. Geochimica et Cosmochimica Acta, 14, 1-27.

Cattermole,P.J. & Jones,A. 1970. The geology of the area around Mynydd Mawr, Nantle, Caernarvonshire. Geological Journal, 7, 111-128.

Cattermole,P.J. & Romano,M. 1981. Geologists Association Excursion Guide No.39, Lleyn Peninsula.

Cave,R. 1965. The Nod Glas sediments of Caradoc age in North Wales. Geological Journal, 4, 279-298.

Chauvel,J.J. 1974. Les minerais de fer de L'Ordovicien Inferieur du Bassin de Bretagne-Anjou, France. Sedimentology, 21, 127-147.

Chauvel,J.J. & Guerrak,S. (in press). Oolitization processes in Palaeozoic ironstones from France, Algeria and Libya. in: Young,T.P. & Taylor,W.E.G. (eds) Phanerozoic Ironstones. Special Publication of the Geological Society of London,

Chowns,T.M. & Maynard,J.B. 1986. Petrology of Lower Jurassic chamosite - siderite ironstones from northeast England (abstract). American Association of Petroleum Geologists Bulletin, 70, 573.

Clark,A.M. 1984. Mineralogy of the Rare Earth Elemnts. in Henderson,P. (ed.) Rare Earth Element Geochemistry, Developments in Geochemistry, 2, Elsevier, Amsterdam, 33-61.

Clemmey,H. 1985. Sedimentary Ore Deposits. in Brenchley,P.J. & Williams, B.P.J. (eds) Sedimentology: recent developments and applied aspects. The Geological Society, Blackwells, 229-247.

Cocks,L.R.M. & Fortey,R.A. 1982. Faunal evidence for oceanic separations in the Palaeozoic of Britain. Journal of the Geological Society, 139, 465-478.

Coward,M.P. & Siddans,A.W.B. 1979. The tectonic evolution of the Welsh Caledonides. in Harris,A.L. Holland,C.H. & Leake,B.E. (eds) The Caledonides of the British Isles-reviewed. Special Publication of the Geological Society of London, 8, Scottish Academic Press, 187-198.

Cox,A.H. 1925. The geology of the Cader Idris range (Merioneth). Quarterly Journal of the Geological Society, 81, 539-592.

Cox,A.H. & Wells,A.K. 1927. The geology of the Dolgelley district, Merionethshire. Proceedings of the Geologists Association, 38, 265-318.

Crimes,T.P. 1969. The stratigraphy, structure and sedimentology of some of the Pre-Cambrian and Cambro-Ordovician rocks bordering the Southern Irish Sea. Unpublished Ph.D. Thesis, University of Liverpool.

Crimes,T.P. 1970. A facies analysis of the Arenig of Western Lleyn, N. Wales. Proceedings of the Geologists Association, 81, 221-239.

Curtis,C.D. 1983. Link between aluminium mobility and destruction of secondary porosity. American Association of Petroleum Geology Bulletin, 67, 380-384.

Curtis,C.D. 1985. Clay mineral precipitation and transformation during burial diagenesis. Philosophical Transactions of the Royal Society of London, A, 315, 91-105.

Curtis,C.D. & Coleman,M.L. 1986. Controls of the precipitation of early diagenetic calcite, dolomite and siderite concretions in complex depositional sequences. in Gautier,D.L. (ed.) Roles of Organic Matter in Sediment Diagenesis, Special Publication of the Society of Economic Palaeontologists and Mineralogists, Tulsa, Oklahoma, 38, 23-33.

Curtis,C.D. Hughes,C.R. Whiteman,J.A. & Whittle,C.K. 1985. Compositional variation within some sedimentary chlorites, and some comments on their origin. Mineralogical Magazine, 49, 375-386.

Curtis,C.D. Pearson,M.J. & Somogyi,V.A. 1975. Mineralogy, chemistry and origin of a concretionary siderite sheet (clay-ironstone band) in the Westphalian of Yorkshire. Mineralogical Magazine, 40, 385-393.

Curtis,C.D. & Spears,D.A. 1968. The formation of sedimentary iron minerals. Economic Geology, 63, 257-270.

Dahanayake,K. 1977. Classification of oncoids from the U. Jurassic carbonates of the French Jura. Sedimentary Geology, 18, 337-353.

Dahanayake,K. & Krumbein,W.E. 1986. Microbial structures in oolitic iron formations. Mineralium Deposita, 21, 85-94.

Davidson,C.F. 1961. Oolitic ironstones of freshwater origin. Mining Magazine, 104, 158-159.

Davies,R.A. 1969. Geological succession and structure of Cambrian and Ordovician rocks in the N.Eastern Carneddau. Unpublished Ph.D. Thesis, University of Wales.

Davies,R.G. 1956. The Pen y Gader dolerite and it's metasomatic effect on the Llyn y Gader sediments. Geological Magazine, 93, 153-172.

Deans,T. 1938. Francolite from sedimentary ironstones of the coal measures. Mineralogical Magazine, 25, 135-139.

Deer,W.A. Howie,R.A. & Zussman,J. 1962a. Rock Forming Minerals, Vol.1 Ortho- and Ring Silicates. Longmans London.

Deer,W.A. Howie,R.A. & Zussman,J. 1962b. Rock Forming Minerals, Vol.3 Sheet Silicates. Longmans London.

Deer,W.A. Howie,R.A. & Zussman,J. 1962c. Rock Forming Minerals, Vol.5 Non-Silicates. Longmans London.

Dexter-Dyer,B. Kretzschmer,M. & Krumbein,W.E. 1984. Possible microbial pathways in the formation of Precambrian ore deposits. Journal of the Geological Society of London, 141, 251-262.

Dimroth,E. 1975. Palaeo-environment of iron-rich sedimentary rocks. Geologische Rundschau, 64, 751-767.

Dimroth,E. 1977. Facies models 6: Diagenetic facies of iron formation. Geoscience Canada, 4, 83-88.

Dreesan,R. (in press). Oolitic ironstones as event-stratigraphical marker beds within the Upper Devonian of the Ardenno-Rhenish Massif. in: Young,T.P. & Taylor,W.E.G. (eds) Phanerozoic Ironstones. Special Publication of the Geological Society of London,

Dunham,K.C. Beer,K.E. Ellis,R.A. Gallagher,M.J. Nutt,M.J.C. & Webb,B.C. 1978. United Kingdom. in Bowie,S.H.U. Kvalheim,A. & Haslam,H.W. (eds). Mineral Deposits of Europe, Volume 1 Northwest Europe, The Institute of Mining and Metallurgy and the Mineralogical Society, London, 263-317.

Dunham,R.J. 1962. Classification of carbonate rocks according to depositional texture. in Ham,W.E. (ed.) Classification of Carbonate Rocks. American Association of Petroleum Geologists, Tulsa, Oklahoma, 108-121.

Dunkley,P.N. 1978. The geology of the South-Western part of the Aran range, Merionethshire - with particular reference to igneous history. Unpublished Ph.D. Thesis, University of Wales.

Eggleton,R.A. 1972. The crystal structure of stilpnomelane. Part II. The full cell. Mineralogical Magazine, 38, 693-711.

Embry,A.F. & Klovan,J.E. 1971. A late Devonian reef tract on northeastern Banks Island Northwest Territories. Bulletin of Canadian Petroleum Geology, 19, 730-781.

Evans,C.D.R. 1968. Geological succession and structure of the area east of Bethesda. Unpublished Ph.D. Thesis, University of Wales.

Fairbridge,R.W. 1983. Syndiagenesis-Anadiagenesis-Epidiagenesis: phases in lithogenesis. in Larsen,G. & Chilingar,G.V.(eds.) Diagenesis in Sediments and Sedimentary Rocks (2). Developments i Sedimentology, 25B, Elsevier, 17- .

Fearnsides,W.G. 1910. The Tremadoc slates and associated beds of south east Carnarvonshire. Quarterly Journal of the Geological Society, 66, 142-188.

Fitches,W.R. & Campbell,S.D.G. 1987. Tectonic evolution of the Bala Lineament in the Welsh Basin. Geological Journal Thematic Issue, 22, 131-153.

Fitches,W.R. & Woodcock,N.H. 1987. Sedimentation and tectonics in the Welsh Basin: introduction. Geological Journal Thematic Issue, 22, 1-5.

Fleet,A.J. 1984. Aqueous and sedimentary geochemistry of the rare earth elements. in Henderson,P. (ed) Rare Earth Element Geochemistry, Developments in Geochemistry 2, Elsevier, Amsterdam, 343-373.

Fortey,R.A. 1984. Global earlier Ordovician transgressions and regressions and their biological implications. in: Bruton,D.L. (ed). Aspects of the Ordovician System. Palaeontological Contributions from the University of Oslo, 295, Universitets-forlaget, 37-50.

Fortey,R.A. & Cocks,L.R.M. 1986. Marginal faunal belts and their structural implications, with examples from the Lower Palaeozoic. Journal of the Geological Society of London, 143, 151-160.

Foster-Smith,J.R. 1977a. The mines of Anglesey and Caernarvonshire. British Mining No.4.

Foster-Smith,J.R. 1977b. The mines of Merioneth. British Mining No.6.

Frankel,R.B. & Blakemore,R.P. 1984. Precipitation of Fe3O4 in magnetotactic bacteria. Philosophical Transactions of the Royal Society London, B, 304, 567-574.

Fryer,B.J. 1983. Rare Earth Elements in Iron-Formations. in Trendall,A.F. & Morris,R.C. (eds). Iron-Formation: Facts and Problems. Developments in Precambrian Geology No.6, Elsevier, Amsterdam, 345-358.

Garzanti,E. Haas,R. & Jadoul,F. (in press). Ironstones in the Mesozoic passive margin sequence of the Tethys Himalaya: sedimentology and metamorphism (Zanskar, Northern India). in: Young,T.P. & Taylor,W.E.G. (eds) Phanerozoic Ironstones. Special Publication of the Geological Society of London,

Gatrall,M. Jenkyns,H.C. & Parsons,C.F. 1972. Limonitic concretions from the European Jurassic, with particular reference to the "Snuff-Boxes" of Southern England. Sedimentology, 18, 79-103.

Gehring,A.U. 1985. A microchemical study of iron ooids. Eclogae Geologica Helvetica, 78, 451-457.

Gehring,A.U. 1986. Mikroorganismen in kondensierten Schichten der Dogger/Malm-Wende im Jura der Nordostschweiz. Eclogae Geologica Helvetica, 79, 13-18.

Gehring,A.U. (in press). The formation of goethitic ooids in condensed Jurassic deposits in Northern Switzerland. in: Young,T.P. & Taylor,W.E.G. (eds) Phanerozoic Ironstones. Special Publication of the Geological Society of London,

George,T.N. 1963. Palaeozoic growth of the British Caledonides. in: Johnson,M.R.W. & Stewart,F.H. (eds) The British Caledonides, Oliver & Boyd, Edinburgh, 1-33.

Gibbons,W. 1987. Menai Strait fault system: an early Caledonian terrane boundary in North Wales. Geology, 15, 744-747.

Gibbons,W. & Gayer,R.A. 1985. British Caledonian terranes. in Gayer,R.A. The Tectonic Evolution of the Caledonide - Appalachian Orogen. Freidr. Vieweg & Son, Braunschweig., 3-16.

Greenland,D.J. 1975. Charge characteristics of kaolinite-iron hydroxide complexes. Clay Minerals, 10, 407-416.

Greenly,E. 1919. The Geology of Anglesey. Memoirs of the Geological Survey of Great Britain, Vol.2.

Greenly,E. 1944. The Ordovician rocks of Arron. Quarterly Journal of the Geological Society, 100, 75-83.

Gromet,L.P. Dymek,R.F. Haskin,L.A. & Koroter,R.L. 1984. The "North American Shale Composite": its compilation, major and trace element characteristics. Geochimica et Cosmochimica Acta, 48, 2469-2482.

Gross,G.A. 1970. Nature and occurence of iron ore deposits. Survey of World Iron Ore Resources, United Nations, New York, 13-31.

Groves,A.W. 1952. Wartime investigations into the haematite and manganese ore resources of Great Britain and Northern Ireland. Permanent Records of Research and Development Ministry of Supply, Report No. 20.703.

Guerrak,S. & Chauvel,J.J. 1985. Les mineralisations ferriferes du Sahara Algerien: Le gisement de fer oolithique de mecheri Abdelaziz (basin de Tindouf). Mineralium Deposita, 20, 249-259.

Gulbrandsen,R.A. 1970. Relation of carbon dioxide content of apatite of the Phosphoria Formation to regional facies. United States Geological Survey Professional Paper, 700-B, B9-B13.

Gygi,R.A. 1981. Oolitic iron formations: marine or not marine? Eclogae Geologica Helvetica, 74/1, 233-254.

Hallam,A. 1975. Jurassic environments. Cambridge University Press, Cambridge.

Hallam,A. & Bradshaw,M.J. 1979. Bituminous shales and oolitic ironstones as indicators of transgressions and regressions. Journal of the Geological Society of London, 136, 157-164.

Hallam,A. & Maynard,J.B. 1987. The iron ores and associated sediments of the Chichali Formation (Oxfordian to Valanginian) of the Trans-Indus salt range, Pakistan. Journal of the Geological Society of London, 144, 107-114.

Halley,R.B. Harris,P.M. & Hine,A.C. 1983. Bank Margin Environment. in Schoelle,P.A. Bebout,D.G. & Moore,C.H. (eds). Carbonate Depositional Environments, American Association of Petroleum Geologists Memoir, 33, 463-506.

Hallimond,A.F. 1924. On stilpnomelane from North Wales. Mineralogical Magazine, 20, 193-197.

Hallimond,A.F. 1925. Iron Ores: Bedded ores of England and Wales. Petrography and Chemistry. Memoirs of the Geological Survey, Special Reports on the Mineral Resources of Great Britain, 24.

Hallimond,A.F. 1951. Problems of the sedimentary iron ores. Proceedings of the Yorkshire Geological Society, 28, 61-66.

Hangari,K.M. Ahmad,J.N. & Perry,E.C. 1980. Carbon and oxygen isotope ratios in diagenetic siderite and magnetite from U.Devonian ironstone, Wadi Shatti district, Libya. Economic Geology, 75, 538-545.

Harder,H. 1978. Synthesis of iron layer silicate minerals under natural conditions. Clays and Clay Minerals, 26, 65-72.

Harder,H. (in press). Mineral formation via hydroxide gels for understanding sedimentary ironstone genesis. in: Young,T.P. & Taylor,W.E.G. (eds) Phanerozoic Ironstones. Special Publication of the Geological Society of London,

Haskin,L.A. Haskin,M.A. Frey,F.A. & Widdeman,T.R. 1968. Relative and absolute terrestrial abundances of the rare earths. in Ahrens,L.H. (ed) Origin and Distribution of the Elements,1. Pergamon Press, Oxford, 889-911.

Hayes,A.O. 1915. The Wabana Iron Ore of Newfoundland. Government Printing Bureau, Ottowa.

Hayes,J.B. 1970. Polytypism of chlorite in sedimentary rocks. Clays and Clay Minerals, 18, 285-306.

Heley,T.P. 1980. Application of statistical analysis to the Slieve Gamph granitic pluton, Ireland. Unpublished M.Phil. thesis (CNAA), Luton College of Higher Education.

Hofmann,H.J. 1975. Bolopora, not a Bryozoan, but an Ordovician phosphatic, oncolitic concretion. Geological Magazine, 112, 523-526.

Howard,A.S. 1985. Lithostratigraphy of the Staithes Sandstone and Cleveland Ironstone Formations (Lower Jurassic) of north east Yorkshire. Proceedings of the Yorkshire Geological Society, 45, 261-275.

Howells,M.F. Reedman,A.J. & Leveridge,B.E. 1985. Geology of the country around Bangor. Explanation of the 1:50,000 sheet, British Geological Survey, sheet 106, England and Wales, HMSO, London.

Hughes,C.R. (in press). The application of analytical transmission electron microscopy in the study of oolitic ironstones: a preliminary study. in: Young,T.P. & Taylor,W.E.G. (eds) Phanerozoic Ironstones. Special Publication of the Geological Society of London,

Hutton,D.H.W. 1987. Strike-slip terranes and a model for the evolution of the British and Irish Caledonides. Geological Magazine, 124, 405-425.

Iijima,A.S. & Matsumoto,R. 1982. Berthierine and chamosite in coal measures of Japan. Clays and Clay Minerals, 30, 264-274.

Isaac,K.P. 1983. Tertiary lateritic weathering in Devon, England, and the Palaeogene continental environment of south west England. Proceedings of the Geologists Association, 94, 105-114.

James,H.E. & Van Houten,F.B. 1979. Miocene goethitic and chamositic oolites, Northeastern Columbia. Sedimentology, 26, 125-133.

James,H.L. 1966. Chemistry of the iron-rich sedimentary rocks. Geological Survey Professional Paper, 440-W.

Jarvis,I. 1980. Geochemistry of phosphatic chalks and hardgrounds from the Santonian to early Campanian (Cretaceous) of Northern France. Journal of the Geological Society of London, 137, 705-721.

Jarvis,I & Jarvis,K.E. 1985. Rare-earth element geochemistry of standard sediments: a study using inductively coupled plasma spectrometry. Chemical Geology, 53, 335-344.

Jones,B. 1933. Geology of the Fairborne-Llwyngwril district Merioneth. Quarterly Journal of the Geological Society, 89, 145-171.

Jones,B. 1988. Biostatistics in Palaeontology. Geoscience Canada, 15, 3-22.

Kandiah,K. Smith,A.J. & White,G. 1975. A pulse processor for X-ray spectrometry with Si(Li) detectors. Paper 2.9 in 2nd ISPRA Nuclear Electronics Symposium, Stressa, Italy.

Kearsley,A.J. (in press). Iron-rich ooids, their mineralogy and microfabric: clues to their origin and evolution. in: Young,T.P. & Taylor,W.E.G. (eds) Phanerozoic Ironstones. Special Publication of the Geological Society of London,

Kidder,D.L. 1985. Petrology and origin of phosphate nodules from the midcontinent Pennsylvanian epicontinental sea. Journal of Sedimentary Petrology, 55, 809-816.

Kimberley,M.M. 1978. Palaeoenvironmental classification of iron formations. Economic Geology, 73, 215-229.

Kimberley,M.M. 1979. Origin of oolitic iron formations. Journal of Sedimentary Petrology, 49, 111-131.

Kimberley,M.M. 1983. Ferriferous Ooids. in Peryt,T.M. (ed) Coated Grains. Springer Verlag, 100-108.

Knox,R.W.O'B. & Fletcher,T.P. (in press). Genesis of a mixed silicate/hydroxide ironstone: the Frodingham Ironstone (Lower Jurassic) of eastern England. in: Young,T.P. & Taylor,W.E.G. (eds) Phanerozoic Ironstones. Special Publication of the Geological Society of London,

Kokelaar,B.P. 1979. Tremadoc to Llanvirn volcanism on the southeast side of the Harlech Dome (Rhobell Fawr), North Wales. in Harris,A.L. Holland,C.H. & Leake,B.E. (eds) The Caledonides of the British Isles-reviewed. Special Publication of the Geological Society of London, 8, Scottish Academic Press, 591-596.

Kokelaar,B.P. Howells,M.F. Bevins,R.E. Roach,R.A. & Dunkley,P.N. 1984. The Ordovician marginal basin of Wales. in Kokelaar,B.P. & Howells,M.F. (eds) Marginal Basin Geology: volcanic and associated sedimentary and tectonic processes in modern and ancient marginal basins. Special Publication of the Geological Society of London, 16, 245-269.

Krauskopf,K.B. 1979. Introduction to Geochemistry. McGraw Hill International Series in the Earth & Planetary Sciences.

Krom,M.D. & Berner,R.A. 1981. The diagenesis of phosphorus in a nearshore marine environment. Geochimica et Cosmochimica Acta, 45, 207-216.

Kronberg,B.I. Fyfe,W.S. Leonardos,O.H. & Santos,A.M. 1979. The chemistry of some Brazilian soils: element mobility during intensive weathering. Chemical Geology, 24, 211-229.

Leggett,J.K. 1980. British Lower Palaeozoic black shales and their palaeo-oceanographic significance. Journal of the Geological Society of London, 137, 139-156.

Leggett,J.K. McKerrow,W.S. Cocks,L.R.M. & Rickards,R.B. 1981. Periodicity in the early Palaeozoic realm. Journal of the Geological Society of London, 138, 167-176.

McClellan,G.H. 1980. Mineralogy of carbonate flourapatites. Journal of the Geological society of London, 137, 675-681.

McKerrow,W.S. 1979. Ordovician and Silurian changes in sea level. Journal of the Geological Society of London, 136, 137-145.

McKerrow,W.S. & Cocks,L.R.M. 1986. Oceans, island arcs and olistostromes: the use of fossils in distinguishing sutures, terranes and environments around the Iapetus Ocean. Journal of the Geological Society of London, 143, 185-191.

Marshall,J.F. 1983. Geochemistry of iron-rich sediments on the outer continental shelf of northern New South Wales. Marine Geology, 51, 163-175.

Martens,C.S. & Harriss,R.C. 1970. Inhibition of apatite precipitation in the marine environment by magnesium ions. Geochimica et Cosmochimica Acta, 34, 621-625.

Matsumoto,R. & Iijima,A.S. 1981. Origin and diagenetic evolution of Ca-Mg-Fe carbonates in some coalfields of Japan. Sedimentology, 28, 239-259.

Matthews,D.W. & Scoon,J.H. 1964. Notes on a new occurrence of stilpnomelane from North Wales. Mineralogical Magazine, 33, 1032-1037.

Maynard,J.B. 1983. Geochemistry of Sedimentary Ore Deposits. Springer Verlag, New York.

Maynard,J.B. 1986. Geochemistry of oolitic iron ores, an electron microprobe study. Economic Geology, 81, 1473-1483.

Mehra,O.P. & Jackson,M.L. 1958. Iron oxide removal from soils and clays by a dithionite-citrate system buffered with sodium bicarbonate. 7th National Conference on Clays and Clay Minerals, 317-327.

Merriman,J. & Roberts,B. 1985. A survey of white mica crystallinity and polytypes in pelitic rocks of Snowdonia and Llŷn, North Wales. Mineralogical Magazine, 49, 305-319.

Myers,K. (in press). Portable Gamma Ray Spectrometry - an important new tool in understanding the origin of the Cleveland Ironstone Formation of northeast Yorkshire. in: Young,T.P. & Taylor,W.E.G. (eds) Phanerozoic Ironstones. Special Publication of the Geological Society of London,

Nahon,D. Carozzi,A.V. Parron,C. 1980. Lateritic weathering as a mechanism for the generation of ferruginous ooids. Journal of Sedimentary Petrology, 50, 1287-1298.

Nair,A.M. & Mathai,T. 1981. Geochemical trends in some laterite profiles of North Kerala. in Laterization Process. Proceedings of the International Seminar on Laterization Processes, Trivandrum, India, 114-119.

Nealson,K.H. 1982. Microbial oxidation and reduction of iron. in Holland,H.D. & Schidlowski,M. Mineral Deposits and the Evolution of the Biosphere. Dahlum Konferenzen, Springer Verlag, 51-65.

Nicholas,T.C. 1915. Geology of the St. Tudwals peninsula. Quarterly Journal of the Geological Society, 71, 83-143.

Oertel,G. & Curtis,C.D. 1972. Clay-ironstone concretion preserving fabrics due to progressive compaction. Geological Society of America Bulletin, 83, 2597-2606.

Pohl,W. Amouri,M. Kolli,O. Scheffer,R. & Zachmann,D. 1986. A new genetic model for the North African metasomatic siderite deposits. Mineralium Deposita, 21, 228-233.

Pulfrey,W. 1933a. The iron ore oolites and pisolites of North Wales. Quarterly Journal of the Geological Society, 89, 401-430.

Pulfrey,W. 1933b. Note on the occurrence of sponge spicules associated with the iron-ores of North Wales. Annual Magazine of the Natural History Series 10, 9, 67-76.

Quade,H. 1976. Genetic problems and environmental features of volcano-sedimentary iron ore deposits of the Lahn-Dill type. in Wolf,K.H. (ed) Handbook of Stratabound and Stratiform Ore Deposits, Volume 7, Elsevier, 255-294.

Ratcliffe,K.T. 1988. Oncoids as environmental indicators in the Much Wenlock Limestone Formation of the English Midlands. Journal of the Geological Society of London, 145, 117-124.

Rawson,P.F. Greensmith,J.T. & Shalaby,S.E. 1983. Coarsening upward cycles in the uppermost Staithes and Cleveland Ironstone Formations (L.Jurassic) of the Yorkshire Coast, England. Proceedings of the Geologists Association, 94, 91-93.

Reedman,A.J. Colman,T.B. Campbell,S.D.G. & Howells,M.F. 1985. Volcanogenic mineralization related to the Snowdon Volcanic Group (Ordovician), Gwynedd, North Wales. Journal of the Geological Society of London, 142, 875-888.

Reedman,A.J. Leveridge,B.E. & Evans,R.B. 1984. The Arfon Group ('Arvonian') of North Wales. Proceedings of the Geologists Association, 95, 313-321.

Reedman,A.J. Webb,B.C. Addison,R. Lynas,B.D.T. Leveridge,B.E. & Howells,M.F. 1983. The Cambrian - Ordovician boundary between Aber and Betws Garmon, Gwynedd, North Wales. Report of the Institute of Geological Sciences, 83/1, 7-10.

Rice,R. Sharp,G.J. 1976. Copper mineralization in the Forest of Coed-y-Brenin, North Wales. Transactions of the Institute of Mining and Metallurgy, 85, Section B, B1-B13.

Richter,D.K. 1983a. Classification of coated grains: discussion. in Peryt,T.M. (ed) Coated Grains. Springer Verlag, New York, 7-8.

Richter,D.K. 1983b. Calcareous ooids: a Synopsis. in Peryt,T.M. (ed) Coated Grains. Springer Verlag, New York, 71-99.

Ridgway,J. 1976. Ordovician palaeogeography of the southern and eastern flanks of the Harlech Dome, Merionethshire, North Wales. Geological Journal, 11, 121-136.

Roberts,B. 1979. Geology of Snowdonia and Llŷn: an outline and field guide. Adam Hilger, Bristol.

Roberts,B. 1981. Low grade and very low grade regional metabasic Ordovician rocks of Llŷn and Snowdonia, Gwynedd, North Wales. Geological Magazine, 118, 189-200.

Roberts,B. Merriman,R.J. 1985. The distinction between Caledonian burial and regional metamorphism in metapelites from North Wales: an analysis of isocryst patterns. Journal of the Geological Society of London, 142, 615-624.

Robinson,D. & Bevins,R.E. 1986. Incipient metamorphism in the Lower Palaeozoic marginal basin of Wales. Journal of Metamorphic Geology, 4, 101-113.

Rohrlich,V. 1974. Microstucture and microchemistry of iron ooids. Mineralium Deposita, 9, 133-142.

Schiavon,N. 1988. Goethite ooids: growth mechanisms and sandwave transport in the Lower Greensand (early Cretaceous, southern England). Geological Magazine, 125, 57-62.

Schoen,R. 1964. Clay minerals of the Silurian Clinton ironstones, New York State. Journal of Sedimentary Petrology, 34, 855-863.

Sellwood,B.W. & Jenkyns,H.C. 1975. Basins and swells and the evolution of an epeiric sea (Pleinsbachian-Bajocian of Great Britain). Journal of the Geological Society of London, 131, 373-388.

Siehl,V.A. & Thein,J. 1978. Geochemische trends in der Minette (Jura, Luxembourg/Lothringen). Geologische Rundschau, 67, 1052-1077.

Siehl,V.A. & Thein,J. (in press). Minette-type ironstones. in: Young,T.P. & Taylor,W.E.G. (eds) Phanerozoic Ironstones. Special Publication of the Geological Society of London,

Slansky,M. 1986. Geology of Sedimentary Phosphates. North Oxford Academic Publishers.

Smith,M. 1987. The Tremadoc 'thrust' zone in southern Central Snowdonia. Geological Journal Thematic Issue, 22, 119-129.

Spears,D.A. (in press). Yorkshire ironstones revisited. in: Young,T.P. & Taylor,W.E.G. (eds) Phanerozoic Ironstones. Special Publication of the Geological Society of London,

Statham,P.J. 1976. A comparative study of techniques for quantitative analysis of the X-ray spectra obtained with a Si(Li) detector. X-ray Spectrometry, 5, 16-28.

Strahan,A. Gibson,W. Cantril,T.C. Sherlock,R.L. & Dewey,H. 1920. Pre Carboniferous and Carboniferous bedded ores of England and Wales. Memoirs Geological Survey - Special report on the mineral resources of Great Britain, Volume 13.

Sweatman,T.R. & Long,J.V.P. 1969. Quantitative electron-probe microanalysis of rock forming minerals. Journal of Petrology, 10, 332-374.

Swett,K. & Crowder,R.K. 1982. Primary phosphatic oolites from the Lower Cambrian of Spitsbergen. Journal of Sedimentary Petrology, 52, 587-593.

Taylor,J.H. 1949. Petrology of the Northampton Sand Ironstone Formation. Memoirs of the Geological Survey of Great Britain, HMSO, London.

Taylor,J.H. 1951. Sedimentation problems of the Northampton Sand Ironstone. Proceedings of the Yorkshire Geological Society, 28, 74-85.

Taylor,R.M. 1987. Non-silicate oxides and hydroxides. in Newman,A.C.D. (ed). Chemistry of Clays and Clay Minerals. Mineralogical Society Monograph, 6, Longmans, 129-201.

Taylor,S.R. & McLennan,S.M. 1985. The continental crust: its composition and evolution. Geoscience Texts Blackwells, Oxford.

Teyssen,T.A.L. 1984. Sedimentology of the Minette oolitic ironstones of Luxembourg and Lorraine: a Jurassic subtidal sandwave complex. Sedimentology, 31, 195-211.

Teyssen,T.A.L. (in press). A depositional model for the Liassic Minette ironstones (Luxembourg, France), in comparison with other Phanerozoic oolitic iron formations. in: Young,T.P. & Taylor,W.E.G. (eds) Phanerozoic Ironstones. Special Publication of the Geological Society of London,

Timofeeva,Z.V. & Balashov,Yu.A. 1972. The distribution of rare earth elements in oolitic iron ores of the Northern Causcus (in Russian). Litologia i Poleznic Isokopaemic, 3, 128-135.

Tremlett,W.E. 1962. The geology of the Nefyn-Llanaelhaiarn area of North Wales. Liverpool & Manchester Geological Journal, 3, 157-176.

Trythall,R.J.B. (in press). The Ordovician oolitic ironstones of North Wales: a field guide. in: Young,T.P. & Taylor,W.E.G. (eds) Phanerozoic Ironstones. Special Publication of the Geological Society of London,

Trythall,R.J.B. Eccles,C. Molyneux,S.G. & Taylor,W.E.G. 1987. Age and controls of ironstone deposition (Ordovician) North Wales. Geological Journal Thematic Issue, 22, 31-43.

Turbitt,T. Barker,E.J. Browitt,C.W.A. Howells,M. Marrow,P.C. Musson,R.M.W. Newmark,R.H. Redmayne,D.W. Walker,A.B. Jacob,A.W.B. Ryan,E. & Ward,V. 1985. The North Wales earthquake of 19 July 1984. Journal of the Geological Society of London, 142, 567-571.

Van Houten,F.B. 1985. Oolitic ironstones and contrasting Ordovician and Jurassic palaeogeography. Geology, 13, 722-724.

Van Houten,F.B. 1986. Search for Milankovitch patterns among oolitic ironstones. Palaeoceanography, 1, 459-466.

Van Houten,F.B. & Arthur,M.A. (in press). Temporal patterns among Phanerozoic oolitic ironstones and oceanic anoxia. in: Young,T.P. & Taylor,W.E.G. (eds) Phanerozoic Ironstones. Special Publication of the Geological Society of London,

Van Houten,F.B. & Bhattacharyya,D.P. 1982. Phanerozoic oolitic ironstones - geological record and facies model. Annual Review of Earth and Planetary Sciences, 10, 441-457.

Van Houten,F.B. & Karasek,R.M. 1981. Sedimentological framework of Late Devonian oolitic iron formation, Shatti Valley, west-central Libya. Journal of Sedimentary Petrology, 51, 415-427.

Van Houten,F.B. & Purucker,M.E. 1984. Glauconite peloids and chamositic ooids - favourable factors, constraints and problems. Earth Science Reviews, 20, 211-243.

Velde,B. 1985. Clay Minerals: a physio-chemical explanation of their occurrence. Developments in Sedimentology, Springer Verlag.

Velde,B. (in press). Chlorite formation in berthierine peloids and iron oolites. in: Young,T.P. & Taylor,W.E.G. (eds) Phanerozoic Ironstones. Special Publication of the Geological Society of London,

Velde,B. Raoult,J.F. & Leikine,M. 1974. Metamorphosed berthierine pellets in mid-Cretaceous rocks from northeast Algeria. Journal of Sedimentary Petrology, 44, 1275-1280.

Webb,B.C. 1983. Early Caledonian structures in the Cambrian slate belt, Gwynedd, North Wales. Report of the Institute of Geological Sciences, 83/1, 1-6.

Weinberg,R.M. 1973. The petrology and geochemistry of the Cambro - Ordovician ironstones of North Wales. Unpublished D.Phil. Thesis, University of Oxford.

Wilkinson,I. 1987. A finite strain study of the Ordovician volcanic rocks of Snowdonia, North Wales, and its implications for a regional strain model. Geological Journal Thematic Issue, 22, 95-105.

Wilkinson,I. & Smith,M. 1988. Basement fractures in North Wales: their recognition and control on Caledonian deformation. Geological Magazine, 125, 301-306.

Williams,A. Strachan,I. Bassett,D.A. Dean,W.T. Ingham,J.K. Wright,A.D. & Whittington,H.B. 1972. A Correlation of the Ordovician Rocks of the British Isles. Special Report of the Geological Society of London, No.3.

Woodcock,N.H. 1984. Early Palaeozoic sedimentation and tectonics in Wales. Proceedings of the Geologists Association, 95, 323-335.

Young,T.P. 1988. The lithostratigraphy of the Upper Ordovician of central Portugal. Journal of the Geological Society of London, 145, 377-392.

Young,T.P. (in press, a). Phanerozoic Ironstones: an introduction and review. in: Young,T.P. & Taylor,W.E.G. (eds) Phanerozoic Ironstones. Special Publication of the Geological Society of London,

Young,T.P. (in press,b). Eustatically controlled oolitic ironstone deposition: facies relationships of the Ordivician open-shelf ironstones of Western Europe. in: Young,T.P. & Taylor,W.E.G. (eds) Phanerozoic Ironstones. Special Publication of the Geological Society of London,

Young,T.P. & Taylor,W.E.G. (eds) (in press). Phanerozoic Ironstones. Special Publication of the Geological Society of London,

APPENDIX 1

TABLE OF LOCALITIES OF IRONSTONE SAMPLES

Table of the localities of all ironstones samples taken for thin section (T.S.)(polished thin sections encircled), point counting, XRD, EPMA, XRF and ICP.

Rock types are as follows:

G - grain-ironstone
P - pack-ironstone
W - wacke-ironstone
M - mud-ironstone
P/M - pack-ironstones lense in mud-ironstone
W/M - wacke-ironstones lense in mud-ironstone
R/P - rud-ironstone in pack-ironstone
R/W - rud-ironstone in wacke-ironstone
F/P - float-ironstone in pack-ironstone
F/W - float-ironstone in wacke-ironstone
F/M - float-ironstone in mud-ironstone
B - bind-ironstone
FG - ferruginous grit
SI - sideritic Ironstone
D - debris flow
V - vein material

SST - sandstone
MDST - mudstone

LOCALITY	SAMPLE No.	ROCK TYPE	GRID REF.	T.S.	POINT COUNT	XRD	EPMA	XRF	ICP
PORTH PADRIG	AA12	SI	3756 9434	X				X	
FFERAM UCHAF	FU1	FG	3626 8775	X					
	FU2	FG		X					
	FU3	FG		X					
TYNRONEN	AA11a	W	4327 7932	X	X				
	AA11b	P		X					
BRYN POETH	BP001	SST	6016 7958	X		X			
	BP1	P/M		X					
	BP2	P/M		X	X				
	BP3	W		X		X			
	BP4	P/M		X		X			
	BP5	W		X		X			
	BP6	P		X		X			
	AA10C	F/W		⊠	X		X		
	AA10D	G		⊠	X				
	AA10E	P		⊠	X		X		
	AA10F	P		X				X	X
	AA10G	P		X	X	X		X	X
	AA15	M		X					
	AA16	M		X					
	AA17	P		X	X				
TREFOR	TF001	M	3715 4747	X					
	TF002	M		X		X			
	TF003	M		X					
	TF004	M		X					
	TF005	M		X					
	TRV1	F/P		X	X				
	TRV2	F/P		X					
	TRV3	F/W		X					
	TRV4	F/P		X	X				
	TRV5	W		X					
	LP68A	M		X					
	LP68B	F/P		X					
	LP68C	F/P		X					
	LP68E	M		X					
	LP68F	F/P		X	X				
	LP68G	F/W		X					
	LP68H	F/W		X					
	LP68I	F/W		⊠					
	LP71A	R/P	3687 4741	X					
	LP71B	W		X					
	LP71C	F/M		X					
	LP71D	R/W		X					

LOCALITY	SAMPLE No.	ROCK TYPE	GRID REF.	T.S.	POINT COUNT	XRD	EPMA	XRF	ICP
TREFOR	LP72A	F/P	3676 4739	⊠			X		
	LP72B	F/P		X					
	LP72C	F/P		X					
	LP72D	F/P		X					
	LP73A	R/W	3672 4739	X					
	LP73B	W		X					
	LP73C	F/W		X					
	LP73D	F/W		X					
	LP73E	F/W		X					
PEN Y GAER	LP19A	W	2982 2832	⊠			X		
	LP19B	P		X				X	
	LP19C	W		X					
	PYG	W		X					
	PYG1	F/P	2984 2829	X		X			
	PYG1A	M		X					
	PYG2	W		X		X			
	PYG2A	M		X					
	PYG2B	M		X					
	LP20A	D		X	X				
	LP20B	F/W		X					
	LP20C	W		X					
	LP22A	P	2990 2821	⊠	X	X	X	X	
	LP22C	W		X					
	LP22D	P		X	X	X	X	X	X
CRAIG--FRYN	LP30A	W/M	2971 2766	X					
	LP30B	D		X					
	LP32	W	2997 2782	X					
CREIGIR UCHAF	LP33	F/W	2989 2806	X	X				
LLANEN--GAN	LP24A	P	2947 2731	X				X	X
	LP24B	W		X					
	LP24C	F/W		X				X	X
	LP24D	W		X	X				
	LP1	W		X					
PIT ABOVE HEN DY CAPEL	LP41A	F/W	2994 2706	X	X				
	LP41B	F/W		X					
	LP41C	W		X					
	LP41D	F/W		X					

LOCALITY	SAMPLE No.	ROCK TYPE	GRID REF.	T.S.	POINT COUNT	XRD	EPMA	XRF	ICP
HEN DY CAPEL	HC	F/W	3002 2714	⊠					
	HCA	F/W		X					
	LP57A	F/W		X					
	LP57B	F/W		X					
	LP57C	F/W		X					
	LP57D	F/W		X					
	LP57E	F/W		X					
	LP57F	F/W		X					
	LP57H	F/M		X					
ABER	SN17A	G	6689 7243	⊠					
	SN17B	G		X					
	AB	G	6693 7245	X				X	
	ABA	P		⊠		X	X	X	X
	ABB	P		⊠					
	SN18A	G		⊠				X	
	SN18B	G		X				X	X
	AB002	V	6699 7296	⊠		X	X		
GORD- -DINOG	SN20A	B	6789 7294	X					
	SN20B	B		X					
	SN20C	R		X					
	SN20D	F/M		X					
	SN20E	B		X					
CWM CASEG	SN26A	W?	6773 6496	X					
	SN26B	W?		X					
	SN26C	W?		X					
A5	SN27A	W?	6429 6224	X					
	SN27B	W?		⊠					
BWLCH Y CYWION	SN21	P	6404 6125	X				X	
	SN22	F/M		X					
LLAN- -BERIS VALLEY	SN16A	D	6114 5801	X					
	SN16B	D		X					
	SN16C	D		X					

LOCALITY	SAMPLE No.	ROCK TYPE	GRID REF.	T.S.	POINT COUNT	XRD	EPMA	XRF	ICP
BETWS GARMON	SN14G	P	5443 5793					X	X
	SN14H	P						X	X
	SN14I	P						X	
	SN14A	F/W	5433 5778	X					
	YF G	F/W	5431 5777	⊠			X	X	
	SN14D	P	5424 5768					X	X
	SN14E	P						X	
	SN14F	P						X	
	SN14B	P	5386 5735	⊠	X			X	X
	YF A	P	LOOSE	⊠	X	X	X	X	
	YF B	W	SAMPLES	⊠		X	X		
	YF C	P	(538 573)	X	X				
	YF E	P		X					
	YF F	W		X	X				
	YF X	P		X					
	SN15A	MDST	5332 5697	X					
	SN15B	P		X	X			X	X
	SN15C	P		⊠			X		
TYDDYN DEUCWM	TD001	P	5442 4099	X					
	TD002	P		X				X	
	TD003	P		X	X	X			
	TD004	P		X					
	SN13A	P		X					
	SN13B	P		X	X			X	
	SN13C	M		X					
TREMADOG	TR	D	5527 4028	X					
	TR1	D		X					
	78144	F/W		X					
	SN12A	D		X					
	SN12C	F/P		X					
	SN12D	F/P		X				X	
	SN12E	P		X	X				
	SN12F	W		X					
PENSY- -FLOG	PSF1	G	5619 3958	X					
	PSF2	B		X					
PEN YR ALLT	SN11A	W	6306 4118	X				X	
	SN11B	W		X	X			X	X
	PYA1	W	6285 4093	X					

LOCALITY	SAMPLE No.	ROCK TYPE	GRID REF.	T.S.	POINT COUNT	XRD	EPMA	XRF	ICP
FFORDD DDU	CI Y	P	6477 1283	X	X				
	CI1B	W		X	X				
	CI	P		⊠			X		
	CI1	W		⊠			X		
	CI2A	M		X	X				
	FD1	P		X		X			
	FD2	P		X		X			
	FD3	W		X		X			
	FD4	P		X		X			
	FD10	W		X					
	FD11	W		X					
	FD12	W		X					
	FD13	R/W		X					
	CI129	W/M		X				X	X
FOXES PATH	CI104	W	7104 1378	X		X			
BWLCH COCH	CI123	M	7495 1557	X		X		X	
	CI130A	M		X	X				
	CI130B	P		X	X			X	X
	CI130C	W		⊠	X	X	X	X	X
CROSS FOXES	CI132	P	7591 1634	X	X				
	CI134	P	7595 1639	X	X			X	
	CI136	P	7602 1647	⊠	X	X		X	X
	CI137	P	7606 1652	⊠		X	X	X	X
TYLLAU MWN	CI200 5	P	8441 2054	X				X	
	CI200 6	P		X					
	CI200 7	P		X					
	CI200 8	P		X					
LLANEG--RYN	CI300	M	5906 0626	X					

APPENDIX 2

COMPOSITIONAL AND GRAIN-SIZE ANALYSIS

Compositional and grain-size analysis data for the North Wales Ironstones (phosphate nodules excluded).

Composition by point counting thin sections (n=300) differentiating between quartz grains, ferruginous allochems and matrix. Lettering for rock types from Appendix 1

Grain-size analysis using an eyepiece graticule and point counter. Data for ooids (including oncoids and peloids) is given as minimum, maximum, mean, median and interquartile range (Q3-Q1), all in millimetres, plus standard deviation and skewness. Lettering for rock type as in Appendix 1.

COMPOSITION (n=300)

AREA	SMPLE	ROCK TYPE	QZ %	OOL %	MAT %
ANGLESEY					
Bryn Poeth	AA10D	G	1.0	63.0	38.0
	AA10C	F/W	2.2	40.3	57.5
	AA10E	P	2.7	44.8	52.8
	AA10G	P	3.2	40.3	56.5
	AA17	P	5.1	40.3	54.6
	BP2	P/M	5.5	37.0	57.5
Tynyronen	AA11A	W	0.0	29.7	70.3
LLYN PENINSULA					
Trefor	TRV1	F/P	1.8	36.8	61.4
	TRV4	F/P	1.5	39.3	59.2
	LP68F	F/P	1.7	37.0	61.3
St. Tudwals	LP22A	P	3.0	62.5	34.5
	LP22D	P	1.2	44.2	54.6
	LP24D	W	1.5	51.2	47.3
	LP33A	F/W	2.7	22.2	75.1
	LP41A	F/W	2.5	31.3	66.2
	LP20A	D	7.7	1.0	91.3
SNOWDONIA					
Betws Garmon	YF-A	P	0.0	62.2	37.8
	YF-C	P	0.0	68.0	32.0
	YF-F	W	0.0	57.6	42.4
	SN14B	P	0.0	74.7	25.3
Tremadog	TD003	P	0.0	72.0	28.0
	SN13B	P	0.0	73.0	27.0
Rhyd	SN11B	W	0.0	28.2	71.8
CADAIR IDRIS					
East	CI130B	P	0.0	63.8	36.2
	CI130C	W	0.0	26.0	74.0
	CI132	P	0.0	42.0	58.0
	CI134A	P	0.0	32.7	67.3
	CI136B	P	0.0	30.0	70.0
	CF2	P	0.0	61.0	39.0
	CI130A	M	0.0	8.3	91.7
West	CIY	P	1.7	68.0	30.3
	CI1B	W	1.3	34.0	64.7
	CI2A	M	0.0	4.0	96.0

GRAIN SIZE ANALYSIS

AREA	SAMPLE	ROCK TYPE	MIN mm	MAX mm	Q3 mm	Q1 mm	MEAN mm	MED. mm	ST. DEV.	SKEW	n
ANGLESEY											
Bryn	AA10D	G	0.24	1.28	1.17	0.59	0.89	0.94	0.38	-.04	30
Poeth	AA10C	F/W	0.24	11.50	1.37	0.49	1.44	0.67	2.30	3.44	31
	AA10E	P	0.15	1.58	0.59	0.30	0.54	0.43	0.36	1.72	30
	AA10G	P	0.18	0.61	0.37	0.31	0.33	0.31	0.08	1.39	30
	AA17	P	0.18	0.49	0.37	0.27	0.33	0.31	0.07	0.24	30
Tynronen	AA11A	W	0.18	1.34	0.43	0.31	0.56	0.49	0.26	0.95	30
LLYN PENINSULA											
Trefor	TRV1	F/P	0.24	1.22	0.54	0.40	0.53	0.49	0.25	1.46	32
	TRV4	F/P	0.37	2.74	0.79	0.40	0.76	0.50	0.64	2.13	30
	LP68F	F/P	0.18	1.34	0.73	0.37	0.58	0.49	0.30	1.14	31
St.	LP22A	P	0.24	1.22	0.81	0.37	0.62	0.67	0.26	0.24	30
Tudwals	LP22D	P	0.24	3.05	0.91	0.43	0.78	0.67	0.53	2.46	31
	LP24D	W	0.18	1.02	0.55	0.31	0.44	0.37	0.19	1.28	31
	LP33A	F/W	0.18	1.83	0.66	0.40	0.59	0.47	0.37	2.02	32
	LP41A	F/W	0.18	1.52	0.85	0.49	0.67	0.66	0.27	0.90	31
SNOWDONIA											
Betws	YF-A	P	0.37	1.31	1.05	0.67	0.87	0.85	0.26	0.03	30
Garmon	YF-C	P	0.37	1.40	0.93	0.64	0.77	0.76	0.23	0.37	30
	YF-F	W	0.18	0.91	0.69	0.37	0.51	0.49	0.20	0.47	30
	SN14B	P	0.43	1.34	0.89	0.66	0.79	0.76	0.23	0.68	30
	SN15B	P	0.24	0.97	0.74	0.43	0.59	0.55	0.20	0.29	30
Tremadog	TD003	P	0.24	0.85	0.62	0.43	0.52	0.49	0.55	0.54	30
	SN12E	P	0.24	1.31	0.98	0.61	0.82	0.82	0.25	0.01	30
	SN13B	P	0.31	1.04	0.62	0.43	0.54	0.49	0.18	0.98	30
Rhyd	SN11B	W	0.12	0.61	0.43	0.31	0.39	0.41	0.10	-.26	30
CADAIR IDRIS											
East	CI130B	P	0.12	0.91	0.40	0.24	0.34	0.29	0.17	1.60	30
	CI130C	W	0.12	0.67	0.40	0.24	0.33	0.32	0.12	0.55	30
	CI132	P	0.18	0.61	0.43	0.27	0.35	0.37	0.10	0.68	30
	CI134A	P	0.12	0.64	0.43	0.24	0.33	0.32	0.13	0.47	30
	CI136B	P	0.18	0.73	0.50	0.27	0.39	0.37	0.14	0.55	30
	CF2	P	0.18	0.73	0.43	0.24	0.35	0.31	0.12	1.23	30
West	CIY	P	0.50	1.58	1.36	0.97	1.15	1.20	0.30	-.68	30
	CI2A	M	0.15	1.22	0.61	0.30	0.48	0.40	0.26	1.23	30

APPENDIX 3

X-RAY DIFFRACTION DATA

X-ray diffraction data for chamosite, apatite, siderite, magnetite and stilpnomelane from the ironstones. All XRD traces contain chamosite and quartz, with varying amounts of apatite, siderite, magnetite and stilpnomelane. Chamosite details are given for each XRD trace. For the other four minerals their identification is taken from the best XRD trace, but also compared to all samples containing that mineral, and are a composite from all the XRD traces.

Samples (at Oxford University) were hand ground in a pestle and mortar with acetone, and pippetted onto a glass slide and allowed to evaporate. Samples were analysed on a Phillips diffractometer (PW1050), with analytical conditions: Cu K^{α} radiation with a monochromator, 45Kv, 32mA, slits 1^{o} divergence, 1^{o} scatter, 0.3mm receiving, chart speed 1^{o} 2θ = 10mm, scan speed 1^{o} 2θ per minute, ratemeter 300 full scale deflection (FSD)(but also 1000 or 3000 FSD), with a graphite monochromator. The minerals were identified using various reference tables, and also by using pure quartz and separated chamosite. The two largest peaks of quartz (100 & 101) were used as an internal standard. This method gives preferred orientation of the chamosite on XRD.

Sample numbers refer to samples listed in Appendix 1. For chamosite data s = siderite peak overlapping, a = apatite peak overlapping, q = quartz peak overlapping. Samples marked with (+) are those whose -10um fraction was analysed, and those marked with (M) have been passed through a magnetic separator. Intensity values for siderite cannot be given as the largest siderite peak (marked *) overlaps with (005) chamosite.

2θ/cm	d/Å	I/I_1	hkl
	BP001		
6.20	14.255	12	001
12.55	7.053	100	002
18.90	4.695	19	003
25.25	3.527	79	004
31.90	2.805	8	005
35.70	2.515	43	202
36.60	2.455	q	?
59.35	1.557	32	060
	BP4$^+$		
6.25	14.141	13	001
12.55	7.053	100	002
19.05	4.659	22	003
25.25	3.527	77	004
32.00	2.797	15	005
33.35	2.687	20	?
35.70	2.515	43	202
42.15	2.144	9	204
51.70	1.768	13	?
59.3	1.558	36	060
	BP6$^+$		
6.30	14.029	9	001
12.60	7.025	100	002
19.00	4.671	16	003
25.30	3.520	78	004
32.00	2.797	s	005
33.30	2.691	15	200
35.75	2.512	40	202
51.70	1.768	13	206/008
59.40	1.556	23	060
	TF002		
6.20	14.255	18	001
12.50	7.018	100	002
18.95	4.450	22	003
25.25	3.527	80	004
59.25	1.560	22	060

2θ/cm	d/Å	I/I_1	hkl
	BP3$^+$		
6.35	13.919	15	001
12.50	7.081	100	002
18.95	4.683	20	003
25.25	3.527	68	004
32.05	2.793	s	005
33.60	2.667	a	?
35.80	2.508	27	202
51.70	1.768	11	?
59.45	1.555	21	060
	BP5$^+$		
6.35	13.919	15	001
12.55	7.053	100	002
19.00	4.671	21	003
25.35	3.513	75	004
31.90	2.805	20	005
33.30	2.691	22	?
35.80	2.508	35	202
42.10	2.146	q	204
51.80	1.765	9	?
59.45	1.555	25	060
	AA10G$^+$		
6.30	14.029	8	001
12.50	7.081	100	002
18.90	4.695	14	003
25.25	3.527	70	004
32.00	2.797	s	005
33.25	2.694	a	?
35.65	2.518	34	202
51.70	1.768	9	?
59.35	1.557	19	060

2θ/cm	d/Å	I/I_1	hkl
	PYG1[+]		
6.35	13.919	11	001
12.55	7.053	100	002
18.95	4.683	16	003
25.25	3.527	66	004
32.00	2.797	s	005
33.15	2.702	16	200
35.70	2.515	20	202
59.30	1.558	19	060
	AB002		
6.20	14.255	9	001
12.45	7.109	100	002
18.80	4.720	19	003
25.25	3.527	94	004
31.70	2.823	14	005
33.30	2.691	2	$20\bar{1}$
34.20	2.622	3	$20\bar{2}$
34.90	2.571	3	201
35.60	2.522	3	?
36.40	2.468	4	$20\bar{3}$
37.40	2.404	3	$20\bar{2}$
38.20	2.360	3	$20\bar{4}$
44.95	2.017	6	007
58.90	1.568	1	?
59.20	1.561	2	060
	YF-B (mud-ironstone)		
6.2	14.255	4	001
12.5	7.081	100	002
19.0	4.671	11	003
25.2	3.534	77	004
32.05	2.793	41	005
33.20	2.698	9	?
35.60	2.522	35	202
59.2	1.561	21	060
	CI130C[+]		
6.30	14.029	10	001
12.55	7.053	100	002
19.05	4.659	16	003
25.25	3.527	82	004
32.05	2.793	29	005
35.70	2.515	41	202
59.25	1.560	27	060

2θ/cm	d/Å	I/I_1	hkl
	LP22A[+]		
6.20	14.255	6	001
12.55	7.053	100	002
19.00	4.671	12	003
25.25	3.527	71	004
32.05	2.797	s	005
35.70	2.515	21	202
59.30	1.558	21	060
	ABA		
6.30	14.029	8	001
12.50	7.081	100	002
18.85	4.708	14	003
25.25	3.527	71	004
32.00	2.797	s	005
35.70	2.515	21	202
59.30	1.558	16	060
	YF-A		
6.30	14.029	4	001
12.50	7.081	100	002
19.00	4.671	10	003
25.25	3.527	58	004
32.10	2.788	s	005
35.60	2.522	38	202
59.20	1.561	13	060
	YF-B (oncoid)		
6.1	14.488	8	001
12.5	7.081	100	002
18.9	4.695	13	003
25.2	3.534	66	004
32.1	2.788	a	005
35.6	2.522	32	202
59.2	1.561	16	060
	CI137[+]		
6?	14?	?	001
12.50	7.081	100	002
19.30	4.599	9	003
25.25	3.527	56	004
32.00	2.797	28	005
32.35	2.767	20	?
35.65	2.518	34	202
41.30	2.186	14	?
59.30	1.558	18	060

2θ/cm	d/Å	I/I_1	hkl
	CI104		
6.25	14.141	11	001
12.5	7.081	100	002
18.9	4.695	21	003
25.25	3.527	81	004
31.7	2.823	13	005
33.5	2.675	4	$20\bar{1}$
34.3	2.614	16	$20\bar{2}$
34.95	2.567	10	$20\bar{1}$
36.5	2.462	13	$20\bar{3}$
37.4	2.404	15	202
45.0	2.014	20	007
58.9	1.568	13	?
59.2	1.561	14	060
	FD1,2,4^{+}		
6?	14?	?	001
12.50	7.081	100	002
19.10	4.647	11	003
25.20	3.534	70	004
32.05	2.793	14	005
33.25	2.694	22	$20\bar{0}$
34.50	2.600	34	$20\bar{2}$
35.70	2.515	57	202
41.30	2.186	17	?
42.30	2.137	17	204
51.60	1.771	13	206/008
53.30	1.719	10	?
57.50	1.603	10	?
59.30	1.558	23	060
	FD3^{+}		
?6.30	14.029	5	001
12.50	7.081	100	002
19.10	4.647	10	003
25.25	3.527	63	004
32.05	2.793	20	005
33.25	2.694	18	?
34.25	2.618	6	?
35.70	2.515	30	202
41.15	2.194	4	?
42.10	2.146	9	204
59.30	1.558	15	060

2θ/cm	d/Å	I/I_1	hkl
	CI1		
6.10	14.488	7	001
12.50	7.081	100	002
19.00	4.671	8	003
25.25	3.527	61	004
32.00	2.797	7	005
33.30	2.691	11	?
34.80	2.578	24	?
35.70	2.515	32	202
41.40	2.181	12	?
42.30	2.137	11	204
51.70	1.768	10	?
59.30	1.558	14	060
	FD1^{+M}		
6.35	13.919	7	001
12.55	7.053	100	002
19.00	4.671	12	003
25.25	3.527	78	004
32.05	2.793	21	005
33.25	2.694	19	$20\bar{0}$
34.25	2.618	6	$20\bar{2}$
35.70	2.515	33	202
42.20	2.141	13	204
47.00	1.933	5	?
49.70	1.834	7	206/008
51.75	1.776	13	205
59.30	1.558	17	060

2θ/cm	d/Å	I/I_1	hkl
	APATITE		
10.90	8.12	5	100
16.80	5.28	3	101
21.90	4.06	7	200
22.95	3.875	7	111
25.85	3.447	34	002?
28.10	3.175	11	102
29.10	3.069	16	210
31.95	2.801	100	211
32.20	2.780	42	112
33.10	2.706	58	300
34.10	2.629	32	202
40.05	2.251	27	310
44.85	2.021	6	113?
46.90	1.937	29	?
48.25	1.886	17	132
49.50	1.841	35	230
50.75	1.799	17	231
51.55	1.773	16	410
52.55	1.751	15	303
53.05	1.726	17	004
	STILPNOMELANE		
7.40	11.946	100	001
14.75	6.006	4	002
22.15	4.013	22	003
29.65	3.013	12	$00\underline{4}$
33.10	2.706	20	$44\underline{5}$
34.95	2.567	38	$44\underline{6}$
38.35	2.347	20	$44\underline{7}$
41.30	2.186	7	$44\underline{\bar{1}}$
42.90	2.108	12	$44\underline{8}$
46.40	1.957	3	440
48.30	1.884	7	$4.4.\underline{\bar{1}\bar{0}}$
58.15	1.586	8	?
58.80	1.570	9	?

2θ/cm	d/Å	I/I1	hkl
	SIDERITE		
24.80	3.590	?	$01\bar{1}2$
31.85	2.810	?	$10\bar{1}4$*
42.20	2.141	?	$11\bar{2}3$
46.10	1.969	?	$20\bar{2}2$
52.70	1.737	?	$01\bar{1}8$
	MAGNETITE		
30.05	2.974	32	220
35.45	2.532	100	311
43.05	2.101	22	400
53.40	1.716	10	422
56.95	1.617	29	511
62.50	1.486	38	440

APPENDIX 4

ELECTRON PROBE MICRO-ANALYSIS DATA

A total of 16 polished thin sections, prepared at Luton College and the Camborne School of Mines, were analysed by EPMA at Cambridge University on aN instrument designed and constructed at Cambridge. Cobalt and olivine were used as standards before analysis.

Hardware: Electron microprobe designed and constructed in Department of Mineralogy and Petrology, Cambridge. Si(Li) detector and Harwell Highspec pulse processor system 3073 (Kandiah et al. 1975) interfaced to Data General Nova 1220 minicomputer with 24K storage.

Analytical conditions:

20 kV accelerating potential
45 nA nominal beam current
(~35 nA at specimen surface)
80 live seconds counting time
5-6 kpps input rate typical
40° take off angle
270 mm specimen - detector distance
Detector resolution ~ 156eV FWHM at MnK@ (5.89keV)

Software: Peaks processed and measured by iterative peak stripping (Statham 1976). Correction methods after Sweatman & Long (1969).

3c detection limits:

Na ~ .25%
Mg ~ .15%
Al,Si ~ .10%
K - Zn ~ .05%

Relative accuracy:

~ 2% for major elements (more than 5% element present).

EPMA data for chamosite siderite stilpnomelane and apatite from the North Wales ironstones. All iron is calculated as FeO. From the EPMA spot-size, only siderite and stilpnomelane could be analysed with confidence. Most chamosite in the North Wales ironstones is too fine-grained to probe individual crystals (Hughes 1989) and therefore it cannot be guaranteed that pure chamosite is being analysed or whether more than one mineral is being probed. However, a simple method (adapted from Curtis et al. 1985) of plotting individual analyses on an $FeO-SiO_2-Al_2O_3$ triangular diagram can show if the analyses are pure (Figure 7.1). The majority of analyses plot over a small area, with tailings toward the SiO_2 and FeO end members. These tailings indicate chamosite mixed with either quartz or magnetite/goethite respectively. These analyses are then ignored and the others are treated as pure chamosite. XRD analysis confirms that the ironstones are are only made of chamosite, quartz and other Fe-oxides.

Confirmation is further given by comparing these analyses with those from chamosite cements and chamosite veins, which have identical compositions, and by comparing with analytical transmission electron microscopy (ATEM) data (Hughes 1989). EPMA analyses of chamosite that also have a small amount of apatite (CaO & P2O5) are included, as the

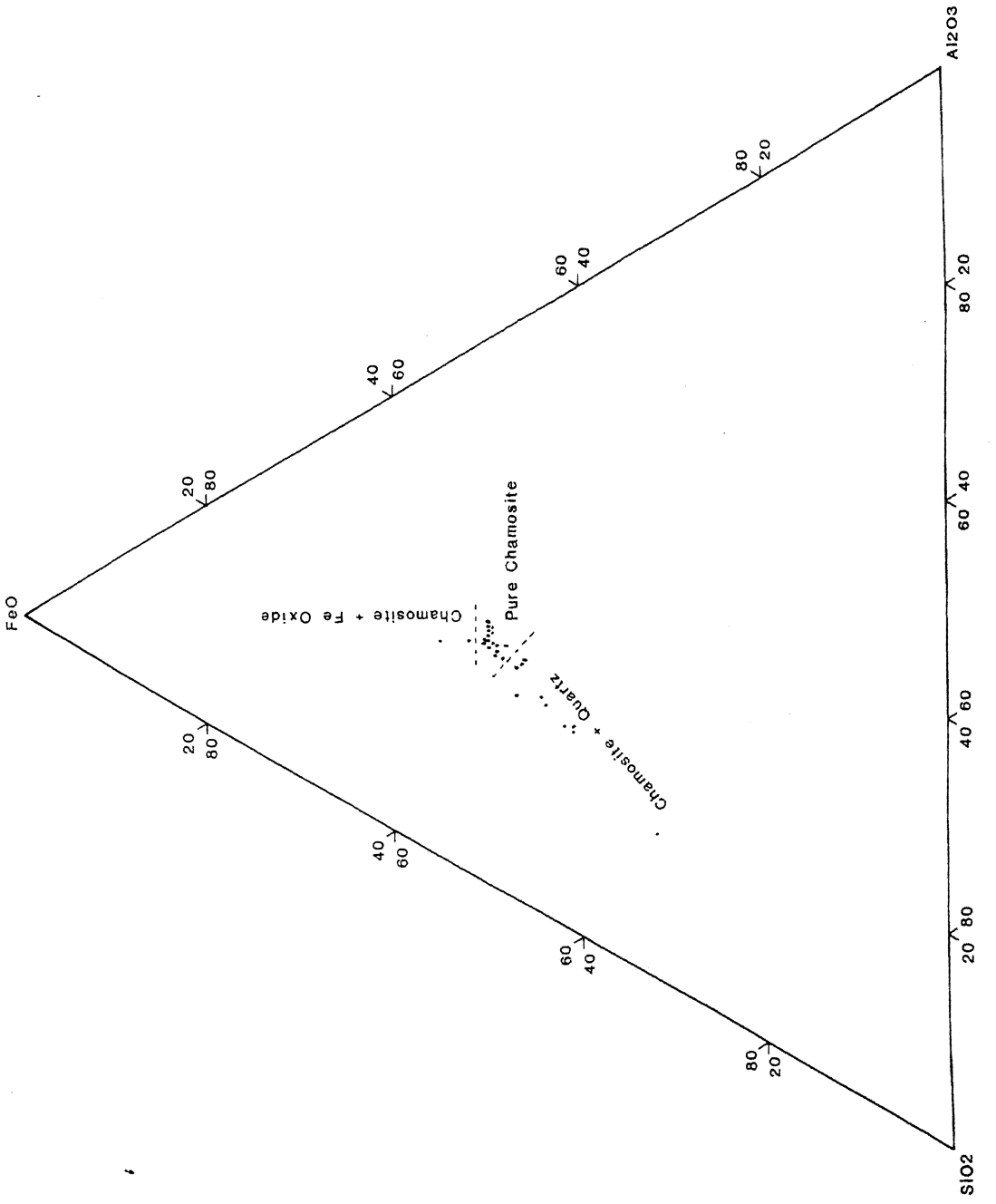

Figure 7.1 EPMA analyses for chamosite plotted on an FeO-SiO2-Al2O3 triangular diagram, to check purity of analysis. The majority of the analyses plot over a small area, and indicate pure chamosite. Individual analyses which trend towards FeO and SiO2 indicate mineral mixing with another phase, these analyses are then ignored.

Fe Si Al Mg ratios are not affected and therefore the chamosite formula can still be calculated. Pure apatite analyses have not been attempted, although the CaO/P_2O_5 ratio has been determined.

Presented first is chamosite EPMA data (mineral formulas calculated to 36 oxygens). Elements also analysed for are Ti (as rutile), Na (not detected), S (not included), Ca & P (as apatite), and Cu & Zn (not detected). Abbreviations: * element not analysed for, - element analysed for but not detected, 0.0 element below detection limits for that analysis but detected on at least one analysis, - total not given due to mixed mineral analysis (apatite), OCT - octahedral total, y - Fe/[Fe+Mg]. Next is data for siderite (differentiated into diagenetic and hydrothermal) where the results have been recalculated to carbonate from oxide. Then stilpnomelane (calculated on the basis of 11 oxygens), and finally a regression line plot for apatite to determine the Ca/P ratio.

AA10C

	2	3	4	6	15	16	18
	o	o	o	o	o	o	o
MgO	2.536	2.729	2.536	2.525	3.017	3.078	2.643
Al2O3	19.143	18.579	20.264	15.490	19.430	19.582	19.917
SiO2	23.368	23.926	23.409	20.957	25.528	24.754	25.189
K2O	-	-	-	-	-	-	-
V2O3	*	*	*	*	*	*	*
Cr2O3	-	-	-	-	-	-	-
MnO	-	-	-	-	-	-	-
FeO	41.683	43.756	43.442	35.298	43.196	43.736	43.311
TOTAL	-	-	-	-	91.171	91.150	91.060
Mg	0.888	0.938	0.862	1.027	0.999	1.025	0.877
Al(T)	2.512	2.480	2.661	2.280	2.329	2.469	2.392
Al(O)	2.788	2.573	2.788	2.704	2.760	2.690	2.836
Al	5.300	5.053	5.449	4.984	5.089	5.159	5.228
Si	5.488	5.520	5.339	5.720	5.671	5.531	5.608
K	-	-	-	-	-	-	-
V	*	*	*	*	*	*	*
Cr	-	-	-	-	-	-	-
Mn	-	-	-	-	-	-	-
Fe	8.187	8.442	8.287	8.057	8.025	8.173	8.064
OCT	11.836	11.953	11.937	11.788	11.784	11.888	11.777
TOTAL	19.836	19.953	19.937	19.788	19.784	19.888	19.777
y	0.902	0.900	0.906	0.887	0.889	0.889	0.902

AA10E

	2	3	8	14	16
	o	o	c	c	o
MgO	2.296	2.577	2.602	2.374	2.035
Al2O3	20.847	20.201	20.087	20.393	18.954
SiO2	23.148	23.726	23.569	23.246	20.485
K2O	-	-	-	-	-
V2O3	*	*	*	*	*
Cr2O3	-	-	-	-	-
MnO	0.0	0.209	0.0	0.173	0.198
FeO	43.053	43.451	43.367	43.560	39.201
TOTAL	-	90.548	89.870	89.851	-
Mg	0.776	0.860	0.884	0.808	0.764
Al(T)	2.750	2.647	2.620	2.694	2.838
Al(O)	2.825	2.726	2.773	2.794	2.796
Al	5.575	5.373	5.393	5.488	5.634
Si	5.250	5.353	5.374	5.306	5.164
K	-	-	-	-	-
V	*	*	*	*	*
Cr	-	-	-	-	-
Mn	0.0	0.040	0.0	0.033	0.042
Fe	8.167	8.198	8.269	8.315	8.262
OCT	11.768	11.824	11.926	11.950	11.864
TOTAL	19.768	19.824	19.926	19.950	19.864
y	0.913	0.905	0.903	0.911	0.915

LP72

	1	2	4	5	6	7	10	11	12
	c	c	c	o	o	o	on	on	on
MgO	1.340	1.798	1.553	1.522	1.940	1.675	1.687	1.714	1.578
Al2O3	19.736	19.817	18.878	19.454	19.350	19.641	19.410	18.911	18.560
SiO2	23.715	23.219	22.913	23.401	23.088	22.736	22.979	22.143	22.688
K2O	-	-	-	-	-	-	-	-	-
V2O3	*	*	*	*	*	*	*	*	*
Cr2O3	0.0	0.0	0.143	0.0	0.0	0.0	0.0	0.0	0.0
MnO	0.195	0.0	0.159	0.0	0.0	0.0	0.128	0.0	0.0
FeO	46.509	46.139	44.168	45.972	46.056	45.241	44.723	43.870	42.619
TOTAL	91.495	90.972	-	90.443	-	89.464	-	-	-
Mg	0.453	0.611	0.546	0.520	0.662	0.579	0.585	0.611	0.566
Al(T)	2.619	2.704	2.598	2.630	2.715	2.730	2.652	2.700	2.540
Al(O)	2.661	2.625	2.649	2.633	2.507	2.637	2.674	2.637	2.725
Al	5.280	5.329	5.247	5.263	5.222	5.367	5.326	5.337	5.265
Si	5.381	5.296	5.402	5.370	5.285	5.270	5.348	5.300	5.460
K	-	-	-	-	-	-	-	-	-
V	*	*	*	*	*	*	*	*	*
Cr	0.0	0.0	0.027	0.0	0.0	0.0	0.0	0.0	0.0
Mn	0.038	0.0	0.031	0.0	0.0	0.0	0.025	0.0	0.040
Fe	8.826	8.802	8.709	8.822	8.817	8.770	8.705	8.783	8.577
OCT	11.978	12.038	11.962	11.975	11.986	11.986	11.989	12.031	11.908
TOTAL	19.978	20.038	19.962	19.975	19.986	19.986	19.989	20.031	19.908
y	0.951	0.935	0.941	0.944	0.930	0.938	0.937	0.935	0.938

LP19A

	5	6	9	12	13	14	15	16	18	19
	o	o	o	o	o	o	o	o	on	on
MgO	0.667	1.052	1.020	0.871	1.130	0.914	1.011	1.268	1.044	1.106
Al2O3	20.968	21.162	20.214	21.388	20.942	21.439	21.202	20.883	21.517	21.051
SiO2	22.703	22.942	21.957	21.400	20.862	22.335	21.857	20.479	22.124	20.924
K2O	-	-	-	-	-	-	-	-	-	-
V2O3	*	*	0.120	0.134	0.130	0.150	0.113	0.0	0.144	0.183
Cr2O3	0.0	0.0	0.0	0.0	0.0	0.117	0.0	0.0	0.0	0.135
MnO	0.126	0.0	0.0	0.0	0.0	0.0	0.0	0.0	0.0	0.0
FeO	44.264	43.034	42.820	41.126	41.679	42.197	42.976	40.545	42.284	42.225
TOTAL	88.728	88.330	86.131	-	-	-	-	-	-	-
Mg	0.231	0.363	0.363	0.312	0.408	0.319	0.355	0.465	0.365	0.396
Al(T)	2.729	2.694	2.752	2.858	2.943	2.772	2.850	2.956	2.814	2.971
Al(O)	3.010	3.075	2.944	3.200	3.041	3.144	3.039	3.107	3.132	2.994
Al	5.739	5.769	5.696	6.058	5.984	5.916	5.889	6.063	5.946	5.965
Si	5.271	5.306	5.248	5.142	5.057	5.228	5.150	5.044	5.186	5.029
K	-	-	-	-	-	-	-	-	-	-
V	*	*	0.023	0.021	0.021	0.023	0.018	0.0	0.022	0.029
Cr	0.0	0.0	0.0	0.0	0.0	0.022	0.0	0.0	0.0	0.026
Mn	0.025	0.0	0.0	0.0	0.0	0.0	0.0	0.0	0.0	0.0
Fe	8.594	8.323	8.560	8.264	8.449	8.260	8.468	8.351	8.289	8.488
OCT	11.860	11.761	11.890	11.797	11.919	11.768	11.880	11.923	11.808	11.933
TOTAL	19.860	19.761	19.890	19.797	19.919	19.768	19.880	19.923	19.808	19.933
y	0.974	0.958	0.959	0.964	0.954	0.963	0.960	0.947	0.959	0.955

LP22A

	1	2	3	5	6	8	9	15	19	26
	on	on	on	c	on	do	do	o	v	c
MgO	1.289	1.426	1.368	1.371	1.563	1.457	1.503	1.671	1.062	1.261
Al2O3	20.257	20.848	21.293	21.479	20.774	20.451	20.427	20.539	21.106	21.580
SiO2	24.018	24.091	24.589	23.391	23.391	23.400	23.114	24.190	22.846	23.285
K2O	-	-	-	-	-	-	-	-	-	-
V2O3	*	*	*	*	*	*	*	*	*	*
Cr2O3	0.0	0.0	0.0	0.0	0.0	0.131	0.0	0.0	0.0	0.0
MnO	-	-	-	-	-	-	-	-	-	-
FeO	43.811	43.607	43.719	44.173	44.673	44.509	44.615	44.617	45.137	44.960
TOTAL	-	90.550	91.625	90.669	90.584	89.949	89.659	91.016	90.283	-
Mg	0.439	0.481	0.455	0.462	0.592	0.496	0.515	0.560	0.362	0.424
Al(T)	2.507	2.544	2.511	2.708	2.684	2.652	2.691	2.555	2.780	2.751
Al(O)	2.956	3.021	3.092	3.022	2.881	2.858	2.840	2.890	2.905	2.984
Al	5.463	5.565	5.603	5.730	5.565	5.510	5.531	5.445	5.685	5.735
Si	5.493	5.456	5.489	5.292	5.316	5.384	5.309	5.440	5.220	5.249
K	-	-	-	-	-	-	-	-	-	-
V	*	*	*	*	*	*	*	*	*	*
Cr	0.0	0.0	0.0	0.0	0.0	0.024	0.0	0.0	0.0	0.0
Mn	-	-	-	-	-	-	-	-	-	-
Fe	8.380	8.259	8.162	8.359	8.491	8.507	8.570	8.391	8.625	8.476
OCT	11.775	11.761	11.709	11.843	11.964	11.885	11.925	11.841	11.892	11.884
TOTAL	19.775	19.761	19.709	19.843	19.964	19.885	19.925	19.841	19.892	19.884
y	0.950	0.945	0.947	0.948	0.935	0.945	0.943	0.937	0.960	0.952

LP22D

	1	2	4	5	7	9
	o	o	o	o	o	o
MgO	1.389	1.212	1.197	1.342	1.076	1.350
Al2O3	20.702	20.227	20.755	20.800	22.138	20.553
SiO2	22.304	21.704	21.456	22.345	22.299	21.978
K2O	-	-	-	-	-	-
V2O3	0.0	0.0	0.126	0.0	0.118	0.184
Cr2O3	-	-	-	-	-	-
MnO	-	-	-	-	-	-
FeO	43.846	42.829	42.837	42.942	43.153	42.624
TOTAL	88.241	85.973	86.371	87.429	88.951	-
Mg	0.483	0.433	0.425	0.469	0.369	0.473
Al(T)	2.794	2.797	2.882	2.760	2.867	2.834
Al(O)	2.903	2.919	2.955	2.991	3.141	2.862
Al	5.697	5.716	5.837	5.751	6.008	5.696
Si	5.206	5.203	5.118	5.240	5.133	5.166
K	-	-	-	-	-	-
V	0.0	0.0	0.024	0.0	0.022	0.035
Cr	-	-	-	-	-	-
Mn	-	-	-	-	-	-
Fe	8.559	8.586	8.546	8.423	8.299	8.379
OCT	11.945	11.938	11.950	11.883	11.831	11.749
TOTAL	19.945	19.938	19.950	19.883	19.831	19.749
y	0.947	0.952	0.953	0.947	0.957	0.947

AB002

	1	2	3	4	5	6
	v	v	v	v	v	v
MgO	1.777	2.444	2.133	2.098	1.881	2.195
Al2O3	21.303	21.144	20.966	21.329	21.335	21.416
SiO2	23.889	23.410	23.144	23.614	22.777	23.129
K2O	-	-	-	-	-	-
V2O3	*	*	*	*	*	*
Cr2O3	-	-	-	-	-	-
MnO	0.150	0.0	0.0	0.0	0.0	0.0
FeO	45.024	43.823	44.290	44.606	44.616	44.389
TOTAL	92.143	90.821	90.534	91.647	90.609	91.129
Mg	0.589	0.819	0.720	0.698	0.636	0.736
Al(T)	2.686	2.735	2.756	2.727	2.832	2.799
Al(O)	2.900	2.871	2.844	2.888	2.875	2.878
Al	5.586	5.606	5.600	5.615	5.707	5.677
Si	5.314	5.265	5.244	5.273	5.168	5.201
K	-	-	-	-	-	-
V	*	*	*	*	*	*
Cr	-	-	-	-	-	-
Mn	0.028	0.0	0.0	0.0	0.0	0.0
Fe	8.376	8.242	8.392	8.331	8.466	8.347
OCT	11.893	11.932	11.956	11.917	11.977	11.961
TOTAL	19.893	19.932	19.956	19.917	19.977	19.961
y	0.934	0.910	0.921	0.923	0.930	0.919

AB-A

	4	9	13	14	17	22	23	24	25
	o	o	o	o	o	o	o	o	o
MgO	2.970	2.408	2.485	2.141	2.222	2.309	2.304	2.605	2.710
Al2O3	21.601	20.445	21.533	20.340	20.503	19.901	21.004	20.588	22.552
SiO2	24.704	22.253	22.912	21.927	22.151	21.559	23.531	22.901	24.455
K2O	-	-	-	-	-	-	-	-	-
V2O3	*	*	*	*	*	*	*	*	*
Cr2O3	0.0	0.0	0.119	0.0	0.0	0.114	0.0	0.0	0.162
MnO	0.192	0.258	0.178	0.183	0.220	0.171	0.207	0.210	0.0
FeO	43.108	41.922	42.233	42.121	42.421	42.458	42.452	42.051	42.186
TOTAL	92.727	87.624	-	-	-	-	89.657	-	-
Mg	0.965	0.838	0.836	0.739	0.768	0.810	0.778	0.857	0.872
Al(T)	2.613	2.806	2.828	2.918	2.862	2.928	2.665	2.840	2.720
Al(O)	2.940	2.820	2.902	2.640	2.745	2.591	2.949	2.629	3.020
Al	5.553	5.626	5.730	5.558	5.607	5.519	5.614	5.469	5.740
Si	5.387	5.194	5.172	5.082	5.138	5.072	5.335	5.160	5.280
K	-	-	-	-	-	-	-	-	-
V	*	*	*	*	*	*	*	*	*
Cr	0.0	0.0	0.021	0.0	0.0	0.021	0.0	0.0	0.028
Mn	0.035	0.051	0.034	0.036	0.043	0.034	0.040	0.040	0.0
Fe	7.861	8.184	7.973	8.165	8.229	8.353	8.044	7.924	7.615
OCT	11.801	11.893	11.766	11.580	11.785	11.809	11.811	11.468	11.537
TOTAL	19.801	19.893	19.766	19.580	19.785	19.809	19.811	19.468	19.537
y	0.891	0.907	0.905	0.917	0.915	0.912	0.912	0.901	0.897

YF-A

	1 m	3 m	4 m	5 m	6 m
MgO	0.592	1.142	1.277	1.044	0.973
Al2O3	14.129	17.501	17.330	17.419	16.122
SiO2	20.241	23.760	23.948	24.025	23.164
K2O	-	-	-	-	-
V2O3	*	*	*	*	*
Cr2O3	-	-	-	-	-
MnO	-	-	-	-	-
FeO	42.099	47.627	47.502	47.970	48.558
TOTAL	-	-	-	90.459	89.181
Mg	0.243	0.397	0.443	0.362	0.347
Al(T)	2.419	2.455	2.420	2.419	2.452
Al(O)	2.173	2.358	2.340	2.351	2.101
Al	4.592	4.813	4.760	4.770	4.553
Si	5.581	5.545	5.580	5.581	5.548
K	-	-	-	-	-
V	*	*	*	*	*
Cr	-	-	-	-	-
Mn	-	-	-	-	-
Fe	9.709	9.293	9.256	9.320	9.727
OCT	12.125	12.048	12.039	12.033	12.175
TOTAL	20.125	20.048	20.039	20.033	20.175
y	0.976	0.959	0.954	0.963	0.966

YF-B

	1 o	3 o	5 o	7 o	9 o	11 m
MgO	2.281	2.142	2.119	1.908	1.704	2.309
Al2O3	18.380	18.272	16.669	16.874	14.373	18.107
SiO2	24.295	24.041	22.052	22.697	18.769	23.989
K2O	-	-	-	-	-	-
V2O3	*	*	*	*	*	*
Cr2O3	0.0	0.0	0.0	0.0	0.132	0.143
MnO	-	-	-	-	-	-
FeO	44.449	45.602	41.266	41.887	36.975	46.003
TOTAL	-	90.407	-	-	-	-
Mg	0.782	0.734	0.795	0.704	0.736	0.789
Al(T)	2.409	2.470	2.450	2.381	2.558	2.498
Al(O)	2.587	2.485	2.469	2.543	2.355	2.389
Al	4.996	4.955	4.919	4.924	4.913	4.887
Si	5.591	5.530	5.550	5.619	5.442	5.502
K	-	-	-	-	-	-
V	*	*	*	*	*	*
Cr	0.0	0.0	0.0	0.0	0.030	0.026
Mn	-	-	-	-	-	-
Fe	8.555	8.773	8.686	8.672	8.966	8.824
OCT	11.924	11.992	11.950	11.919	12.087	12.028
TOTAL	19.924	19.992	19.950	19.919	20.087	20.028
y	0.916	0.923	0.916	0.925	0.924	0.918

YF-G

	6 m	7 m	8 m	9 m
MgO	2.390	2.609	2.594	2.082
Al2O3	19.920	20.158	19.797	16.350
SiO2	24.099	24.541	23.016	19.773
K2O	-	-	-	-
V2O3	*	*	*	*
Cr2O3	0.0	0.151	0.0	0.0
MnO	-	-	-	-
FeO	43.393	43.521	43.427	37.588
TOTAL	-	-	-	-
Mg	0.809	0.870	0.893	0.844
Al(T)	2.525	2.511	2.684	2.625
Al(O)	2.808	2.804	2.707	2.615
Al	5.333	5.315	5.391	5.240
Si	5.474	5.489	5.316	5.375
K	-	-	-	-
V	*	*	*	*
Cr	0.0	0.027	0.0	0.0
Mn	-	-	-	-
Fe	8.243	8.140	8.389	8.546
OCT	11.860	11.841	11.989	12.005
TOTAL	19.860	19.841	19.989	20.005
y	0.911	0.903	0.904	0.910

SN15C

	6 m	7 m	9 m	10 m
MgO	2.249	2.188	2.190	2.096
Al2O3	19.233	19.430	19.503	19.874
SiO2	24.059	24.332	24.023	23.364
K2O	-	-	-	-
V2O3	*	*	*	*
Cr2O3	0.118	0.0	0.141	0.0
MnO	-	-	-	-
FeO	45.467	45.919	45.770	45.476
TOTAL	91.281	91.870	91.711	90.907
Mg	0.759	0.732	0.735	0.710
Al(T)	2.552	2.536	2.589	2.685
Al(O)	2.583	2.608	2.590	2.644
Al	5.135	5.144	5.179	5.329
Si	5.448	5.464	5.411	5.315
K	-	-	-	-
V	*	*	*	*
Cr	0.021	0.0	0.025	0.0
Mn	-	-	-	-
Fe	8.611	8.624	8.623	8.651
OCT	11.974	11.964	11.973	12.005
TOTAL	19.974	19.964	19.973	20.005
y	0.919	0.922	0.922	0.924

CI1

	1 o	2 o	5 o	6 o	7 o	8 o	9 o	10 o	13 o	16 o	18 o
MgO	1.641	1.572	1.697	1.797	1.303	1.446	1.526	1.445	1.633	1.539	1.529
Al2O3	16.315	15.386	15.008	16.164	15.104	15.545	15.879	14.965	15.589	15.127	15.997
SiO2	25.461	26.315	26.358	26.086	26.486	25.882	26.101	27.856	25.272	25.573	25.808
K2O	0.165	0.114	0.149	0.176	0.201	0.095	0.178	0.165	0.193	0.219	0.147
V2O3	*	*	*	*	0.104	*	*	0.088	0.131	0.0	0.084
Cr2O3	0.0	0.0	0.156	0.0	0.0	0.0	0.0	0.0	0.0	0.0	0.095
MnO	0.264	0.207	0.195	0.171	0.221	0.173	0.206	0.198	0.132	0.207	0.216
FeO	45.959	46.676	46.535	46.388	46.082	46.708	46.711	45.719	46.161	47.042	46.752
TOTAL	89.916	90.271	90.202	90.781	89.657	89.849	90.748	90.581	89.257	89.836	90.702
Mg	0.565	0.540	0.584	0.612	0.451	0.500	0.521	0.489	0.569	0.535	0.524
Al(T)	2.113	1.934	1.914	2.037	1.853	1.995	2.016	1.671	2.085	2.032	2.070
Al(O)	2.334	2.247	2.171	2.319	2.279	2.257	2.276	2.338	2.144	2.129	2.263
Al	4.447	4.181	4.085	4.356	4.132	4.252	4.292	4.009	4.299	4.161	4.333
Si	5.887	6.066	6.086	5.963	6.147	6.005	5.984	6.329	5.911	5.968	5.930
K	0.049	0.033	0.044	0.051	0.059	0.028	0.052	0.048	0.058	0.065	0.043
V	*	*	*	*	0.019	*	*	0.016	0.025	0.0	0.015
Cr	0.0	0.0	0.028	0.0	0.0	0.0	0.0	0.0	0.0	0.0	0.017
Mn	0.052	0.040	0.038	0.033	0.043	0.034	0.040	0.038	0.026	0.041	0.042
Fe	8.887	8.998	8.986	8.868	8.944	9.063	8.956	8.687	9.030	9.181	8.984
OCT	11.838	11.825	11.807	11.832	11.736	11.854	11.793	11.568	11.794	11.886	11.845
TOTAL	19.887	19.858	19.851	19.883	19.795	19.882	19.845	19.616	19.852	19.951	19.888
y	0.940	0.943	9.925	0.935	0.952	0.948	0.945	0.948	0.941	0.945	0.945

CI

	1 on	2 on	3 on	4 on	5 on	6 on	8 on	9 on	12 on	13 o	14 o	15 o
MgO	0.733	1.475	1.305	1.529	1.480	1.626	1.438	1.497	1.387	1.633	1.436	1.537
Al2O3	10.038	14.067	13.878	13.845	14.277	14.450	14.173	13.842	14.086	14.791	14.426	14.587
SiO2	19.906	25.880	25.953	26.650	25.866	26.072	26.027	22.907	25.935	25.408	25.808	25.444
K2O	0.0	0.0	0.0	0.0	0.0	0.0	0.0	0.0	0.076	0.0	0.0	0.0
V2O3	0.0	0.0	0.0	0.198	0.0	0.0	0.0	0.0	0.0	0.0	0.181	0.130
Cr2O3	0.0	0.0	0.0	0.0	0.0	0.0	0.0	0.0	0.0	0.0	0.0	0.0
MnO	0.0	0.0	0.0	0.0	0.0	0.0	0.0	0.0	0.0	0.129	0.0	0.0
FeO	35.943	45.283	45.595	45.669	45.398	45.834	44.823	41.261	46.513	46.047	46.441	46.607
TOTAL	-	87.375	87.393	88.529	87.907	88.650	87.123	-	88.412	88.174	88.292	88.544
Mg	0.345	0.527	0.467	0.540	0.527	0.573	0.514	0.584	0.492	0.576	0.507	0.542
Al(T)	1.717	1.791	1.764	1.690	1.818	1.837	1.758	2.007	1.833	1.985	1.893	1.984
Al(O)	2.018	2.188	2.168	2.175	2.205	2.190	2.250	2.262	2.116	2.143	2.131	2.082
Al	3.735	3.979	3.932	3.865	4.023	4.027	4.008	4.269	3.949	4.128	4.024	4.066
Si	6.283	6.209	6.236	6.310	6.182	6.163	6.242	5.993	6.167	6.015	6.107	6.016
K	0.0	0.0	0.0	0.0	0.0	0.0	0.0	0.0	0.023	0.0	0.0	0.0
V	0.0	0.0	0.0	0.037	0.0	0.0	0.0	0.0	0.0	0.0	0.034	0.025
Cr	0.0	0.0	0.0	0.0	0.0	0.0	0.0	0.0	0.0	0.0	0.0	0.0
Mn	0.0	0.0	0.0	0.0	0.0	0.0	0.0	0.0	0.0	0.026	0.0	0.0
Fe	9.487	9.086	9.163	9.043	9.074	9.061	8.991	9.027	9.250	9.117	9.191	9.215
OCT	11.850	11.801	11.798	11.795	11.806	11.824	11.755	11.873	11.858	11.862	11.863	11.864
TOTAL	19.850	19.801	19.798	19.795	19.806	19.824	19.755	19.873	19.858	19.862	19.863	19.864
y	0.965	0.945	0.952	0.944	0.945	0.941	0.946	0.939	0.950	0.941	0.948	0.945

CI cont

	16 o	17 o	19 o	20 o
MgO	1.582	1.320	1.776	1.547
Al2O3	16.032	14.972	14.998	15.363
SiO2	24.279	26.246	25.411	25.068
K2O	0.0	0.0	0.0	0.0
V2O3	0.136	0.0	0.0	0.0
Cr2O3	0.129	0.0	0.0	0.0
MnO	0.0	0.0	0.0	0.0
FeO	45.432	45.485	46.090	45.193
TOTAL	87.592	88.023	88.432	87.170
Mg	0.561	0.463	0.620	0.550
Al(T)	2.218	1.823	2.010	2.022
Al(O)	2.283	2.331	2.158	2.297
Al	4.501	4.154	4.168	4.319
Si	5.782	6.177	5.990	5.978
K	0.0	0.0	0.0	0.0
V	0.026	0.0	0.0	0.0
Cr	0.024	0.0	0.0	0.0
Mn	0.0	0.0	0.0	0.0
Fe	9.048	8.952	9.087	9.014
OCT	11.942	11.746	11.895	11.861
TOTAL	19.942	19.746	19.895	19.861
y	0.942	0.951	0.936	0.943

CI130C

	6 o	7 o	8 o	9 o	10 o
MgO	2.684	2.543	2.241	2.561	2.669
Al2O3	17.987	17.467	14.841	17.972	17.715
SiO2	24.385	24.360	19.952	24.317	23.782
K2O	-	-	-	-	-
V2O3	*	*	*	*	*
Cr2O3	-	-	-	-	-
MnO	-	-	-	-	-
FeO	44.916	44.820	37.375	45.415	44.525
TOTAL	90.764	89.924	-	-	-
Mg	0.916	0.877	0.928	0.874	0.925
Al(T)	2.442	2.397	2.458	2.429	2.471
Al(O)	2.415	2.366	2.394	2.425	2.385
Al	4.857	4.763	4.852	4.854	4.856
Si	5.585	5.634	5.542	5.571	5.529
K	-	-	-	-	-
V	*	*	*	*	*
Cr	-	-	-	-	-
Mn	-	-	-	-	-
Fe	8.604	8.670	8.683	8.702	8.658
OCT	11.986	11.985	12.005	12.001	11.968
TOTAL	19.986	19.985	20.005	20.001	19.968
y	0.904	0.908	0.903	0.909	0.904

CI137

	1 on	2 on	3 on	4 on	5 on	6 on	7 on	8 on
MgO	1.915	1.717	1.250	1.861	1.906	1.983	1.947	1.931
Al2O3	15.527	14.823	11.584	14.259	15.824	14.883	14.039	15.327
SiO2	25.391	25.492	19.663	24.359	25.562	26.450	26.558	26.265
K2O	0.0	0.0	0.0	0.0	0.0	0.0	0.087	0.0
V2O3	*	*	*	*	*	*	*	*
Cr2O3	0.0	0.0	0.0	0.0	0.0	0.0	0.0	0.0
MnO	0.0	0.0	0.0	0.0	0.0	0.132	0.0	0.0
FeO	46.873	46.664	38.127	45.028	46.688	47.424	47.952	47.442
TOTAL	90.027	-	-	-	-	-	-	-
Mg	0.662	0.603	0.558	0.679	0.657	0.679	0.671	0.659
Al(T)	2.107	1.991	2.115	2.036	2.085	1.927	1.855	1.981
Al(O)	2.141	2.128	1.972	2.079	2.233	2.102	1.975	2.159
Al	4.248	4.119	4.087	4.115	4.318	4.029	3.830	4.140
Si	5.893	6.009	5.885	5.964	5.915	6.073	6.145	6.019
K	0.0	0.0	0.0	0.0	0.0	0.0	0.026	0.0
V	*	*	*	*	*	*	*	*
Cr	0.0	0.0	0.0	0.0	0.0	0.0	0.0	0.0
Mn	0.0	0.0	0.0	0.0	0.0	0.026	0.0	0.0
Fe	9.098	9.200	9.543	9.220	9.036	9.107	9.280	9.092
OCT	11.901	11.931	12.073	11.978	11.926	11.914	11.952	11.910
TOTAL	19.901	19.931	20.073	19.978	19.926	19.914	19.952	19.910
y	0.932	0.939	0.945	0.931	0.932	0.931	0.933	0.932

Diagenetic siderite compositions for the Bryn Poeth (AA10E) Pen Y Gaer (LP 19A, 22A, 22D) and Trefor (LP72) ironstones. Carbonate values are recalculated from oxide values given by the probe data. Some analyses have been recalculated because of mixing with apatite. The Ca values are recalculated subtracting CaO in the ratio CaO:P2O5 1:1.27. Additionally, some silica is present in some of the analyses and is included to balance the totals. Ca values marked with an asterix are probe analyses with apatite in the analysis, and therefore recalculated in the ratio (CaO:P2O5 1:1.27) before converting to carbonate values. SiO2 represents silica in the analysis which reduces the total. Siderite form is: R - rhomb, C - cement, O - replacing ooid.

Sample No.		$FeCO_3$	$MgCO_3$	$CaCO_3$	$MnCO_3$	TOTAL CARBONATE	SiO_2
AA10E							
6	O	82.53	2.39	8.70	3.15	96.77	4
7	O	86.37	2.15	8.65	3.13	100.30	0
9	C	81.90	1.87	8.42	6.32	98.51	0
11	R	63.72	2.76	5.12	30.09	101.69	0
12	R	14.92	1.77	5.60	70.11	92.40	14
13	R	78.73	2.67	11.13	10.15	102.68	0
15	O	87.54	4.12	3.08	5.03	99.77	0
19	O	86.23	2.48	8.26	3.32	100.29	0
LP19A							
17	C	89.15	3.21	*0.72	3.79	96.87	0
21	R	89.00	5.80	*1.78	1.04	97.62	0
22	R	88.00	5.26	*1.74	1.13	96.13	0
23	R	89.00	4.63	*1.88	0.73	96.24	0
25	R	89.19	5.23	*1.76	0.61	96.79	0
26	R	90.80	4.31	*1.72	0.41	97.24	0
27	C	88.83	3.68	*1.95	0.88	95.34	0
28	C	87.61	5.05	*2.34	0.70	95.70	0
LP22A							
10	R	90.60	5.91	*2.10	1.11	99.72	0
11	R	83.64	3.97	*1.73	1.44	90.78	10
12	R	93.05	5.69	*1.14	0.97	100.85	0
13	R	92.66	6.11	*1.73	0.45	100.95	0
14	R	91.11	4.59	*1.05	0.92	97.67	2
24	C	94.95	4.22	*2.66	1.03	102.86	0
28	C	93.75	2.46	*0.36	5.58	102.15	
LP22D							
12	R	89.88	5.87	1.24	0.48	97.47	0
13	R	90.11	5.52	0.83	0.55	97.01	0
14	R	90.41	5.81	0.85	0.89	97.96	0
15	R	89.37	5.68	1.32	0.75	97.12	0
16	R	88.71	5.66	1.22	0.78	96.37	0
LP72							
13	R	89.63	4.41	0.78	3.28	98.10	0
14	R	87.85	5.34	1.41	3.89	98.49	0
15	R	74.66	3.63	0.49	10.31	89.09	9
16	R	85.79	5.08	0.98	9.15	101.00	0

EPMA analyses of hydrothermal siderites in weight % of carbonate for the Aber (AB-A) and Betws Garmon (SN15C and YFA) ironstones. SiO_2 values are silica in the siderite analyses which otherwise reduce the total.

Sample No.	$FeCO_3$	$MgCO_3$	$CaCO_3$	$MnCO_3$	TOTAL CARBONATE	SiO_2
AB-A						
6	81.81	3.27	5.57	12.71	103.36	0
7	88.71	1.93	3.84	6.13	100.61	0
8	96.11	1.37	3.04	0.75	101.27	0
19	85.53	3.34	3.82	9.07	101.76	0
20	81.45	3.23	5.40	12.09	102.17	0
21	81.33	3.09	5.78	12.09	102.29	0
SN15C						
4	83.00	3.26	0.55	0.38	87.19	19
5	98.07	4.44	0.54	0.00	103.05	0
12	86.96	2.47	0.79	0.27	90.49	13
13	89.09	2.49	0.87	0.31	92.79	11
14	80.97	2.04	0.82	0.00	83.83	19
15	93.22	2.08	1.25	0.50	97.05	6
16	77.08	2.91	0.75	0.33	81.07	26
17	92.07	3.54	0.78	0.27	96.66	8
18	84.63	3.15	1.32	0.37	89.47	14
20	85.55	3.10	2.00	0.40	91.05	12
YFA						
1	98.26	2.89	1.64	0.00	102.79	1
7	101.33	0.00	0.52	0.00	101.85	1

EPMA data for stilpnomelane from Cadair Idris east. CI130C is from a stilpnomelane-rich ironstone, while CI137 is from a magnetite-rich ironstone. All iron is expressed as FeO. Na and Ti were also analysed for but not detected. TET - tetrahedral, OCT - octahedral, INT - interlayer sites.

	CI130C:1	CI130C:2	CI130C:4	CI130C:5	CI137:10	CI137:11	CI137:13	CI137:14	CI137:17
SiO2	45.865	44.917	44.848	43.474	44.714	41.747	44.091	44.145	42.067
Al2O3	6.300	6.395	6.160	6.110	6.112	6.057	6.100	6.119	6.231
FeO	34.543	34.804	34.900	36.099	37.983	36.592	38.390	37.335	41.096
MnO	0.363	0.330	0.414	0.360	-	-	-	-	-
MgO	2.720	2.831	2.663	2.576	0.904	0.954	0.812	0.882	0.942
CaO	0.458	0.193	0.254	0.175	0.797	2.807	0.827	1.160	0.300
K2O	2.884	3.227	2.108	3.202	2.736	2.935	2.527	2.508	2.222
Total	93.133	92.698	91.347	91.995	93.247	91.093	92.747	92.149	92.858
	FORMULA (based on 11 oxygens)				FORMULA (based on 11 oxygens)				
Si	3.641	3.607	3.636	3.562	3.618	3.506	3.598	3.609	3.489
Al(T)	0.359	0.393	0.364	0.438	0.382	0.494	0.402	0.391	0.511
Al(O)	0.233	0.215	0.221	0.152	0.201	0.101	0.186	0.198	0.097
Fe	2.296	2.334	2.369	2.470	2.573	2.567	2.618	2.554	2.851
Mn	0.024	0.024	0.029	0.025	-	-	-	-	-
Mg	0.325	0.338	0.322	0.315	0.107	0.121	0.098	0.108	0.115
Ca	0.038	0.015	0.024	0.015	0.068	0.252	0.074	0.103	0.025
K	0.296	0.328	0.214	.335	0.282	0.312	0.264	0.265	0.239
TET	4.000	4.000	4.000	4.000	4.000	4.000	4.000	4.000	4.000
OCT	2.878	2.911	2.941	2.962	2.881	2.789	2.902	2.860	3.063
INT	0.334	0.343	0.238	0.350	0.350	0.564	0.338	0.368	0.264
OCT+INT	3.212	3.254	3.179	3.312	3.231	3.353	3.240	3.228	3.327
TOTAL	7.212	7.254	7.179	7.312	7.231	7.353	7.240	7.228	7.327

EPMA data for apatite plotted as CaO against P2O5 to calculate the Ca/P ratio.

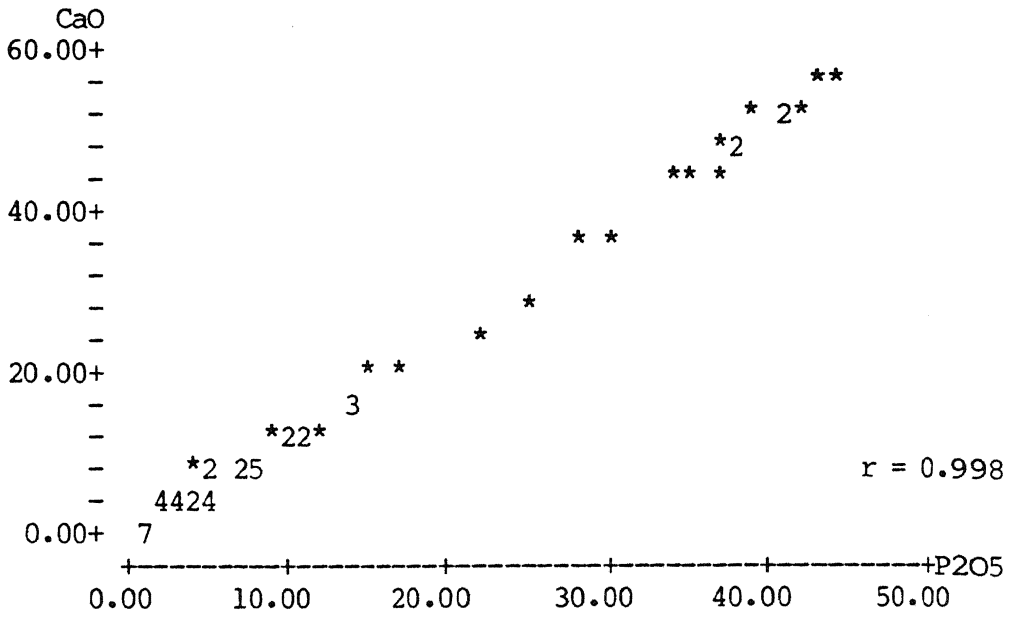

THE REGRESSION EQUATION IS

CaO = 1.27 P2O5 - 0.651

APPENDIX 5

X-RAY FLUORESENCE AND INDUCTIVELY COUPLED PLASMA SPECTROMETRY DATA

The ironstone were prepared by rock crushing at the Open University. Rock samples were broken down to roughly 3cm pieces by a hydraulic breaker. These were then broken into 5mm pieces with a jaw crusher. Between each sample the jaws of the crusher were cleaned with a wire brush and acetone. 100g of sample was then placed in an agate tema and ground for roughly 7 minutes. Between each sample the tema was cleaned by grinding with a little quartzite, and then cleaning with a dusting brush and acetone.

The ironstones were analysed by XRF (PW1400) at Nottingham University (analysts Dr. P.K. Harvey & Dr. B.P. Atkin) for the major elements on fused glass beads and for 18 trace elements on pressed powder pellets. These analyses give total iron [Fe_2O_3(T)] in the form of Fe_2O_3. Ferrous iron was calculated by titrations against potassium dichromate and the remaining iron was assigned as ferric iron. O.R.I. represents the oxidation/reduction state of the ironstone and is $FeO/[FeO + Fe_2O_3]$. Major elements are expressed as weight percent oxide and trace and rare earth elements as ppm. XRF values below the (2s) detection limit are quoted as zero.

ICP analysis at Oxford Polytechnic (analyst Dr. W. Perkins) for the REE of only selected samples. Cerium and yttrium were analysed by both XRF and ICP. XRF values for these are given for all ironstone samples in the trace elements, while ICP values are only for those selected for REE analysis. Those REE values in brackets represent unreliable data and a value is determined by interpolating between adjacent elements on a chondrite normalised plot, and used only for calculating REE totals.

The location of samples is given in Appendix 1, the nomenclature for rock-types is given in Appendix 1.

Sample No.	AA10F	AA10G	AA12A	LP22A	LP22D	LP19B	LP24A	LP24C	SN18A	SN18B	ABA
Analysis No.	015	016	017	028	029	030	031	032	018	019	020
Rock Type	P	P	S	P	P	P	W	F	G	G	P
SiO2	13.21	19.39	16.28	19.80	21.48	17.78	28.52	30.61	17.04	10.27	18.01
Al2O3	7.75	10.83	3.61	6.86	6.61	5.51	9.14	13.02	9.35	7.03	9.82
TiO2	0.36	0.46	0.18	0.39	0.32	0.28	0.47	0.76	0.62	0.53	0.59
Fe2O3(T)	56.66	47.53	47.53	44.46	47.82	52.81	41.68	40.56	50.74	57.40	49.98
FeO	6.20	31.73	23.38	30.63	33.42	22.08	30.10	27.94	37.48	35.92	30.67
Fe2O3	49.77	12.27	21.55	10.42	10.68	28.29	8.22	9.51	9.09	17.49	15.90
MgO	0.97	1.86	1.97	1.15	0.96	0.65	1.40	1.42	1.63	1.37	1.69
CaO	3.93	3.52	5.15	6.57	4.09	4.63	4.08	2.58	2.19	1.97	1.82
Na2O	0.47	0.29	0.00	0.19	0.08	0.00	0.00	0.03	0.13	0.00	0.00
K2O	0.05	0.00	0.00	0.00	0.01	0.02	0.00	0.01	0.00	0.00	0.00
MnO	1.33	1.44	0.29	0.29	0.13	0.15	0.28	0.35	0.85	0.63	1.49
P2O5	3.56	1.72	3.34	4.76	2.84	3.57	2.84	1.76	1.22	1.01	1.01
LOI	10.79	12.73	21.53	14.94	15.82	14.09	11.87	9.13	16.12	19.07	14.84
TOTAL	99.08	99.76	99.90	99.41	100.17	99.50	100.30	100.22	99.89	99.29	99.25
ORI	0.122	0.742	0.547	0.766	0.777	0.465	0.803	0.766	0.821	0.695	0.682
As	61	21	27	852	31	49	36	40	4	8	0
Ba	207	85	48	100	120	199	72	95	59	89	52
Ce	516	283	188	157	173	173	137	186	174	122	114
Co	94	115	46	38	25	26	28	62	36	31	40
Cr	243	129	107	140	195	176	165	159	200	172	192
Cu	60	21	45	25	32	30	30	17	26	28	62
Hf	5	4	0	4	0	8	6	0	3	13	4
Ni	165	414	37	47	36	19	44	121	50	54	63
Nb	9	15	5	10	8	6	9	18	15	14	16
Pb	81	26	17	39	26	26	21	22	11	8	11
Rb	8	10	9	10	10	10	7	10	11	11	10
S	4366	1563	24784	20645	6606	7321	7796	0	841	1879	1051
Sc	23	32	10	11	9	7	15	25	44	43	35
Sr	221	154	177	369	240	510	147	139	32	34	18
V	484	245	246	253	319	305	249	230	238	236	226
Y	124	100	91	72	74	85	68	82	63	47	61
Zn	213	167	41	108	103	91	127	195	143	127	163
Zr	86	147	53	79	64	48	91	182	144	116	135
La	43.48	36.05	-	-	40.42	-	32.87	36.63	-	18.25	27.76
Ce	165.18	134.27	-	-	87.88	-	75.94	91.22	-	48.87	68.04
Pr	(15.40)	(12.54)	-	-	(11.09)	-	(9.41)	10.92	-	(6.16)	8.82
Nd	81.35	66.50	-	-	51.62	-	45.94	46.14	-	31.90	43.10
Sm	21.03	16.86	-	-	10.76	-	10.80	12.14	-	7.92	10.91
Eu	5.27	4.37	-	-	2.39	-	2.43	2.68	-	1.97	2.57
Gd	24.97	20.59	-	-	12.25	-	12.44	14.10	-	8.59	11.43
Tb	3.54	2.88	-	-	1.50	-	1.45	2.02	-	(1.42)	1.99
Dy	22.07	19.63	-	-	11.05	-	10.77	12.72	-	8.91	11.27
Ho	4.10	3.88	-	-	2.15	-	2.03	2.44	-	1.74	2.18
Er	11.25	10.88	-	-	5.89	-	5.57	6.89	-	5.46	6.63
Tm	1.52	1.64	-	-	0.81	-	0.79	(1.08)	-	0.91	(1.04)
Yb	9.50	10.46	-	-	4.78	-	4.78	7.19	-	6.09	6.95
Lu	1.29	1.53	-	-	0.64	-	0.64	1.07	-	0.89	1.04
Y	117.05	99.16	-	-	65.91	-	61.94	61.47	-	45.01	53.07
Ce/Ce*	1.48	1.47	-	-	0.96	-	1.00	1.09	-	1.06	1.00
Eu/Eu*	0.71	0.72	-	-	0.64	-	0.64	0.66	-	0.73	0.71
REE	409.95	342.08	-	-	243.23	-	215.86	246.61	-	149.08	203.73
REE+Y	527.00	442.24	-	-	309.14	-	277.80	308.08	-	194.09	256.80
La/Lu	33.71	23.56	-	-	63.16	-	51.40	34.23	-	20.51	26.69
La/Sm	2.07	2.14	-	-	3.76	-	3.04	3.02	-	2.30	2.55
Gd/Lu	19.36	13.46	-	-	19.14	-	19.44	13.18	-	9.65	10.99
Sm/Ho	5.13	4.35	-	-	5.01	-	5.32	4.98	-	4.55	5.01
Ho/Lu	3.18	2.54	-	-	3.36	-	3.17	2.28	-	1.96	2.10

Sample No.	AB	SN21	SN14D	SN14E	SN14F	SN14G	SN14H	SN14I	YF	SN14B	SN15B
Analysis No.	021	040	001	002	003	004	005	006	007	008	009
Rock Type	G	P	P	P	P	P	P	P	P	P	P
SiO2	18.51	17.02	12.11	15.62	11.94	13.59	14.49		12.90	11.27	14.26
Al2O3	8.14	8.82	4.88	6.13	4.97	5.95	5.64		5.97	4.38	5.03
TiO2	0.60	0.36	0.23	0.29	0.24	0.27	0.28		0.23	0.20	0.19
Fe2O3(T)	48.91	41.88	56.38	53.61	61.15	64.25	68.12		65.94	61.56	49.88
FeO	31.43	30.32	40.87	36.32	36.10	27.45	29.74	25.74	33.04	39.37	35.69
Fe2O3	13.98	8.18	10.95	13.25	21.05	33.74	35.07		29.22	17.81	10.22
MgO	1.65	3.19	0.84	1.02	1.00	1.04	0.99		0.79	0.64	1.56
CaO	2.49	13.40	5.88	5.83	6.00	6.01	3.76		5.32	3.82	5.78
Na2O	0.12	0.00	0.00	0.01	0.00	0.00	0.02		0.00	0.00	0.00
K2O	0.00	0.22	0.00	0.00	0.00	0.00	0.00		0.00	0.00	0.00
MnO	1.52	0.53	0.05	0.01	0.04	0.05	0.07		0.03	0.02	0.24
P2O5	1.40	7.82	4.11	4.13	4.19	4.42	2.68		3.79	2.62	3.91
LOI	16.29	6.49	14.86	13.49	9.69	3.54	3.06		4.26	15.37	18.97
TOT	99.63	99.74	99.34	100.16	99.22	99.13	99.10		99.24	99.87	99.81
ORI	0.714	0.805	0.806	0.753	0.656	0.475	0.485		0.557	0.711	0.795
As	0	6	0	11	2	13	29	0	26	5	1
Ba	52	44	77	79	93	127	164	120	115	109	54
Ce	154	314	225	185	182	288	327	234	225	205	185
Co	35	8	28	34	32	47	32	37	24	29	23
Cr	192	231	255	309	284	399	325	317	346	275	220
Cu	37	43	23	34	31	36	40	49	30	20	21
Hf	8	7	0	3	10	0	6	0	11	4	6
Ni	65	19	30	30	27	37	49	37	35	41	37
Nb	15	9	7	7	4	7	7	2	7	5	5
Pb	16	13	9	29	21	7	21	15	17	13	12
Rb	10	25	12	10	10	12	14	13	14	11	10
S	792	82979	1821	26005	12172	5109	3185	4046	1546	8270	6487
Sc	39	19	12	13	15	11	12	9	13	12	16
Sr	33	215	459	426	434	554	375	443	422	474	481
V	237	403	358	424	420	584	495	469	463	428	416
Y	67	159	99	94	82	111	81	99	103	77	101
Zn	145	27	78	163	130	169	348	401	201	70	71
Zr	137	79	56	68	59	68	69	59	65	50	54
La	-	-	36.73	-	-	49.88	42.71	-	-	27.14	39.69
Ce	-	-	88.75	-	-	112.09	107.25	-	-	72.30	101.84
Pr	-	-	9.89	-	-	(14.00)	(11.76)	-	-	(7.95)	(11.42)
Nd	-	-	48.97	-	-	67.07	55.52	-	-	39.31	54.80
Sm	-	-	11.83	-	-	14.99	13.23	-	-	9.33	12.36
Eu	-	-	2.67	-	-	3.34	2.90	-	-	2.12	2.87
Gd	-	-	12.53	-	-	16.32	14.48	-	-	10.88	14.66
Tb	-	-	1.87	-	-	2.03	1.97	-	-	(1.66)	1.81
Dy	-	-	10.01	-	-	13.57	11.57	-	-	9.71	11.87
Ho	-	-	1.78	-	-	2.59	2.11	-	-	1.82	2.22
Er	-	-	5.13	-	-	6.92	5.76	-	-	5.02	5.98
Tm	-	-	(0.71)	-	-	(0.97)	(0.81)	-	-	0.69	(0.86)
Yb	-	-	4.10	-	-	5.77	4.80	-	-	5.51	5.26
Lu	-	-	0.59	-	-	0.76	0.65	-	-	0.59	0.70
Y	-	-	56.94	-	-	75.66	58.32	-	-	52.31	66.68
Ce/Ce*	-	-	1.06	-	-	0.97	1.11	-	-	1.15	1.11
Eu/Eu*	-	-	0.67	-	-	0.65	0.64	-	-	0.65	0.65
REE	-	-	235.56	-	-	310.30	275.52	-	-	194.03	266.34
REE+Y	-	-	292.50	-	-	385.96	333.84	-	-	246.34	333.02
La/Lu	-	-	62.26	-	-	65.63	65.71	-	-	46.00	56.70
La/Sm	-	-	3.11	-	-	3.33	3.23	-	-	2.91	3.21
Gd/Lu	-	-	21.24	-	-	21.47	22.28	-	-	18.44	20.94
Sm/Ho	-	-	6.64	-	-	5.79	6.27	-	-	5.13	5.57
Ho/Lu	-	-	3.02	-	-	3.41	3.25	-	-	3.09	3.17

Sample No.	YF-G	YF-F	SN12D	SN13B	TD002	SN11	SN11A	CI130B	CI130C	CI134A	CI136B
Analysis No.	033	034	025	026	027	023	024	010	011	012	013
Rock Type	F	W	F	P	P	W	W	P	W	P	P
SiO2	38.07	25.67	34.48	8.74	8.76	21.03	24.07	23.75	25.03	17.70	25.57
Al2O3	8.07	7.78	10.19	4.29	3.57	6.68	8.50	7.20	7.75	7.41	9.15
TiO2	0.36	0.36	0.33	0.18	0.15	0.30	0.51	0.37	0.40	0.35	0.45
Fe2O3(T)	33.05	45.24	28.02	76.05	77.44	62.51	55.16	55.80	48.21	61.39	50.38
FeO	5.79		16.52	19.53	19.27	27.09	26.05	23.62	28.53	26.60	25.96
Fe2O3	26.62		9.67	55.37	56.02	34.40	26.21	29.54	16.50	31.83	21.53
MgO	1.04	1.31	1.00	0.39	0.27	1.47	1.51	1.37	2.00	1.31	1.71
CaO	6.33	4.34	11.59	3.70	3.48	1.72	1.85	3.92	3.89	4.40	4.30
Na2O	0.00	0.06	0.00	0.13	0.00	0.14	0.15	0.00	0.00	0.00	0.00
K2O	0.00	0.00	0.00	0.00	0.01	0.39	0.37	0.40	0.71	0.07	0.31
MnO	0.00	0.06	0.08	0.08	0.06	0.49	0.58	0.11	0.22	0.04	0.13
P2O5	4.76	3.10	9.19	2.96	2.78	1.13	1.27	2.88	2.68	3.23	3.04
LOI	8.56	12.22	5.17	2.29	2.89	3.98	5.15	3.79	9.29	3.43	5.04
TOTAL	100.24	100.14	100.06	98.82	99.39	99.84	99.11	99.59	100.18	99.34	100.07
ORI	0.196		0.655	0.282	0.277	0.467	0.525	0.471	0.658	0.482	0.573
As	310	26	0	0	0	114	56	5	5	3	8
Ba	36	67	0	75	42	50	97	116	154	81	92
Ce	155	184	77	241	259	238	232	318	147	236	189
Co	41	22	41	52	92	94	54	26	49	33	27
Cr	129	263	238	377	375	90	141	257	160	259	173
Cu	105	42	15	29	22	24	30	19	93	26	23
Hf	4	5	0	16	0	14	16	8	4	12	7
Ni	30	29	60	25	34	127	60	35	29	41	33
Nb	8	8	12	8	5	22	16	10	9	8	10
Pb	26	12	12	19	8	16	8	7	14	46	10
Rb	7	8	10	13	15	48	57	50	68	22	40
S	71199	18895	2816	1005	677	16961	10171	1243	101997	20	5676
Sc	12	10	20	19	21	16	27	14	11	10	15
Sr	558	628	194	114	84	47	90	119	126	128	148
V	217	412	463	575	562	177	310	416	296	489	324
Y	62	91	105	98	99	45	58	82	63	83	63
Zn	117	151	100	43	37	91	220	40	39	98	69
Zr	81	96	87	53	55	106	116	71	75	80	83
La	-	-	-	-	-	-	25.62	60.51	44.43	-	30.06
Ce	-	-	-	-	-	-	72.61	141.31	102.97	-	73.22
Pr	-	-	-	-	-	-	7.07	14.49	11.34	-	7.92
Nd	-	-	-	-	-	-	30.92	68.31	53.28	-	38.44
Sm	-	-	-	-	-	-	8.07	14.98	11.07	-	9.37
Eu	-	-	-	-	-	-	1.80	2.74	2.19	-	1.90
Gd	-	-	-	-	-	-	9.44	15.69	12.58	-	9.71
Tb	-	-	-	-	-	-	1.48	2.40	1.71	-	(1.60)
Dy	-	-	-	-	-	-	9.37	14.13	10.90	-	9.83
Ho	-	-	-	-	-	-	1.97	2.68	2.04	-	(2.01)
Er	-	-	-	-	-	-	5.64	7.38	5.80	-	5.45
Tm	-	-	-	-	-	-	(0.88)	(1.03)	(0.80)	-	(0.75)
Yb	-	-	-	-	-	-	5.75	6.20	4.76	-	4.28
Lu	-	-	-	-	-	-	0.80	0.84	0.69	-	0.63
Y	-	-	-	-	-	-	47.74	74.91	59.47	-	53.30
Ce/Ce*	-	-	-	-	-	-	1.25	1.10	1.00	-	1.09
Eu/Eu*	-	-	-	-	-	-	0.63	0.55	0.56	-	0.61
REE	-	-	-	-	-	-	180.79	352.69	264.56	-	195.17
REE+Y	-	-	-	-	-	-	228.53	427.60	324.03	-	248.47
La/Lu	-	-	-	-	-	-	32.03	72.04	64.39	-	47.71
La/Sm	-	-	-	-	-	-	3.18	4.04	4.01	-	3.21
Gd/Lu	-	-	-	-	-	-	11.80	18.68	18.23	-	15.41
Sm/Ho	-	-	-	-	-	-	4.10	5.59	5.43	-	*
Ho/Lu	-	-	-	-	-	-	2.46	3.19	2.96	-	*

Sample No.	CI137	CI129	CI123	CI200E
Analysis No.	014	035	036	022
Rock Type	P	W	M	P
SiO2	17.79	42.27	45.13	17.80
Al2O3	6.77	12.16	16.60	4.51
TiO2	0.35	0.54	0.79	0.33
Fe2O3(T)	61.39	30.60	19.34	69.60
FeO	27.20	20.13	11.95	27.42
Fe2O3	31.17	8.22	6.06	39.13
MgO	0.93	1.37	1.64	1.04
CaO	5.51	4.78	4.46	2.30
Na2O	0.00	0.08	0.04	0.02
K2O	0.13	0.00	2.44	0.32
MnO	0.06	0.06	0.04	0.06
P2O5	3.22	3.52	3.44	1.62
LOI	3.12	4.99	5.21	1.64
TOTAL	99.28	100.38	99.13	99.24
ORI	0.492	0.731	0.687	0.438
As	0	41	121	0
Ba	66	34	5545	111
Ce	266	185	153	150
Co	36	25	17	42
Cr	204	247	159	69
Cu	21	32	13	28
Hf	5	5	0	0
Ni	32	70	58	58
Nb	7	16	16	6
Pb	16	59	13	8
Rb	23	7	84	27
S	2840	0	0	10622
Sc	8	23	12	6
Sr	148	32	81	67
V	418	371	110	268
Y	91	119	79	49
Zn	94	147	112	160
Zr	68	128	129	64
La	56.63	21.83	-	-
Ce	134.98	73.78	-	-
Pr	(15.12)	7.71	-	-
Nd	69.61	31.93	-	-
Sm	14.63	10.29	-	-
Eu	3.30	1.72	-	-
Gd	16.79	15.70	-	-
Tb	2.31	2.21	-	-
Dy	15.56	14.41	-	-
Ho	3.03	3.02	-	-
Er	8.27	7.16	-	-
Tm	1.14	1.03	-	-
Yb	6.53	7.91	-	-
Lu	0.87	1.16	-	-
Y	88.84	69.94	-	-
Ce/Ce*	1.06	1.31	-	-
Eu/Eu*	0.65	0.46	-	-
REE	348.77	199.86	-	-
REE+Y	437.61	269.80	-	-
La/Lu	65.09	18.82	-	-
La/Sm	3.87	2.12	-	-
Gd/Lu	19.30	13.54	-	-
Sm/Ho	4.83	3.41	-	-
Ho/Lu	3.48	2.60	-	-

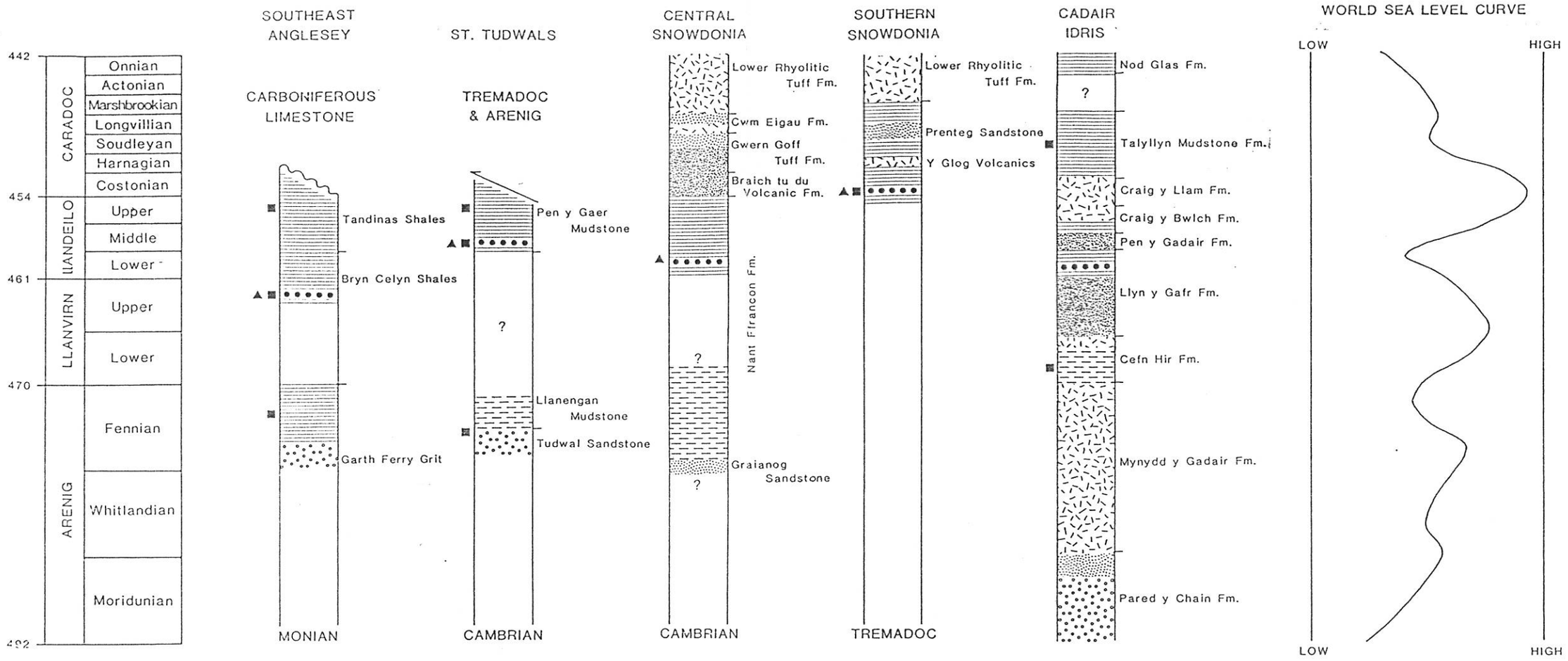

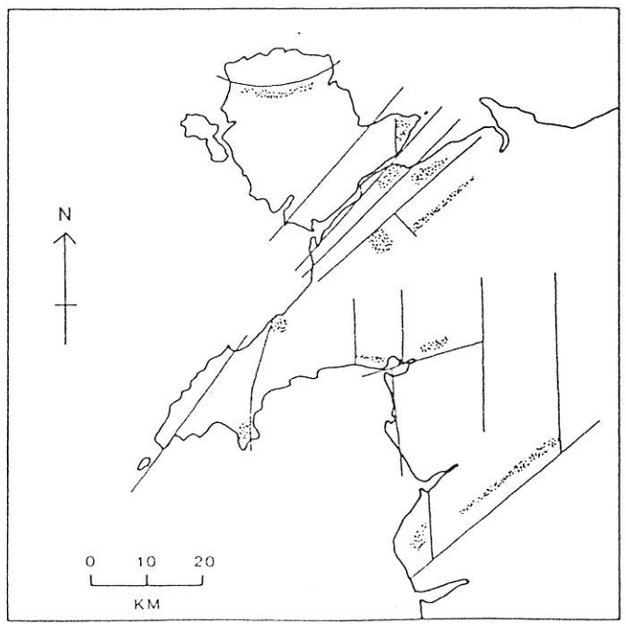

Figure A. Generalised stratigraphy of the North Wales Ordovician, from Beckley (1987), Williams et al. (1972) and: Southeast Anglesey (Bates 1972), St. Tudwals (Crimes 1969), Central Snowdonia (BGS 1985b), Southern Snowdonia (Smith 1987) and Cadair Idris (Cox 1925) and Ridgway (1976). Graptolite control from the above authors. Acritarchs from Trythall et al. (1987). Gaps in the stratigraphic columns represent hiatuses. World Sea Level Curve from Cocks & Fortey (1986). Inset map demonstrates the relationship between faulting and ironstone sedimentation (stipple), faulting pattern after Figure 1.3.

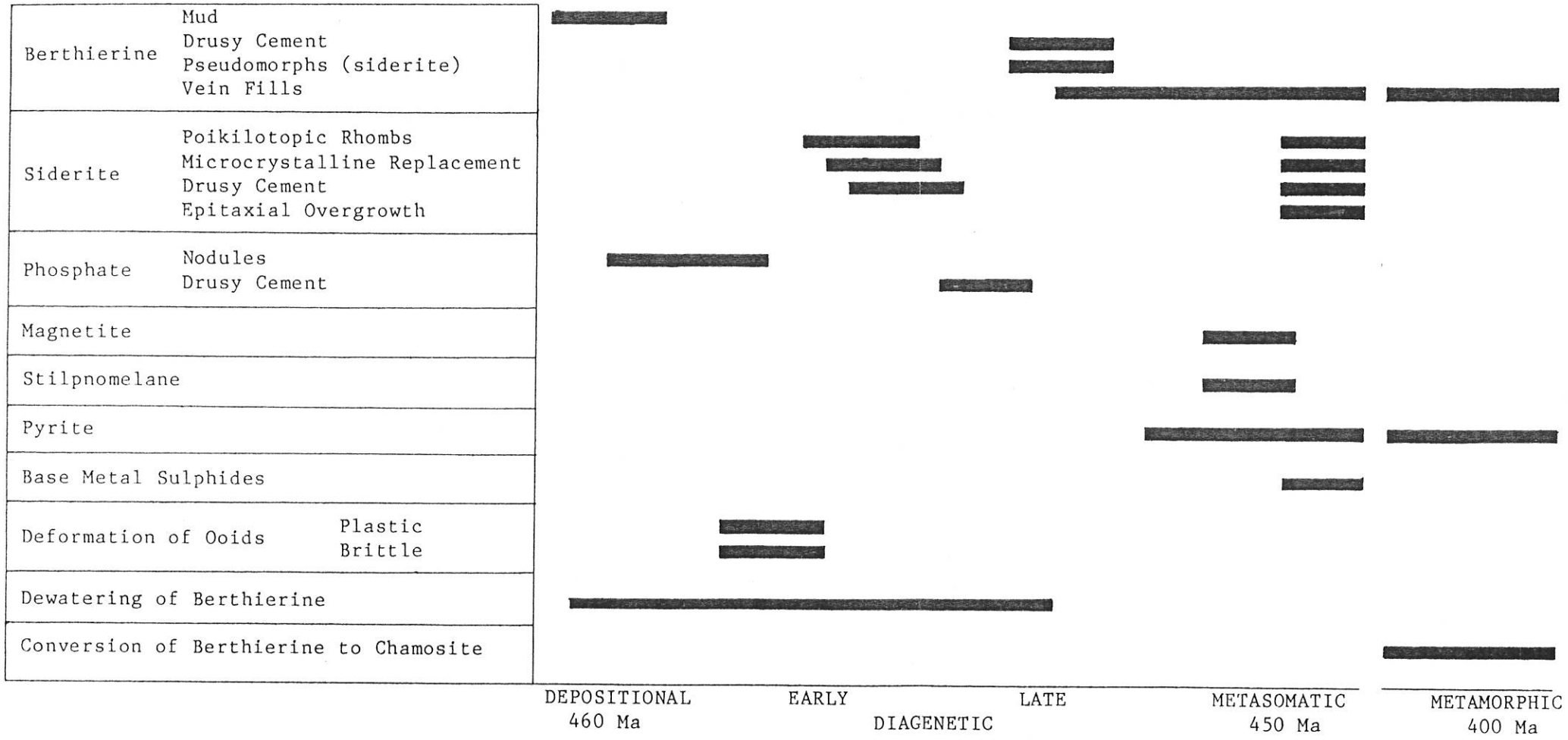

Figure B. Paragenetic sequence of diagenetic, metasomatic (and hydrothermal) and metamorphic processes within the Noh oolitic ironstones. Timings for the different events are given for scale.